②

RESOLVE Project Final Report

Visibility Conditions and Causes of Visibility Degradation In the Mojave Desert of California

by

John Trijonis, Santa Fe Research Corp
Michael McGown and Marc Pitchford, EPA-EMSL
Donald Blumenthal and Paul Roberts, Sonoma Technology
Warren White and Edward Macias, Washington University
Raymond Weiss and Alan Waggoner, Waggoner Electronics
John Watson and Judith Chow, Desert Research Institute
Robert Flocchini, University of California at Davis

DTIC
ELECTED
MAR 3 1 1989
D

for the
R2508 Joint Planning and Policy Board
Visibility Protection Program
Environmental Division
Public Works Department

JULY 1988

NAVAL WEAPONS CENTER
CHINA LAKE, CA 93555-6001

88 3 31 011

Naval Weapons Center

FOREWORD

This report documents air quality studies in the Mojave Desert of California initiated and authorized by the Joint Policy Planning Board (JPPB) of the R-2508 Restricted Airspace. This study, called RESOLVE (Research on Operations Limiting Visual Extinction), is part of a Department of Defense (DOD) program to protect flight and weapons test operations in this airspace from adverse impacts caused by degraded visibility

The RESOLVE study was carried out in three overlapping phases: the design and planning phase from 1983 to mid-1984; the data collection phase from August 1983 through August 1985, with various special field experiments carried out intermittently during 1984 through 1986. and midcourse, on-line data analysis begun in late 1984 and completed in late 1985.

REPORT DOCUMENTATION PAGE

1a REPORT SECURITY CLASSIFICATION UNCLASSIFIED		1b RESTRICTIVE MARKINGS			
2a SECURITY CLASSIFICATION AUTHORITY		3 DISTRIBUTION/AVAILABILITY OF REPORT A statement: public release: 8 October 1987			
2b DECLASSIFICATION/DOWNGRADING SCHEDULE					
4 PERFORMING ORGANIZATION REPORT NUMBER(S) NWC TP 6869		5 MONITORING ORGANIZATION REPORT NUMBER(S)			
6a NAME OF PERFORMING ORGANIZATION Naval Weapons Center	6b OFFICE SYMBOL (If Applicable)	7a NAME OF MONITORING ORGANIZATION			
6c ADDRESS (*City, State, and ZIP Code*) China Lake, CA 93555-6001		7b ADDRESS (*City, State, and ZIP Code*)			
8a NAME OF FUNDING/SPONSORING ORGANIZATION	8b OFFICE SYMBOL (If Applicable)	9 PROCUREMENT INSTRUMENT IDENTIFICATION NUMBER			
8c ADDRESS (*City, State, and ZIP Code*)		10 SOURCE OF FUNDING NUMBERS			
		PROGRAM ELEMENT NO.	PROJECT NO.	TASK NO.	WORK UNIT NO.

11 TITLE (*Include Security Classification*)

RESOLVE PROJECT FINAL REPORT, Visibility Conditions and Causes of Visibility Degradation in the Mojave Desert of California

12 PERSONAL AUTHOR(S)

Trijonis, McGown, Pitchford, Blumenthal, Roberts, White, Macias, Weiss, Waggoner, Watson. Chow. Flocchini

13a TYPE OF REPORT Final	13b TIME COVERED From 1983 To 1986	14. DATE OF REPORT (*Year, Month, Day*) 1988, July	15. PAGE COUNT 182

16 SUPPLEMENTARY NOTATION

17 COSATI CODES			18. SUBJECT TERMS (*Continue on reverse side if necessary and identify by block number*)
FIELD	GROUP	SUB-GROUP	Degradation, visibility, aerosol mass, extinction, emission, variations, air particles, particulate matter, nitrates, organic

19 ABSTRACT (*Continue on reverse side if necessary and identify by block number*)

(U) The Department of Defense has been conducting an extensive air-quality study called RESOLVE (Research On Operations Limiting Visual Extinction). The RESOLVE study is part of a DOD program to protect flight and test operations in the Mojave Desert of California from adverse impacts caused by degraded visibility. Historically, the Mojave Desert in Southern California has represented an ideal region for test and training operations because of excellent visibility, dependably good weather, and large areas of unused land and airspace. Since the 1940s a decrease in visibility in the airspace has been occurring and DOD is concerned about potential adverse effects on operations from further declines in visibility. Highlighted in this study are the major conclusions that pertain directly to the two RESOLVE objectives: documenting baseline visibility conditions in the study region and characterizing the causes and source areas of visibility degradation.

20 DISTRIBUTION/AVAILABILITY OF ABSTRACT ☐ UNCLASSIFIED/UNLIMITED ☒ SAME AS RPT. ☐ DTIC USERS	21 ABSTRACT SECURITY CLASSIFICATION UNCLASSIFIED	
22a NAME OF RESPONSIBLE INDIVIDUAL J. O'Gara	22b TELEPHONE (*Include Area Code*) (619) 939-3411 x378	22c. OFFICE SYMBOL Code 266

DD FORM 1473, 84 MAR   83 APR edition may be used until exhausted
All other editions are obsolete

CONTENTS

1.0 INTRODUCTION

For several years, the Department of Defense (DOD) has been conducting an extensive air-quality study in the Mojave Desert of California. This study, called RESOLVE (Research On Operations Limiting Visual Extinction), is part of a DOD program to protect flight and test operations in the desert from adverse impacts caused by degraded visibility. Within the overall program to protect operations, the purpose of RESOLVE is to provide a fundamental understanding of visibility conditions and visibility-related atmospheric processes. The two major objectives of RESOLVE are (1) to document baseline visibility conditions in the study region and (2) to characterize the causes and source areas of visibility degradation.

The RESOLVE study was carried out in three overlapping phases: design, data collection, and data analysis. The design and planning phase took a year and a half (1983 to mid-1984), although additions and modifications to the plan occurred throughout the course of the study. The data-collection phase included routine monitoring from August 1983 through August 1985 at seven locations, plus various special field experiments carried out intermittently from 1984 through 1986. Midcourse, online data analysis was begun in late 1984 and was concluded a year later. This document is the culmination of the data analysis effort.

1.1 BACKGROUND

Historically, the Mojave Desert in Southern California has represented an ideal region for DOD test and training operations because of excellent visibility, dependably good weather, and large areas of unused land and airspace. Because of these advantages, DOD located a number of major facilities in the region (designated the R-2508 airspace) shown in Figure 1. The DOD facilities include Edwards and George Air Force Bases, the Naval Weapons Center (NWC), and Fort Irwin Army National Training Center (FINTC). Together, these facilities employ approximately 37,000 people with a budget of 1.5 billion dollars per year.

Since the mid-1940s, when the facilities were established, a decrease in visibility in the R-2508 airspace has been occurring. Sometimes visibility degradation is now severe enough to adversely affect the optical data for certain tests or to force changes in operational procedures. Visibility conditions are still generally adequate for the types of test and training activities conducted at the facilities. However, DOD is concerned about potential adverse effects on operations from further declines in visibility.

The Joint Policy Planning Board (JPPB) of DOD has the goal of developing a management strategy to maintain and optimize the operational capabilities of the test facilities. In addressing this goal, JPPB initiated studies and discussions of the visibility issue, which, in turn, have led to the formation of a DOD Visibility Protection Program (VPP). The VPP consists of four parts: (1) a project to evaluate the operational impacts of visibility impairment at the DOD facilites, (2) the RESOLVE study to document baseline visibility and characterize sources of visibility impairment, (3) a long-term monitoring network to measure future visibility trends and associated causes, and (4) a policy
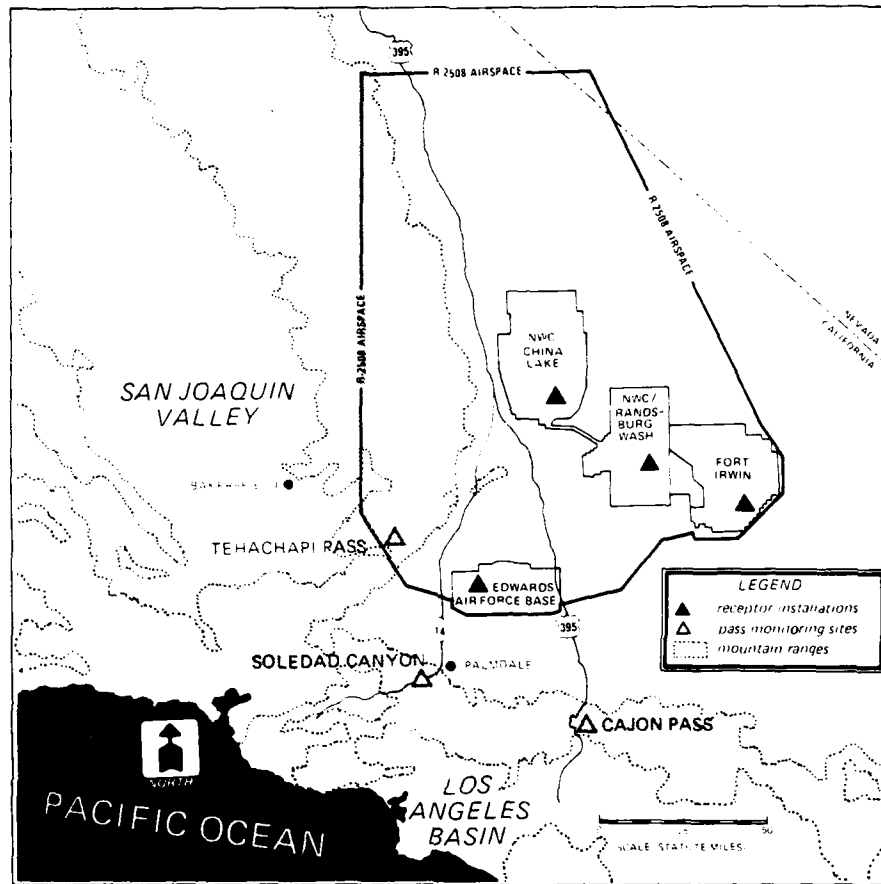
FIGURE 1. RESOLVE Study Area Monitoring Sites.

planning study to identify the best strategies for protecting operations. As noted, this report presents the results of the second part of the program—the RESOLVE visibility study.

Several publications have been issued as part of the RESOLVE program. The most significant are a protocol for the monitoring program (Reference 1), a data analysis plan (Reference 2), a design evaluation based on historical data and error analysis (Reference 3), a quality assurance paper (Reference 4), and annual/quarterly data summary reports (References 5 and 6). The monitoring program protocol (Reference 1) is particularly important because it explains the assumptions, design considerations, and plans behind RESOLVE.

1.2 STUDY PHILOSOPHY

The RESOLVE program interests many organizations, among which are potential conflicts. In addition to DOD, numerous Federal and state agencies are concerned. Some of these are the U.S. Environmental Protection Agency (EPA), the National Park Service (NPS), the Forest Service (FS), the Bureau of Land Management (BLM), the California Air Resources Board (CARB), the Department of Forestry, the Department of Food and Agriculture, and the Energy Commission. Interested parties also include industry,

agriculture, utilities, developers, and local and county governments in the Mojave Desert and in the upwind air basins. The two upwind regions of most concern are the Los Angeles basin (the South Coast Air Basin of California) and the San Joaquin Valley.

Because of the potential for conflicts, a statement about study philosophy is included here. To deal effectively with visibility as a resource, DOD needs to develop an understanding of visual air quality that is not only comprehensive but also accurate. If the results of RESOLVE are biased in any way, DOD will be hampered in its management effort. In other words, DOD has a vested interest in not wrongly implicating any one type of pollutant or any one source area. In designing the RESOLVE program, conducting the monitoring, and analyzing the data, the basic philosophy has always been to seek the best possible, unbiased scientific results.

To achieve the best possible technical results from RESOLVE, DOD gathered input from other interested parties. One area where other organizations have given assistance is in research support. Western Oil and Gas Association (WOGA) sponsored four important projects in support of RESOLVE: (1) high-sensitivity X-ray fluorescence (XRF) analysis of RESOLVE particle filters, (2) a study of organic particle origins, (3) a heated/ambient nephelometer experiment, and (4) a data-base documentation effort. The Las Vegas EPA Laboratory contributed personnel, computer time, and equipment that went well above the requirements of the RESOLVE Interagency Agreement between EPA and DOD.

The second major area of input was in the review process. To keep other parties abreast of RESOLVE, DOD members participated in SCENES (Subregional Cooperative Electric Utility, Department of Defense, National Park Service, Environmental Protection Agency Study) and CDAWG (California Desert Air Working Group). The RESOLVE program plan (Reference 1) and data analysis plan (Reference 2) were widely disseminated among interested parties and publicly presented at workshops. These plans were significantly modified based on resulting comments. Interim products from the study (e.g., data summaries and research papers) were also subject to public scrutiny. This final report has undergone a similar process of review and modification.

An idea that was highlighted in the review of the program protocol was the need to quantify uncertainties. This idea was made a part of the RESOLVE approach and, in fact, comprehensive treatment of uncertainties is one of the unique features of RESOLVE. The precisions of the data sets have been documented, and key policy results (e.g., causes and source areas of visiblity degradation) have been subjected to error analyses. All the uncertainties are specified as single standard errors.

1.3 TERMINOLOGY AND BASIC CONCEPTS OF VISIBILITY

The air quality issue of interest in this study is atmospheric visibility. Visibility can be defined quantitatively in terms of contrast (the relative brightness of various features in a scene), discoloration (shifts in the wavelength distribution of light produced by the atmosphere), visual range (the farthest distance that an observer is able to distinguish a large black object against the horizon sky), and extinction coefficient (the fraction of light that is attenuated per unit distance as a light beam traverses the atmosphere). As illustrated in the following paragraphs, these visibility indices are all interrelated.

Among the four visibility indices, extinction coefficient is most directly related to the composition of the atmosphere. Visibility through the atmosphere is restricted by the scattering and absorption of light by both gases and particles. The extinction coefficient, "B"

in conventional units of Mm^{-1}, is simply the sum of those four components, $B = Bsg + Bag + Bsp + Bap$. Here,

Bsg = light scattering by air molecules (Rayleigh or natural blue-sky scatter). This term is on the order of 10 to 12 Mm^{-1}, depending on altitude.

Bag = light absorption by gases. Nitrogen dioxide (NO_2) is the only common gaseous species that significantly absorbs light.

Bsp = light scattering by particles. This term is usually dominated by fine particles because scattering efficiency per unit particle mass exhibits a pronounced peak in the size range of 0.1 to 1.0 micrometers.

Bap = light absorption by particles. This term arises nearly entirely from elemental carbon (soot) particles.

Once the extinction coefficient and the properties of a scene have been fully characterized, the other three indices of visibility can be calculated in a straightforward manner. For example, in a uniform atmosphere, visual range (V) and extinction coefficient are related by the simple Koschmeider formula, $V = k/B$, where k is a constant that depends on the contrast detection threshold of the observer. A "standard" observer is defined as one with a 2% contrast threshold; in this case, $k = 3.9$.

Because extinction coefficient is directly related to atmospheric composition, and because other visibility indices can be calculated from extinction coefficient, the visibility results in this report are presented in terms of extinction coefficient (or its simple inverse, standard visual range). In some cases, we report specific measured components of extinction, such as nephelometer particle scattering (Bscat). Note, however, that Bscat is not exactly equal to real particle scattering (Bsp) because of measurement limitations of the nephelometer. As explained in Section 3.3 of this report, adjustments are made for measurement biases when calculating extinction coefficient or visual range.

Recognizing that Rayleigh scatter by air molecules is purely natural and basically constant, some of the analyses herein focus on non-Rayleigh extinction, rather than total extinction (or visual range). Essentially all of non-Rayleigh extinction in the RESOLVE area comes from atmospheric particles (gaseous NO_2 is found to contribute only about 3% on the average). Furthermore, although coarse-particle extinction is not negligible, fine particles (≤ 2.5 micrometers in diameter) usually dominate non-Rayleigh extinction. Because of these reasons, and because the size and chemical composition of particles reflect their origin, many of the analyses in this report revolve around the mass, size (fine versus coarse), and chemical composition of ambient particles.

With respect to chemical composition, in most areas only five types of species account for essentially all of particle mass and associated light extinction. These five types are organics, sulfates, nitrates, elemental carbon, and soil dust. Formulas for calculating the mass of these species from the RESOLVE data are given later in the text.

1.4 SUMMARY OF MAJOR CONCLUSIONS

We highlight here the major conclusions that pertain directly to the two RESOLVE objectives: documenting baseline visibility conditions in the study region and characterizing the causes and source areas of visibility degradation.

Baseline Visibility Conditions

- For average extinction levels, visual range at NWC is 89 kilometers (55 miles). Worst tenth-percentile days have a visual range of 59 kilometers, with the best tenth-percentile days at 143 kilometers. Edwards AFB averages about 15% worse than NWC, while Fort Irwin NTC averages about 15% better. Edwards AFB experiences especially severe worst-case days, while Fort Irwin NTC has especially clear best-case days.

- A map was prepared illustrating the geographical pattern of visibility within the study region (Figure 2). This map should provide a reasonable estimate of average visibility at any point of interest in the study region.

- From lowest visibility to highest visibility, the ranking of the calendar quarters is Jul.-Sep., Apr.-Jun., Oct.-Dec., and Jan.-Mar. The summer quarter average for total extinction is one and a half times the winter extinction average. The seasonal pattern for worst-case conditions is similar to, but not as pronounced as, the seasonal pattern for average conditions.

- At the desert receptor locations, visibility tends to be lowest just before midnight and highest in the early afternoon. The daytime (0800 to 1600) average for light extinction is about 10% lower than the 24-hour average.

Causes and Sources of Visibility Degradation

- Averaged over the three receptor sites, the allocation of visibility degradation by species is as follows: organics 26% ± 9%; sulfates 24% ± 5%; elemental carbon 19% ± 6%; soil dust 18% ± 8%; and nitrates plus NO_2 13% ± 5%. The extinction budget shows some minor variations from site to site. The main seasonal variation occurs for the nitrates plus NO_2 percentage, which becomes as large as the other categories in the winter, but which is especially small in the summer. The extinction budget for worst-case days is almost identical to the one for average conditions.

- Various analyses indicate that organics sulfates, elemental carbon, and nitrates plus NO_2 are dominated by man-made sources from upwind air basins. Estimates indicate that slightly over three-fourths of non-Rayleigh extinction is from anthropogenic sources.

- On the average, the single most significant source of visibility degradation in the study region appears to be anthropogenic transport from the San Joaquin Valley, accounting for about one-half (maybe somewhat more) of non-Rayleigh extinction. In the northern majority of the study region (NWC), the remainder of non-Rayleigh extinction comes from natural sources. Along the southern edge of the study region, contributions from Los Angeles and local and natural sources are significant. For the worst-case days at Edwards AFB and Fort Irwin NTC, transport from the Los Angeles basin appears to be more important than it is for average contributions.

- Three individual source categories contribute significantly to man-made extinction in the RESOLVE region: diesel vehicles and equipment, the petroleum industry, and gasoline vehicles. Together, these sources account for about 60% of anthropogenic extinction, with the diesel category alone contributing about one-quarter of man-made extinction. No other source categories individually account for more than 5% of man-made extinction in the region as a whole.

FIGURE 2. Spatial Pattern of Visual Range (for 2% Contrast and Average Extinction Levels) In and Near the RESOLVE Study Area.

NOTES:

- Circled data points represent RESOLVE monitoring data. The entire 2 years of RESOLVE data were used, with nephelometer scattering factored to non-Rayleigh extinction using site-specific RESOLVE base-year relationships and 11 Mm⁻¹ added for Rayleigh scatter.
- Smaller print data points are based on particle-scattering data in and near Searles Valley. The data are factored to total extinction using RESOLVE relationships.
- Other data points are based on median airport data calibrated to RESOLVE data.
- The dashed lines indicate uncertainty in the isopleths near Searles Valley.
- Isopleths near the border of the map are guided by nephelometer data at Death Valley as well as data from other airports in California and Nevada.
- The Beaumont (Banning Pass) value, shown in parentheses, is inconsistent (higher) than surrounding stations. This inconsistency may be because of the high altitude of that site (790 meters) or because of uncertainties associated with the limited visibility markers at that site.
- The following abbreviations are used in this figure for the stations: Edwards AFB, EDW; NWC, CHL; Fort Irwin NTC, FOR; Soledad Pass, SOL; Cajon Pass, CAP; Tehachapi Pass, TEH; and Randsburg Wash, RAW

2.0 MONITORING AND DATA OVERVIEW

2.1 MONITORING DESIGN CONSIDERATIONS

Most of the military operations sensitive to visibility occur in the southern half of the R-2508 restricted airspace (see Figure 1). Aircraft measurements in the region show that visibility degradation is primarily confined to the lower troposphere below the level of the maximum afternoon mixing heights, i.e., less than about 3,000 meters mean sea level (MSL) altitude* (References 7 and 8). Thus, the RESOLVE monitoring program was focused within the mixing layer in the southern R-2508 region.

In designing the RESOLVE monitoring network, the results of prior aerometric studies in the region were reviewed and critical aspects of the design were evaluated using historical data and error analysis (Reference 3). Based on this review and evaluation, several assumptions were made in formulating the monitoring program. These assumptions were subsequently reassessed during RESOLVE through data analyses and special measurements. Some of the critical assumptions affecting the program design were as follows:

- It was assumed that particulate matter, not NO_2, is the dominant contributor to non-Rayleigh extinction in the study region (Reference 3). It was further understood that, although fine particles should dominate non-Rayleigh extinction, coarse particle contributions would not be negligible (References 9 and 10). The major aerosol constituents of interest should include organics, sulfates, elemental carbon, soil dust, and nitrates (References 10 and 11).

- It was assumed that the visibility degrading aerosol in the Mojave Desert would include contributions from the Los Angeles urban area (References 7, 12, and 13); the San Joaquin Valley (References 14 and 15); wind-blown dust from desert sources (References 16 and 10); and, on a localized basis, certain industrial complexes, urban areas, and roads in the desert.

- Since, at least under some circumstances, the aerosol species from the Los Angeles basin and the San Joaquin Valley should have different chemical compositions, it was assumed that a combination of chemically resolved particle data (from both source and receptor regions) and meteorological data would help to distinguish aerosols from the Los Angeles basin from those originating in the San Joaquin Valley.

- Because of high correlations between daytime and 24-hour particle averages, because of the similarity between daytime and 24-hour particle composition, and because of some military interest in nighttime as well as daytime visibility, it was assumed that 24-hour particle samples (used in conjunction with continuous nephelometer data) would be appropriate for characterizing the nature and scope of the visibility-reducing aerosol (Reference 3). Particulate data on a 24-hour basis (rather than on an 8-hour basis) should also provide greater measurement precision with less operational difficulties and smaller expenses.

- Based on the results of preliminary error analysis (Reference 3), it was understood that the monitoring program should minimize measurement uncertainties, maximize the number of sampling cases, and provide documentation on precision and accuracy.

---

* All references to altitude in this report refer to height above sea level.

2.2 ROUTINE MONITORING NETWORK

The routine RESOLVE monitoring network, operated from August 1983 through August 1985, included continuous measurements of light scattering, contrast, and meteorological parameters as well as daily particle sampling. Monitoring was conducted at three important receptor sites in the desert (Edwards AFB, NWC at China Lake, and Fort Irwin NTC); three pass sites leading into the desert (Soledad, Cajon, and Tehachapi); and Randsburg Wash, part of NWC. Refer to Figure 1 for the location of the RESOLVE network. Note that the following abbreviations will sometimes be used herein for the stations: Edwards AFB, EDW; NWC, CHL; Fort Irwin NTC, FOR; Soledad Pass, SOL; Cajon Pass, CAP; Tehachapi Pass, TEH; and Randsburg Wash, RAW.

The monitoring equipment operated at each site is listed in Table 1. The measurements at all sites included continuous light scattering coefficient, continuous meteorological parameters, and daily collection of fine (< 2.5 micrometers) and total (< 10 micrometers) particle filter samples. In addition, contrast measurements and/or photographs were obtained at the receptor sites. Radiosonde measurements of wind, temperature, and relative humidity were made on most days at both Edwards AFB and NWC by DOD; and National Weather Service (NWS) synoptic weather data were acquired for all study days.

TABLE 1. RESOLVE Monitoring Stations and Equipment.

Equipment	Monitoring stations							
	EDW	CHL	FOR	RAW	TEH	SOL	CAP	Total
VISIBILITY								
Nephelometer (continuous)	1	1	1	1	1	1	1	7
Teleradiometer (hourly)	2	1	3					6
Camera	2	1	3	1				7
AEROSOL								
RESOLVE 2x4 sampler[a] (24-hour)	1	1	1	1	1	1	1	7
DRUM[b] particle sampler (4-hour)	1	1			1	1		4
METEOROLOGY								
Wind speed/direction and temperature	1	1	1	1	1	1	1	7
Dewpoint	1	1	1	1				4
Relative humidity					1	1	1	3
Radiosonde (upper air wind, temperature, and RH)	1[c]	1[c]						2
DATA RECORDING								
Satellite data system	1	1	1	1	1	1	1	7
Cassette tape data system	1	1	1	1				4
Strip chart recorders	1	1	1	1	1	1	1	7

[a] 2x4 refers to collection in two size ranges of a total of four simultaneous samples (1 total, d < 10 micrometers; 3 fine, d < 2.5 micrometers.
[b] Multistage rotating DRUM impactor. These samplers were usually at the sites indicated, but were occasionally moved between sites.
[c] Not co-located with monitoring site. Operated by DOD personnel.

The fine and total particle measurements at all sites were made using the RESOLVE 2x4 sampler, which acquired one total and three fine filter samples. The 2x4 samplers were operated on a 24-hour basis (midnight to midnight*) each day. The total filter and two of the fine filters were made of Teflon and provided data on mass, absorption, and elemental composition. The second fine Teflon filter served as a data quality check and as a means to document precision. The third fine particle filter, composed of quartz, was used for elemental and organic carbon determination. In addition, five Davis Rotating Universal Multistage (DRUM) impactor samplers were operated at various sites during the program. The DRUM samplers obtained size-segregated samples for elemental analysis by proton-induced X-ray emission (PIXE) with a time resolution of 4 hours. These samplers are described in more detail in other RESOLVE reports (References 3 and 4).

For each site/day, all three Teflon filters (one total and two fine) were analyzed for particle mass and light absorption. For every third day at the receptor sites, for every sixth and twelfth day at the other sites, and for selected other days, one fine Teflon filter was analyzed for elemental composition by PIXE and high-sensitivity XRF, and the fine quartz filter was analyzed for organic and elemental carbon. The substrates and types and frequency of analyses for the 2x4 samples at the various sites are summarized in Table 2.

The existence of both PIXE and XRF data for some elements raised the question as to what values to use in the data analysis. Table 3 lists the measured elements and the percent of values above the detection thresholds for both methods. For each element, we chose to use the values from the method that had the lower detection threshold for that element (i.e., the method with the higher percentage in Table 3).

Extensive quality-control procedures were developed and documented for all measurements, and quality-assurance audits were performed semiannually at all sites by a contractor (References 4 and 17). To document the performance of the 2x4 particle samplers, the seven RESOLVE samplers were operated side-by-side in a comparison test with two virtual impactors (Sierra Instruments Model 244) at EPA in Las Vegas, Nev. (Reference 18). The 2x4 sampler was also included in another comparison test at Reno, Nev., using various samplers involved in the SCENES program (Reference 19). In addition, the 2x4 sampler was designed so that one fine filter was redundant. Accordingly, the quality of the data could be checked and the internal precision of the sampler could be assessed by comparing the mass and absorption measurements on the simultaneously collected filters.

2.3 MONITORING SCHEDULE AND DATA RECOVERY

Figure 3 illustrates the period covered by the RESOLVE monitoring program. The RESOLVE network operated from August 1983 through August 1985. Because of initial difficulties with the 2x4 samplers, however, the 2x4 samplers were not deployed until April, May, or June 1984, depending on the site. Thus, the daily particle sampling encompasses about 15 to 17 months of the 2-year program.

As shown in Figure 3, the period July 1984 through June 1985 is designated as the "RESOLVE base year." This period consists of the 4 calendar quarters when the particle samplers were fully operational. To avoid seasonal biases, many of the analyses reported

---

* All references to hours in this report refer to Pacific Standard Time.

TABLE 2. RESOLVE 2x4 Sampler Filter Analyses.

2x4 filter number	Size of particles on filter, μm	Gravimetric mass	PIXE,[a] OAT,[b] XRF[c]	Carbon[d]	Quality control and special studies
NWC, Edwards AFB, Fort Irwin NTC					
1 Total Teflon	<10	All filters	Every third filter (day) plus ~40 additional filters per site.[e]		
2 Fine Teflon	<2.5	All filters	Every third filter (day) plus ~40 additional filters per site.[e]		Selected filters
3 Fine Teflon	<2.5	All filters			
4 Fine quartz	<2.5			Every third filter (day) plus ~40 additional filters per site.[e]	Selected filters
Tehachapi, Soledad Pass, Cajon Pass, Randsburg Wash					
1 Total Teflon	<10	All filters	Routine plus ~40 additional filters per site.[e]		
2 Fine Teflon	<2.5	All filters	Routine plus ~40 additional filters per site.[e]		Selected filters
3 Fine Teflon	<2.5	All filters			
4 Fine quartz	<2.5			Routine plus ~40 additional filters per site.[e]	Selected filters

[a] PIXE - Elemental analysis by proton-induced X-ray emission technique.
[b] OAT - Light absorption and elemental carbon by optical absorption technique.
[c] XRF - special sensitivity X-ray fluorescence; performed on fine filters only.
[d] Organic, elemental, and total.
[e] Selected based on the results of the routine analyses.

TABLE 3. Percent of XRF and PIXE Data
Above Detection Thresholds.

Chemical	XRF	PIXE
Si	---	99.6
Al	---	89.4
Na	---	82.0
Mg	---	44.5
P	---	39.2
Au	---	5.1
Pt	---	.9
Ru	---	.6
S	100.0	100.0
Fe	99.7	99.3
Ca	99.6	99.0
K	100.0	98.4
Zn	100.0	80.7
Pb	99.9	72.2
Ti	85.6	72.3
Br	100.0	54.2
Cu	96.6	54.5
Ni	95.8	52.4
Mn	91.7	43.1
V	81.8	53.0
Cr	77.2	40.0
Sr	97.4	2.1
Se	93.9	3.3
Rb	93.6	.9
Cl	37.4	38.8
Hg	33.1	.6
Cd	8.3	.5
Pd	3.7	.6
As	1.8	1.4
Ag	2.4	.5
Sn	2.0	.2
Ba	1.2	.3
Mo	.7	.8
Zr	.4	.6
Y	76.7	---
Ga	10.8	---
In	1.2	---
Sb	1.0	---
La	.8	---
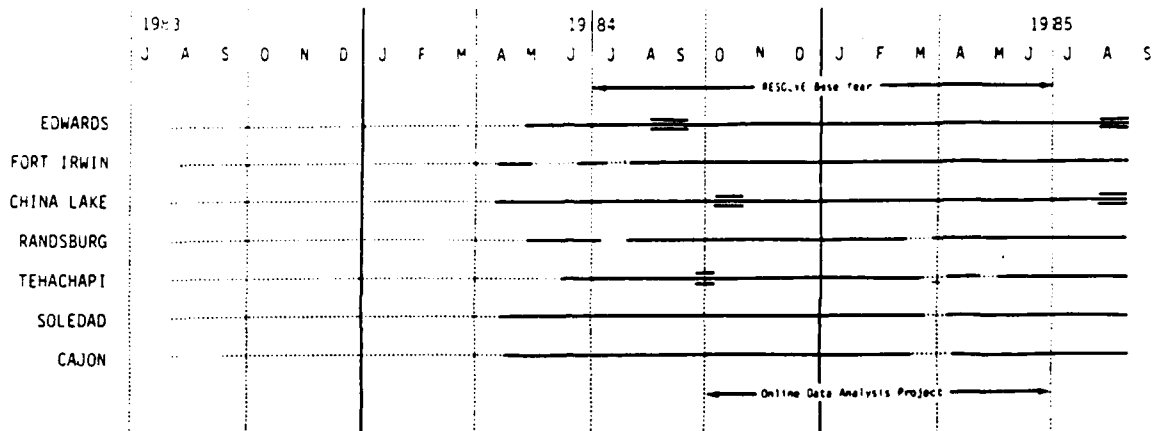
NOTES:
- Operation without 2x4 particle sampler = ...
- Operation with 2x4 particle sampler = _____
- Special study experiments = ≡
- In addition to the special study experiments indicated above, a heated/ambient nephelometer study was conducted at Edwards AFB and NWC from November 1984 to August 1985, an insulated nephelometer study was conducted at Edwards AFB during the fall/winter of 1985-86 and summer of 1986, a winter nitrate study was conducted at Edwards AFB and NWC in January-February 1986, and an organic origins study was conducted at Edwards AFB and NWC in the winter and summer of 1986.
- Chart includes all data gaps exceeding 7 days.
- Absorption measurements are missing for November-December 1984 at all sites and also for January 1985 at NWC.

FIGURE 3. RESOLVE Monitoring Schedule.

herein are restricted to data from the RESOLVE base year. When seasonal biases are unimportant, or when the biases can be easily discounted, the analysis is conducted for the entire 15- to 17-month program, or for the entire 2 years of the program.

Figure 3 also illustrates all significant data gaps that occurred during the monitoring program. The two most noteworthy data gaps were

1. In late March 1985, the 2x4 samplers were inoperative for about 1 to 3 weeks (depending on the site) because of a temporary disruption in the supply of Teflon filters.

2. Absorption measurements were missing during November and December 1984 because the quality assurance program detected unreliable blank values for that period caused by a deteriorating laboratory instrument.

No serious consequences developed from either data gap because the RESOLVE data set consists of a large number of measurements and the gaps did not represent a critical fraction of the data.*

---

* The one data gap with potentially serious consequences was the missing absorption data set that might have introduced a significant seasonal bias. However, we tested our major findings using explicit seasonal adjustments and found that the effect of the missing absorption data on our conclusions was negligible.

The period for the Online Data Analysis Project is indicated on Figure ꞈelow the last entry on the chart. The purpose of the Online Data Analysis Project was to analyze the incoming data and recommend midcourse correction to the program—extensions to the routine monitoring and additions to the special intensive studies. As it turned out, the Online Data Analysis Project was critical to the successful completion of the RESOLVE program (see further discussion in Section 2.4).

Figure 4 illustrates the completeness of the data for daily averages. We chose to define a daily average as valid or nonmissing if the instrument operated for at least two-thirds of the day. Figure 4 shows percent completeness on a monthly basis for the 2x4 samplers, meteorological sensors, nephelometers, and teleradiometers. With the exception of start-up months and the March 1985 gap for the 2x4 sampler, the monthly data recovery always exceeded 80% and usually exceeded 90% for all four types of instrumentation. Considering the entire period after instrument start-up, the average fractions of daily data recovery were as follows:

2x4 samplers	90%
meterological data	95%
nephelometers	92%
teleradiometers	95%

For the continuous monitors, if we examine data completeness on an hourly basis rather than a daily average basis, the fractions of data recovery were as follows:

meteorological data	95%
nephelometers	95%
teleradiometers	95%

Note the size of the routine RESOLVE data set with respect to the number of recorded observations. For the 2 years of continuous monitoring, about 115,000 hourly nephelometer averages, 463,000 meteorological data points (114,000 to 117,000 each for four meteorological variables), and 32,000 teleradiometer observations were recorded. For the 16-month period of particle sampling, approximately 3100 site-days, when three Teflon filters and one quartz filter were exposed in the 2x4 samplers, led to about 9000 filter mass measurements and 8000 absorption measurements. Analyses by PIXE, high-sensitivity XRF, and the carbon technique were performed on about 800 of the 3100 site-days with particle sampling.

2.4 SPECIAL STUDIES

Although the routine monitoring network provides most of the data needed to attain the RESOLVE objectives, the network does not provide all of the measurements required for the program goals. The remainder of the requisite information is furnished by intensive field experiments and other special studies carried out for limited time periods and/or at a limited number of sites. In the planning work for RESOLVE, the decision as to whether a certain measurement should be done routinely or as part of a special study was based on an evaluation of the trade-offs between the needs for complete data coverage and the costs of conducting the measurements.
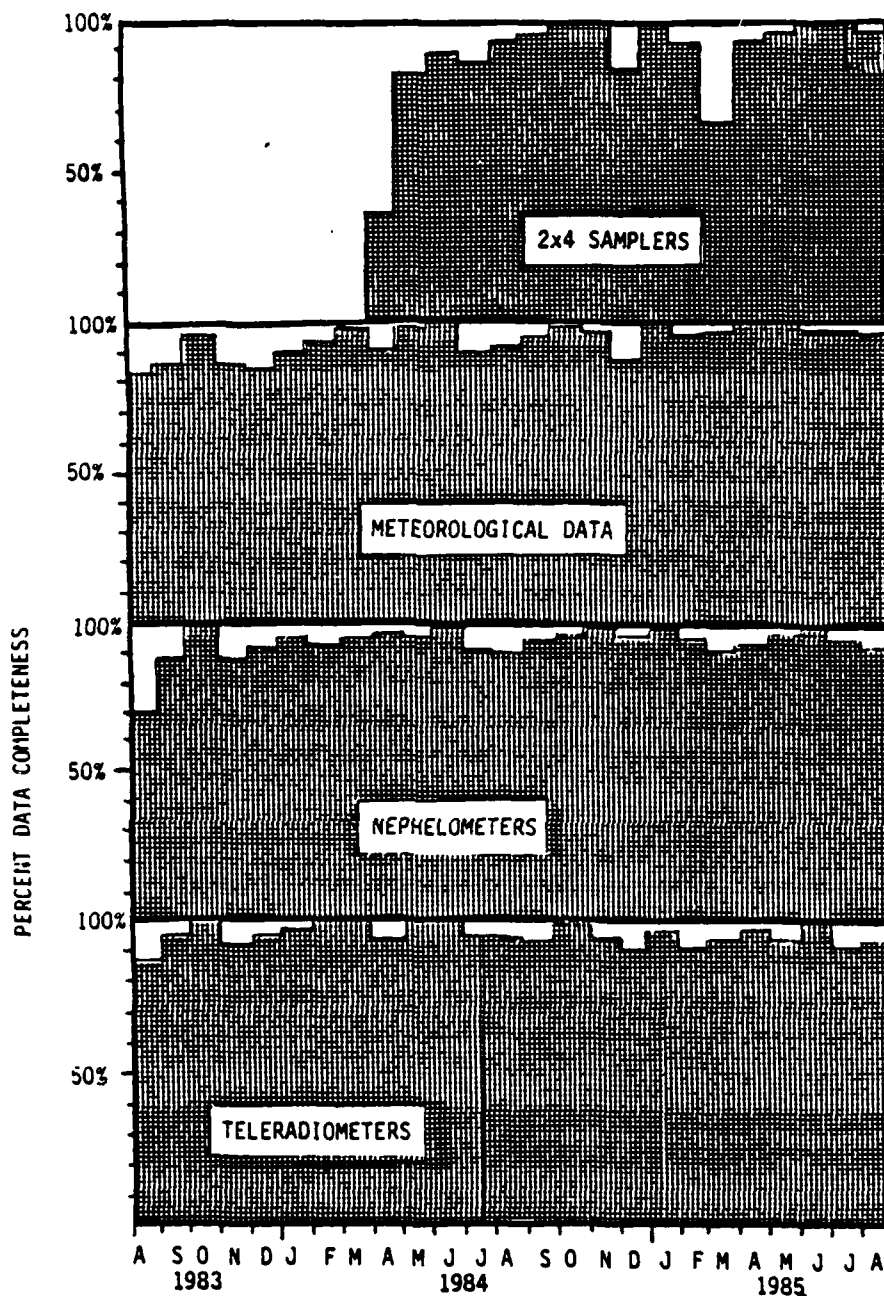
FIGURE 4. Completeness of RESOLVE Data Collection.

Some of the special studies (Organic Origins, Insulated Nephelometer, Local Emission Inventory, Nuclepore Filter Data) were not formulated until the majority of the routine monitoring was completed. The need for these studies was identified by the Online Data Analysis Project carried out from late 1984 through the middle of 1985. The Online Data Analysis Project also led to midcourse adjustments in the routine monitoring program (e.g., a time extension from April 1985 to August 1985, and the addition of high-sensitivity XRF analysis for the Teflon filters).

The RESOLVE special studies are briefly described in the following paragraphs. The descriptions cover when, where, and why the studies were performed as well as how the data are used in this report. All of the field experiments except for the Organic Origins Study were carried out by Alan Waggoner and Raymond Weiss. The last two studies deal with literature reviews of emission-type data rather than field measurements. The Organic Origins and Heated/Ambient Nephelometer Studies, plus the high-sensitivity XRF analysis in the routine program, were funded by WOGA as research contributions in support of RESOLVE.

High-Sensitivity NO_2

In the summer of 1984, a high-sensitivity instrument was used to measure NO_2 concentrations at Edwards AFB, NWC, and Tehachapi. These measurements, along with data from other previous studies, provided information on the contribution of NO_2 absorption to the light extinction budget (see Section 7.2.1).

True Particulate Nitrate

During the summers of 1984 and 1985 and the winter of 1986, particulate nitrate concentrations at Edwards AFB and NWC were measured using a nylon filter preceded by a nitric-acid denuder. These data were used to estimate nitrate contributions to the light extinction budget (see Section 7.2.3) and to investigate the role of nitrate in the aerosol mass balance (see Section 3.3).

Thermidograph Nephelometer

A cyclone (fine particle) nephelometer that heated atmospheric samples to 350°C was deployed at Edwards AFB in the summer of 1984. This instrument indicated what fraction of fine particle scattering was caused by refractory materials as opposed to evaporable compounds. The data provided an important check on the allocation of fine-particle light scattering among aerosol components (see Section 7.2.3).

Cyclone Nephelometer

During the summers of 1984 and 1985, a nephelometer with an on-off cyclone to eliminate coarse particles was operated at Edwards AFB and NWC. The data from this experiment were used to estimate the contribution of coarse-particle scattering to the light extinction budget (see Section 7.2.3) and to evaluate the accuracy of the nephelometer as a measure of total particle scattering (see Section 3.2.2).

Organic Origins

During the winter and summer of 1986, organic particle samples were collected on an episodic basis at Edwards AFB and NWC under a WOGA contract to Global Geochemistry Corp. These samples were analyzed with respect to carbon-12/carbon-14 isotope ratios and with respect to molecular composition. The results provided information on the origin of the organic aerosol in terms of contemporary versus fossil and in terms of natural versus anthropogenic (see Section 8.1).

Coarse-Particle Carbon

Coarse-particle samples for carbon analysis were collected on quartz fiber filters at Edwards AFB in the summer of 1985. This data set was used to help determine the relative contributions of elemental carbon and soil dust to coarse-particle absorption (see Section 7.2.2).

Heated/Ambient Nephelometer

Special nephelometers were operated at Edwards AFB and NWC from November 1984 through August 1985 under a WOGA contract to Waggoner and Weiss. These nephelometers sampled air that was cycled from near-ambient temperature to an elevated temperature (+ 15°C) that would evaporate absorbed water in the aerosol. The resulting information on light scattering by water was useful in interpreting the light scattering budget (see Section 7.2.3) and in evaluating the accuracy of the routine RESOLVE nephelometers (see Section 3.2.2).

Nuclepore-Filter Data

During the summer of 1985, fine-particle samples were collected at Edwards AFB on nuclepore filters. The nuclepore filter data were used to evaluate the accuracy of the routine RESOLVE Teflon data. This accuracy evaluation was especially important with respect to the Teflon absorption measurements (see Section 3.2.2).

Insulated Nephelometer

For 9 months during the fall and winter of 1985 and 1986 and the summer of 1986, an insulated/ambient nephelometer was operated in conjunction with the routine RESOLVE nephelometer at Edwards AFB. This experiment provided information on the accuracy of the RESOLVE nephelometer relative to ambient conditions and on the precision of the nephelometer data (see Section 3.2.2 and Appendix A).

Diurnal Particle Composition

In the summer of 1985, the 2x4 samplers at Edwards AFB and NWC were operated on an 8-hour basis rather than on a 24-hour basis. Particle composition analyses were conducted on all samples over a 3-week period. The purpose of this intensive study was to investigate whether the 24-hour composition data were representative of shorter time periods (see Section 3.5).

Dust Characterization

A literature review was conducted by AeroVironment, Inc., to characterize the chemical composition of dust sources in the RESOLVE study region. The information was needed to help evaluate the origins of soil dust particles (see Section 8.1).

Local Emission Inventory

An emission inventory for sources of primary particulate matter in the RESOLVE study region was assembled by Nero and Associates, Inc. This inventory included resolution by particle size and chemical composition. The results were useful in evaluating the contributions of local desert source categories to extinction (see Section 8.4 and Appendix B)

3.0 DATA QUALITY AND REPRESENTATIVENESS

Chapter 2.0 dealt with the scope and quantity of the RESOLVE data. Chapter 3.0 focuses on the quality of the data set. Understanding the quality of the data is important in providing a sense of the amount of confidence that can be placed in the subsequent conclusions.

Several reasons account for the good quality of the RESOLVE data base: care in designing the monitoring network, especially the selection of instrumentation and the provision for a quality assurance program; attentiveness in operating and maintaining the monitoring stations; using the On-Line Data Analysis Program; examining the data set while the data were being collected; and subjecting the final data set to an intense screening process to flag erroneous or suspicious values.

3.1 DATA-SCREENING PROCEDURES

Once the RESOLVE data base was assembled, the critical air quality parameters (daily averages of nephelometer data and particle mass/absorption/carbon/PICE/XRF data) were subjected to a careful screening process to flag erroneous values. Such a screening procedure is an absolute necessity with most air-quality data sets because erroneous values do become recorded and because just a few such outliers can have a substantial effect on the data analysis results (especially those that involve least-squares methods or variance-related techniques.) However, to avoid biases produced by preconceived ideas as to what relationships or models the data should follow, the screening process was performed before starting any of the key data-analysis studies (i.e., extinction budget regressions, receptor modeling analyses, spatial/temporal descriptions, etc.).

The screening process for the RESOLVE data was facilitated and made especially purposeful by several duplications built into the monitoring system. List No. 1 in Table 4 indicates pairs of data-base parameters that were essentially duplicate measurements of the same phenomenon. Scrutinizing these duplicate measurements was the most important aspect of the screening procedure.

The screening process included the following steps to identify and flag outliers:

1. For each of the seven sites individually, special scatterplot outputs were prepared for 24 pairs of closely associated parameters. These pairs included the duplicate parameters (List No. 1 of Table 4) as well as other closely related parameters (List No. 2 of Table 4). The scatterplot outputs contained not only a routine scatter diagram of the data but a listing of the date and data values as well as markings indicating the number of standard deviations that each observation varied from a least-squares line fit to the data.

2. For each site, the scatterplot outputs were scrutinized to identify anomalous data points. When an anomaly was identified on one scatterplot, the anomaly was then circled and marked on all scatterplots pertaining to that parameter.

TABLE 4. Plots Prepared for Each Site as Part of
the Data-Screening Process.

List No. 1: Scatterplots of Duplicate Parameters
    Two alternate fine masses
    Each fine mass versus sum of chemical species (organics + sul-
        fates + elemental carbon + soil)
    Two alternate fine absorptions
    Fine absorption versus elemental carbon
    PIXE S versus XRF S
    PIXE Fe versus XRF Fe
    PIXE Ca versus XRF Ca
    PIXE K versus XRF K
    PIXE Ti versus XRF Ti
    PIXE Pb versus XRF Pb
    PIXE Zn versus XRF Zn

List No. 2: Scatterplots of Closely Related Parameters
    Total mass versus each fine mass
    Each fine mass versus Bsp
    Total mass versus Bsp
    Total absorption versus each fine absorption
    Each fine mass versus each fine absorption
    Total mass versus total absorption
    Each fine mass versus organics
    Each fine mass versus sulfur
    Each fine mass versus elemental carbon
    Bsp versus organics
    Bsp versus sulfur
    Bsp versus elemental carbon
    Organics versus elemental carbon

List No. 3: Time Series Plots of Daily Averages
    Ratio of each fine mass to Bsp
    Ratio of each fine mass to total mass
    Ratio of each fine absorption to Bsp

3. The day in question was found on three time-series plots of daily "key ratios" (see List No. 3 in Table 4; also see Figure 5 for an example). This information allowed a test to be made as to whether the anomaly occurred just for the date in question (or also for surrounding dates) and whether the anomaly occurred just at the site in question (or also for surrounding sites). In the process of checking the scatterplots of duplicate parameters, the scatterplots of other closely related parameters, and the spatial/temporal patterns in the time series plots, it often became obvious that a specific data value was actually erroneous.

4. The fourth step was to make a judgment whether the data value was erroneous and to write down the reasons for the error. A file of these reasons was assembled.

5. The last step was to label certain data values as "definitely" or "probably" erroneous and to flag them as such in the RESOLVE data archive.

The causes for the erroneous data were investigated by checking the monitoring station logs and the original data recordings. In some cases, a correctable mistake (e.g., a transcription error) was found and the flagged data point was fixed. For some cases, a likely cause was found, but no way was found to correct the data. Sometimes, no obvious cause was identified.
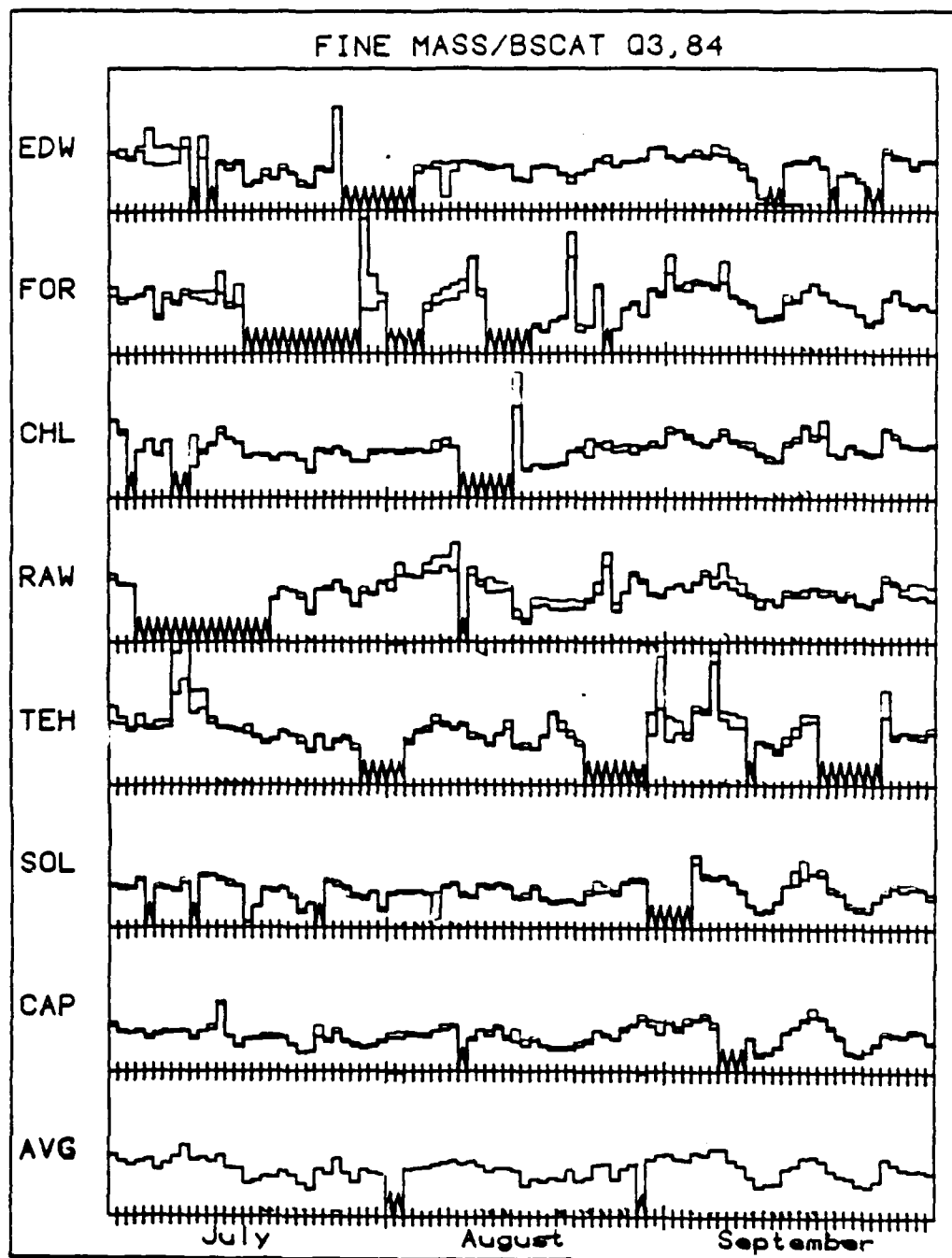
FIGURE 5. Time Series Plot For Data Screening. The two lines
for each site represent the ratio of each fine-mass channel to
nephelometer scattering.

Table 5 summarizes the amount of data points flagged by the above procedure.
Generally, about 1 to 2% of the data points were flagged for particle mass, particle
absorption, and PIXE analysis. None of the XRF data and almost none of the nephelometer
data appeared to be erroneous. About 5 to 7% of the carbon data were flagged. The thermal
separation technique for organic/elemental carbon is an evolving and uncertain approach

that has not yet been standardized and carbon measurements tend to be the least precise of all the RESOLVE data sets.

TABLE 5. Percent of Daily Average Data Flagged
By the Data Quality Screening Process.

Nephelometer Scattering	0 1
Fine-Particle Mass	2 2
Total Particle Mass	1 0
Fine-Particle Absorption	2 2
Total Particle Absorption	1 3
Fine-Organic Carbon	5 4
Fine-Elemental Carbon	6 9
PIXE Analysis	0 8
XRF Analysis	0 0

With respect to erroneous values for fine-particle mass and absorption. the flagging process produced essentially no loss in the total number of daily observations. For the data set used in this report (which excludes flagged values), the two simultaneous fine mass or absorption measurements were averaged together, but just the single valid measurement was used if the other measurement was missing or erroneous.

Figures 6, 7, and 8 illustrate some of the flagged data by showing scatterplots (for all sites combined) of the two alternative fine-mass values, the two alternative fine-absorption values, and fine-absorption versus fine-elemental carbon. The flagging procedure was not based on these scatterplots alone, but rather on an examination of all the graphic outputs listed in Table 4.
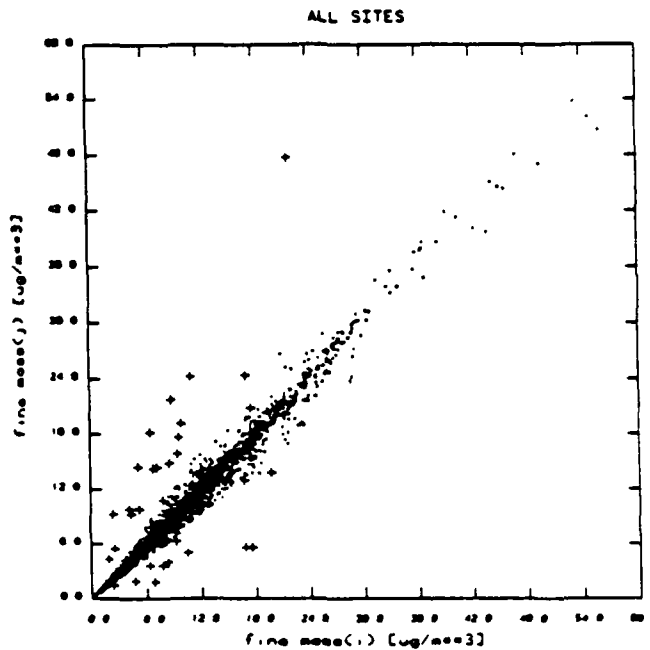

FIGURE 6. Scatterplot of Alternate Fine-Mass Channels, Showing Flagged Data (+).
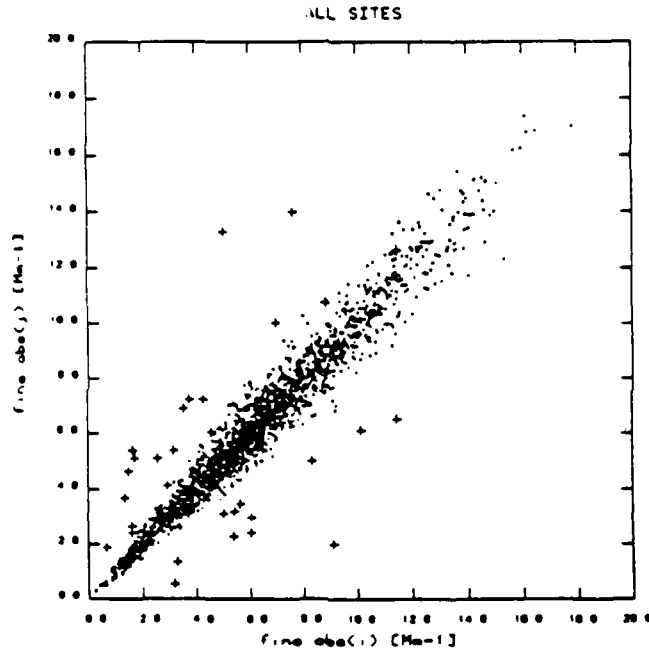
FIGURE 7. Scatterplot of Alternate Fine-Absorption Channels, Showing Flagged Data (+).
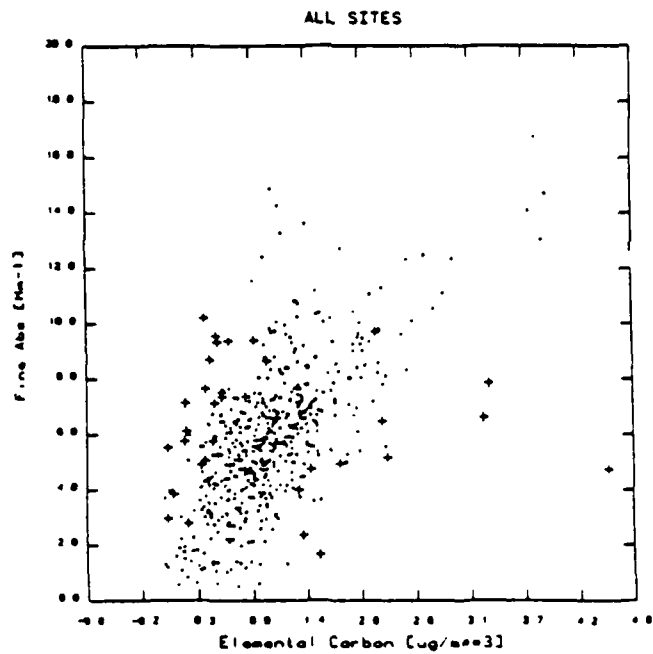
FIGURE 8. Scatterplot of Fine-Absorption Versus Fine-Elemental Carbon, Showing Flagged Data (+).

In addition to the discussed process for identifying erroneous daily averages, other screening and flagging procedures were applied to the RESOLVE data set. For example, all daily averages based on less than 16 hours of sampler operation were flagged as incomplete. Also, certain teleradiometer measurements were flagged as erroneous when extremely low (often negative) extinction coefficients resulted because of a problem with the inherent contrast values in the fall season under certain sky and cloud conditions. A brief screening process was also applied to the meteorological data set, but none of the meteorological data that had passed the initial field examination were found to be erroneous.

3.2 PRECISION AND ACCURACY

This section discusses the precision and accuracy of the RESOLVE measurements. Precision refers to the degree of reproducibility of the measurement; imprecision thus represents *random* error. Accuracy refers to the lack of a consistent bias in the measurements; inaccuracy thus represents *systematic* error.

3.2.1 Precision Estimates

Precision is defined here as ±1 standard error of measurement reproducibility. Precision can be conceptualized as the standard deviation of the data set that would occur if a particular parameter were measured simultaneously by a large number of equivalent monitors. In practice, precision is often determined by operating two equivalent monitors together over a large number of sampling periods. In the latter case, the deviation between the two monitors includes the imprecision of both, and the total deviation is thus (by simple error propagation) $\sqrt{2}$ times the individual imprecision. Thus, for the two-monitor case, precision is estimated as the standard deviation of the difference between the two monitors divided by $\sqrt{2}$.

Appendix A derives precision estimates for the critical air-quality parameters in RESOLVE–particle mass, absorption, scattering, and composition (carbon/PIXE/XRF). For particle mass and absorption, the precision is determined directly from the duplicate measurements provided by the 2x4 sampler. For the other parameters, total imprecision is estimated by error propagation techniques applied to various components of the measurement uncertainty.

Table 6 summarizes the precision results (and, for convenient reference, average parameter values at the receptor sites). The precisions for most of the key air-quality parameters are generally about 5 to 10%. The main exceptions are fine elemental carbon and coarse absorption, both of which have high relative imprecision because they are of small magnitude. For fine elemental carbon, an alternative, more precise measurement is available (fine-particle absorption). Coarse absorption is very imprecise (on a percentage basis) because it is obtained by subtraction of two parameters of relatively large magnitude. Fortunately, it is not critical to the data analysis that coarse absorption be known precisely on a daily basis.

To get a better feeling for the precision estimates, refer to the scatterplots in Figures 6, 7, and 8 (neglecting the flagged, erroneous data). The high precision of particle mass and absorption is evident in Figures 6 and 7. Figure 8 reflects the lower precision of the elemental carbon data. Figure 9 illustrates the precision of the PIXE and XRF analyses for the four elements (S, K, Ca, and Fe) that are nearly always above detection limits for both methods.

TABLE 6. Precision of RESOLVE 24-Hour Data.

Elements	Average precision[a]	Average base-year concentrations		
		Edwards AFB	NWC	Fort Irwin NTC
Scattering and Absorption				
Particle scattering	± 2%	31.2 Mm⁻¹	25.7 Mm⁻¹	20 3 Mm⁻¹
Fine-particle absorption[b]	± 5%	5.2 Mm⁻¹	5 8 Mm⁻¹	4 1 Mm⁻¹
Total particle absorption	± 7%	6.4	7 2	5.1
Coarse-particle absorption	(± 45%)[c]	1.2	1.4	1 0
Particle Mass				
Fine-particle mass[b]	± 5%	8 3 µg/m³	9.0 µg/m³	6.5 µg/m³
Total particle mass	± 5%	17.8	18.0	13 6
Coarse-particle mass	(±12%)[c]	9 5	9.0	7 1
Critical Elements (Fine)				
Fine-organic carbon	± 8%	2.1 µg/m³	1.9 µg/m³	1 1 µg/m³
Fine-elemental carbon	± 23%	54	49	42
XRF S	± 5%	51	.67	45
PIXE Si	± 10%	51	35	47
PIXE Al	± 12%	21	.14	.17
XRF Ca	± 6%	093	.073	088
XRF Fe	± 5%	.11	.082	085
XRF Mn	± 11%	.0037	.0023	0024
PIXE Mg	± 12%	.042	032	062
XRF K	± 5%	095	.078	.070
XRF Pb	± 8%	.016	.021	0094
XRF Ni	± 6%	.0028	.0032	0019
Other elements of interest[d]				
XRF V	± 25%	.0022 µg/m³	0022 µg/m³	0015 µg/m³
PIXE Cl	± 8%	.067	.034	025
PIXE Na	± 15%	.22	.19	15
XRF Zn	± 16%	.0068	.0099	0076
XRF Br	± 7%	.0043	.0051	0029

[a] Precision uncertainty represents a single standard error.

[b] Reported precision pertains to the *average* of the two fine 2x4 values (as used in the RESOLVE DATA ANALYSIS). The imprecision of a single fine channel would be greater by a factor of $\sqrt{2}$.

[c] Obtained by subtraction of fine from total.

[d] The RESOLVE special experiments for fine particulate nitrate involved just a few weeks of sampling at Edwards AFB and NWC. The data suggest annual average NO_3 concentrations of about 1.2 µg/m³ at Edwards AFB and 0.5 µg/m³ at NWC (see Section 7.3). The precision of an individual 24-hour sample is dominated by flow rate uncertainties and is estimated as ±5% (Reference 20).
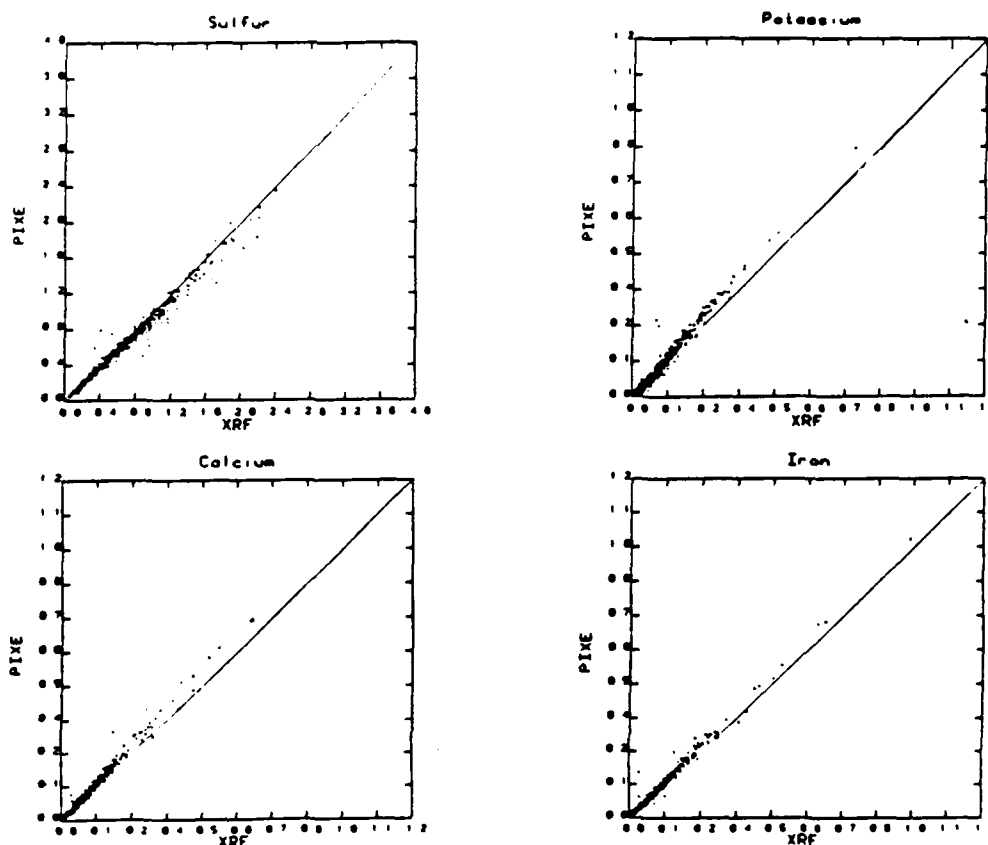
FIGURE 9. Comparison of PIXE and XRF Analyses for Four Elements (in μg/m³) That Are Highly Detectable by Both Methods.

All of the major conclusions of the data analysis are based on longer term averages of the RESOLVE data. For a longer term average of N data points, the error in the average due to measurement imprecision is reduced by a factor of $\sqrt{N}$. Because of this effect, and because measurement precision is generally quite good, we found that measurement imprecision is a negligible component of the overall uncertainty level in our conclusions.

3.2.2 Accuracy Considerations

In analyzing the RESOLVE data, we adopted the approach of correcting for any inaccuracies that were known to be significant. We do not mean that all inaccuracies were removed from the data. On the contrary, the potential for unknown or miscorrected inaccuracies represents one of the main sources of uncertainty in the results. Nevertheless, we did attempt to make corrections whenever they were appropriate.

Two of the important RESOLVE measurements are known to be inaccurate—particle absorption and particle scattering. Absorption measurements on Teflon filters tend to overestimate atmospheric particle absorption because of internal filter reflectance (References 21, 22, and 23). Nephelometers may mismeasure scattering from volatile components (especially water) by altering the temperature and relative humidity of the

sample. Nephelometers also miss much of coarse particle scattering because of a loss of coarse particles in the sampling train and because of a systematic underestimate of the scattering from coarse particles.

Two methods are used here to estimate an accuracy calibration factor for the Teflon absorption measurements. The first is based on a comparison of RESOLVE fine absorption levels to RESOLVE fine-elemental-carbon concentrations. Although the RESOLVE elemental carbon data are not very precise, they are (on the average) accurate, at least in terms of agreement with other researchers (Reference 24). To make the RESOLVE absorption data set consistent with values found in the literature, the absorption data set can be calibrated against elemental carbon concentrations using the literature consensus of 9 m^2/g as the absorption efficiency for fine elemental carbon (Reference 25). This procedure yields a correction factor of 0.6 for the Teflon absorption data.

The second method is based on a 3-week experiment at Edwards AFB comparing RESOLVE Teflon absorption to nuclepore absorption using the integrating plate method, which, in turn, has been calibrated against an optical extinction cell (Reference 26). Some problems developed in interpreting the data from this experiment, but the result yielded the same correction factor—0.6. The 0.6 accuracy factor (applied to all particle absorption values before placing the values into the RESOLVE data base) is not without uncertainty, despite the fact that the two methods agreed.

The issue of volatile aerosols in the nephelometer was addressed by two RESOLVE special studies. The Insulated Nephelometer Study compared a routine RESOLVE nephelometer to an ambient nephelometer (one that is designed to produce only a very slight temperature change from ambient conditions). This study indicated that, on the average, the RESOLVE nephelometer was only about 1 to 2% lower than the ambient nephelometer. The difference (which showed considerable random scatter) was greater at high relative humidities. However, even above 70% relative humidity, which occurred less than 10% of the time, the average difference was only a factor of about 1.1. The Heater/Ambient Nephelometer Study cycled nephelometers from near-ambient conditions to a heated condition (+15°C) to measure the percent of scattering by water and other easily volatilized species. The volatilized component averaged less than 3% at NWC and less than 7% at Edwards AFB, and was almost always less than 20%.

The Insulated Nephelometer Study demonstrated that the RESOLVE nephelometers closely approximate ambient scattering conditions with respect to volatile aerosols (to within 1 to 2% on the average). The Heated/Ambient Nephelometer Study explained why this was reasonable by showing that water and other easily volatilized species are not very significant aerosol components in the study region. We decided not to apply any accuracy correction factor to the RESOLVE nephelometer data to account for volatilized species because the observed correction factor was so small and variable.

With respect to the issue of missing coarse-particle scattering, the inaccuracy of the RESOLVE nephelometer data is more significant. We estimate that the RESOLVE nephelometers miss about one-half of coarse-particle scattering based on Stokes theory calculations of sampling train losses, Mie theory results for scattering efficiencies, Mie theory calculations of nephelometer truncation errors, and crude size distribution data available in the literature. In Section 7.2.3, we conclude that average coarse-particle scattering is about 0.6 m^2/g times average coarse (2.5 to 10 micrometers) mass, which amounts to 5 Mm^{-1} as a mean value over the three RESOLVE receptor locations. This information implies that 2.5 Mm^{-1} of coarse-particle scattering is missing on the average, which is about 10% of the three-site mean nephelometer value (25.5 Mm^{-1}). The corrected three-site mean for total-particle scattering would thus be 28 Mm^{-1}.

One method to use to correct for the coarse-scattering inaccuracy would be to adjust each individual 24-hour nephelometer value in the data base by adding 0.3 m²/g times the daily coarse-particle mass. We decided against this approach, however, for the following three reasons: (1) The outputs based on 24-hour nephelometer data would not be consistent with outputs based on the hourly nephelometer data (which could not be corrected because of the lack of hourly coarse-mass data), (2) a multiplication of missing values would be present because both nephelometer and coarse-mass data would have to be available on a given day, and (3) significant imprecision would be added to the nephelometer data base because the coarse-particle scattering correction of 0.3 m²/g times coarse-particle mass is very imprecise on a daily basis (because of imprecision in coarse-particle mass data and because of variations in daily average coarse-scattering efficiency). Rather, we decided to add the correction during the data analysis whenever we calculated total extinction or visual range. Thus, when nephelometer readings are reported here (sometimes labeled as Bscat), they represent raw nephelometer data with no correction made for coarse-particle scattering. But, whenever we sum all extinction components or report visual range, the results always include the correction for missing coarse-particle scatter.

3.3 MASS AND EXTINCTION BALANCES

One of the most important quality checks for the particle and extinction data bases in RESOLVE involves comparing the whole to the sum of the parts. Does the sum of the major aerosol chemical constituents approximate measured aerosol mass? Does the sum of particle scattering and absorption plus gaseous scattering and absorption equal measured total extinction?

Table 7 presents average fine-particle mass balances for all seven stations based on the routine data during the RESOLVE base year (July 1984 to June 1985). About 10 to 20% of the fine-particle mass is not accounted for by organics, sulfates, soil, and elemental carbon. This remaining mass is believed to be mostly nitrates* plus very minor contributions from miscellaneous species. For Edwards AFB and NWC, if we add the measured particle nitrate mass (using the denuder technique that should yield a somewhat greater value than the nitrate on Teflon filters) and the mass of other miscellaneous elements (about 3%), the total mass accounted for is 104% at Edwards AFB and 97% at NWC. Thus, the average mass balance for fine particles seems to be quite reasonable.

Figure 10 shows how the sum of chemical components (organics plus sulfates plus elemental carbon plus soil dust plus miscellaneous measured elements) compares to fine mass on a daily basis for the entire data set. Although the relationship is not extremely precise, the correlation is fairly good (R = 0.79). Thus, both for the average and individual days, the fine-particle-mass balance is indicative of good data quality.

Table 8 compares teleradiometer measurements of total extinction (available for the three RESOLVE receptor sites) to the sum of extinction components. As discussed in Section 7.2, the sum of extinction components—averaged over the three sites—consists of 24% from Rayleigh scatter by air molecules (assumed to be a constant 11 Mm⁻¹), 2% from light absorption by gaseous NO_2 (based on special study NO_2 data), 61% from light scattering by particles (50% from fine particles and 11% from coarse particles based on nephelometry and coarse-particle data), and 13% from light absorption by elemental

---

* Several indications are present that the remaining mass mostly represents nitrates. One important piece of evidence is that nitrates and unaccounted-for mass are the only two aerosol components that show a winter maximum rather than a summer maximum (see data and discussion in Section 7.3.2).

TABLE 7. Fine-Particle Mass Balances Calculated
for the RESOLVE Base Year.

Elements	Mass components divided by total measured fine mass by site						
	EDW	CHL	FOR	RAW	TEH	SOL	CAP
Organics[a]	32%	37%	29%	30%	34%	30%	36%
Sulfates[a]	30%	24%	28%	32%	26%	32%	27%
Elemental carbon	6%	6%	7%	5%	4%	8%	7%
Soil[a]	16%	20%	27%	17%	15%	10%	8%
Unaccounted for[b]	16%	13%	9%	16%	21%	20%	22%
Number of days[c]	85	87	80	26	26	30	33

[a] To include the mass of associated ions, the following conventions are adopted throughout this report: sulfates = 4.12 x S (assuming ammonium sulfate), organics = 1.5 x Organic C (accounting for associated hydrogens and other ions), and soil = 2.14 Si + 1.67 Al + 1.44 Ca + 1.40 Fe + 1.66 Mg + 1.22 K + 1.44 Mn (accounting for common soil compounds).

[b] This category represents the fine-particle mass not accounted for by the other four categories. It is thought to be mostly nitrates. True particulate nitrate by the denuder/nylon-filter method, which would tend to be greater than the nitrate collected on the routine Teflon filters, is approximately 17% of fine mass at Edwards AFB and 7% at NWC. The mass of miscellaneous other species measured by PIXE or XRF (e.g., lead salts) accounts for about 3% of the total at all seven sites.

[c] This table is restricted to days in the RESOLVE base year with data available for fine mass and all chemical components.
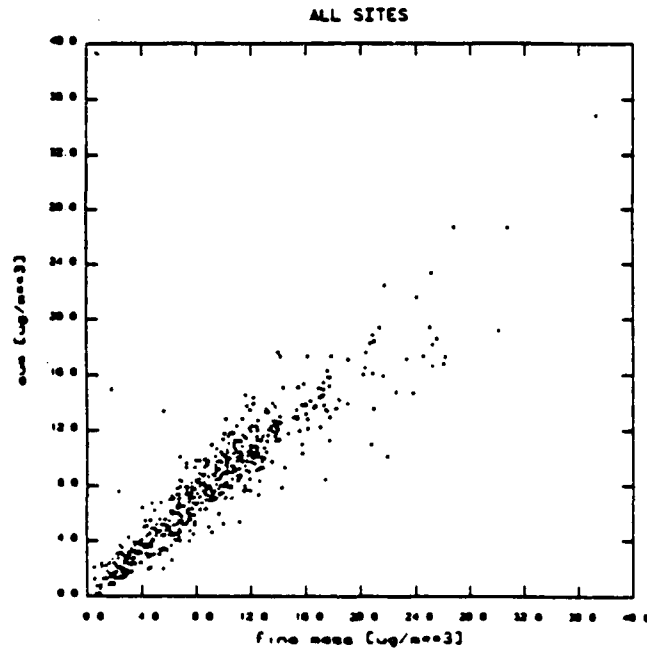

FIGURE 10. Scatterplot of Sum of Measured Fine Aerosol
Components Versus Total Fine Mass.

TABLE 8. Comparison of Teleradiometer Total Extinction to
the Sum of Extinction Components.

Site and teleradiometer targets	Ratio of teleradiometer to sum of components*		Correlation of daily teleradiometer to sum of components	
	All data	Clear skies	All data	Clear skies
Edwards AFB				
Target 1	88	87	90 (335)**	92 (98)
Target 2	84	85	78 (308)	70 (35)
Fort Irwin NTC				
Target 1	84	81	78 (188)	84 (10)
Target 2	82	82	82 (259)	89 (33)
Target 3	73	79	77 (261)	91 (18)
NWC				
Target 1	78	83	79 (322)	89 (47)

* Comparisons are carried out using daily averages. The sum of components is calculated in Mm $^{-1}$ as

$$11 + \left[(B_{scat24} + .3CP) + .04 B_{scat24} + B_{ap24} \right] \cdot \frac{B_{scat8}}{B_{scat24}}$$

The first term is Rayleigh scatter. The value in parentheses represents particle scatter, adjusted to account for the missing part of coarse-particle scattering. The second and third terms in the brackets are NO_2 and particle absorption, respectively. The subscript "24" refers to 24-hour averages. The last ratio in the formula factors the result to an 8-hour daytime basis to be consistent with the daytime data for teleradiometer extinction. For the short period of missing absorption data, B_{ap24} is estimated as a constant fraction of B_{scat24}.

** () = Sample size.

carbon (based on routine particle absorption data). Results are presented for all teleradiometer data (regardless of sky conditions) and for clear skies (when the data quality should be best). The data are for daily averages, with the sum of extinction components adjusted from a 24-hour basis to an 8-hour basis using the diurnal pattern of Bscat (see footnote to Table 8).

As indicated in the left-hand side of Table 8, teleradiometer extinction is generally about 15 to 25% less than the sum of components. This amount is qualitatively consistent with expectations. The sum of extinction components is based on ground-level, point measurements. The teleradiometer, on the other hand, represents an average over a line of sight from ground level to elevated targets (mountains). It is very reasonable to expect somewhat lower extinction levels at higher elevations (particularly at elevations above the mixing layer).

The right-hand side of Table 8 presents the correlation between daily values for teleradiometer extinction and sum of components. Most of the correlations range from about 0.75 to 0.9, which is good, especially considering the potential problems with

teleradiometer data* (References 27, 28, and 29) and the fact that point measurements are being correlated with line-of-sight measurements. Thus, both with respect to averages and daily correlations, the teleradiometer data appear to corroborate the good quality of the data sets for extinction components (i.e., scattering and absorption).

3.4 INTERPARAMETER CORRELATIONS

Table 9 summarizes the correlations that exist among the important aerosol and extinction parameters. The correlations are based on all daily averages from the three receptor sites during the RESOLVE base year. For each parameter, the other parameters are listed below it in order of descending degree of correlation. The correlations can be interpreted in terms of physical and chemical relationships as well as in terms of data quality. Here, we focus mainly on the data quality implications.

One feature shown in Table 9 is the consistently good correlation (generally about 0.75 to 0.80) that exists among particle scattering (Bscat), fine-particle absorption (Fabs), fine-particle mass (Fmass), organics (Org), and sulfates (Sul). These are the main measures or components of fine-particle mass and fine-particle extinction—they all show summertime peaks and they all are thought to originate mostly from man-made sources. That the parameters show fairly good levels of correlation despite the fact that none are really duplicate measures of the same phenomenon suggests good data quality. More significantly, the fact that each of these parameters consistently shows about the same degree of correlation with the others suggests that none of these parameters has uniquely poor data quality.

Elemental carbon shows a somewhat lesser correlation with the above five parameters—about 0.6 to 0.7. Even for fine absorption, a duplicate measure of the same phenomenon, only a 0.6 correlation with elemental carbon is present. The reason for this is the relatively low precision of the elemental carbon data (see Table 6).

The soil variable and the major soil elements (Si, Al, Fe, and Ca) all intercorrelate at very high levels—generally 0.9 to 1.0. This high intercorrelation is a reflection of the good precision in the PIXE and XRF analyses.

The elements Ni and Pb do not correlate as high with the other key air-quality parameters (Bscat, Fabs, Fmass, Org. Sul, and EC) as the soil variable and soil elements intercorrelate. Generally, Ni and Pb correlate at a level of 0.25 to 0.40. This fact should not represent a data quality problem, because precision is quite good for Ni and Pb (see Table 6). Rather, the explanation for the lower correlations lies in some of the findings of Chapter 8. Ni and Pb are used as tracer elements to investigate contributions from different source areas (San Joaquin Valley (Ni rich) versus Los Angeles and desert sources (both Pb rich)). Tracer element fraction of fine mass in air leaving the source areas exhibits a significant

---

* The potential for imprecision in the teleradiometer measurements is suggested by some correlation studies with the RESOLVE data sets. Comparing hourly teleradiometer data for different targets at the same site yields correlations around 0.65 to 0.80. Comparing hourly teleradiometer data with hourly nephelometer data yields correlations around 0.6 to 0.8.

TABLE 9. Correlation Coefficients Between Key Extinction
and Aerosol Parameters.

Mean	Std. Dev.	Mean	Std. Dev.	Mean	Std. Dev.	Mean	Std. Dev.	Mean	Std. Dev.
24.8 Bscat	15.7	2.7 Org	1.8	1.7 Soil	2.0	0.10 Fe	0.11	.004 Ni	.003
Fmass	0.84	Fabs	0.79	Si	1.00	Soil	0.98	Fabs	0.43
Fabs	0.79	Fmass	0.76	Fe	0.98	Si	0.97	Pb	0.36
Sul	0.79	Bscat	0.74	Al	0.95	Ca	0.95	Oc	0.36
Oc	0.74	Ec	0.68	Ca	0.94	Al	0.94	Sul	0.30
Ec	0.61	Sul	0.65	K	0.88	K	0.89	Bscat	0.28
Rem	0.40	Pb	0.38	Fmass	0.54	Fmass	0.59	Fmass	0.22
Pb	0.40	K	0.36	Sul	0.16	Sul	0.23	Ec	0.21
K	0.36	Ni	0.36	Bscat	0.16	Bscat	0.22	Rem	0.16
Ni	0.28	Fe	0.18	Oc	0.10	Oc	0.18	K	-.04
Fe	0.22	Al	0.12	Ec	0.08	Ec	0.14	Fe	-.09
Al	0.19	Rem	0.11	Fabs	0.06	Fabs	0.14	Soil	-.15
Soil	0.16	Soil	0.10	Ni	-.15	Ni	-.09	Si	-.16
Si	0.14	Ca	0.10	Pb	-.19	Pb	-.16	Ca	-.17
Ca	0.13	Si	0.07	Rem	-.23	Rem	-.22	Al	-.17

Mean	Std. Dev.	Mean	Std. Dev.	Mean	Std. Dev.	Mean	Std. Dev.	Mean	Std. Dev.
5.1 Fabs	2.0	2.2 Sul	1.4	0.44 Si	0.55	0.10 Ca	0.11	.018 Pb	.017
Bscat	0.79	Bscat	0.79	Soil	1.00	Fe	0.95	Fabs	0.46
Oc	0.79	Fabs	0.78	Fe	0.97	Soil	0.94	Bscat	0.40
Sul	0.78	Fmass	0.76	Al	0.94	Si	0.92	Oc	0.38
Fmass	0.76	Oc	0.65	Ca	0.92	Al	0.88	Ni	0.36
Ec	0.66	Ec	0.59	K	0.86	K	0.82	Ec	0.33
Pb	0.46	Pb	0.32	Fmass	0.52	Fmass	0.47	Sul	0.32
Ni	0.43	K	0.31	Bscat	0.14	Sul	0.16	Rem	0.30
Rem	0.27	Ni	0.30	Sul	0.14	Bscat	0.13	Fmass	0.28
K	0.25	Fe	0.23	Oc	0.07	Oc	0.10	K	-.12
Fe	0.14	Al	0.20	Ec	0.06	Ec	0.07	Fe	-.16
Al	0.07	Soil	0.16	Fabs	0.04	Fabs	0.04	Al	-.17
Soil	0.06	Ca	0.16	Ni	-.16	Ni	-.17	Soil	-.19
Si	0.04	Si	0.14	Pb	-.20	Pb	-.21	Si	-.20
Ca	0.04	Rem	0.08	Rem	-.22	Rem	-.32	Ca	-.21

Mean	Std. Dev.	Mean	Std. Dev.	Mean	Std. Dev.	Mean	Std. Dev.	Mean	Std. Dev.
8.1 Fmass	4.4	0.48 Ec	0.34	0.17 Al	0.21	0.09 K	0.09	0.79 Rem	1.6
Bscat	0.84	Oc	0.68	Soil	0.95	Fe	0.89	Bscat	0.40
Fabs	0.76	Fabs	0.66	Si	0.94	Soil	0.88	Fmass	0.33
Oc	0.76	Fmass	0.61	Fe	0.94	Si	0.86	Pb	0.30
Sul	0.76	Bscat	0.61	Ca	0.88	Al	0.83	Fabs	0.27
K	0.69	Sul	0.59	K	0.83	Ca	0.82	Ni	0.16
Ec	0.61	Pb	0.33	Fmass	0.54	Fmass	0.69	Oc	0.11
Fe	0.59	K	0.23	Su.	0.20	Bscat	0.36	Sul	0.08
Al	0.54	Ni	0.21	Bscat	0.19	Oc	0.36	Ec	0.08
Soil	0.54	Fe	0.14	Oc	0.12	Sul	0.31	K	-.08
Si	0.52	Al	0.11	Ec	0.11	Fabs	0.25	Fe	-.22
Ca	0.47	Soil	0.08	Fabs	0.07	Ec	0.23	Si	-.22
Rem	0.33	Rem	0.08	Pb	-.17	Ni	-.04	Al	-.23
Pb	0.28	Ca	0.07	Ni	-.17	Rem	-.08	Soil	-.23
Ni	0.22	Si	0.06	Rem	-.23	Pb	-.12	Ca	-.32

NOTES:
- All means and standard deviations are in Mm^{-1} or µg/m^2
- Data are for all 24-hour averages during the RESOLVE base year at the three receptor sites.

degree of variability.* In fact, at the passes, the critical tracer elements (Ni at Tehachapi and Pb at Soledad and Cajon) exhibit correlations of only 0.3 to 0.7 with the other key air-quality variables. At the receptor sites, the correlations should be even lower, because Ni (or Pb) can further vary independently of the other air-quality parameters, depending on the relative contributions of the various source areas.

3.5 DIURNAL AND VERTICAL REPRESENTATIVENESS

In this section we discuss two aspects of the temporal/spatial representativeness of RESOLVE data. Specifically, we address the questions (1) are the 24-hour particulate samples adequate for characterizing air quality during daytime hours (when visibility is of special concern), and (2) are the ground-level measurements adequate to characterize visibility at higher altitudes within the mixing layer?

Particle scattering levels at the RESOLVE receptor sites show a distinct diurnal pattern. A minimum occurs in the early afternoon, so that daytime (0800 to 1600) particle scattering averages about 10 to 15% lower than the 24-hour mean. This fact, in itself, does not negate the use of 24-hour particle data to characterize daytime air quality. Perhaps the 24-hour particle data can simply be factored by the diurnal variations in the nephelometer if daytime visibility per se becomes an issue. The key to this question is whether or not particle composition (which serves as the basis for the extinction budget allocations and aerosol origin allocations) shows a significant diurnal variation.

To address the question of diurnal variations in particle composition, a special field experiment was conducted at Edwards AFB and NWC for 3 weeks during August 1985. The experiment involved operating the 2x4 particle samples on an 8-hour basis rather than a 24-hour basis. Table 10 compares average fine-particle composition for the daytime and 24-hour periods. With only two exceptions—denuder nitrates at Edwards AFB and organics at NWC (both of which may have involved sampling problems)**—the average particle compositions are nearly identical for the daytime and 24-hour periods. These data are consistent with the conclusions of a RESOLVE planning study (Reference 3) that found identical daytime and nighttime particle compositions at NWC based on the data by Ouimette (Reference 30).

The earlier RESOLVE planning study by Trijonis, et al. (Reference 3) also noted a close coupling of daytime and 24-hour air quality as evidenced by high correlations between 0800-1600 and 0000-2400 averages of nephelometer data. These high correlation levels, typically about 0.9, are confirmed in the RESOLVE data set.** Thus, both with respect to correlation of loadings and overall aerosol composition, we conclude that the 24-hour particle samples are adequate for characterizing air quality during daytime hours.

---

* Day-to-day fluctuations in the Ni mass fraction at Tehachapi or the Pb mass fraction at the Los Angeles passes can be explained by at least three factors: (1) variation in the secondary versus primary makeup of fine mass, (2) variation in trajectories (and therefore source exposure) within the upwind air basins, and (3) variations in source emissions.

** The RESOLVE planning study has also been verified in another sense. The planning study warned of data quality and precision problems for 8-hour sampling as opposed to 24-hour sampling. During the 8-hour sampling of August 1985, it was found that (1) precision was generally a factor of 2 or 3 worse than for the routine 24-hour sampling; (2) the number of values flagged by the data-screening procedure increased by an order of magnitude; and (3) the sampling protocol was more problematical, leading to several questions regarding data quality.

TABLE 10. Fine-Particle Mass Balances,
Daytime (0800-1600) Versus 24-Hour.

Elements	Mass components plus total measured fine mass by site and period			
	Edwards AFB		NWC	
	Daytime	24-Hour	Daytime	24-Hour
	Mass components ÷ total measured fine mass			
Organics[a]	35%	36%	50%	41%
Sulfates[a]	37%	36%	32%	32%
Elemental carbon [b]	7%	6%	6%	6%
Soil[a]	15%	13%	24%	22%
Unaccounted for[c]	6%	9%	– 12%	– 1%
Total fine mass	7.1	10.0	8.8	10.3(µg/m³)
Days of sampling[d]	14	14	12	14

[a] To account for the mass of associated ions, the following conventions were adopted throughout this report: sulfates = 4.2 S, organics = 1.5 Organic C, and soil = 2.14 Si + 1.67 Al + 1.44 Ca + 1.40 Fe + 1.66 Mg + 1.22 K + 1.44 Mn.

[b] Computed from particle absorption because of poor-quality, elemental-carbon data during the special study.

[c] This category represents the fine-particle mass not accounted for by the other four categories. It is thought to be mostly nitrates. True particulate nitrate by the denuder/nylon-filter method, which would tend to be greater than the nitrate collected on the routine Teflon filters, averaged 12% over the 24-hour periods and 21% over the daytime periods during this set of sampling days.

[d] Sample is restricted to periods without missing data for all key parameters.

The question of vertical representativeness can be investigated using data from a nephelometer network operated by NWC. In addition to a station at NWC adjacent to the RESOLVE site, NWC operates stations at B Mountain (370 meters higher than NWC at 7 kilometers SSE) and Laurel Mountain (710 meters higher than NWC at 19 kilometers south). To compare NWC with the two elevated sites, particle scattering data were assembled for the three sites over the 2-year RESOLVE period (September 1983 to August 1985).

Over the 2 years, particle scattering at B Mountain and Laurel Mountain averaged 64% and 89%, respectively, of that at NWC. These averages are consistent with the conclusion that extinction levels are somewhat lower at higher elevations. It is puzzling that the higher mountain (Laurel) shows the higher particle scattering, but this could be explained by the closer proximity of Laurel Mountain to flow from the San Joaquin Valley.

The correlation coefficient for daily average particle scattering is 0.77 between NWC and B Mountain, and 0.75 between NWC and Laurel Mountain. These correlations are quite good, especially considering that this situation represents a "worst-case" or "conservative" evaluation of vertical representativeness. As noted in Sections 4.3.2 and 4.3.3, NWC is the RESOLVE receptor site that is most subject to influence by local sources. NWC is also separated from the other two sites, not only vertically, but horizontally. Horizontal inhomogeneities seem significant because a correlation of only 0.79 is obtained even when the two mountain sites are compared. Good correlations, despite the horizontal distances, show that (at least on a daily basis; on an hourly basis, the correlations are not as

good–0.66 between NWC and B Mountain, and 0.61 between NWC and Laurel Mountain) ground-level air quality is not severely decoupled from elevated air quality.

4.0 CLIMATE AND METEOROLOGY

The two major objectives of RESOLVE are to document existing visibility conditions in the study region and to characterize the causes and sources of visibility degradation. In addressing each of these objectives, it is important to have an understanding of the meteorology of the study region.

4.1 CLIMATE OF THE RESOLVE STUDY REGION

4.1.1 Temperature and Moisture

The RESOLVE study region encompasses much of the California high desert, including the western half of the Mojave Desert and the southern portion of the Owens Valley (see Figure 1). The region includes many desert valleys and dry lakes with elevations of 600 to 1000 meters and several mountain ranges with peaks of 1500 to 2500 meters.

The climate of the study area is strongly influenced by the mountain ranges that border the desert on the south and west. The Sierra Nevada and Tehachapi Mountains on the west and the San Gabriel Mountains on the south intercept the storms that bring rain to the coastal regions of California. Air masses crossing these mountains typically drop much of their moisture on the mountain barriers and become warmer and drier as they move down the slopes into the desert.

Average rainfall in the desert region ranges from about 10 to 25 centimeters per year (Reference 31). Most of the rain occurs from December through March in winter storms that come from the Pacific. Some rainfall occurs in the summer and is associated with tropical, unstable air masses coming from the southeast. An average of only about 25 days per year having over .025 centimeter of precipitation occurs at Edwards AFB.

As a result of the trapping of moisture by the mountains, the desert region is relatively dry and free of clouds. Solar heating and nighttime radiational cooling result in average diurnal temperature variations of 15 to 20°C. As an example of the desert climate, the monthly temperature, precipitation, and relative humidity averages for Edwards AFB are presented in Table 11.

TABLE 11. Climatic Data for Edwards AFB.

	Jan	Feb	Mar	Apr	May	Jun	Jul	Aug	Sep	Oct	Nov	Dec
Surface temperature summary, °C												
Average maximum	13.3	16.1	17.8	22.2	26.7	32.2	36.7	35.6	32.8	25.6	18.9	13.9
Average minimum	–1.1	1.1	3.9	6.7	10.0	14.4	18.9	17.8	14.4	7.8	2.2	–1.1
Mean hourly	6.1	8.9	11.1	14.4	18.9	23.3	27.8	26.7	23.9	16.7	10.6	6.7
Average surface relative humidity, %	56	52	52	45	38	33	27	31	40	37	47	52
Average precipitation, mm (monthy totals)	22.6	23.6	21.8	6.6	1.8	1.0	1.3	4.8	4.6	0.0	14.0	17.5

NOTE: Data obtained from monthly weather summaries (Reference 32).

4.1.2 Wind-Flow Patterns

The air masses that affect California tend to travel from west to east, bringing clean ocean air into the state. In the desert region, above the influence of the terrain, the prevailing flows tend to be from the west or northwest most of the year (Reference 33), with a shift to southwesterly flows in the summer (Reference 34). The actual flow patterns and wind directions in the lower levels of the atmosphere are controlled by the locations of high- and low-pressure systems and by the topography.

The weather in California is strongly affected by the location of the semipermanent high-pressure area in the northern Pacific Ocean (Reference 33). In summer, this pressure center remains to the north, blocking Pacific storms and low-pressure systems. In the winter, this pressure center weakens and moves south, allowing storms to enter California. As storms and low-pressure systems cross the state, the upper air winds can vary greatly in speed and direction. However, since storm periods tend to be times of good ventilation and good visibility, most of our discussion will focus on nonstorm flow patterns.

In the absence of storms in the summer, and between storms in the winter, the prevailing flow patterns tend to be dominated in the lower levels by the topography and by thermal effects. Without the convective mixing associated with storms, the air in the RESOLVE region and in the air basins to the west and south tends to be stable, with mixing depths well below the heights of the mountain ranges that separate the desert from the coastal valley (Reference 35). Thus the prevailing westerly flows tend to be channeled into the desert through passes in the mountain ranges. The most frequent morning and afternoon surface streamlines for January and July in the southern part of the study region have been determined by Smith, et al. (References 7 and 35) and are shown in Figures 11 and 12. Winter and summer predominant 24-hour surface wind flow patterns for all of California are illustrated in Figures 11 and 12.

The winter months are characterized by calm winds in the desert and in the mountain passes during the night and morning, and light flows into the desert during the afternoon (see Figure 11). In the winter, radiative cooling creates very stable air near the surface, with the surface flows essentially decoupled from the flows aloft during much of the day. In fact, near the surface in winter, drainage flows from the mountains tend to counteract the prevailing westerlies. As seen in Figure 13, the result on a 24-hour-average basis is a tendency for offshore flows out of the coastal valleys. Even in winter, however, by midafternoon, solar heating tends to dissipate the drainage flows, and the prevailing westerlies, reinforced by heating inland, push some air into the desert from the San Joaquin Valley and the Los Angeles basin (see Figure 11).

An important feature of the winter regime in the desert is the relatively light wind at the surface. Calms are reported 26% of the hours in November, December, and January at NWC (Reference 36) and 37% at Edwards AFB (Reference 37). This percentage contrasts with May through July, when only 6% of the hours at NWC and 10% at Edwards AFB are reported as calm. The large percentage of winter calms allows the potential buildup of local emissions from wood burning, motor vehicles, and industrial sources to supplement the pollutants transported into the desert from upwind source areas.

In the summer months (see Figures 12 and 14), the transport is more consistent throughout the day. Solar heating in the desert creates a thermal low-pressure area that tends to persist through the night, generating flow into the desert for almost the entire 24-hour day. The wind speeds, however, are typically much higher in the afternoon than in the late night and morning.

Figures 12 and 14 indicate that the San Joaquin Valley is the primary source of summer air for most of the study region, with the Los Angeles basin (and possibly Ventura County) influencing the southern part of the region. The San Joaquin Valley is the dominant source of summer air at NWC and the primary source at Fort Irwin NTC. The San Joaquin Valley may also be the primary source of summer air at Edwards AFB, although Edwards AFB frequently receives air from the Los Angeles basin late in the day.

The convergence zone to the east of Fort Irwin NTC in Figure 12 is a typical summer feature. On occasion, this zone shifts to the west, allowing emissions transported from the Imperial Valley (southeast of Palm Springs) to impact the Fort Irwin NTC region.
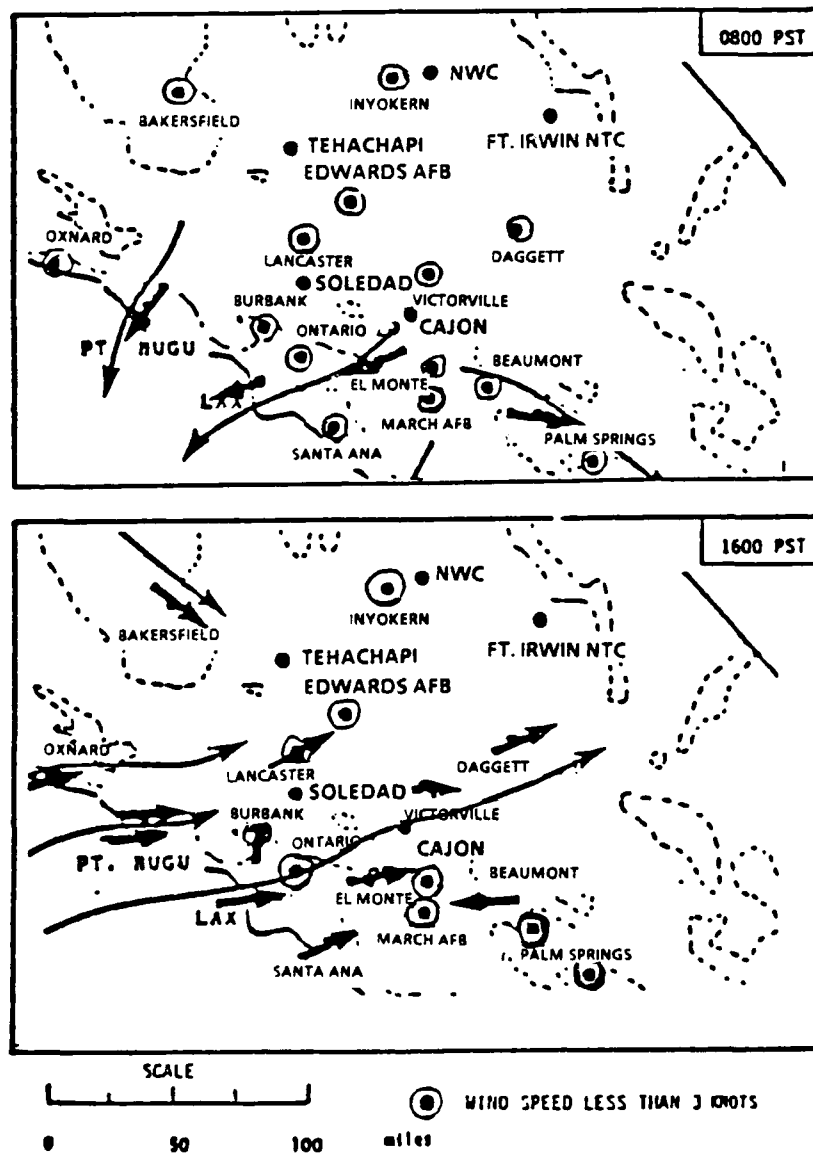

FIGURE 11. Most Frequent Wind Directions in the Mojave Desert for 0800 and 1600 PST for January 1979 and 1980. Heavy arrows indicate observed most-frequent wind directions.
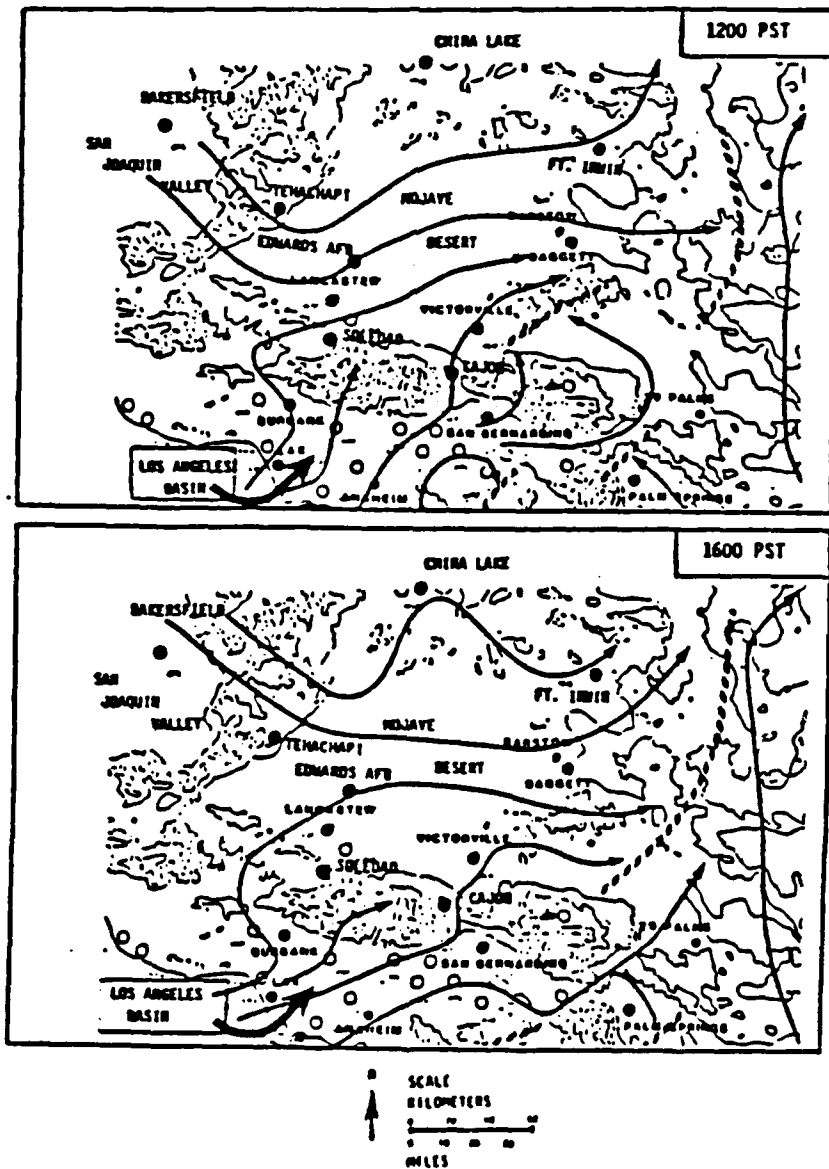
FIGURE 12. Most Frequent Wind Directions in the Mojave Desert for 1200 and 1600 PST for July and August 1979 and 1980. Convergence zones are indicated by hatched lines.
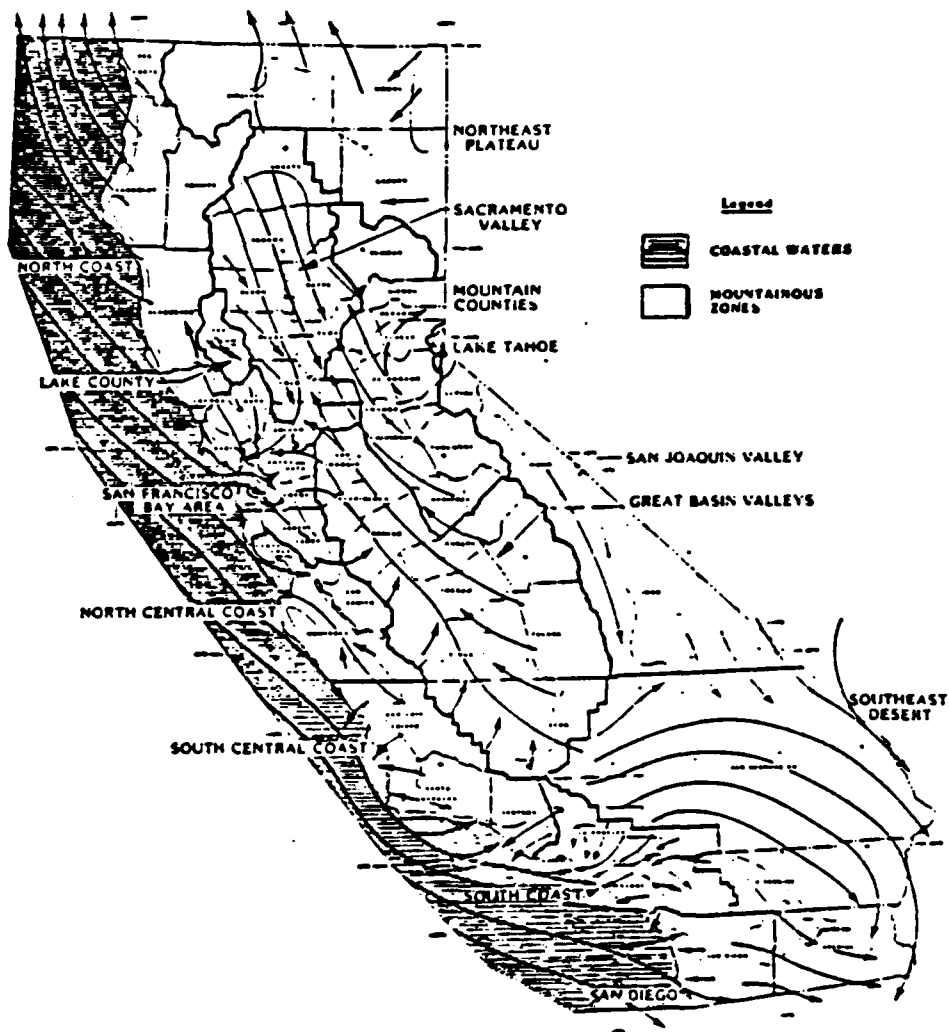
FIGURE 13. California Predominant Surface Wind-Flow
Patterns for the Winter (December to February). (Reference 38).
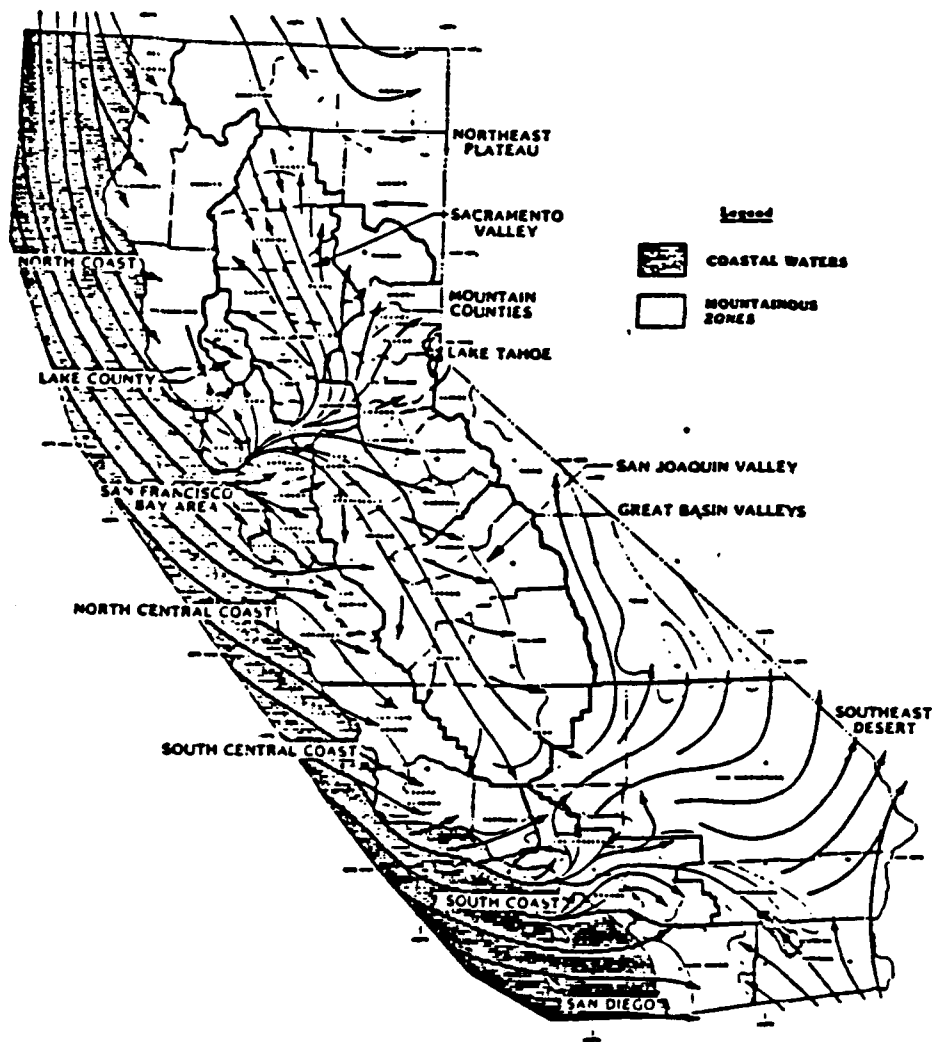
FIGURE 14. California Predominant Surface Wind-Flow
Patterns for the Summer (June to August). (Reference 38.)

4.1.3 Source Regions and Resulting Visual Range Distribution

Figure 15 shows 1983 emissions reported for the RESOLVE study area (western Southeast Desert Air Basin and southern Great Basin Air Basin) and the major upwind basins (San Joaquin Valley, Los Angeles, and South Central Coast) for PM10, SO_x, and NO_x. Although emissions of SO_x in the San Joaquin Valley and the South Coast changed somewhat between 1983 and the 1984-85 RESOLVE period, the general spatial distribution remained similar. The emission estimates are those reported by the local air pollution control districts, and the methods of estimating emissions may not be consistent between districts. Nevertheless, it is clearly shown in Figure 15 that reported emissions of the air basins upwind of the RESOLVE region (San Joaquin Valley, Los Angeles, and South Central Coast) are much greater than those of the RESOLVE study area. Total emissions reported for the three upwind basins are a factor of 13 times greater than those for the RESOLVE study area for SO_x, a factor of 12 times greater for NO_x, and a factor of 17 times greater for PM10.

The emission patterns are reflected in the spatial distribution of visibility illustrated in Figure 16 (Reference 40). The median airport visual range for the upwind air basins is in the 15- to 40-kilometer range. Airport visual ranges in the RESOLVE area are on the order of 50 to 100 kilometers, with the worst visibility in the areas nearest the upwind air basins. It is clear from Figures 15 and 16 that air masses transported into the desert from the upwind counties have the potential to degrade visibility in the desert.

## 4.2 RESOLVE METEOROLOGY AND COMPARISON TO LONG-TERM AVERAGES

In this section we describe the meteorology of the RESOLVE study period and compare the RESOLVE period to long-term averages. We made the comparisons using parameters for which historical data are readily available at Edwards AFB and NWC.

### 4.2.1 Temperature and Moisture

Annual and quarterly maps for temperature and relative humidity at the RESOLVE measurement sites for July 1984 through June 1985 are presented in Figures 17 and 18. It is apparent from Figure 17 that the desert sites average 3 to 5°C warmer than the pass sites during all seasons. This difference in temperature reflects three factors: (1) Cooler marine air from the upwind valleys is transported through the passes, (2) increased solar heating is present in the desert, and (3) the pass sites are higher in elevation than the desert.

The transport of air from the upwind valleys into the desert is also evident in the relative humidity spatial distribution shown in Figure 18. The pass sites have higher average relative humidity values than the desert sites. Relative humidity at Edwards AFB is higher than at the other desert sites, reflecting closer proximity of Edwards AFB to the passes and the impact of moist marine air from the Los Angeles basin.

Average diurnal patterns for temperature and relative humidity are plotted in Figure 19 for Edwards AFB, NWC, and Fort Irwin NTC. NWC has the greatest daily temperature extremes, probably because of its location in a dry lake bed where the effects of daytime heating and nighttime drainage are both maximized. The impact of marine air at Edwards AFB late in the afternoon is indicated by the temperature starting to decrease earlier in the day than at the other sites, and by the relative humidity being higher (especially in the late afternoon).
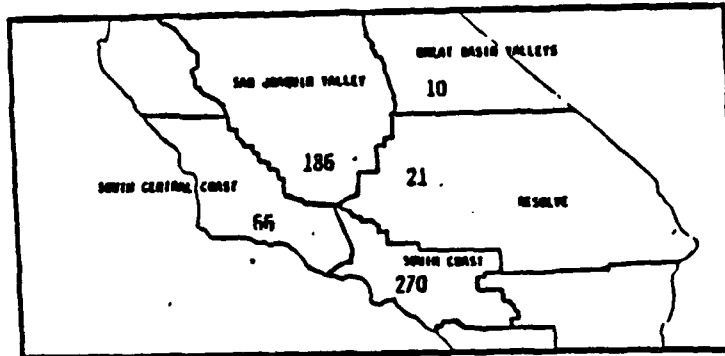
a. Particulate Matter less than 10 µm (1000 tons/yr)
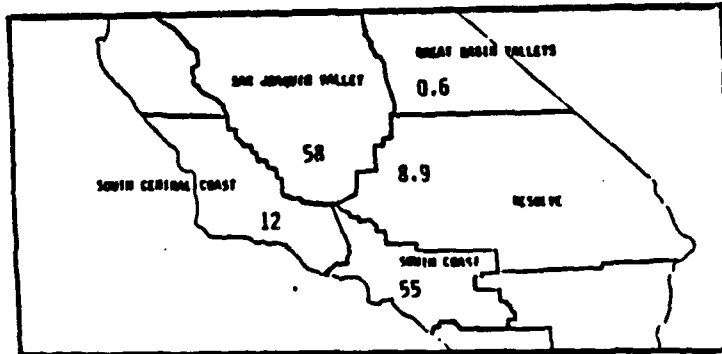
b. Sulfur Oxides (1000 tons/yr)
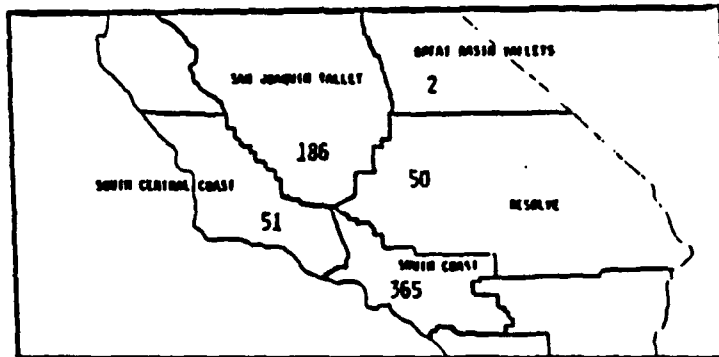
c. Nitrogen Oxides (1000 tons/yr)

FIGURE 15. 1983 Emissions in the RESOLVE Region and Upwind Air Basins (Reference 39).
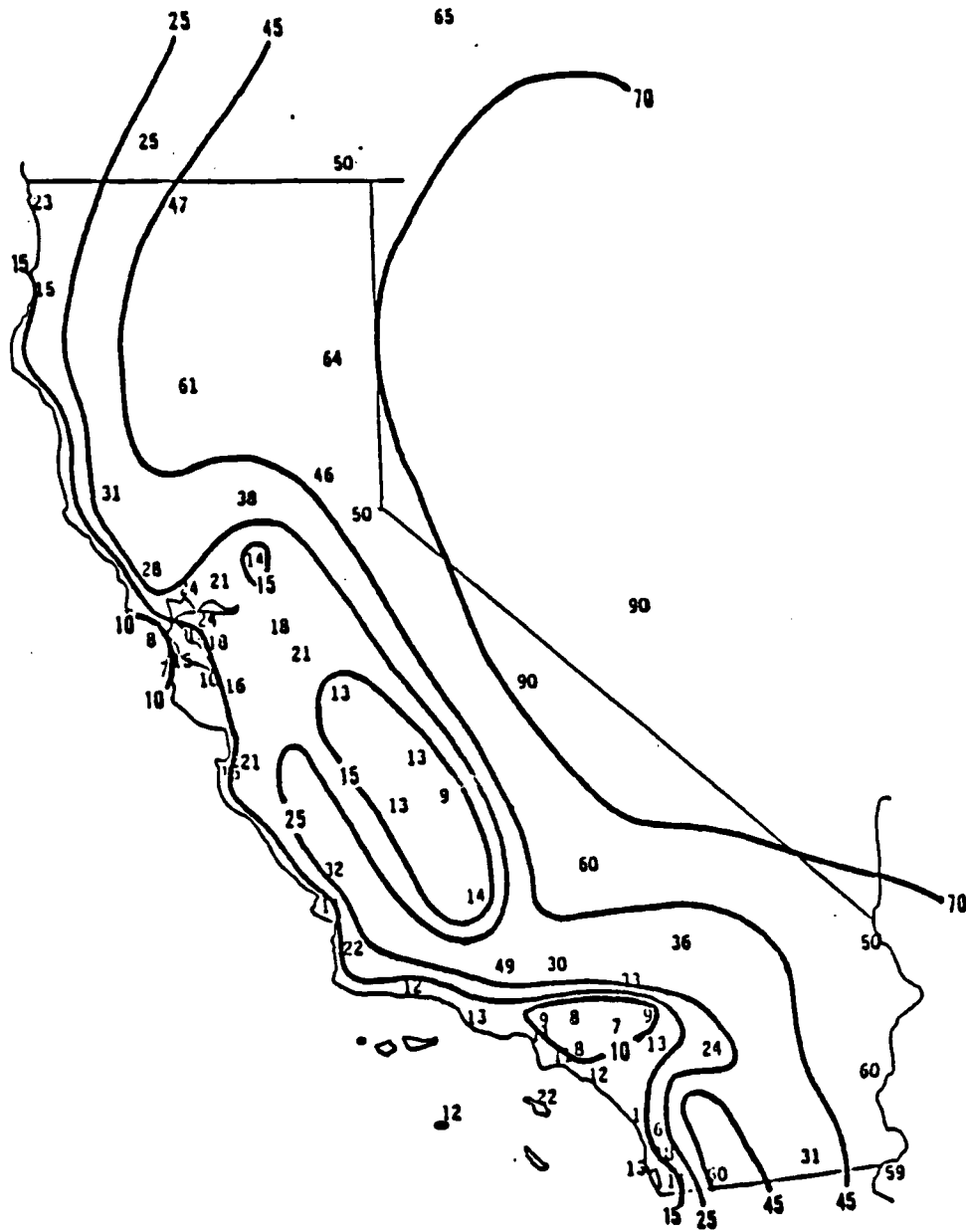
FIGURE 16. Median 1 P.M. Airport Visual Range (in Miles) for
California (1974 to 1976 Data).
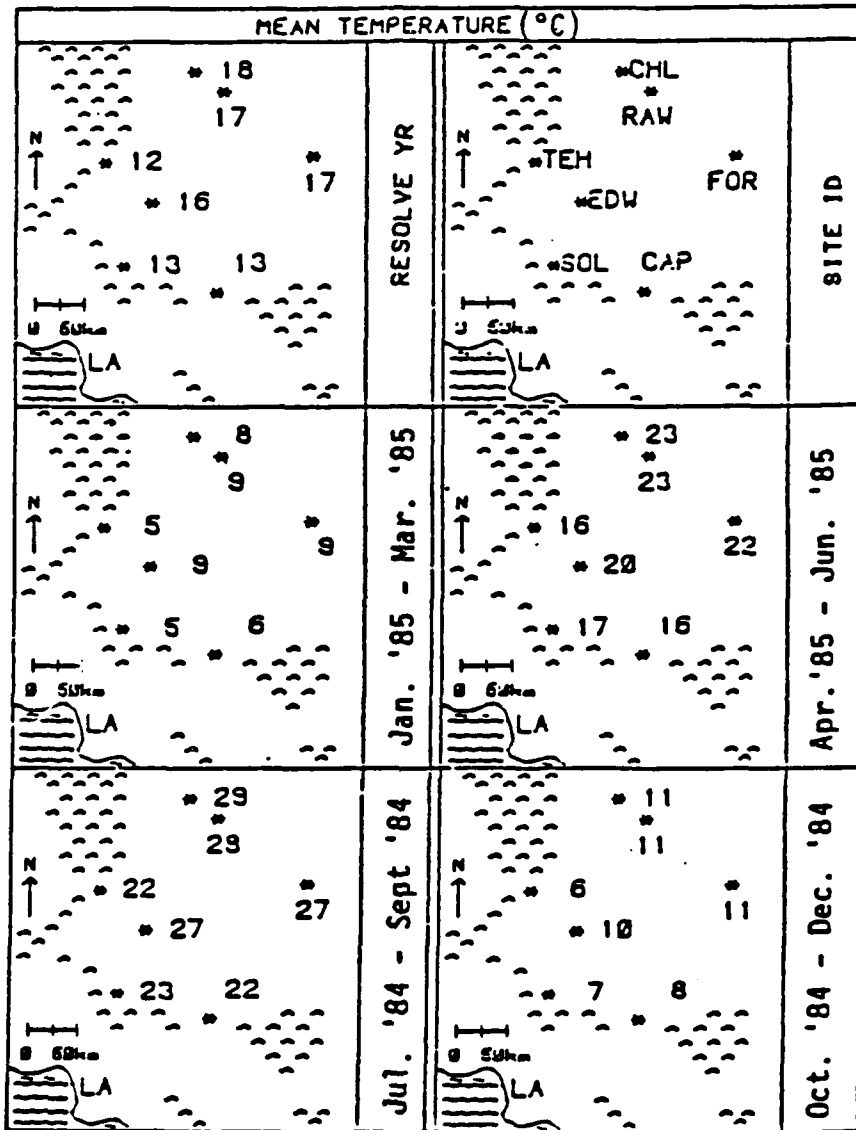
FIGURE 17. Annual and Quarterly Average Temperature (°C) at the RESOLVE Sites for July 1984 through June 1985.
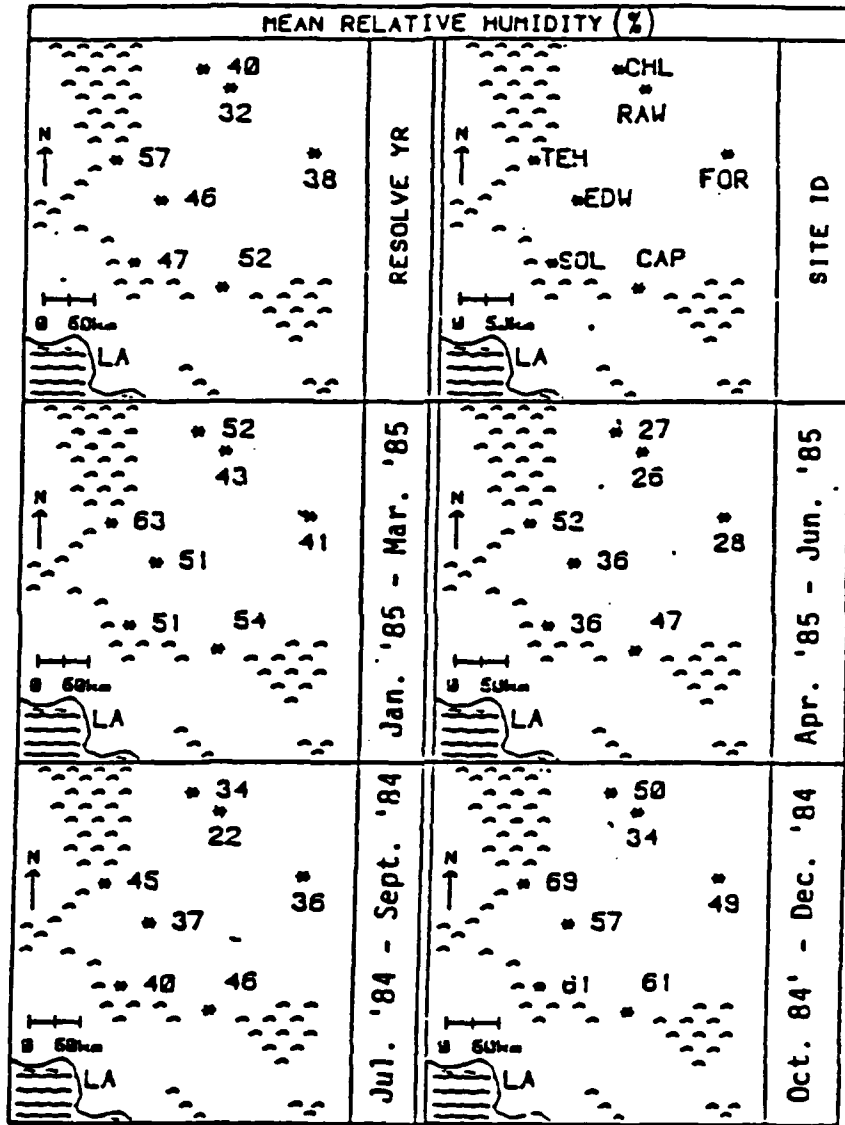
FIGURE 18. Annual and Quarterly Average Relative Humidity
(%) at the RESOLVE Sites for July 1984 through June 1985.
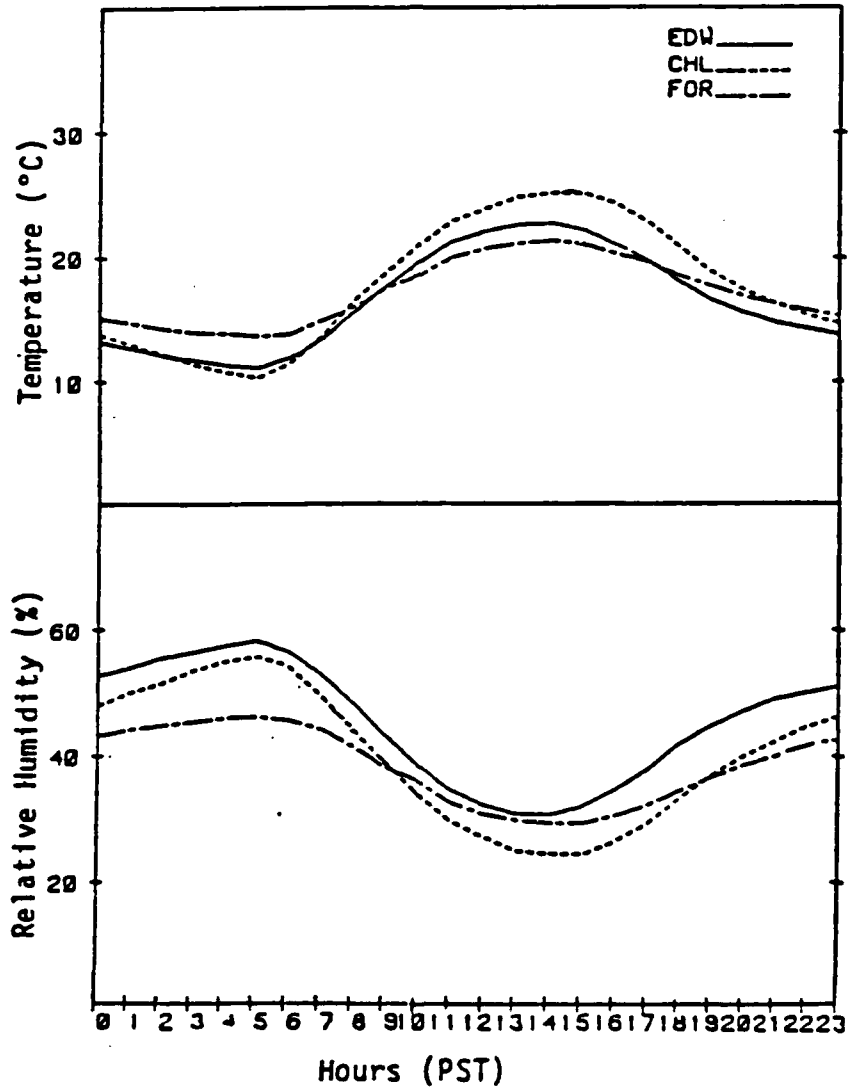
FIGURE 19. Annual Average Temperature and Relative
Humidity Diurnal Patterns at Edwards AFB, NWC, and Fort
Irwin NTC.

The surface temperature, precipitation, and relative humidity for the RESOLVE year (July 1984 to June 1985) are compared with the long-term averages at Edwards AFB and NWC in Figures 20 through 22 (References 32 and 41). From Figure 20, the average maximum temperature at both Edwards AFB and NWC was within 3°C of the long-term averages for all months except December 1984 and April and June 1985. The December average maximum was substantially cooler than average at both locations. This cooling was because December was exceptionally stormy, with record rainfall (see Figure 21) (Reference 41) and very high average relative humidity (see Figure 22). April and June at both sites were somewhat warmer than normal. During the late winter and spring, both sites experienced below normal rainfall and relative humidity.

The NWC precipitation and relative humidity distributions are similar to those at Edwards AFB for the RESOLVE period except for July and August 1984. During the summer of 1984, unusual thunderstorms occurred over the Sierra Nevada. These storms affected the NWC site but not the Edwards AFB site.

Upper-air temperatures are an indication of the stability of the atmosphere. Typically, temperatures above about 20°C at 850 mb (about 1500 m/ms 1) in the summer are associated with high photochemical pollution potential in Southern California. The average monthly 850 mb temperatures from the Edwards AFB and Vandenberg AFB soundings during RESOLVE are plotted in Figure 23, along with the long-term averages. (Vandenberg AFB is located on the coast, west of the RESOLVE study area.) Generally, significantly warmer 850 mb temperatures than the rest of the year occur from June through September. These months can be considered a "summer" regime with the greatest potential for photochemical pollutants.

For the RESOLVE period, the 850 mb temperatures for most months at both sites were reasonably close to the long-term averages. However, the October through December 1984 period averaged about 4 degrees cooler than normal, reflecting increased frontal system activity during that period. The May 1985 850 mb temperatures at Edwards AFB were over 5 degrees higher than normal, making the air in the desert more stable than usual during that month.

4.2.2 Winds and Flow Patterns

The predominant flow patterns for winter and summer are shown in Figures 11 to 14. Annual wind roses for the RESOLVE sites are shown in Figure 24. The positions of the roses on the page reflect their geographic locations. The predominant wind directions in Figure 24 are consistent with the summer flow patterns in Figures 12 and 14, and with the general winter afternoon flows in Figures 11 and 13.

Long-term monthly average wind data from Edwards AFB (Reference 31) and NWC (Reference 41) are compared with data obtained during the RESOLVE year in Figures 25 and 26, respectively. During RESOLVE, the wind directions in all months at both sites were quite close to their long-term means, but a slight variation toward more southerly flow is evident for a few months at both sites. This more southerly flow might have slightly increased the effect of the Los Angeles basin compared to the San Joaquin Valley at Edwards AFB during RESOLVE.
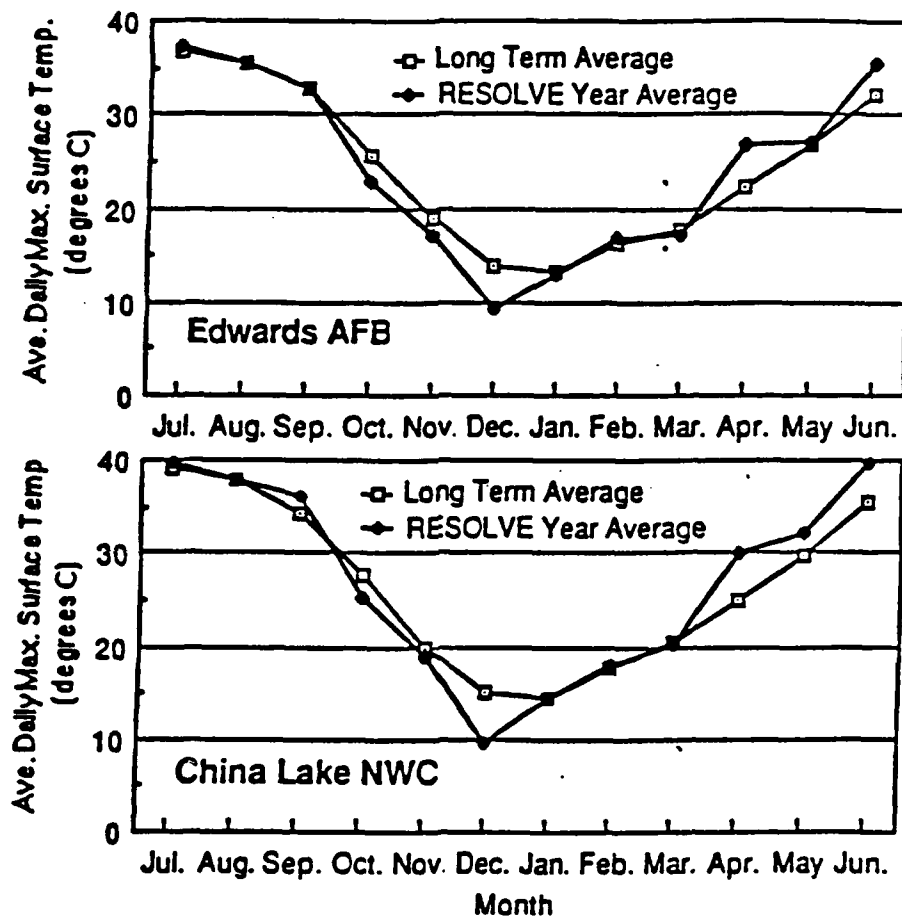
FIGURE 20. Comparison of Long-Term and RESOLVE Year Average Daily Maximum Surface Temperatures at Edwards AFB and NWC.
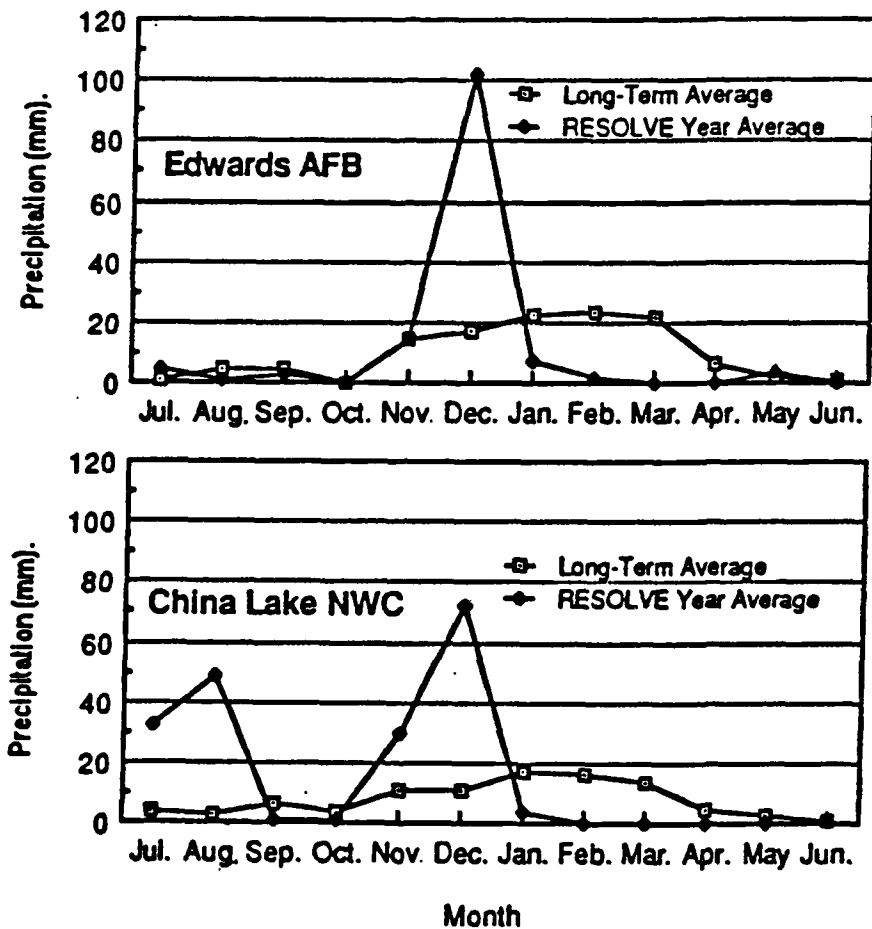
FIGURE 21. Comparison of Long-Term and RESOLVE Year
Precipitation at Edwards AFB and NWC.
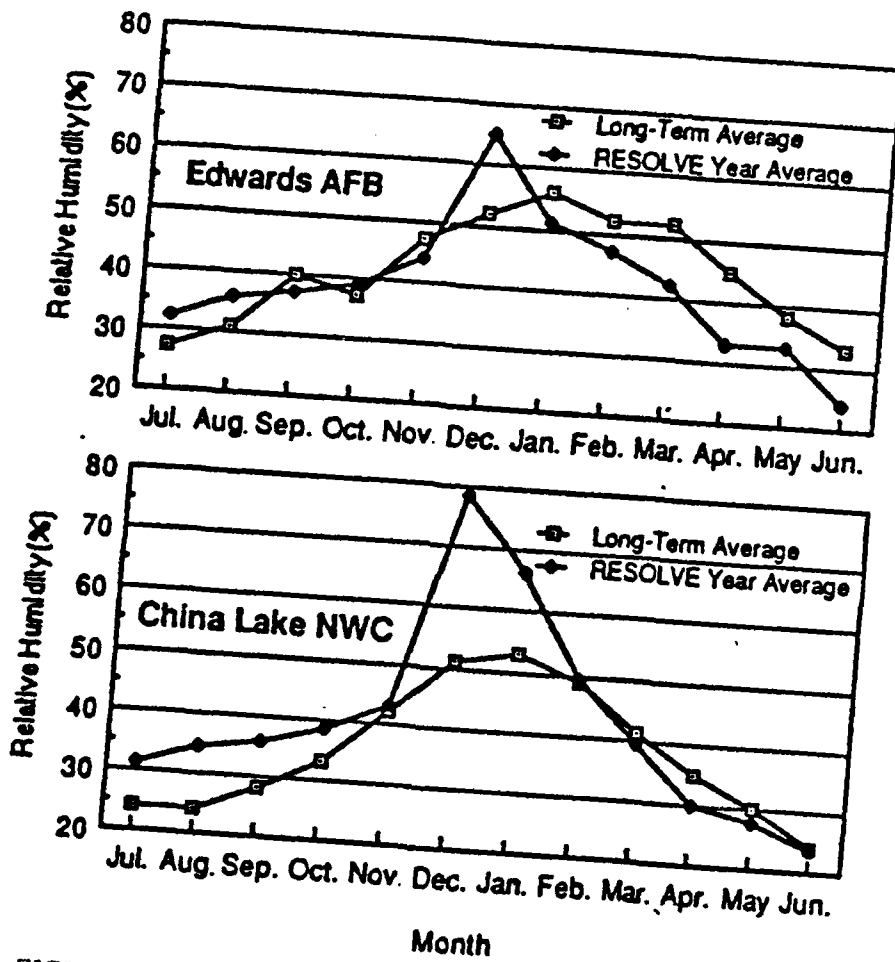
FIGURE 22. Comparison of Long-Term and RESOLVE Year Relative Humidity at Edwards AFB and NWC. Long-term and RESOLVE measurements at NWC are from different measurement stations.
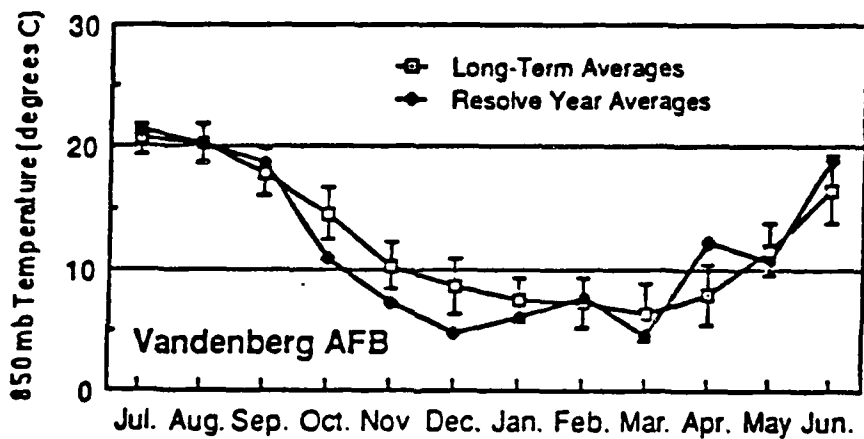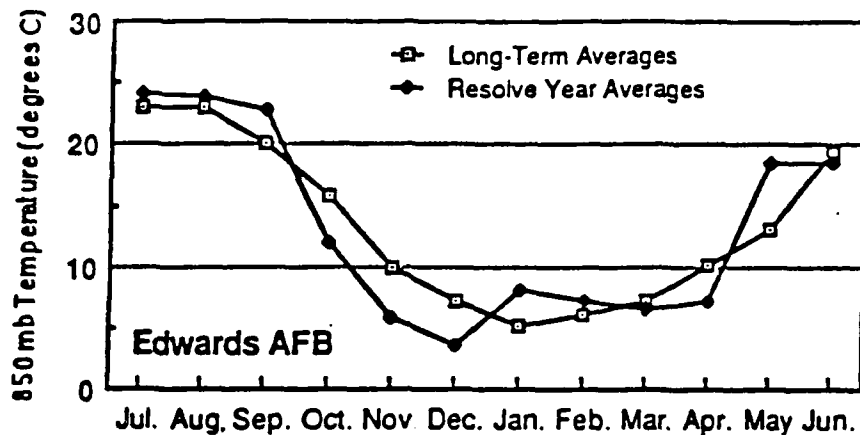
FIGURE 23. Comparison of Long-Term and RESOLVE Year 850 mb Temperatures From the Edwards AFB and Vandenberg AFB Soundings (References 32, 42 and 43). Error bars for Vandenberg AFB are 1 standard deviation of 30-year monthly averages.
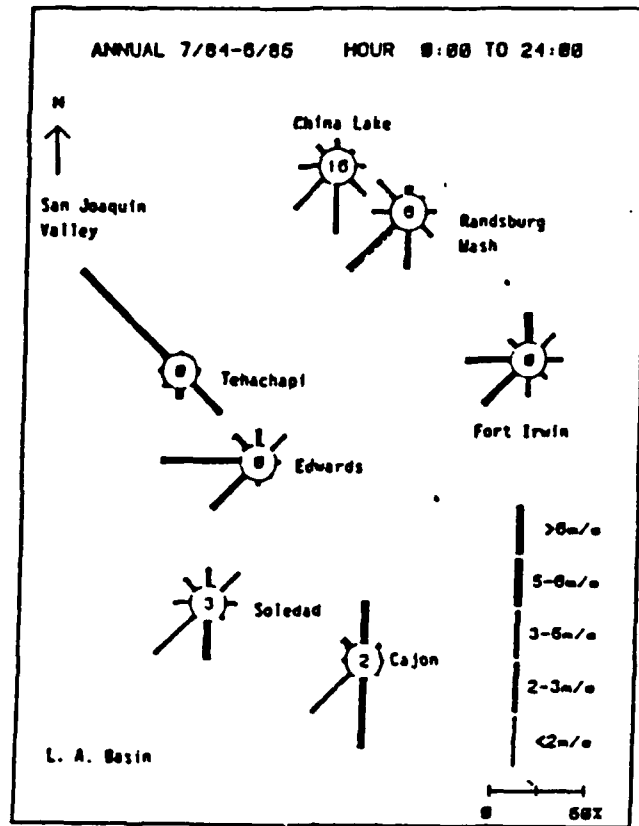
FIGURE 24. Annual Surface Wind Roses for the RESOLVE Network. Average wind speed for each direction is indicated by the bar style; and the percent of hours with wind in the direction is shown by the length of the bar. The percentages of hours with calm winds are shown in the circles.
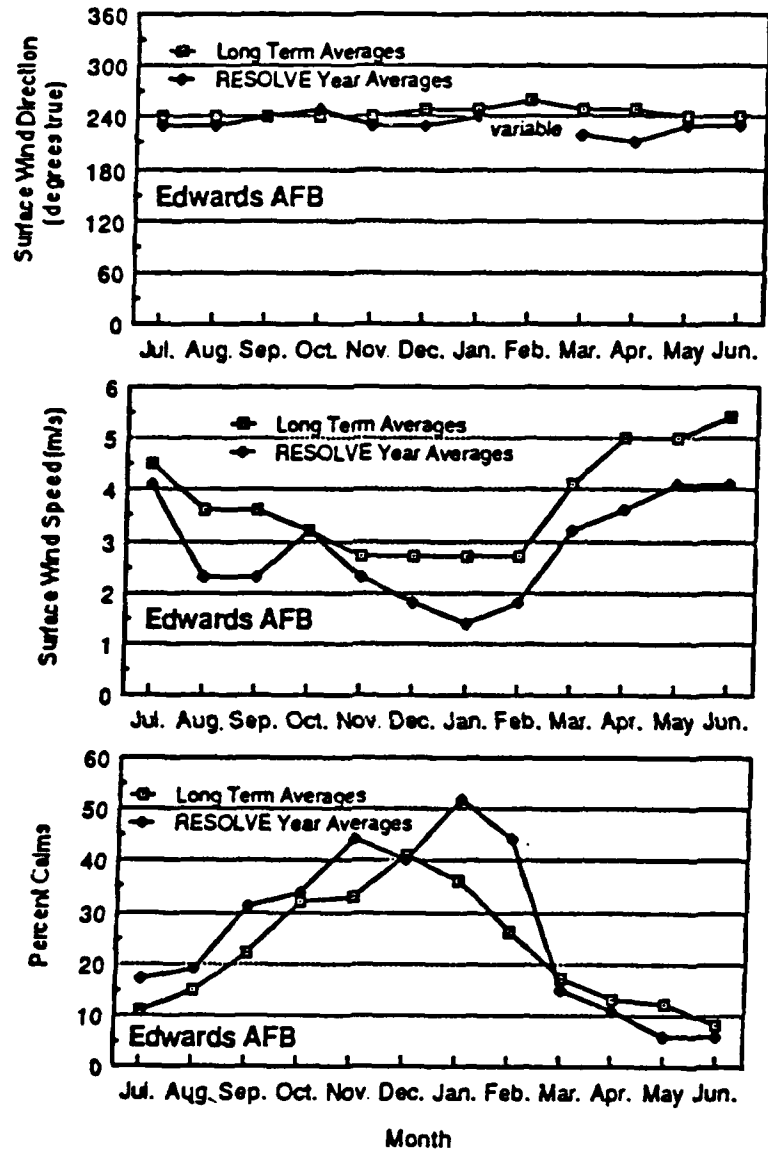
FIGURE 25. Comparison of Long-Term and RESOLVE Year
Surface Winds at Edwards AFB. Median direction and average
speed are shown.
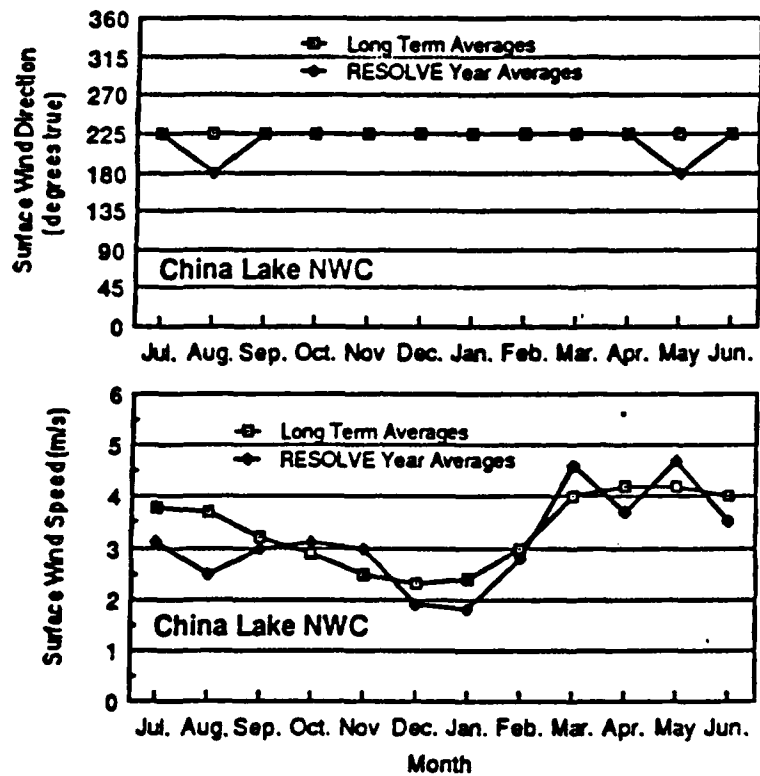
NOTE: No data on RESOLVE year calms were easily available from NWC.

FIGURE 26. Comparison of Long-Term and RESOLVE Year
Surface Winds at NWC. Prevailing direction and average speed
are shown.

The average wind speeds at NWC during RESOLVE were representative of normal
condition.. At Edwards AFB, however, the wind speeds appeared to be lower than normal
during RESOLVE, and the percentage of calms reported was higher. These differences are
not consistent with the data from NWC, and we do not have an obvious explanation for
them. It is possible that the differences are an artifact of instrument placement or
instrument type. Small changes in instrument placement can cause large changes in speed
and direction. (An example of substantial differences between nearby sites can be seen by
comparing the Edwards AFB airfield data in Figure 25 with the RESOLVE site data in
Figure 24. However, the weather office at Edwards AFB says that the sensor type and
placement has remained consistent for the period of record.)

4.2.3 Visual Range

To examine the climatological representativeness of visibility conditions during
RESOLVE, nephelometer data obtained by a long-term DOD monitor adjacent to the
RESOLVE NWC site are plotted in Figure 27. Monthly averages of scattering coefficient for
1979 through 1985 at the site are compared to monthly averages from the same site during
the RESOLVE year. With the exception of December 1984, light scattering during
RESOLVE was similar to, but slightly greater than, the longer term data. The base-year
mean is 7% higher than the long-term mean. The December average during RESOLVE was

47 Mm⁻¹ compared to the 7-year average of 34 Mm⁻¹. December 1984 was the wettest December on record at NWC, and the high Bscat levels are probably related to the high relative humidity and fog recorded that month.
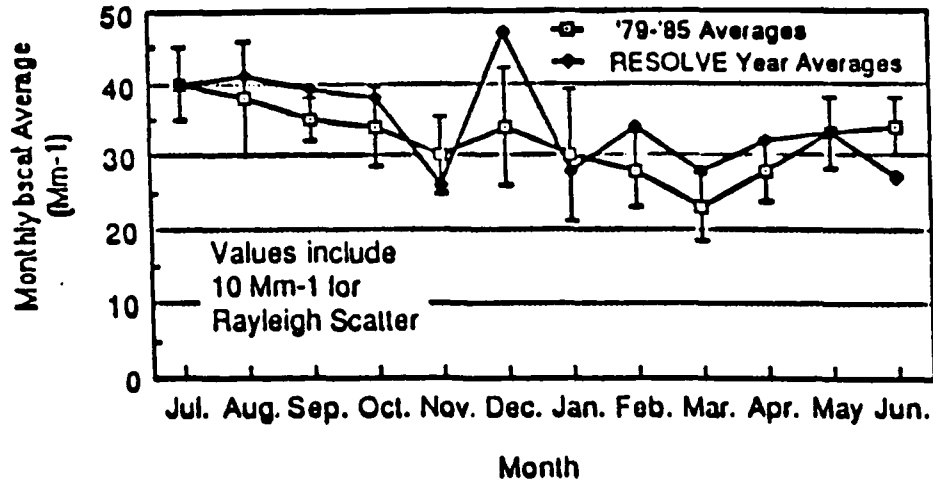
FIGURE 27. Comparison of 1979 to 1985 Average Bscat Data at NWC Range Trailer With RESOLVE Year Monthly Averages. Error bars are 1 standard deviation of the 7-year monthly averages.

4.2.4 Summary of Climatological Representativeness

Earlier, we compared the RESOLVE year to climatic norms for several meteorological indicators. In general, surface temperature, upper air temperature, and wind-flow patterns during the RESOLVE year were reasonably normal. In contrast, the rainfall amounts and, in some months, the relative humidity were quite different from long-term averages, especially in July 1984, which had near-record rain at NWC, and December 1984, which had record precipitation. Rainfall, however, is highly variable from year to year, and rain typically falls during short storm periods in any one year. It is not unusual to have the rainfall concentrated during a few months, and summer rains are also not rare.

To help assess the representativeness of the study period, it is useful to know the standard deviations of the long-term averages. For the parameters discussed in the first three sections of this chapter, we were able to determine the standard deviations only for 850 mb temperature at Vandenberg AFB and Bscat at NWC. For these parameters, the RESOLVE year months were generally within 1 standard deviation, and always within 2 standard deviations, of the long-term monthly averages. Thus, except for the heavy rainfall in 2 months, it does not appear that the RESOLVE year was an outlier.

For a visibility study, the major climatological norm of interest is the one for Bscat. The nephelometer monthly averages at NWC were similar to their 7-year averages for all months except December 1984. The conclusions about visibility, drawn from the RESOLVE data, should generally be representative, although some caution should be exercised in interpreting data from December 1984, especially at NWC.

4.3 RELATIONSHIP OF VISIBILITY TO METEOROLOGY

Within any season, visibility fluctuates substantially day to day because of meteorological variations. In this section, we examine the relationships between visibility and several meteorological parameters to identify meteorological situations that produce degraded visibility in the desert and to develop hypotheses about the sources of visibility degrading aerosols.

4.3.1 Synoptic Conditions Leading to Visibility Degradation

A synoptic typing scheme developed for use in the California Central Valley (Reference 44) was applied for each day of the 2-year RESOLVE nephelometer record. It was found that low visibility in the desert occurs primarily under two types of synoptic patterns, but the occurrence of these patterns does not always result in low visibility. Certain mesoscale features that happen frequently on low-visibility days during both synoptic patterns were also identified. These features are onshore flow below about 3000 m/ms 1 and a deep enough mixing layer to allow marine air to flow through the passes or over the mountains into the desert. Examples of the two synoptic conditions, under which similar mesoscale transport of pollutants from the upwind basins to the desert can occur, are shown in Figures 28A and 28B. The thermal low-pressure condition in Figure 28A is frequent in the summer, while the prefrontal condition in Figure 28B typically occurs in other seasons.

Another condition that occasionally leads to degraded visibility in the desert is a strong pressure gradient aligned with the north-south desert valleys (see Figure 28C). This condition generates strong northerly winds that entrain and transport dust from dry lake beds.

4.3.2 Surface Flow Patterns Related to High Bscat

Wind roses for the days from August 1983 through August 1985 that had the 25% highest and 25% lowest maximum hourly Bscat for each RESOLVE site are shown in Figure 29. The wind roses for the days of highest Bscat (see Figure 29a) show that the winds on the days of worst visibility are similar to the annual average winds shown in Figure 24, and reflect the prevailing transport from the Los Angeles basin and San Joaquin Valley. Wind roses for the best visibility days (see Figure 29b) are significantly different, however, and reflect the desert origin of the air on clean days. The high percentage of calms at NWC in Figure 29a is indicative of a potential contribution to visibility impairment from local sources on the worst days. The reduction in the percent of flow from the southwest at Edwards AFB on the best days is indicative of the reduced importance of the Los Angeles basin on clean days at that site.

4.3.3 Relationship of Diurnal Air-Quality Variations to Flow Patterns

The diurnal patterns of light scattering coefficient on best-case and worst-case days at the RESOLVE pass and receptor sites are presented in Figures 30 and 31. These figures are consistent with the streamlines in Figures 11 and 12 as well as with the wind roses for the high Bscat days in Figure 29a.

Figure 30 shows that, on hazy (high Bscat) days, the Bscat values in the passes peak in the evening. This is consistent with typical ventilation patterns of the upwind basins (References 7, 35, and 45). Figure 31 shows that, again on hazy days, the maximum Bscat

FIGURE 28. Example of Synoptic Conditions Leading to Degraded Visibility in the California Deserts.

LEGEND

H, L ...... Surface pressure centers

⊤ ...... Surface fronts

━━●━━ ...... Surface isobars (every 4 mb)

━━━━ ...... Flow lines at 500 mb

Surface   500 mb

(A) Thermal Low (8/20/84)

(B) Prefrontal (2/07/85)

(C) Blowing Dust (2/20/85)
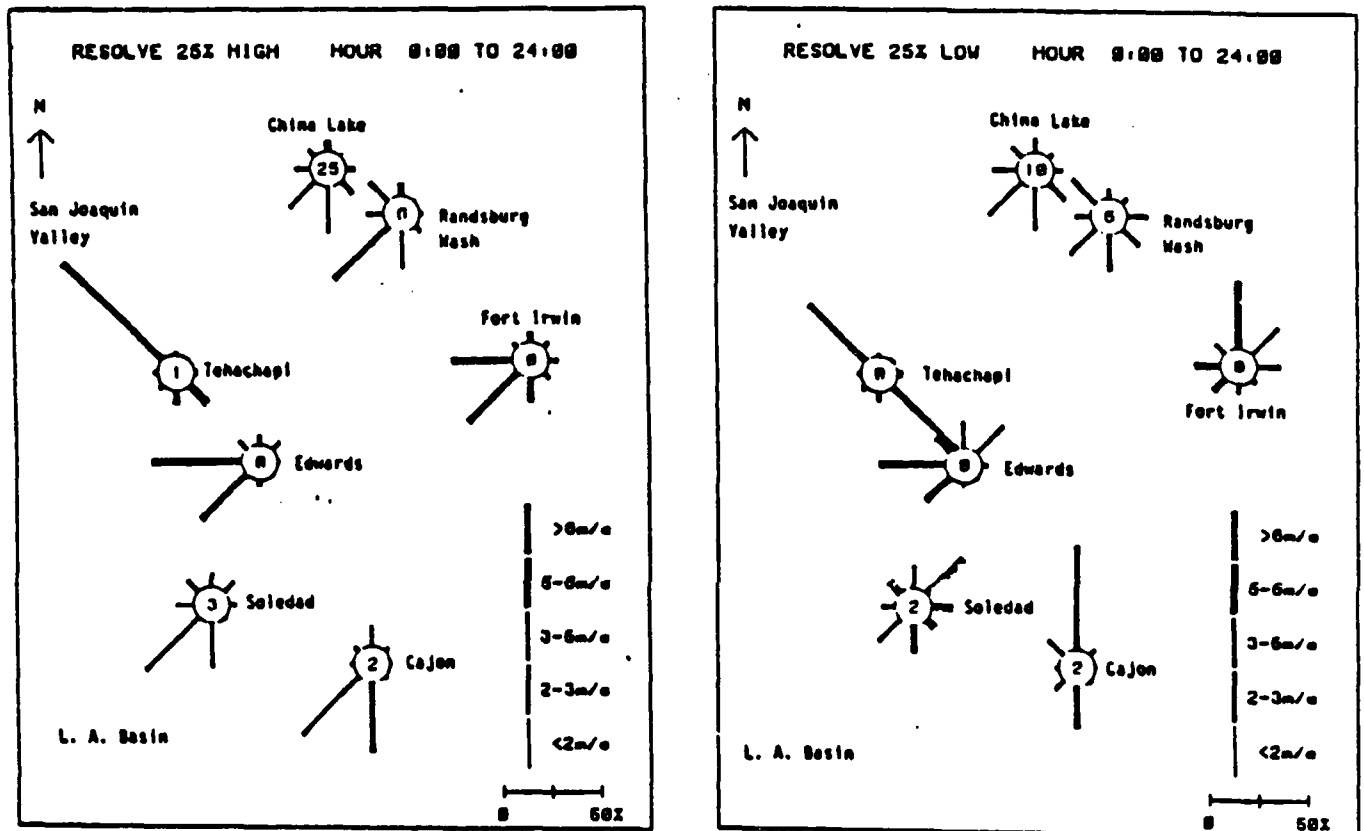
(a) Highest Bscat.

(b) Lowest Bscat

FIGURE 29. Twenty-Four-Hour Surface Wind Roses for the RESOLVE Network for the Days of the 25% Highest (a) and Lowest (b) Daily Maximum Bscat Values at Each Site. Average wind speed for each direction is indicated by the bar style, and percent of hours with wind in the direction is shown by the length of the bar. The percentages of hours with calm winds are shown in the circles.
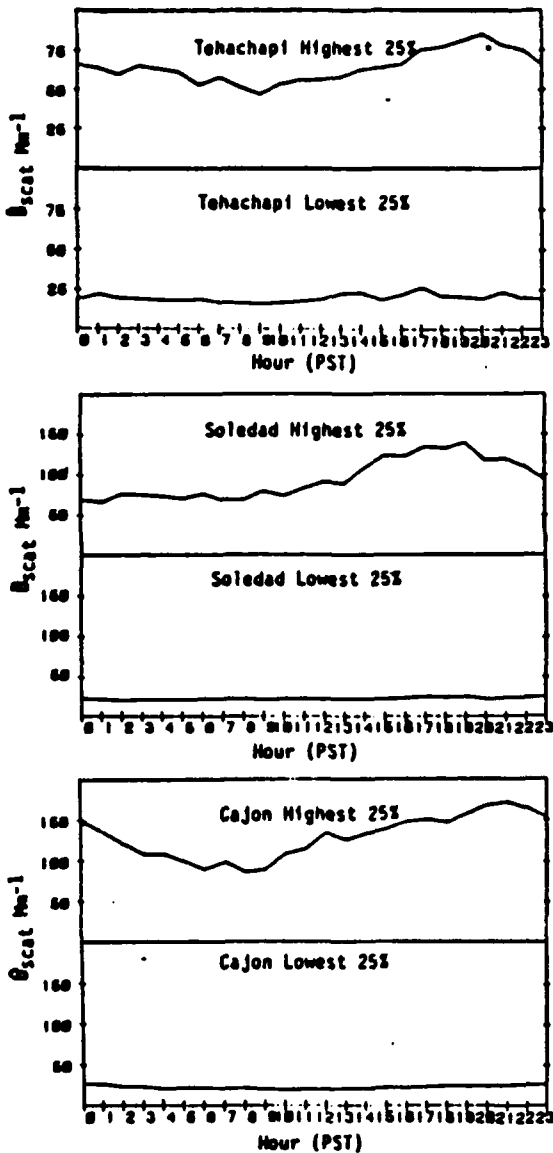
FIGURE 30. Diurnal Average Bscat for
RESOLVE Sampling Period for 25%
Highest and 25% Lowest Daily Average
Bscat at RESOLVE Pass Sites.
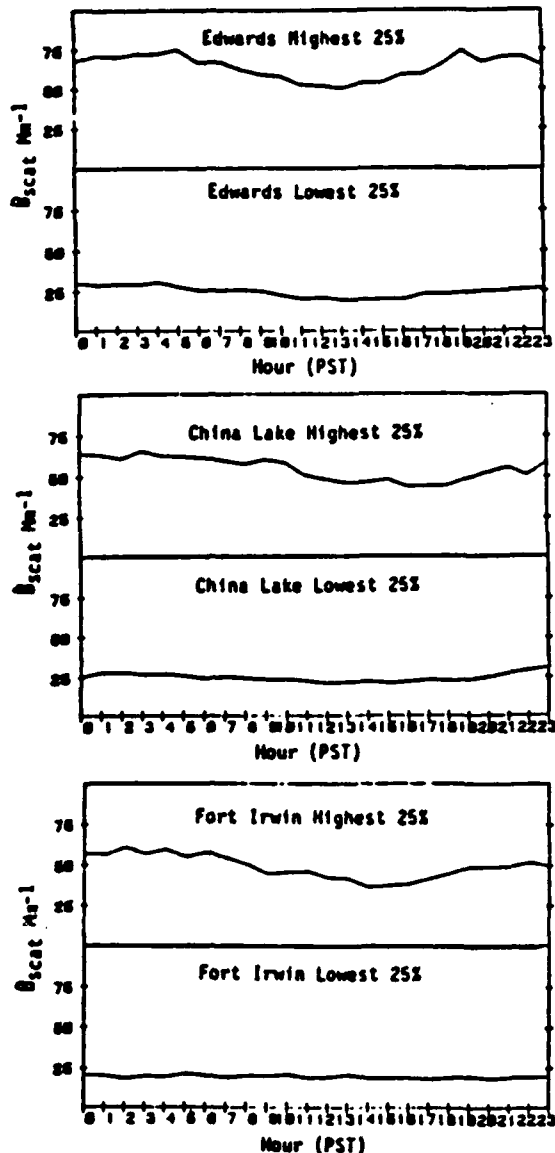
FIGURE 31. Diurnal Average Bscat for
RESOLVE Sampling Period for 25%
Bscat at Highest and 25% Lowest Daily
Average RESOLVE Receptor Sites.

values at the receptor sites occur during the late night and early morning. This phenomena is consistent both with transport of the evening peaks from the upwind passes and with the added early morning contribution of local sources (such as wood burning and traffic in the residential areas near NWC). For clean days, the diurnal variations are much less pronounced, or even absent, suggesting that different transport processes may be occurring on those days.

4.3.4 Relationship of Mean Bscat to Wind Speed

Figures 32 and 33 display the relationship of 24-hour mean Bscat to wind speed at the pass and receptor sites, respectively. Three types of relationships are apparent in the figures. The Soledad and Cajon Pass sites are on the desert sides of the passes. For these sites, Bscat increases with wind speeds up to 4 or 5 m/s and then decreases with high wind speeds. This phenomenon can be interpreted as follows. At very low speeds, Bscat is low because the effects of transport are minimal and because local sources are evidently unimportant. At slightly higher speeds, the impact of the Los Angeles basin becomes more apparent. At still higher speeds, the decrease in Bscat is probably due to better ventilation related to the higher winds.

A second type of pattern is a decrease in Bscat as speed increases from calm to relatively low speeds, followed by a subsequent increase with wind speed. This phenomen occurs at Edwards, NWC, Randsburg Wash, and Tehachapi. The initial decrease may be from a dilution of emissio..s from local sources (however, it is not obvious what the local sources at Tehachapi are). The subsequent increases with speed might be attributed to transport of pollutants from other locations, and to wind-blown dust at higher speeds.

At Fort Irwin NTC, the trend is a steady increase with wind speed suggesting a lack of local sources.

4.3.5 Transport Direction for Days of High and Low Bscat

To assess the relative frequency of occurrence of air mass transport into the desert from the various upwind regions, we examined the 850 mb winds measured in the morning at Edwards AFB. Edwards AFB is in flat terrain at the center of the RESOLVE monitoring region, so the winds there should be reasonably representative of the transport in the region. The morning soundings (between midnight and noon) were chosen to be representative of synoptically driven transport without distortion by afternoon thermally driven flows. The 850 mb height was chosen to be above local nighttime drainage flows but still representative of the afternoon mixed layer.

The frequencies and average speeds of the 850 mb winds for each direction are shown in Figure 34. It is evident that, on an annual basis, the prevailing boundary layer flow is from the southwest through west. However, in the winter months, the flow is bimodal with about equal frequency from the northeast and west.

Figure 35 presents similar frequency distributions of the Edwards AFB 850 mb winds for the days with the 25% highest and 25% lowest 24-hour average Bscat at the three RESOLVE receptor sites. From Figure 35, it is evident that the days of worst visibility at the receptor sites are dominated by flow from the southwest, and the days of best visibility typically occur with flow from the northeast. This distribution is consistent with a strong contribution to the desert Bscat from the San Joaquin Valley and/or Los Angeles basin. Then, the flow on 61% of all days originates in these regions. In contrast, 77% of the worst-case days and only 26% of the best-case days at Edwards AFB have flow from these regions. The results are similar for the other receptor sites.
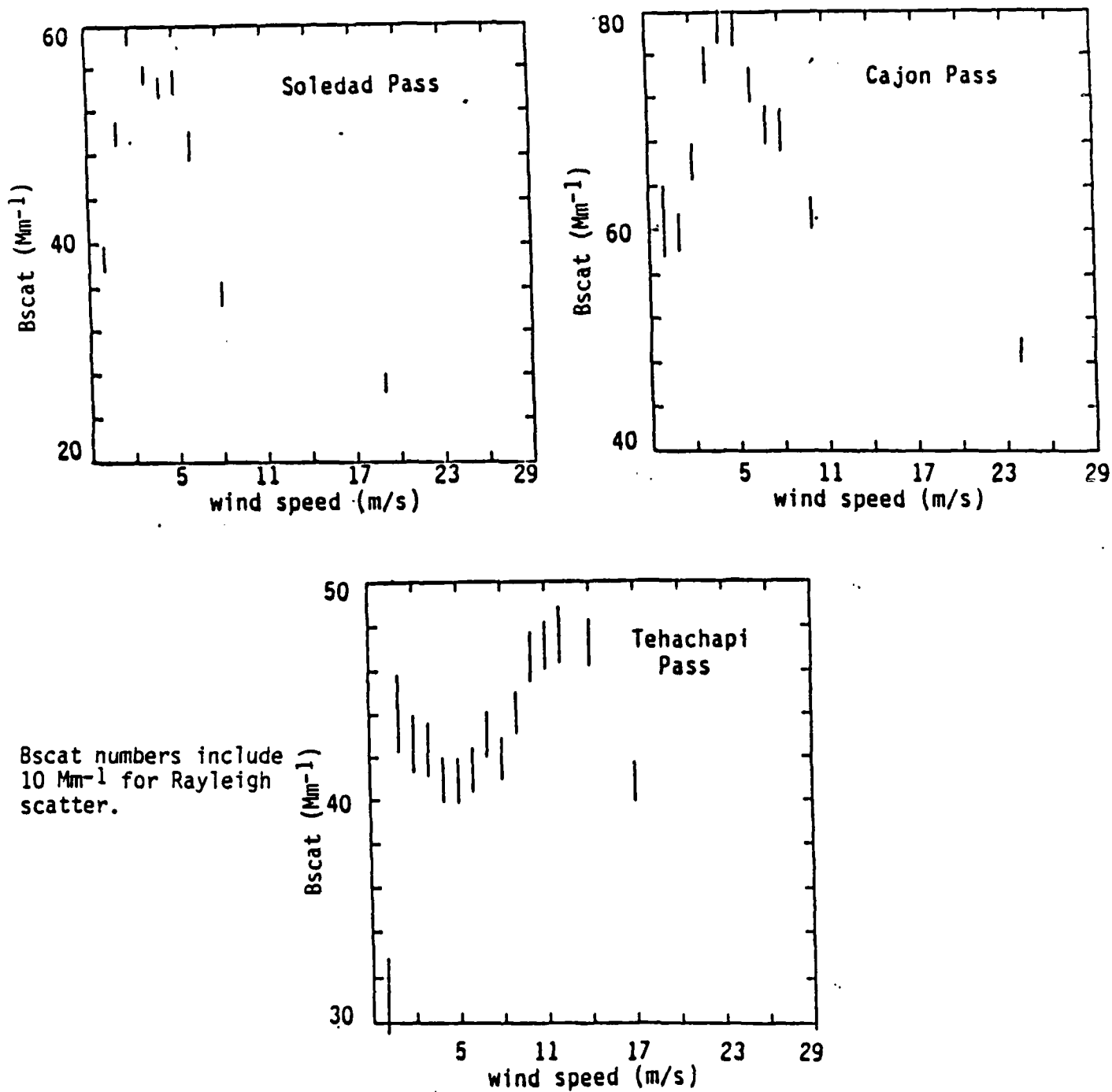
FIGURE 32. Mean Bscat for Each Wind Speed Category at the Pass Sites. Error bars indicate ±1 standard deviation of Bscat. Note that Bscat scales vary between plots.
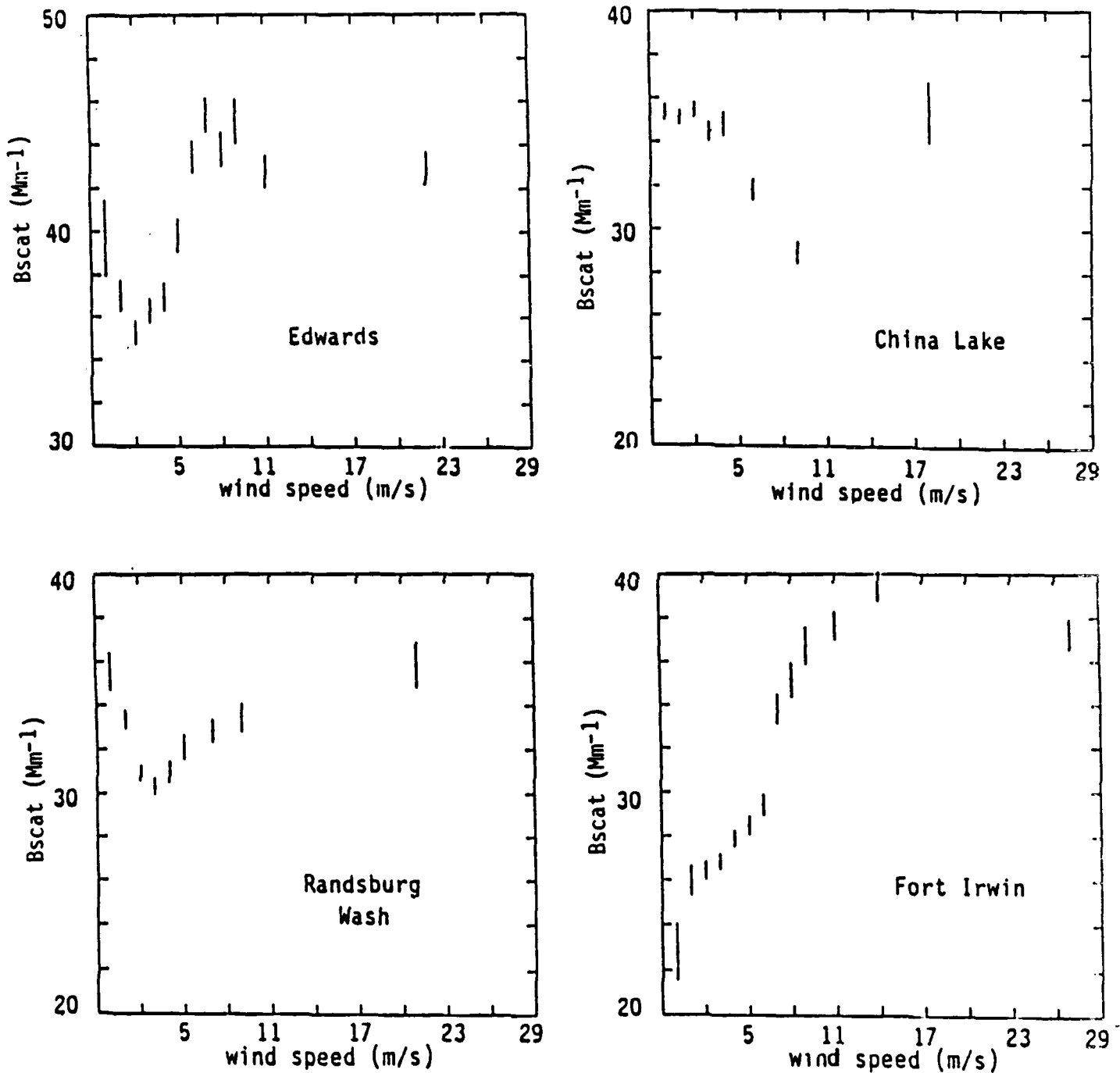
Bscat numbers include 10 Mm^{-1} for Rayleigh scatter

FIGURE 33. Mean Bscat for Each Wind Speed Category at the Receptor Sites. Error bars indicate ±1 standard deviation of Bscat. Note that Bscat scales vary between plots.
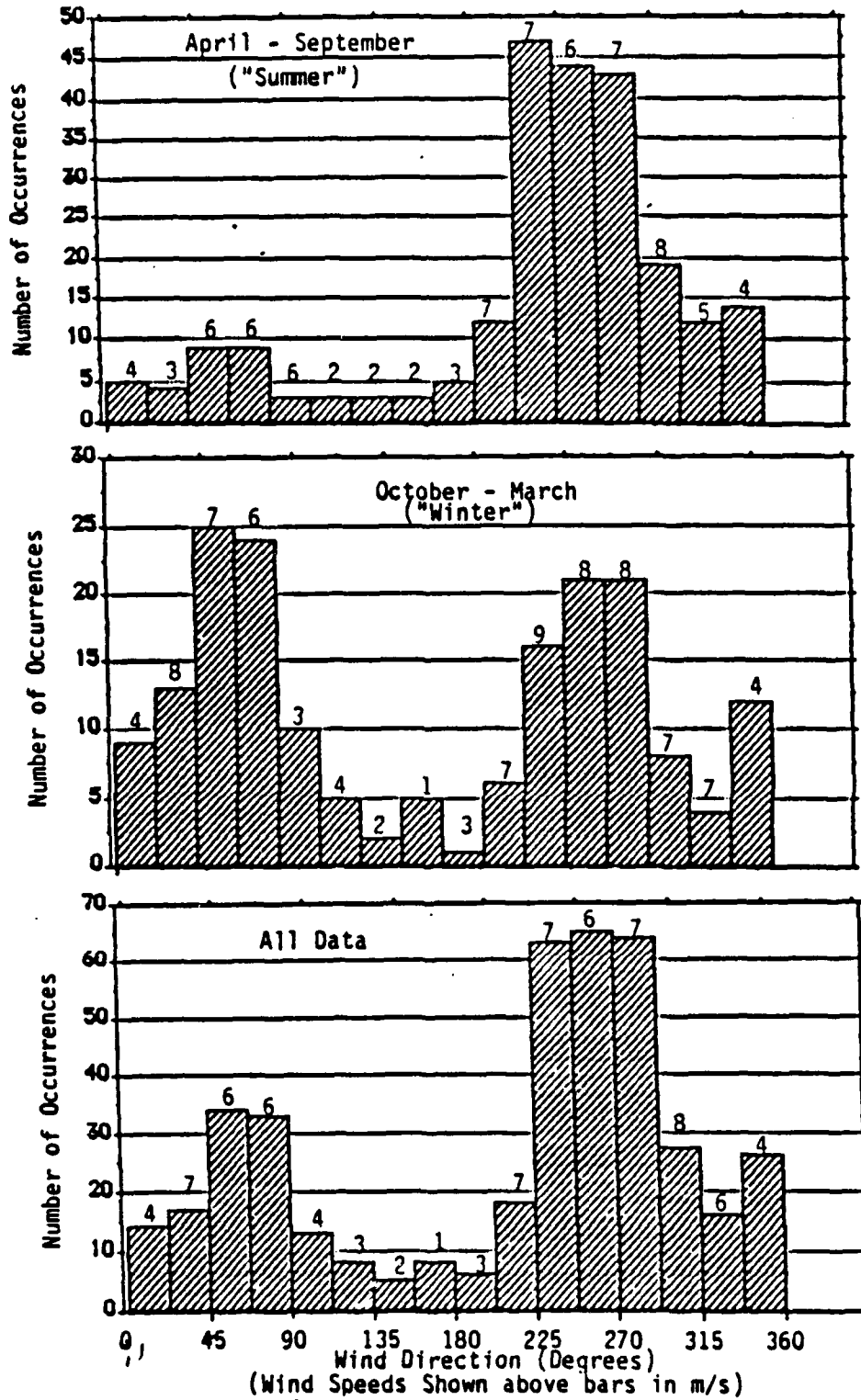
FIGURE 34. Frequency and Average Speed of Edwards AFB 850
mb Winds for Each Direction for AM Soundings. Data are from
August 1983 through July 1985. Note that 417 days of soundings
are available. The missing days include February through April
1984 plus other randomly distributed days.
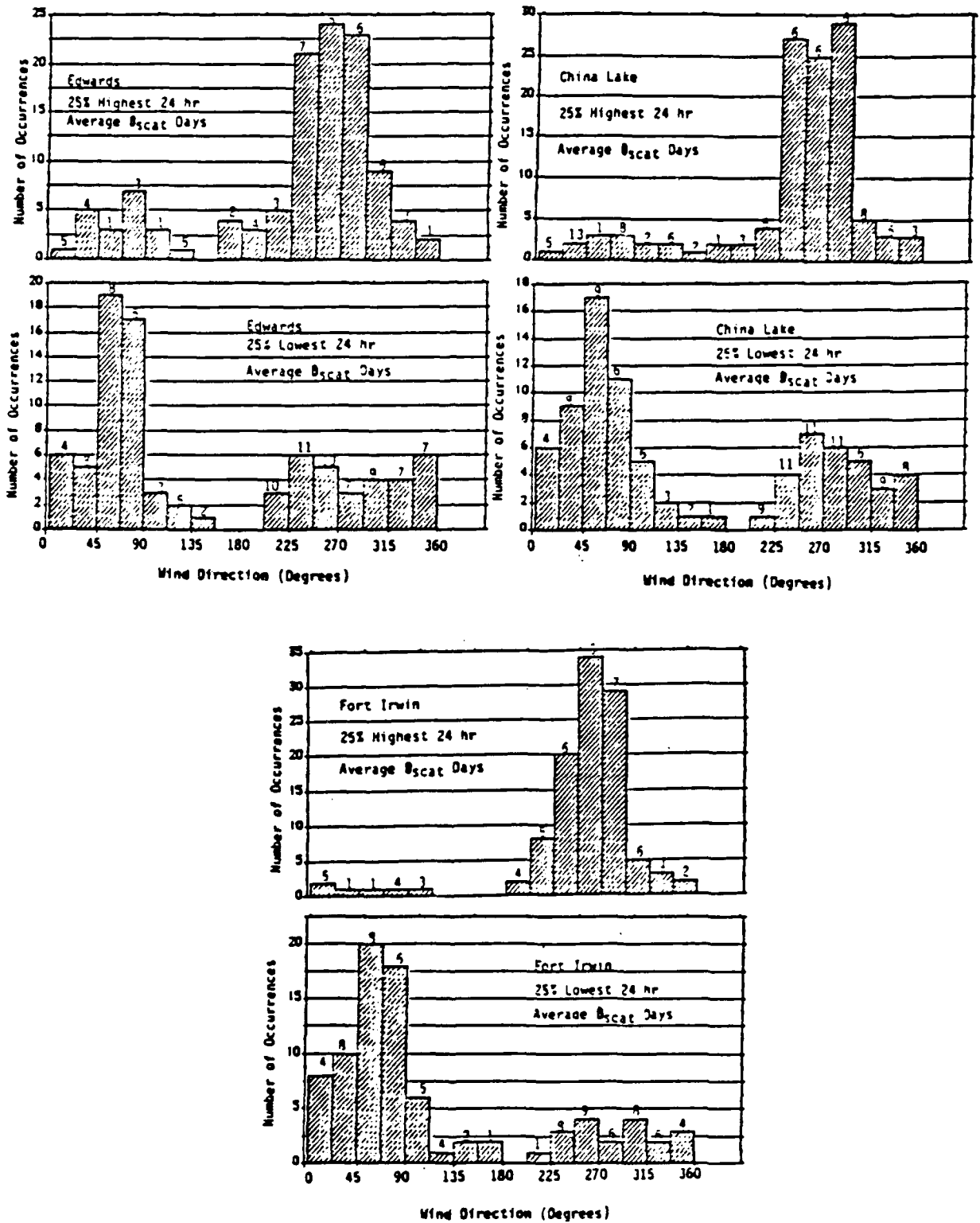
FIGURE 35. Frequency and Average Speed of Edwards AFB 850 mb Winds for Each Direction for AM Soundings on the 25% Highest and 25% Lowest 24-Hour Bscat Days at Edwards AFB, NWC, and Fort Irwin NTC. Data base is the same as for Figure 34.

Some exceptions exist to these generalizations. In Figure 35, on days of high Bscat with winds from the north through east, the 850 mb winds are often very light, especially in winter. These stagnation conditions may allow the buildup of local desert emissions and may represent a significant, though infrequent, contribution to visibility impairment by local emissions. On a few other of the low-visibility days with northerly winds, the wind speeds were quite high (above 15 m/s), indicating visibility impairment due to wind-blown dust. This condition occurred only a few days per year, however. From Figure 35, it is also evident that, when clean days occurred with winds from the southwest, the wind speeds were high, suggesting possible frontal conditions with good mixing and ventilation.

4.4 DEFINITION OF FLOW REGIMES

In analyzing the contributions of various regions to visibility degradation at the RESOLVE desert sites, it is useful to have a daily indicator of air mass origin for each site. The simplest approach is to use the direction of the upper winds in the region as an indicator of air mass movement. The most easily accessible and appropriate parameter is the morning 850 mb wind at Edwards AFB.

The definitions of the source regions and associated wind sectors are presented in Table 12. At each desert site, the days are divided into five classes, each representing potential transport from a specific source region.

It is interesting to assess the percent of variance that can be explained by the classes for various measures of aerosol mass, extinction, and composition. In general, the classes are not very successful at explaining the variance in air quality. About 7 to 20% of the variance at Edwards AFB and NWC and 20 to 40% of the variance at Fort Irwin NTC is explained by the classification scheme. This result is not unexpected, however, since the purpose of the scheme is to assess transport directions, not aerosol concentrations.

TABLE 12. Definition of Wind-Flow Classes for Desert Sites.

Class	Wind direction sectors for each site			
	Edwards AFB	NWC	Randsburg Wash	Fort Irwin NTC
Northern desert sources and local (includes Searles Valley at Randsburg Wash)	315° – 67.5°	315° – 45°	315° – 22.5°	315° – 45°
Eastern desert sources and local (includes Searles Valley at NWC and Imperial Valley at Fort Irwin)	67.5° – 135°	45° – 135°	22.5° – 135°	45° – 180°
Southern Mojave Desert, Los Angeles basin, and upwind coastal counties (Ventura, Santa Barbara) sources	135° – 247.5°	135° – 225°	135° – 225°	180° – 202.5°
Los Angeles basin, coastal counties, San Joaquin Valley, and western desert sources	247.5° – 270°	225° – 270°	225° – 270°	247.5° – 270°
San Joaquin Valley and western desert sources	270° – 315°	270° – 315°	270° – 315°	270° – 315°

5.0 SPATIAL PATTERNS OF VISIBILITY

The first objective of the RESOLVE program is to characterize baseline visibility in the RESOLVE study region. One of the most important aspects of this objective is to develop an understanding of geographical air-quality patterns.

5.1 AIR-QUALITY MAPS

The most straightforward method of illustrating the spatial features of the RESOLVE data is to plot averages (or other statistics) for each site on a map of the study area. The RESOLVE Annual and Quarterly Data Summary Reports (References 5 and 6) include numerous maps of this type. Figure 36 presents some examples – maps of annual averages for total scattering (particle plus Rayleigh), particle absorption, fine mass, coarse mass, organics, and sulfates. The Data Summary Reports also include tables listing statistical parameters for selected particle and extinction measurements; Table 13 presents some examples for total scattering and particle absorption. Using the data in such tables, it is possible to prepare maps for many statistical parameters.

Figure 36 does reveal some of the more salient spatial features of air quality in the RESOLVE study area. For example, it is obvious that the worst visual air quality occurs along the southern edge of the study area (at the pass sites near the Los Angeles basin), and that the best visual air quality occurs in the northeastern part of the study area. However, the maps of Figure 36 are not really satisfactory in terms of giving a comprehensive and vivid picture of spatial air-quality patterns.

To obtain a better picture of visual air quality in and around the RESOLVE study region, the RESOLVE data were combined with data from other sources. Most of the other data were based on airport visibility observations (References 40 and 46), although we also used nephelometer recordings from Death Valley (Reference 47) and Searles Valley (Reference 48). In combining the data sets, the most significant step was to calibrate the airport data to the more accurate RESOLVE instrumental observations for total extinction. The airport data are not equivalent to the RESOLVE data for at least the following three reasons.

1. Airport visibility readings depend on the properties of the observer, the target, and the illumination conditions. The airport readings generally correspond to an observer contrast threshold of at least 5% (i.e., a Kischmeider constant at least 1.3 times smaller than the constant for a 2% contrast threshold).

2. The airport data taken from the literature represent median extinction levels, not average extinction levels.

3. The published airport data correspond to the periods 1977 to 1979 in Los Angeles and 1974 to 1976 at the other California sites, and do not correspond to the RESOLVE study period.

The calibration factor for the airport data was derived by comparing the RESOLVE data to nearby airport visibilities. We found that median airport visual range should be multiplied by a factor of 1.4 to be equivalent to a visual range based on average RESOLVE extinction data (sum of Rayleigh scatter, fine scatter, coarse scatter, NO_2 absorption, and particle absorption). The most significant uncertainty in the resulting visibility map (Figure 37) is whether the spatial patterns of airport visibility in the southern half of
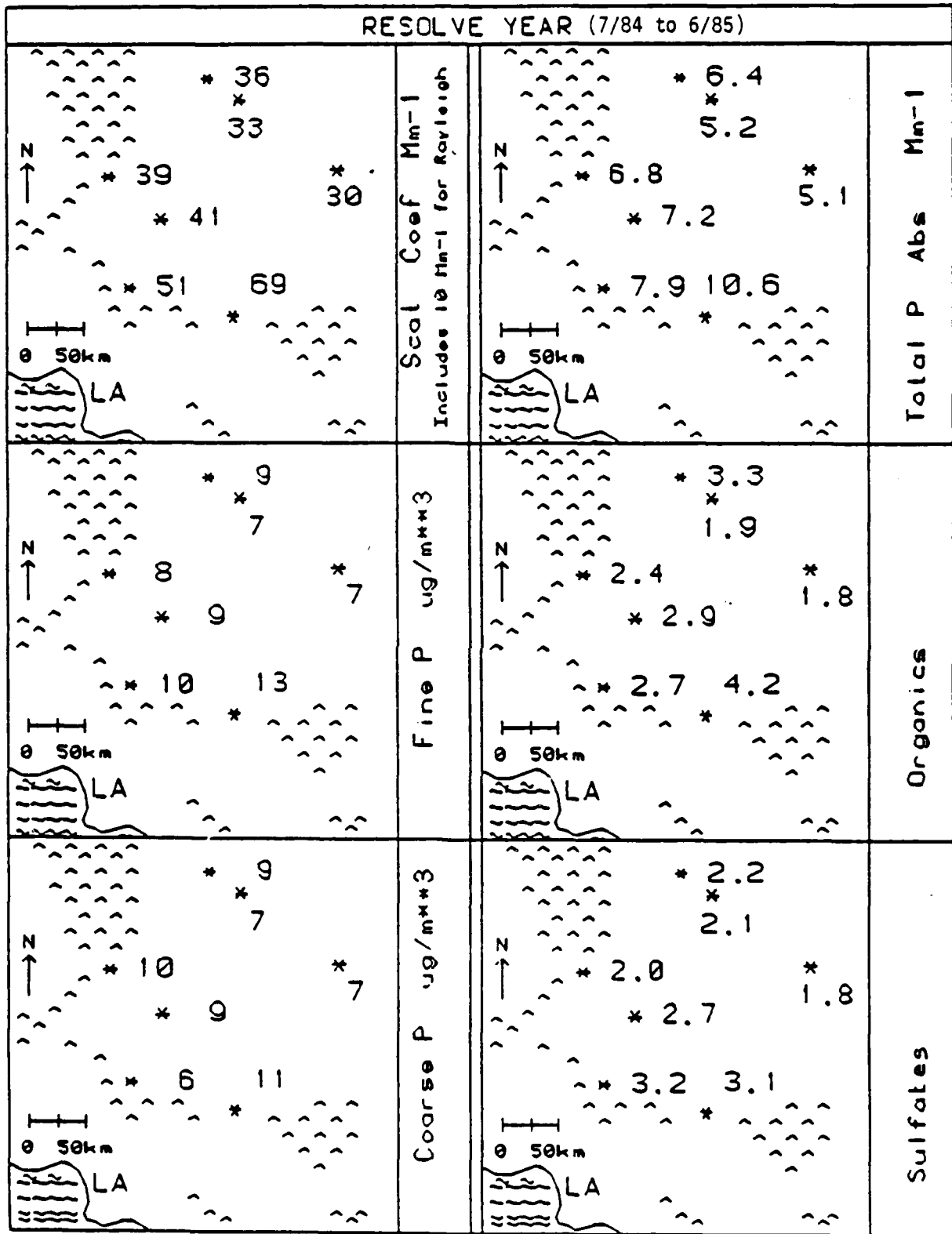
FIGURE 36. Maps of Air Quality for Selected Parameters and Annual Averages Over the RESOLVE Base Year.

TABLE 13. Examples of Tables for Statistical Parameters and Distributions.
RESOLVE year (7/84 to 6/85) — Distribution of data.

Site	No. of obs.	Max	Min	Arithmetic		Geometric		Values equaled or exceeded by stated percentage of observations								
				Mean	Std dev	Mean	Std dev	1	5	10	25	50	75	90	95	99
Hourly nephelometer scattering (Mm⁻¹) (includes 10 Mm⁻¹ for Rayleigh scatter)																
Edwards AFB	8132	318	10	40.9	26.6	34.4	1.8	141	91	73	52	34	23	15	14	12
Fort Irwin	8313	237	10	30.3	19.2	26.0	1.7	100	65	54	38	25	17	13	12	11
NWC	8226	369	6	35.7	21.8	31.4	1.6	125	71	58	43	31	22	17	15	12
Randsburg	8282	396	11	33.2	22.9	28.5	1.7	118	71	57	41	27	19	15	13	12
Tehachapi	7844	373	8	39.0	28.5	31.3	1.9	132	93	74	52	32	18	13	12	10
Soledad	8523	398	10	51.3	44.5	38.7	2.1	217	139	106	65	37	22	15	13	11
Cajon	8541	396	1	69.9	65.7	47.6	2.4	311	212	162	93	45	23	15	13	11
Daily nephelometer scattering (Mm⁻¹) (includes 10 Mm⁻¹ for Rayleigh scatter)																
Edwards AFB	356	167	13	41.2	19.9	37.0	1.6	105	81	65	51	39	29	19	16	13
Fort Irwin	363	91	11	30.3	14.1	27.3	1.6	75	56	51	39	28	19	14	13	11
NWC	358	110	14	35.7	15.1	33.2	1.5	95	62	52	43	33	26	21	19	15
Randsburg	355	148	12	33.2	16.3	30.0	1.6	90	62	52	41	31	22	16	15	13
Tehachapi	343	111	10	38.8	19.9	33.6	1.7	91	78	67	51	38	21	15	13	12
Soledad	365	228	12	51.2	30.9	43.0	1.8	137	107	92	69	44	29	17	15	13
Cajon	365	275	12	70.4	44.1	56.1	2.1	184	147	134	98	65	32	18	15	12
Daily total particle absorption (Mm⁻¹)																
Edwards AFB	256	14	1	7.2	2.6	6.6	1.5	13	11	10	9	7	5	4	3	2
Fort Irwin	246	13	0	5.1	2.5	4.4	1.9	12	9	8	7	5	3	2	1	0
NWC	228	14	1	6.4	2.3	5.9	1.5	13	10	9	8	6	5	4	3	2
Randsburg	251	12	0	5.2	2.7	4.1	2.3	11	10	9	7	5	3	2	1	0
Tehachapi	225	16	0	6.8	3.2	5.6	2.0	13	12	11	9	7	4	2	1	0
Soledad	245	16	0	7.9	3.2	6.9	1.8	15	13	12	10	8	6	3	2	0
Cajon	250	19	1	10.6	3.9	9.5	1.7	18	17	15	13	11	9	5	3	2

California have changed substantially from the mid- to late 1970s to the early to mid-1980s. Available data (References 40, 46, 49, and 50) suggest that such changes were probably not large.

In essence, Figure 37 is a more detailed, "blown-up" picture of the California visibility map presented previously as Figure 16 and is also the same as Figure 2, repeated here for the convenience of the reader. The California visibility map shows that two pockets of low visibility exist in the state: the Los Angeles basin and the San Joaquin Valley. Trijonis (Reference 40) demonstrated that these two pockets of low visibility are caused by man-made air-quality variations rather than purely natural factors. Figures 16 and 37 reveal that the RESOLVE study area is in the air-quality gradient associated with those two regions. The shape of the isopleths (i.e., the form of the gradient) suggests that the NWC receptor site is much more affected by the San Joaquin Valley than by the Los Angeles basin. Fort Irwin NTC and Edwards AFB appear to be affected significantly by both source regions. These conclusions agree quite well with the qualitative description of transport relationships found in Section 4.1.2.

NOTES:

- Circled data points represent RESOLVE monitoring data. The entire 2 years of RESOLVE data were used, with nephelometer scattering factored to non-Rayleigh extinction using site-specific RESOLVE base-year relationships and 11 Mm⁻¹ added for Rayleigh scatter.
- Smaller print data points are based on particle-scattering data in and near Searles Valley. The data are factored to total extinction using RESOLVE relationships.
- Other data points are based on median airport data calibrated to RESOLVE data.
- The dashed lines indicate uncertainty in the isopleths near Searles Valley.
- Isopleths near the border of the map are guided by nephelometer data at Death Valley as well as data from other airports in California and Nevada.
- The Beaumont (Banning Pass) value, shown in parentheses, is inconsistent (higher) than surrounding stations. This inconsistency may be because of the high altitude of that site (790 meters) or because of uncertainties associated with the limited visibility markers at that site.

FIGURE 37. Spatial Pattern of Visual Range (for 2% Contrast and Average Extinction Levels) In and Near the RESOLVE Study Area.

5.2 INTERSTATION RELATIONSHIPS

This section examines the degree to which air quality at each site is related to air quality at the other sites. One measure of this commonality is the correlation coefficient between daily average concentrations for each pair of sites. The correlation coefficient indicates the correspondence between high and low concentrations at two sites or, because correlations usually are dominated by the highest concentrations, the correspondence between episode conditions at the two sites. Correlations between sites are not necessarily representative of source/receptor relationships because of lag times in source-to-receptor impacts, and because of potential negative aspects of source/receptor associations (for example, a receptor site being impacted on days when strong transport (and good ventilation) exists at a pass site).

Table 14 presents interstation correlation coefficients for daily averages of particle scattering and particle absorption. All data available from the 2 years of routine monitoring are used to derive the table, so the sample sizes are quite large — around 600 to 700 for Bsp, and 250 to 350 for Bap. The greatest correlations are marked by circles (R > .70) and underlining (R > .60).

Two important features appear in Table 14: (1) All of the stations correlate fairly well, with even the smallest correlation coefficients (NWC versus the Los Angeles pass sites) being about 0.40; (2) the four desert sites generally tend to correlate higher than pass sites versus desert sites or pass sites versus pass sites.

TABLE 14. Interstation Correlation Coefficients for Daily Particle Scattering and Daily Particle Absorption.

Site	Particle scattering						Total absorption					
	EDW	FOR	CHL	RAW	TEH	SOL	EDW	FOR	CHL	RAW	TEH	SOL
EDW												
FOR	(.70)						(.71)					
CHL	.55	59					.60	66				
RAW	.68	(.77)	(.83)				.69	(85)	(.72)			
TEH	.57	51	.43	48			68	61	.55	(73)		
SOL	(.72)	66	.41	52	44		66	59	44	58	67	
CAP	54	58	36	44	45	(73)	59	63	45	63	65	(72)

These two observations indicate that the whole study region, especially the desert part of the study region, tends to have at least some degree of homogeneity in terms of air-quality variations. That the air-quality variations are not perfectly uniform, however, can be appreciated by noting that a correlation of .80 represents only 64% variance explained, and a correlation of .40 represents only 16% variance explained. Among the three key receptor sites (Edwards AFB, Fort Irwin NTC, and NWC) it is NWC that shows the most independence from the other two (i.e., the least correlations). Upon examining the pass sites, we find a salient feature is the high correlation between Soledad and Cajon, indicating that (when the Los Angeles basin ventilates to produce high concentrations at the passes) the ventilation tends to occur at both passes together. Other features are the relatively high correlation between Soledad and Edwards AFB, and the tendency for Cajon to be the pass site least correlated with the desert sites (except Cajon versus Fort Irwin NTC).

Factor analysis was also used to investigate the spatial interrelationships of daily particle scattering among the seven sites. The analysis was segregated into annual (September 1984 to August 1985), quarterly, and monthly data sets. The annual results place all sites into one factor with Edwards AFB, Fort Irwin NTC, and Randsburg Wash having the highest factor loadings. These results are consistent with the discussion of Table 14 and reflect the general correlation of all the sites, especially the desert sites.

The results for quarters 2 and 3 look very similar to those of the annual data set; again all sites fall into 1 factor. Quarters 1 and 4 (fall and winter) divide the sites into 2 factors. In general, factor 1 includes the pass sites, and factor 2 the desert sites. In quarter 4, Edwards AFB could be grouped with either pass or desert sites; and Fort Irwin NTC is grouped with the pass sites.

Factor analysis performed month by month provides 1, 2, or 3 factors depending on the particular month. Site groupings within these factors vary and it is difficult to interpret what the factors actually represent. Table 15 is a summary of the monthly factor analysis and shows how often one site is in the same factor with another. Table 15 shows that NWC, Randsburg Wash, and Fort Irwin NTC are normally in the same factor as Soledad-Cajon, Edwards AFB-Soledad, and Edwards AFB-Randsburg Wash. Also, NWC and Randsburg Wash are not highly correlated with either of the Los Angeles pass sites. All of these results seem consistent with the previous interpretation of Table 14.

TABLE 15. Summary of the Monthly Factor Analyses.

Number of months in which sites occur in the same factor (24 months total).

Site	EDW	FOR	CHL	RAW	TEH	SOL	CAP
EDW							
CHL	15						
FOR	16	18					
RAW	18	21	21				
TEH	15	15	13	13			
SOL	18	8	15	11	13		
CAP	15	11	13	10	13	20	

6.0 TEMPORAL PATTERNS OF VISIBILITY

Two temporal patterns of interest exist: seasonal variations over the time of year and diurnal variations over the time of day.

6.1 SEASONAL VARIATIONS

Figure 38 presents the seasonal pattern for particle scattering at the three receptor sites on a quarterly basis. The average, the best-case tenth percentile, and the worst-case tenth percentile are presented both for hourly averages and daily averages during the entire 2 years of nephelometer monitoring. Incidentally, the observed seasonal patterns in particle scattering are representative of seasonal patterns in total extinction because the seasonal variation in particle absorption closely resembles that of particle scattering.
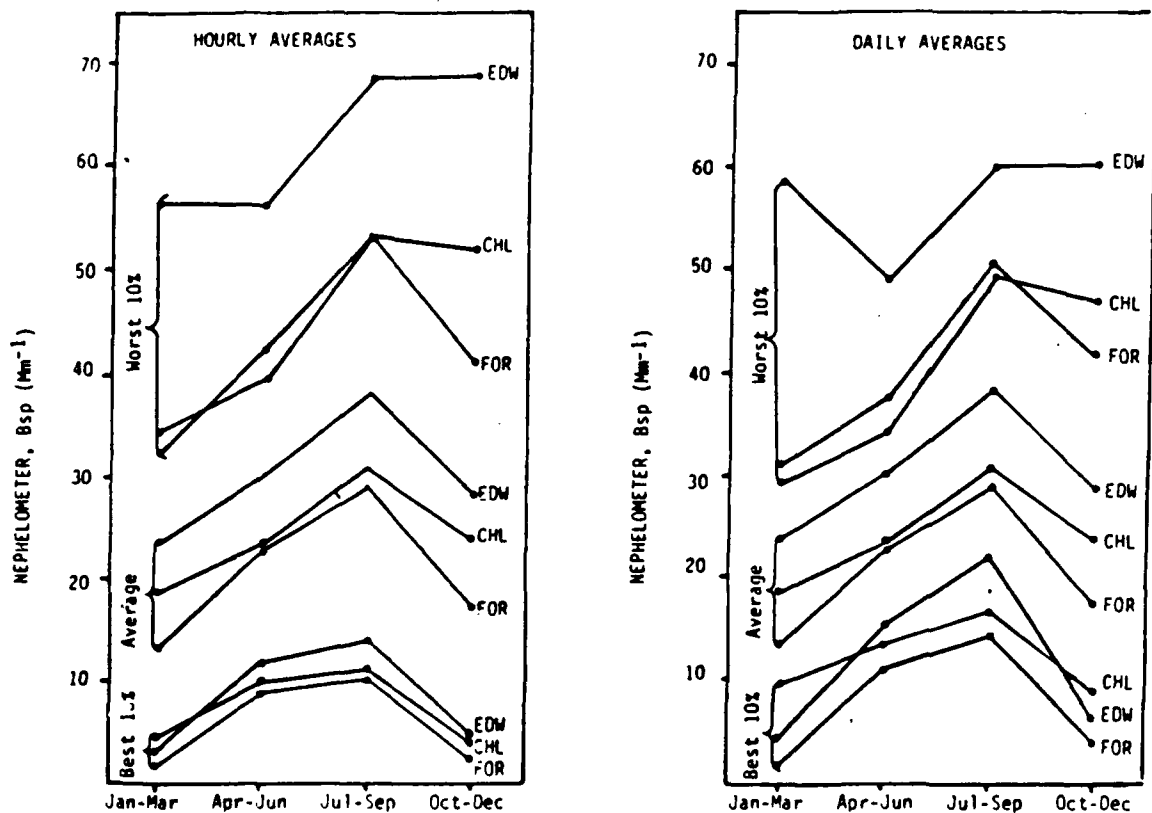
FIGURE 38. Quarterly Patterns in Hourly and Daily Averages for Particle Scattering.

At least four major points are to be made with respect to Figure 38.

1. The ranking of the three receptor sites with respect to light extinction is Edwards AFB highest, then NWC, then Fort Irwin NTC. Basically, NWC experiences about average

particle scattering among the three receptor sites, with Edwards AFB about 20% worse, and Fort Irwin NTC about 20% better.

2.   Average light scattering at all three sites demonstrates the same distinct seasonal pattern. Average visibility is worse in the summer (third) quarter and best in the winter (first) quarter. Average visibility in the spring and fall quarters is intermediate, with the spring quarter tending to be slightly worse than the fall quarter.

3.   An interesting relationship exists among the sites for the best-case and worst-case tenth percentiles. For the worst tenth percentile, NWC is about the same as Fort Irwin NTC, with Edwards AFB showing more severe worst-case conditions than those two sites. For the best tenth percentile, NWC and Edwards AFB are close together, with Fort Irwin NTC demonstrating especially good best-case conditions. Basically, regarding NWC as the average site, apparently Edwards AFB has lower average visibility than NWC, mostly because Edwards AFB has more severe worst-case conditions. On the other hand, Fort Irwin NTC has higher average visibility than NWC, mostly because Fort Irwin NTC experiences especially good best-case conditions.

4.   The seasonal pattern is not as constant or strong for the worst-case tenth percentile as it is for the average. Essentially, this fact reflects the phenomena that worst-case conditions are nearly as frequent in fall and other seasons as they are in summer, even though average visibility is lowest during summer.

Figures 39, 40, and 41 illustrate the seasonal variation in the key atmospheric parameters on a monthly basis. The data in these figures cover the entire 17-month period of particle sampling. The figures reveal the following features:

● Particle scattering peaks in the third quarter (July through September). The local maximum in July is due to data from July 1985 when the RESOLVE network was affected by very severe brush and forest fires in Southern California.

● Organics, sulfates, and elemental carbon (or equivalently, particle absorption) all show a broad summertime maximum from May through Sepember. This condition may reflect the strong transport conditions from the upwind source regions during summer (see Section 4.1.2) and may suggest the importance of transport for each of these three aerosol components. The localized peak for organics during July is associated with the wildfires of July 1985.

● Fine-particle soil reaches a maximum from March through May when wind speeds are at a maximum. Coarse-particle mass (dominated by soils) shows a broad summertime peak. The disagreement in seasonal patterns for fine-soil and coarse particles may reflect different source processes for fine soil versus coarse soil and/or strong seasonal patterns in the small nonsoil component of coarse particles (e.g., coarse nitrates, organics, sulfates, and elemental carbon.)

● The remaining unaccounted-for fine mass is slightly greater in winter than in summer. As discussed in Section 3.3, the unaccounted-for component probably mostly represents nitrate aerosol (which was found to have a winter peak—see Section 7.3). Higher nitrate concentrations in winter than in summer would likely reflect the strong temperature dependence of the equilibrium between ammonium nitrate aerosol and its precursor gases, HNO_3 and NH_3 (References 51 and 52). That is, even though transport from the upwind source regions is greatest during summer, the thermodynamic processes seem to be the controlling factor for the seasonal pattern of aerosol nitrate.

• Fine-mass concentration exhibits a broad maximum from April through October. Essentially, the May through September peak for organics, sulfates, and elemental carbon is extended to April because of fine soil in spring, and to October because of unaccounted-for fine mass (nitrates) in fall.

An additional aspect of seasonal patterns is the seasonal variation in the light extinction budget. This aspect is discussed in Section 7.3.2.
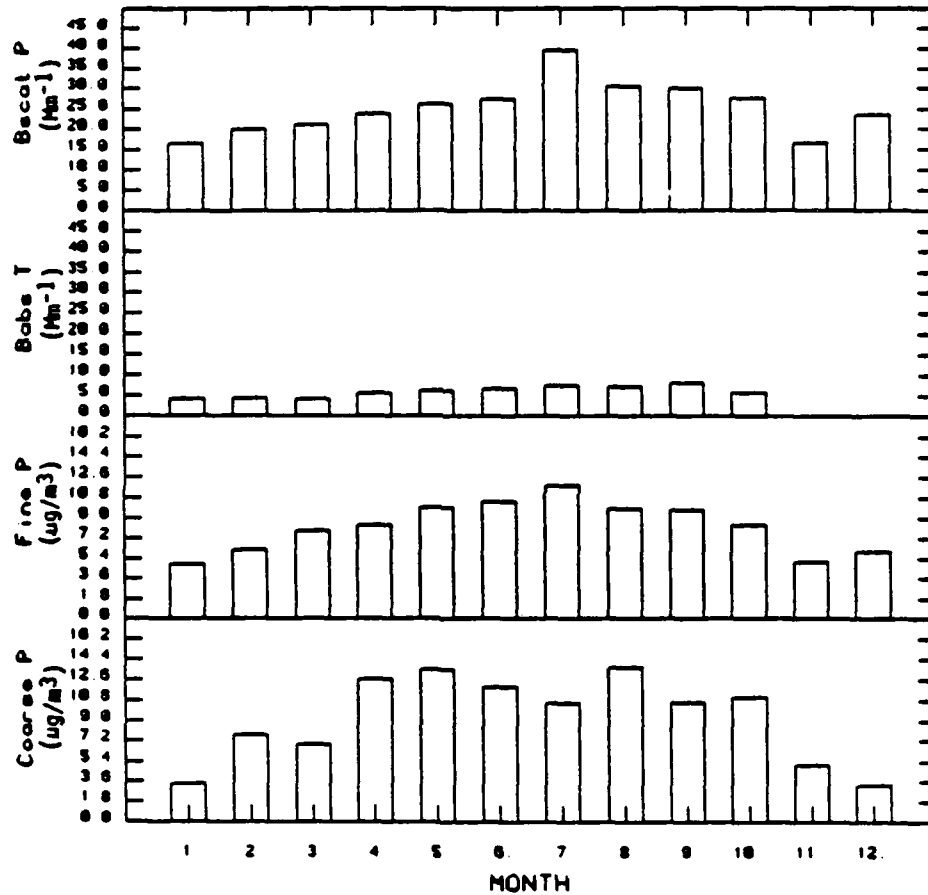
FIGURE 39. Monthly Variations in Particle Scattering, Absorption, and Mass Averaged Over the Three Receptor Sites.
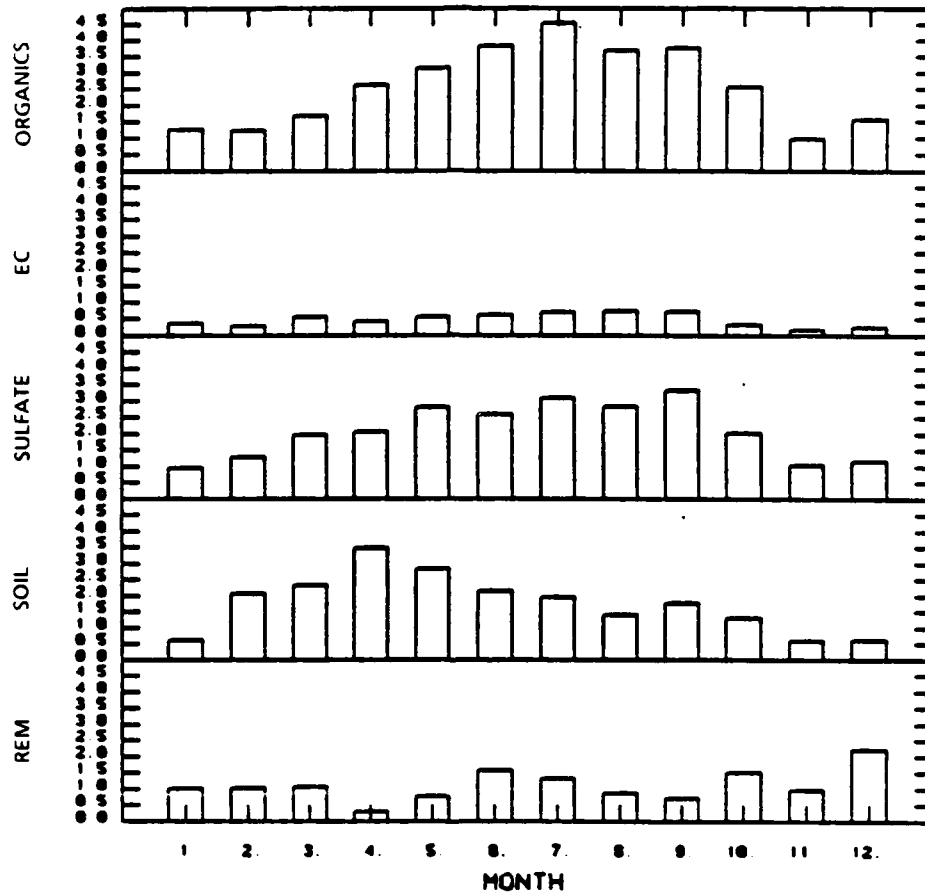
FIGURE 40. Monthly Variations in the Chemical Components of Fine-Particle Mass Averaged Over the Three Receptor Sites (All in $\mu g/m^3$).
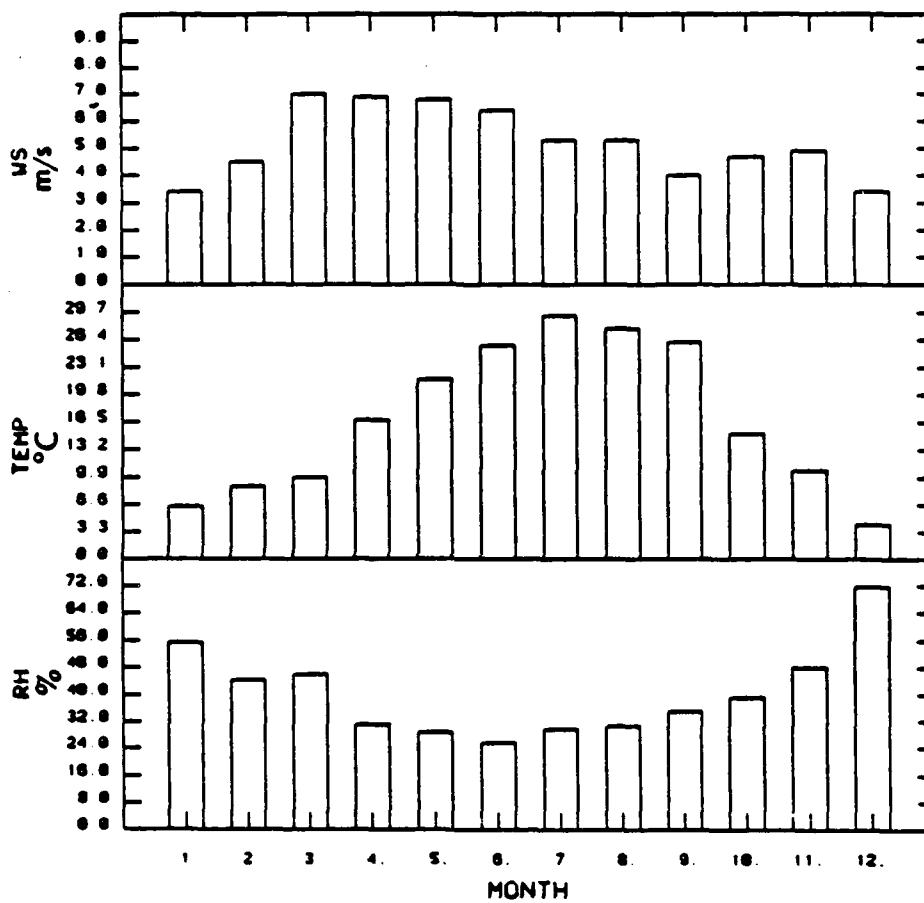
FIGURE 41. Monthly Variations in Meteorological Parameters Averaged Over the Three Receptor Sites.

6.2 DIURNAL VARIATIONS

Diurnal variations in air quality were discussed in previous chapters. In this section, we present the overall average diurnal patterns for particle scattering. As indicated on the right-hand side of Figure 42, the diurnal patterns at the pass sites show increasing concentrations, starting at midday, that lead to peaks in aerosol scattering during the evening. These data are consistent with the typical ventilation pattern for air masses leaving the upwind source areas. At the desert sites, aerosol scattering tends to decrease in late morning, leading to a minimum in early afternoon. This fact most likely reflects greater dispersion in the morning because of the elevation of mixing heights and the increase in wind speeds. Aerosol concentrations in the desert start to rise in the afteroon, leading to a peak late at night and early in the morning. This phenomenon is consistent with transport from the upwind basins during the afternoon and evening (References 7 and 14). Also consistent with the transport hypothesis is the fact that the diurnal variations are most pronounced at the sites nearest the upwind basins, and least pronounced at the sites most distant from the upwind basins.
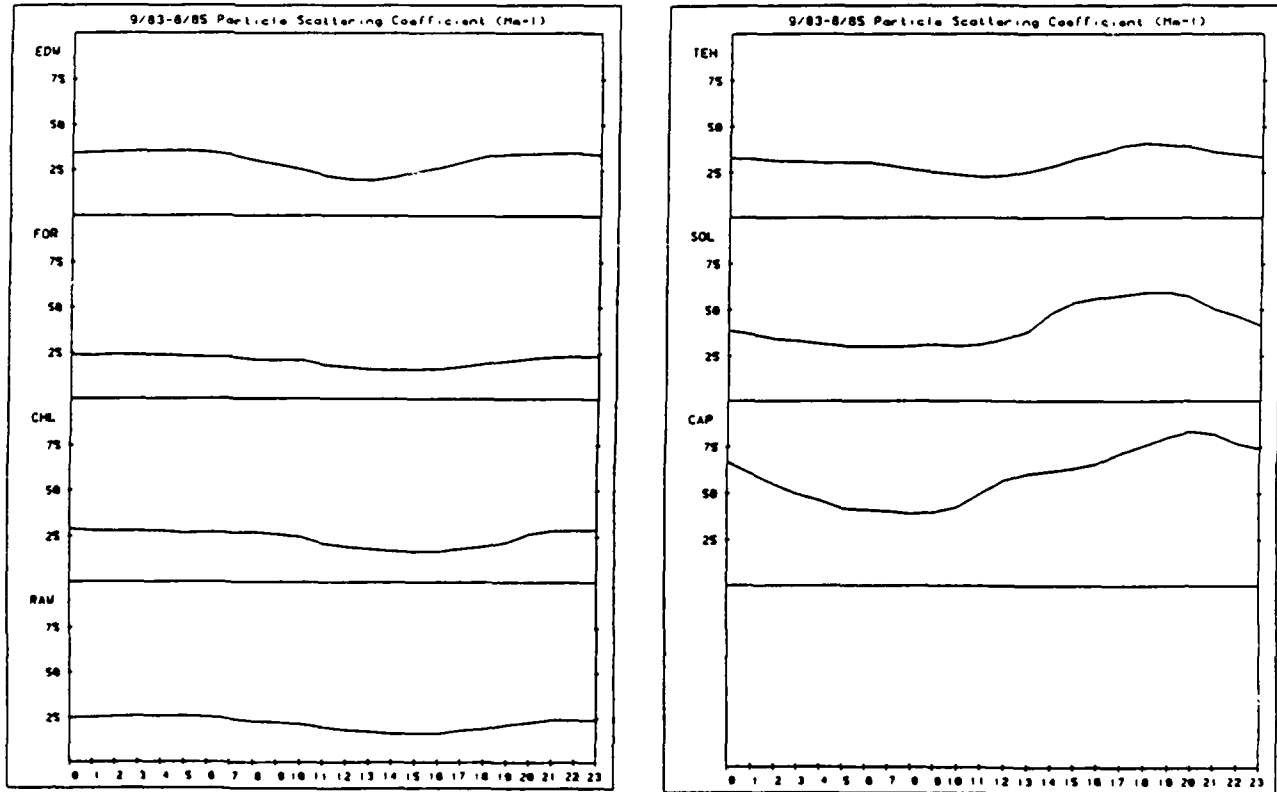
FIGURE 42. Average Diurnal Patterns for Particle Scattering.

6.3 TIME-SERIES PLOTS

Figures 43 through 45 provide time-series plots of extinction and aerosol data for Edwards AFB, NWC, and Fort Irwin NTC, respectively. The top row in each figure presents nephelometer particle scattering as well as the sum of nephelometer particle scattering and particle absorption. The second row pertains to fine-particle mass, and the next five rows give the components of fine mass (all in µg/m³). The last row presents the ratio of nickel to lead.

The top two rows are used to identify episodes of poor air quality. The next two rows characterize the aerosol components causing the episodes. The Ni/Pb ratio provides information on source areas (see Section 8.2).

Table 16 provides a list of days when standard visual range was 50 kilometers or less at any of the three RESOLVE receptor sites. As discussed previously (see Figure 38), Edwards AFB has significantly more low-visibility days than NWC or Fort Irwin NTC—the latter two sites being about equivalent in frequency of low-visibility days. It is also apparent that worst-case days can occur in any season. Table 16 and Figures 43 through 45 were used to select episodes for the illustrative case studies of Chapter 9.
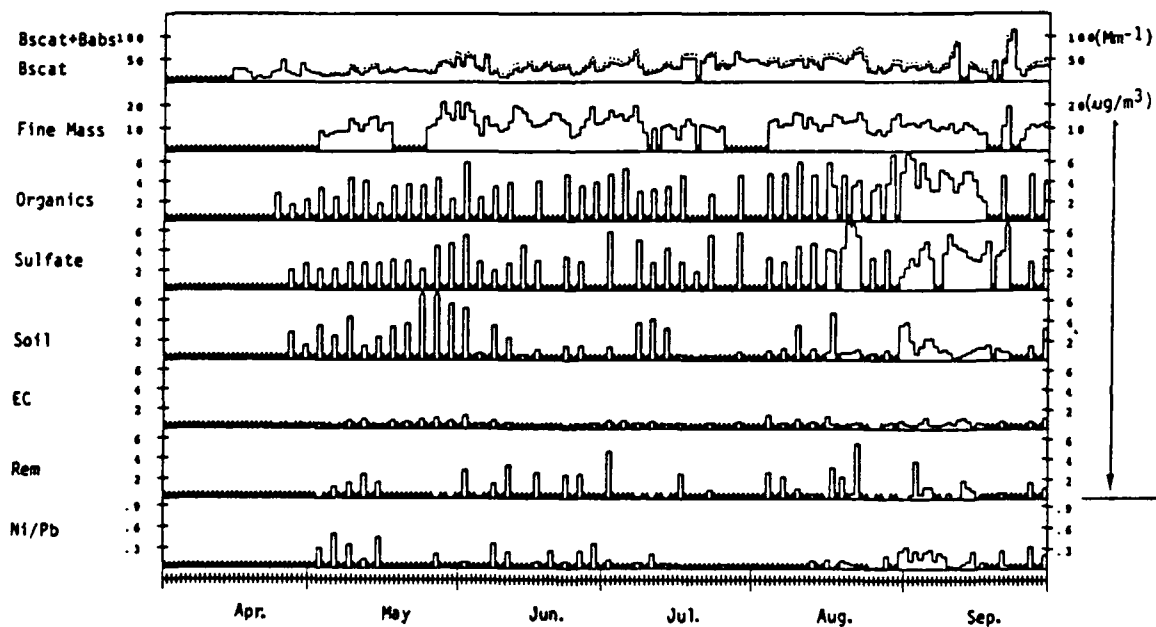
NOTES:
- Bscat represents nephelometer particle scattering without correction for coarse-particle scattering. The dashed line in the first row is Bscat plus particle absorption.
- "Rem," fine mass minus the next 4 components, should qualitatively reflect fine nitrates.

FIGURE 43a. Time Series of Daily Averages at Edwards AFB (April 1984 to September 1984).
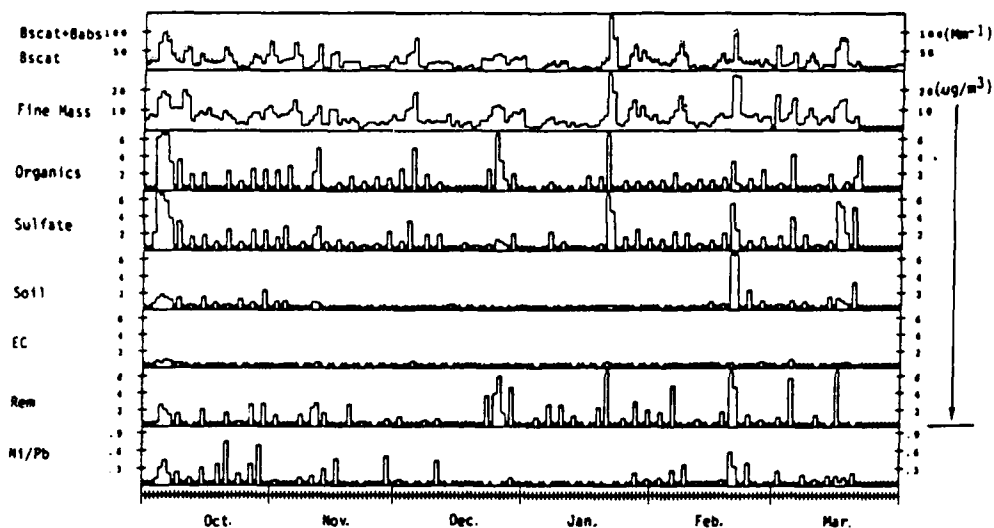
NOTES:
- Bscat represents nephelometer particle scattering without correction for coarse-particle scattering. The dashed line in the first row is Bscat plus particle absorption.
- "Rem," fine mass minus the next 4 components, should qualitatively reflect fine nitrates.

FIGURE 43b. Time Series of Daily Averages at Edwards AFB (October 1984 to March 1985).
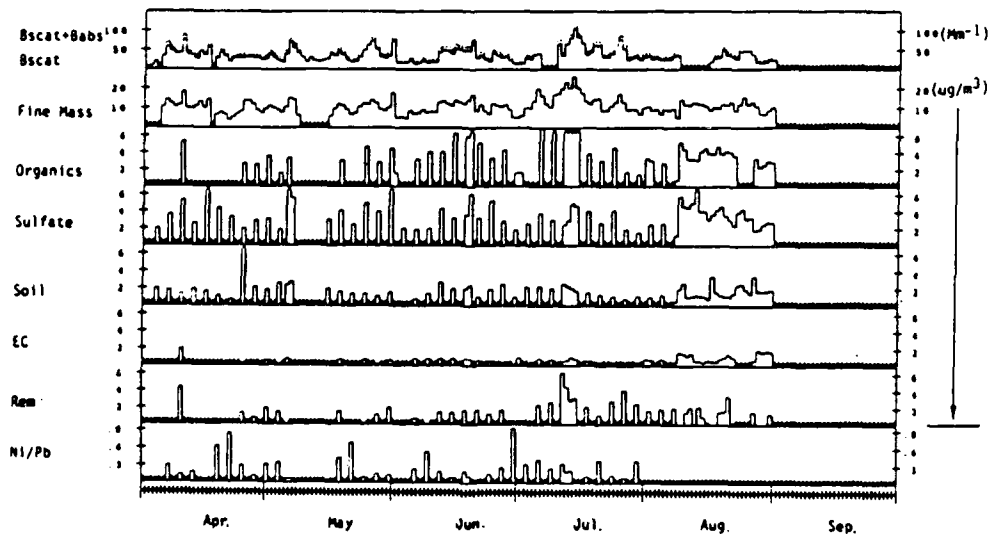
NOTES:
- Bscat represents nephelometer particle scattering without correction for coarse-particle scattering. The dashed line in the first row is Bscat plus particle absorption.
- "Rem," fine mass minus the next 4 components, should qualitatively reflect fine nitrates.

FIGURE 43c. Time Series of Daily Averages at Edwards AFB (April 1985 to August 1985).
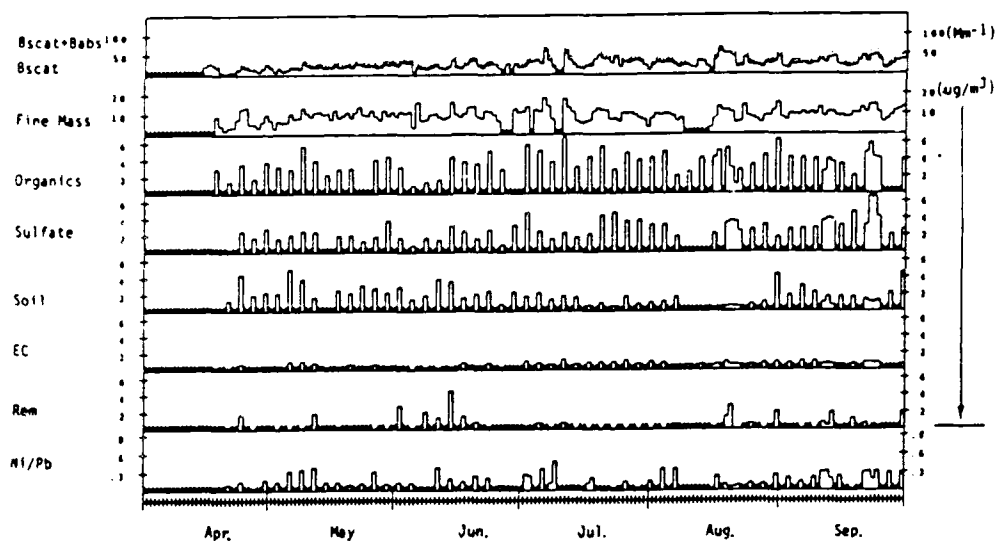
NOTES:
- Bscat represents nephelometer particle scattering without correction for coarse-particle scattering. The dashed line in the first row is Bscat plus particle absorption.
- "Rem," fine mass minus the next 4 components, should qualitatively reflect fine nitrates.

FIGURE 44a. Time Series of Daily Averages at NWC (April 1984 to September 1984).
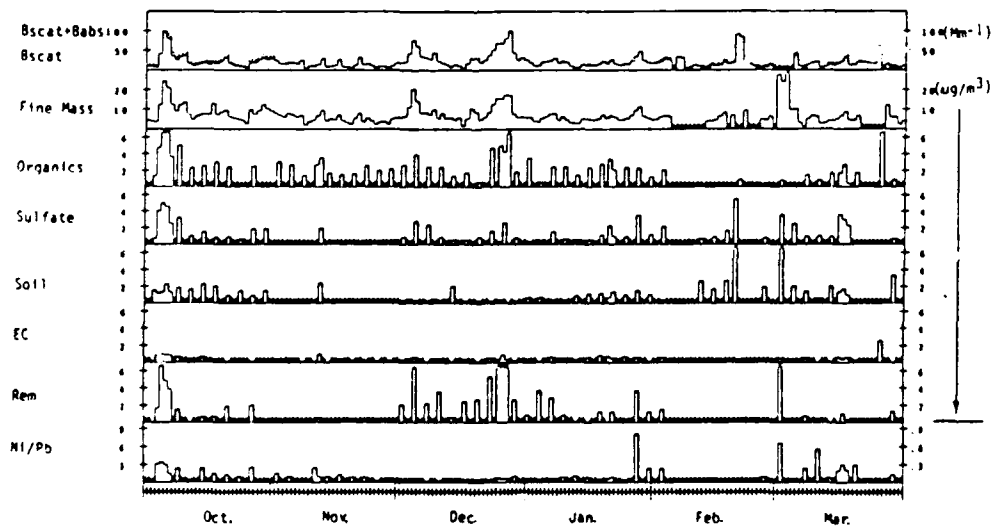
NOTES:
- Bscat represents nephelometer particle scattering without correction for coarse-particle scattering. The dashed line in the first row is Bscat plus particle absorption.
- "Rem," fine mass minus the next 4 components, should qualitatively reflect fine nitrates.

FIGURE 44b. Time Series of Daily Averages at NWC (October 1984 to March 1985).
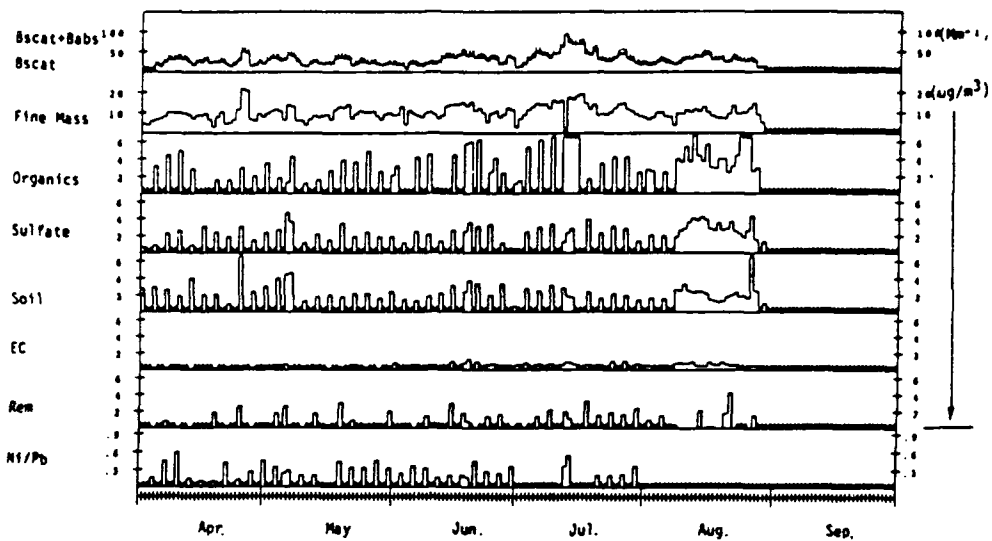
NOTES:
- Bscat represents nephelometer particle scattering without correction for coarse-particle scattering. The dashed line in the first row is Bscat plus particle absorption.
- "Rem," fine mass minus the next 4 components, should qualitatively reflect fine nitrates.

FIGURE 44c. Time Series of Daily Averages at NWC (April 1985 to August 1985).
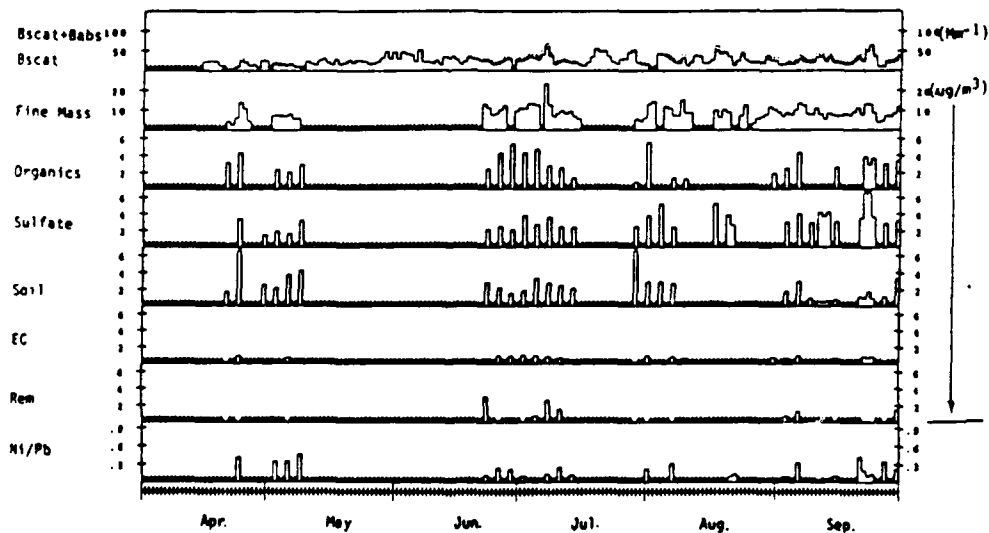
NOTES:
- Bscat represents nephelometer particle scattering without correction for coarse-particle scattering. The dashed line in the first row is Bscat plus particle absorption.
- "Rem," fine mass minus the next 4 components, should qualitatively reflect fine nitrates.

FIGURE 45a. Time Series of Daily Averages at Fort Irwin NTC (April 1984 to Sepember 1984).
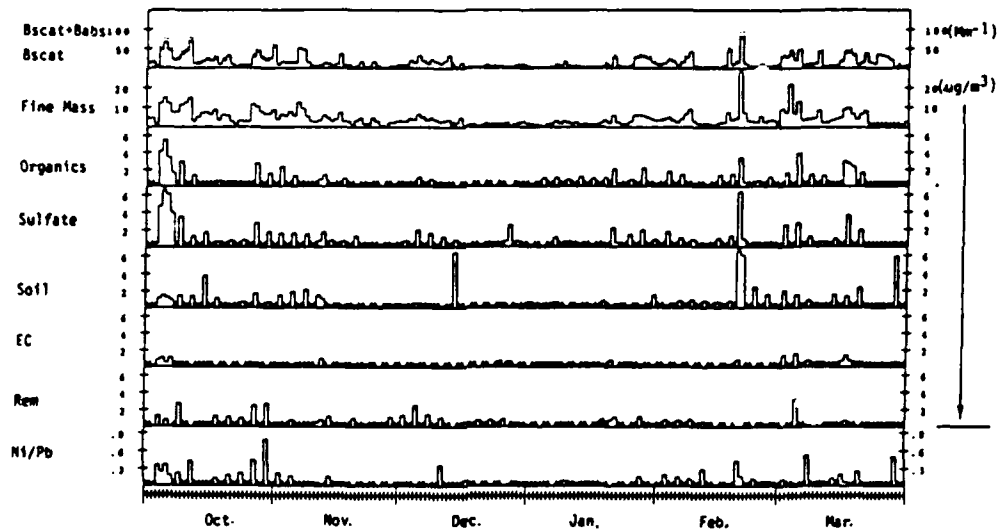
NOTES:
- Bscat represents nephelometer particle scattering without correction for coarse-particle scattering. The dashed line in the first row is Bscat plus particle absorption.
- "Rem," fine mass minus the next 4 components, should qualitatively reflect fine nitrates.

FIGURE 45b. Time Series of Daily Averages at Fort Irwin NTC (October 1984 to March 1985).
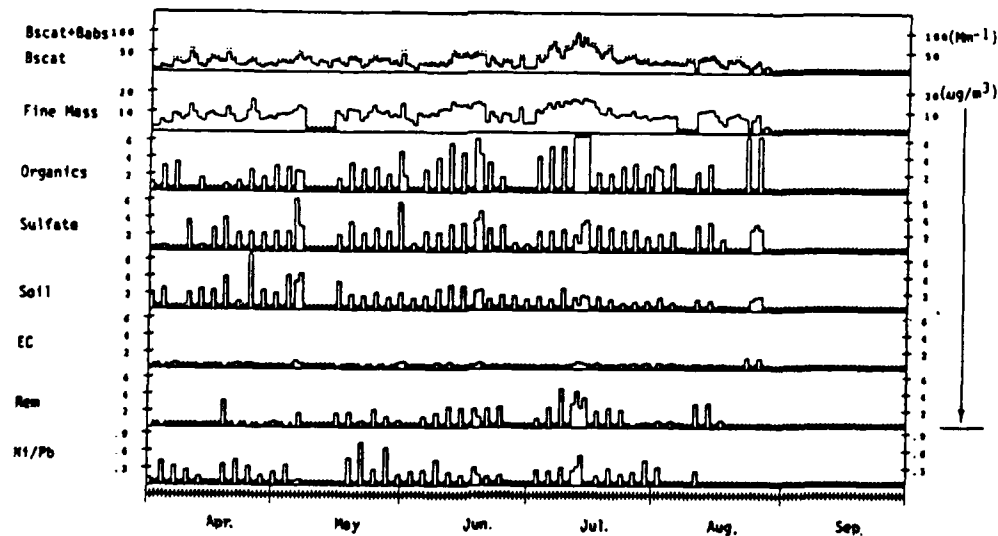
NOTES:
- Bscat represents nephelometer particle scattering without correction for coarse-particle scattering. The dashed line in the first row is Bscat plus particle absorption.
- "Rem," fine mass minus the next 4 components, should qualitatively reflect fine nitrates.

FIGURE 45c. Time Series of Daily Averages at Fort Irwin NTC (April 1985 to August 1985).

TABLE 16. Days When Standard Visual Range* at the RESOLVE Receptor
Sites Was 50 Kilometers or Less—April 1984 to August 1985.

| Date	Visual range, Km				Date	Visual range, Km		
	EDW	NWC	FOR			EDW	NWC	FOR
Second Quarter 1984					**First Quarter 1985**			
4/25	50	---	---		1/21	21	---	---
5/29	---	---	49		1/22	37	---	---
5/31	47	---	---		1/27	47	---	---
6/2	46	---	---		2/7	42	---	---
6/3	50	---	---		2/20	28	28	3:
6/6	50	---	46		2/21	---	30	---
					3/1	38	---	---
Third Quarter 1984					3/5	---	---	50
7/6	---	46	36		3/16	38	---	---
7/7	43	---	40		3/17	39	---	---
7/11	---	49	---		3/25	---	39	---
7/18	50	---	---					
7/19	---	---	44		**Second Quarter 1985**			
7/20	---	---	49		4/6	46	---	---
7/21	---	---	49		4/10	36	---	---
7/23	49	---	---		4/16	45	---	---
7/26	45	---	---		4/19	---	---	49
7/28	38	---	46		4/25	---	43	---
7/29	47	---	---		4/26	---	46	---
7/31	49	---	---		5/6	40	---	---
8/1	50	---	---		5/7	47	---	---
8/9	50	---	---		5/25	43	---	---
8/17	---	47	48		5/26	40	---	---
8/21	44	---	---		5/31	38	---	---
8/22	42	---	---		6/15	47	---	---
8/31	---	50	---		6/19	40	---	---
9/10	49	---	---					
9/11	38	---	---		**Third Quarter 1985**			
9/22	33	---	---		7/5	---	---	48
9/23	23	---	38		7/6	---	---	41
					7/9	---	---	47
Fourth Quarter 1984					7/10	41	---	45
10/4	38	---	---		7/11	---	44	39
10/5	30	30	43		7/12	38	27	33
10/6	37	36	---		7/13	36	40	43
10/11	49	---	39		7/14	30	42	37
10/31	41	---	---		7/15	35	41	42
11/6	35	---	47		7/16	42	41	43
11/12	37	---	---		7/19	44	49	---
11/16	49	---	---		7/20	44	---	45
12/4	---	33	---		7/24	49	---	---
12/5	30	40	---		7/25	37	---	---
12/23	---	47	---		7/26	49	---	---
12/24	---	36	---		8/8	---	---	45
12/25	---	36	---		8/9	---	---	46
12/26	---	31	---		8/24	50	---	---
12/27	---	26	---					

*Standard visual range is 3 9/Bext, where Bext is total instrumental extinction. Based on the discussions of Sections 3 2.2 and 7 2, total extinction is calculated as the sum of 11 Mm⁻¹ (Rayleigh scatter), Bext (nephelometer particle scattering), 3 CP (the sum of coarse-particle scattering missed by the nephelometer), 04 Bext (an estimate of NO_2 absorption), and Bap (total particle absorption) If CP and/or Bap are missing, total extinction is estimated as 11 + 1 4 Bscat (see Section 7 2)

7.0 CAUSES OF LIGHT EXTINCTION

The results for the light extinction budget—the allocation of extinction contributions among atmospheric species—is presented in this chapter. In addition to natural Rayleigh scattering by air molecules, just five types of aerosol (plus gaseous NO_2) usually contribute nearly all of ambient light extinction. These five categories are sulfates (from SO_x emissions), nitrates plus NO_2 (from NO_x emissions), elemental carbon, organics, and soil dust. The first three categories are generally dominated by man-made emissions, while the last two aerosol types (organics and soil dust) arise from a wide variety of both natural and anthropogenic sources. Knowledge of the extinction contributions from Rayleigh scatter and these five categories already provide important insights about the nature and origins of visibility degradation in the Mojave Desert.

7.1 SCOPE OF THE ANALYSIS

The right-hand column of Table 17 lists annual average non-Rayleigh extinction for Edwards AFB, NWC, and Fort Irwin NTC. As explained later in this chapter, these estimates of non-Rayleigh extinction are calculated from RESOLVE data for particle scattering, particle absorption, and NO_2 concentrations, with appropriate accuracy and correction factors applied. Moving leftward in the table, the addition of Rayleigh scatter yields total extinction coefficients that can, in turn, be translated into visual ranges using the Koschmeider relationship.

TABLE 17. Average Extinction Coefficients for RESOLVE Base Year.

			Bext	=	Bsg	+	Bag	+	Bsp	+	Bap
					Rayleigh Scatter		Non-Rayleigh				
Visual Range (2% contrast)	Site	Bext			Units = $[Mm^{-1}]$						
73 km	EDW	53	=		11	+			42		
83 km	CHL	47	=		11	+			36		
100 km	FOR	39	=		11	+			28		
83 km	Average	46	=		11	+			35		

Several aspects of the scope of this chapter can be explained in relation to Table 17.

1. Nearly all of the discussion herein pertains to average results over the three receptor locations.

2. The analysis focuses on a budget for non-Rayleigh extinction. Although Rayleigh scatter contributes 20 to 30% of average extinction at the receptor sites, the Rayleigh scatter component is natural and constant.

3. The results presented here are for the RESOLVE base year, July 1984 through June 1985. The RESOLVE particle samplers operated for 16 months (May 1984 through August 1985), but we have restricted the data to the four complete quarters to avoid seasonal bias.

4. The definition of aerosol species deserves a brief explanation. To account for the mass of associated ions, the following conventions are adopted:

$$\text{Sulfates} = 4.12[S]$$
$$\text{Nitrates} = 1.29[NO_3]$$
$$\text{Organics} = 1.5[\text{Organic C}]$$
$$\text{Soil} = 2.14\,Si + 1.67\,Al + 1.44\,Ca + 1.40\,Fe + 1.66\,Mg + 1.22\,K + 1.44\,Mn$$

7.2 EXTINCTION ALLOCATION PROCEDURE

Figure 46 presents an overview of the entire extinction allocation procedure. Total non-Rayleigh extinction at the three desert receptor sites, 35 Mm^{-1}, consists of contributions from absorption by gases (1 Mm^{-1}), scattering by particles (28 Mm^{-1}), and absorption by particles (6 Mm^{-1}). The boxes in the figure indicate the techniques used to determine and allocate the contributions. The following three subsections expound on these determinations and allocation methods.

7.2.1 Nitrogen Dioxide Absorption

The only gas that contributes significantly to atmospheric light absorption is nitrogen dioxide. Absorption by NO_2 is determined from measured NO_2 concentrations by the formula, Bag = .33 $[NO_2]$, where the units of absorption are Mm^{-1} and the units of $[NO_2]$ are ppb[2,3,4]. Special high-sensitivity NO_2 data collected for RESOLVE at Edwards AFB and NWC during the summer/fall 1984 indicate that NO_2 absorption is about 4% of particle scattering in the Mojave Desert. This result is consistent with an analysis of long-term routine data sets for the desert by Trijonis, et al. (Reference 3) as well as with other special field programs (References 53 and 54). Applying this 4% factor to the average particle scattering measured at the receptor sites yields a value for NO_2 absorption of only 1 Mm^{-1} (see Figure 46).

7.2.2 Particle Absorption

The extinction budget analysis for particle absorption is illustrated on the right-hand side of Figure 46. Particle absorption measurements with the daily RESOLVE Teflon filters were made at the University of California, Davis, using the integrating plate method and were corrected for accuracy as described in Section 3.2.2. Based on the routine RESOLVE data, total particle absorption is 6 Mm^{-1}, consisting of 5 Mm^{-1} from fine particles and 1 Mm^{-1} from coarse particles.

The next step is to allocate the absorption among aerosol components. In the literature, it is almost always assumed that particle absorption arises entirely from elemental carbon concentrations. Some speculation, however, has been made that soil dust might also contribute significantly to absorption, especially in the coarse-particle size range. Three methods were used to estimate soil dust contributions to coarse-particle absorption. As indicated by Table 18, all three methods implied that absorption from coarse soil dust is small, only about 20% of the 1 Mm^{-1} total coarse absorption. The same methods show that absorption from fine soil dust is negligible. Accordingly, assuming that 20% of coarse-particle absorption is from soil dust, we arrive at the result in Figure 46 that absorption arises almost entirely from elemental carbon.

$B_{\text{Non-Rayleigh}}$ = Bag + Bsp + Bap

| Analysis of existing NO₂ data. RESOLVE special NO₂ data. | Routine RESOLVE data. RESOLVE special experiment. | Routine RESOLVE data. RESOLVE special experiments. |

$35 \, \text{Mm}^{-1}$ = 1 + 28 + 6

| RESOLVE special experiment. Literature review. RESOLVE Mie Theory. | Routine RESOLVE data. |

FINE 23   COARSE 5   FINE 5   COARSE 1

| RESOLVE regressions. Mie Theory. Literature review. Sloane Interactive Theory. | Routine RESOLVE data. | Literature review. RESOLVE experiment. RESOLVE Mie Theory. |

Species contributions = NO₂: 1
(Mm⁻¹)

Organics: 8½
Sulfates: 8
Soil dust: 2
Elemental carbon: ½
(RESOLVE special experiment) Nitrates: 4

Soil dust: 4⁺
Organics ⎫
Sulfates ⎬ : 1⁻
Elemental C ⎪
Nitrates ⎭

Elemental carbon: 6⁻
Soil dust: 0⁺

FIGURE 46. Extinction Allocation Procedure.

TABLE 18. Estimation of Soil Dust Contribution to Coarse Absorption.

Methodology	Percentage of coarse absorption allocated to soil dust
Coarse EC absorption estimated from RESOLVE special study measurements of coarse EC with published absorption efficiencies for coarse EC (References 11 and 57). Coarse-soil absorption obtained by subtraction.	0-40%
Coarse-soil absorption calculated from Mie theory using RESOLVE DRUM sampler data for soil elements (Reference 58), with imaginary refractive index for soil of ≤ .004i (Reference 59), and with adjustments to account for entire coarse-soil distribution.	0-30%
Coarse-soil absorption estimated from experimental measurements of soil absorption efficiency by Draftz (Reference 60), with RESOLVE soil concentrations adjusted to account for entire coarse-soil distribution.	10-30%

7.2.3 Particle Scattering

Particle scattering is the most complex part of the extinction budget analysis. The average particle scattering measured by the routine RESOLVE nephelometers at the three receptor sites is 25.5 Mm^{-1}. As discussed in Section 3.2.2, special intensive experiments demonstrated that the RESOLVE nephelometers operate near ambient conditions with respect to relative humidity. Consequently, no significant accuracy correction is required for changes in water scattering. Calculations regarding the collection and measurement efficiency of the nephelometer for coarse particles, however, indicate that the nephelometer misses one-half of coarse-particle scattering (later estimated to be 5 Mm^{-1}). When adjusted for this missing coarse-particle scattering, the corrected total particle scattering becomes 28 Mm^{-1} (see Figure 46).

Three methods are used here to estimate the portion of particle scattering due to coarse particles. To derive a factor that can be applied to averages of the routine RESOLVE coarse-mass data, and to provide a common basis for comparison, the results of all three methods are specified in terms of a pseudo coarse-particle scattering efficiency in m^2/g, defined as [total coarse-particle scattering]/[particle mass from 2.5 to 10 μm]. Table 19 describes the three methods and summarizes the results. In our opinion, the most relevant result is that from the first method (RESOLVE Cyclone Nephelometer Study) that was designed specifically to address this issue. As a concensus finding, we have chosen a pseudo coarse-particle scattering efficiency of 0.6 m^2/g.

Applying the 0.6 m^2/g pseudo coarse-scattering efficiency to the average coarse mass at the three receptor sites yields a coarse-scattering value of 5 Mm^{-1}. This 5 Mm^{-1} is allocated among species according to their percentage contributions to measured coarse mass (2.5 to 10 micrometers): 85% soil dust*, 5% nitrates **, 4% organics**, 3% sulfates*, and 3% elemental carbon*, where * refers to values based on RESOLVE monitoring data and ** refers to values estimated from engineering judgments. Two major potential sources of error exist in this allocation, but, fortunately, they tend to cancel. First, soil dust contributions may be underestimated because soil dust might account for even more than 85% of the coarse mass greater than 10 micrometers. Second, soil dust contributions may be overestimated because coarse scattering efficiencies should be greater for the other four

components. The other four components will tend to occur in smaller coarse particles, and coarse-particle scattering efficiency is approximately proportional to the reciprocal of particle diameter.

TABLE 19. Estimation of Pseudo Coarse-Particle Scattering Efficiency.

Methodology	Pseudo coarse-scattering efficiency*
RESOLVE cyclone nephelometer experiment, with adjustments for nephelometer collection efficiency and nephelometer measurement efficiency for coarse particles.	6 m²/g
Mie theory calculation (Reference 58) based on RESOLVE DRUM sampler data for soil, with adjustments to account for entire coarse-particle size distribution.	3- 5 m²/g
Regressions based on teleradiometer data and fine-/coarse-particle data. Conventional regression (Reference 61) Zero interception (References 9 and 61)	4 m²/g .7-1.3 m²/g

*Total coarse-particle scattering/Particle mass from 2.5 to 10μm

The fine scattering of 23 Mm^{-1} in Figure 46 is allocated among species according to fine-particle scattering efficiencies. As shown in Table 20, four methods are used to determine the scattering efficiencies of fine organics, sulfates, elemental carbon, and soil dust. The scattering efficiency of fine nitrates is assumed to be the same as that of fine sulfates (References 11, 55, 56, and 57).

Note that good agreement is found among the methods, within about ±1 m²/g, on the scattering efficiencies for organics, sulfates, and soil dust. High uncertainty exists with respect to the scattering efficiency of elemental carbon, but this is of little consequence because elemental carbon occurs in such small concentrations. The consensus scattering efficiencies are based on discussions among RESOLVE team members about the merits and limitations of the various methods. The consensus values are reported as whole numbers with fractions rather than decimals as a better reflection of the uncertainties. The uncertainties in the scattering efficiencies and the resulting potential errors in the extinction budget are quantified in Appendix A.

In Table 20 we chose to include the scattering contribution from aerosol water as a part of the scattering efficiencies (i.e., the scattering efficiencies are inflated above "dry efficiencies" to represent aerosol water). With respect to regression formulations, this means that we are using strictly linear regression forms rather than regression forms that include nonlinear relative humidity (RH) terms. The strictly linear regressions achieve a slightly better statistical fit with the RESOLVE data. In any case, aerosol water is not a critical factor in the RESOLVE study area. The Heated/Ambient Nephelometer Special Study indicated that, on the average, aerosol water contributes only 7% to fine-particle scattering at Edwards AFB and 3% at NWC.

To obtain a fine-scattering budget, the consensus scattering efficiencies of Table 20 are multiplied by average concentrations for organics, sulfates, elemental carbon, and soil dust

TABLE 20. Determination of Fine-Particle Scattering Efficiencies.

Methodology	Scattering efficiencies (m²/g)			
	Organics	Sulfates	Elemental carbon	Soil dust
REGRESSION ANALYSIS (based on routine RESOLVE data at the three receptor sites)				
Conventional regression	3.7	5.0	0.6[b]	0.4
Structural regression[a]	3.8	5.1	– 1.8[b]	0.5
LITERATURE REVIEW (20 studies with the following adjustments for consistency)				
Nephelometer calibration	2-3	3-6	(2-3)[c]	1-2½
Airport contrast = 5%				
Nephelometer λ = 530 nm				
Organics = 1.5 · OC				
Relative humidity = 40%				
MIE THEORY (for Mojave Desert data)				
Ouimette and Flagan (Reference 49)	2.5[d]	3.2	NA	1.4
RESOLVE DRUM sampler data	NA	3.2	NA	1.4
INTERACTIVE MIE THEORY (based on Detroit size distributions, Reference 62)	3.8	4.7	(3.8)[c]	1.3
CONSENSUS	3½	4½	1½	1¼

[a] As in Madansky (Reference 63) and White and Macias (Reference 64).
[b] Difference from zero not statistically significant.
[c] Elemental carbon grouped with organic carbon.
[d] Mie theory based on volume size distribution for all material, not just organics.

as well as special-study concentrations for denuder difference nitrates.* The addition of the five resulting components yields a scattering level that is 13% greater than measured fine scattering. To achieve the species allocation of the 23 Mm⁻¹ listed in Figure 46, the five calculated components are each divided by a factor of 1.13.

* The RESOLVE special studies for fine particulate nitrate using the denuder difference method found the following (sample size in parentheses):

	Fine NO₃ concentrations, µg/m³	
	Edwards AFB	NWC
SUMMER		
1984 Study	5 (27 day)	.4 (25 day)
1985 Study	1 1 (22 day/20 night)	
WINTER		
1986 Study	1 6 (12 day/9 night)	6 (9 day/8 night)

Multiplying by 1.29 to account for the cation mass, we conclude that the average fine NH_4NO_3 concentrations are approximately 1.55 µg/m³ (1.0 µg/m³ summer/2.0 µg/m³ winter) at Edwards AFB and .65 µg/m³ (.5 µg/m³ summer, .8 µg/m³ winter) at NWC. Nitrate data were not gathered at Fort Irwin NTC. Fort Irwin NTC is more similar to NWC than to Edwards AFB both in terms of distance from upwind source areas and in terms of percentage of fine mass not accounted for by non-nitrate components. Scaling the NWC data by fine mass, we estimate that average fine NH_4NO_3 concentrations are approximately .46 µg/m³ (.4 µg/m³ summer, .5 µg/m³ winter) at Fort Irwin NTC.

A special experiment with a thermidograph nephelometer that heats samples to 350°C provides a check on the nature of the fine-particle-scattering budget. According to the RESOLVE thermidograph experiment, 87% of the fine aerosol scattering should be nonrefractory species—organics, sulfates, and nitrates. The corresponding result predicted by our fine-scattering budget is 89%. Basically, the thermidograph nephelometer verifies that the refractory species (soil dust and elemental carbon) do have much lower scattering efficiencies than fine organics, sulfates, and nitrates, and that these latter three species do dominate fine scattering in the RESOLVE area.

7.3 EXTINCTION BUDGET RESULTS

Table 21 presents the final extinction budget obtained by adding all of the species contributions listed along the bottom of Figure 46. (Table 21 is more precise than Figure 46 in the sense that a decimal point was added to the calculations.) The results indicate that all five major species contribute significantly to non-Rayleigh extinction, with organics and sulfates most important, and the nitrates plus NO_2 category least important.

TABLE 21. Average Extinction Budget Calculated
for the Three RESOLVE Receptor Sites.

Total Non-Rayleigh:	35.4 Mm⁻¹
Organics:	9.1 (26%)
Sulfates:	8.5 (24%)
Elemental carbon:	6.8 (19%)
Soil dust:	6.4 (18%)
NO_2 + nitrates:	4.6 (13%)

It is interesting to compare the extinction budget results with the previous extinction budget published by Ouimette and co-workers (References 10 and 49) using data for NWC during 1979. Our results are similar to those of Ouimette in terms of fine-particle scattering, fine-particle absorption, and the extinction contributions from sulfates and elemental carbon. Ouimette, however, had a much smaller contribution from organics and a larger contribution from coarse-particle scattering (and therefore soil dust). His low organic concentrations may represent a measurement problem for organics (note that the aerosol chemical species fell substantially short of closing a mass balance in his data). The coarse-particle scattering in the 1979 study may be overestimated because of potential problems with the optical particle counter in the coarse-particle range.

7.3.1 Site-to-Site Variations

Table 22 presents extinction budgets for the three sites individually. The values in Table 22 were derived by using the assumptions and parameters of Sections 7.2.1 to 7.2.3 in conjunction with aerosol composition data (e.g., FP versus CP, Bsp versus Bap, and FP chemical speciation) that is specific to each site.

The most notable site-to-site variations in the extinction budgets are the extra importance of organics at NWC and nitrates at Edwards AFB. Generally, however, the percentage contributions are fairly similar at all three locations, a reflection of similar aerosol composition at the three locations.

TABLE 22. Site-to-Site Variations in Extinction Budgets.

Non-Rayleigh total		Organics	Sulfates	Elemental carbon	Soil dust	Nitrates + NO_2
Absolute contribution (Mm⁻¹)						
EDW	42	10	10½	8	6½	7
CHL	36	10½	8	7	7	3½
FOR	28	6½	7½	5½	5½	3
Relative contribution (%)						
EDW	100	24	25	19	15	17
CHL	100	29	22	19	20	10
FOR	100	23	26	20	21	10

7.3.2 Seasonal Variations

Table 23 presents extinction budgets for summer and winter.* Total non-Rayleigh extinction is nearly 50% higher in summer than in winter, basically because of a near doubling of organic, sulfate, and soil dust concentrations in summer compared to winter. In contrast, nitrate concentrations are higher in winter than in summer. As a result, the nitrate plus NO_2 category, that accounts for only 9% of the total in summer, contributes about 20% in winter.

TABLE 23. Extinction Budgets for Summer Versus Winter.

	Non-Rayleigh total	Organics	Sulfates	Elemental carbon	Soil dust	Nitrates + NO_2
Absolute contribution (Mm⁻¹)						
Summer (April-September)	41½	11½	10½	7½	8	4
Winter (October-March)	28½	6	6	5½	5	5½
Relative contribution (%)						
Summer (April-September)	100	28	25	18	20	9
Winter (October-March)	100	23	21	19	17	20

* In this section, to make maximum use of the RESOLVE data set, all 17 months (6 winter and 11 summer) of particle data are used in sorting by winter/summer or calendar quarter.

Complete extinction budgets are not possible on a quarterly basis because of the lack of quarterly nitrate data. As the next best alternative, Table 24 lists the components of particle extinction and fine-particle mass on a quarterly basis. Table 24 shows that the ranking of particle extinction and mass (from the highest quarter to the lowest quarter) is 3-2-4-1. The percentage contributions of absorption, coarse scatter, and fine scatter to total particle extinction are generally about the same for all quarters, with the exception of a greater fraction of coarse-particle scatter in spring (because of relatively higher dust concentrations during that windy season). Organics and sulfates show a second-third quarter peak (especially the third quarter). Fine soil dust, like coarse-particle mass, peaks in the second quarter. The unaccounted-for fine mass is greatest during the first and fourth quarters; these data agree with the special-study data that show a wintertime nitrate peak.

TABLE 24. Quarterly Variations in the Components of Particle
Extinction and Fine Particle Mass.

	Calendar quarter			
	1 January-March	2 April-June	3 July-September	4 October-December
Contributions = absolute (%)				
Total particle extinction	25 Mm^{-1}	36 Mm^{-1}	44$\frac{1}{2}$ Mm^{-1}	30$\frac{1}{2}$ Mm^{-1}
Particle absorption	4 (17%)	6$\frac{1}{2}$ (17%)	7$\frac{1}{2}$ (17%)	6 (19%)
Coarse-particle scatter	3$\frac{1}{2}$ (14%)	7$\frac{1}{2}$ (21%)	5$\frac{1}{2}$ (13%)	4 (13%)
Fine-particle scatter	17$\frac{1}{2}$ (69%)	22 (62%)	31$\frac{1}{2}$ (70%)	20$\frac{1}{2}$ (68%)
Total fine-particle mass	5.7 µg/m^3	10.2 µg/m^3	10.6 µg/m^3	6.4 µg/m^3
Organics	1.4 (25%)	3.3 (32%)	4.0 (38%)	1.9 (30%)
Sulfates	1.3 (23%)	2.6 (26%)	3.1 (29%)	1.5 (23%)
Elemental carbon	.4 (6%)	.6 (5%)	.7 (7%)	.3 (5%)
Soil dust	1.4 (25%)	2.7 (27%)	1.7 (16%)	.9 (14%)
Unaccounted-for	1.2 (21%)	1.0 (10%)	1.1 (10%)	1.8 (28%)

7.3.3 Quartile Variations

Although a complete extinction budget sorted by percentiles of visibility is not possible because of the lack of detailed nitrate data, it is possible to examine how the components of particle extinction and fine-particle mass vary with overall visibility levels. Table 25 lists extinction components and fine-mass components averaged over the best 25% of days, all days, and worst 25% of days.

Proceeding from best-case days, to average days, to worst-case days, a tendency exists for an increased fraction of extinction caused by fine-particle scatter, and decreased fractions caused by particle absorption and coarse-particle scatter. Also, a tendency exists for a higher percentage fine-mass contribution from "unaccounted-for" (nitrates?), and a lower percentage contribution from soil dust. Although these tendencies are statistically significant, they are of minor practical importance. The average of worst-case days closely resembles the average of all days in terms of extinction contributions and is nearly identical in terms of fine-mass contributions. Even examining the highest 10% of worst-case days, we do not find dramatic shifts in the composition of particle extinction or fine mass.

TABLE 25. Components of Particle Extinction and Fine Particle Mass
for Best, Average, and Worst Visibility Conditions.*

	Average of best 25% of days	Average of all days	Average of worst 25% of days
Contributions = absolute (%)			
Total particle extinction	13 Mm⁻¹	34.5 Mm⁻¹	59.5 Mm⁻¹
Particle absorption	3 (23)	6.5 (18)	8.5 (15)
Coarse-particle scatter	2.5 (18)	5 (15)	8 (13)
Fine-particle scatter	7.5 (59)	23 (67)	43 (72)
Total fine-particle mass	3.6 µg/m³	8.4 µg/m³	13.0 µg/m³
Organics	1.1 (30)	2.8 (33)	4.1 (32)
Sulfates	.9 (25)	2.3 (27)	3.7 (28)
Elemental carbon	.2 (6)	.5 (6)	.8 (6)
Soil dust	1.0 (28)	1.7 (20)	2.4 (19)
Unaccounted-for	.4 (11)	1.1 (13)	2.0 (15)

* Sorting of days at each site is according to the sum of all extinction components
at that site. Averages are then taken over the three sites together

7.4 UNCERTAINTY ESTIMATES

Appendix C presents a detailed uncertainty analysis for the extinction budget results.
Error propagation techniques are applied to judgmental estimates of uncertainty that
encompass instrument imprecisions, climatological variations, potential measurement
inaccuracies, and potential modeling errors (e.g., in the extinction efficiencies). The
estimated uncertainties (single standard error) for the non-Rayleigh extinction budget are
as follows:

Species	Contribution ± uncertainty
Organics	26% ± 9%
Sulfates	24% ± 5%
Elemental carbon	19% ± 6%
Soil dust	18% ± 8%
Nitrates plus NO_2	13% ± 5%

The errors in the species contributions range from 5% to 9% of non-Rayleigh extinction,
with the greatest absolute errors being in the organics and soil-dust categories.

An important benefit of the error propagation analysis is that it reveals the relative
magnitude of the different sources of uncertainty (i.e., imprecision versus climatological
representativeness versus measurement inaccuracy versus modeling error). For example,
the uncertainties in the organic and sulfate categories are dominated by potential errors in
the scattering efficiencies to be used with these components. (Note that errors introduced by
sampling artifacts are included within the uncertainties of the scattering efficiencies. See
Appendix B for details.) Uncertainty in the accuracy correction factor for Teflon abosrption
accounts for the major part of the error in the elemental-carbon category. Error in the soil-
dust category arises essentially all from uncertainty in our estimate of total coarse-particle

scattering. Uncertainty in the nitrate-plus-NO_2 category is about one-half because of error in the scattering efficiency for nitrates, and one-half because of error in the concentration of nitrate particles. Uncertainties related to measurement imprecision and climatological representativeness are quite negligible (except for the sparse nitrate sampling) because of the large number of observations in the RESOLVE data set.

8.0 SOURCES OF ATMOSPHERIC LIGHT EXTINCTION

One of the main objectives of the RESOLVE program is to determine the sources of light extinction–to understand the origins, source areas, and source categories of visibility reducing particles in the R-2508 study region.

The source allocation techniques used in Sections 8.1 and 8.2 are founded on measurements of aerosol composition–composition either with respect to the five major aerosol components or with respect to tracer elements. As such, these techniques fall within the framework of "receptor" modeling (modeling centered on empirical data collected at receptor sites). The RESOLVE monitoring program was designed specifically around the receptor modeling approach (Reference 1). An alternative approach, "source-oriented" or "mathematical diffusion" modeling, may also be possible in the long term. The development of source-oriented models, however, may be extremely difficult.*

8.1 NATURAL VERSUS MAN-MADE SOURCES

In Chapter 7, contributions to non-Rayleigh extinction were allocated among five categories: sulfates, nitrates plus NO_2, elemental carbon, organics, and soil dust. By considering the origins of each of these categories individually, we can derive an overall estimate regarding natural versus man-made contributions to light extinction.

Trijonis (Reference 40) evaluated natural versus anthropogenic origins for sulfates, nitrates, and elemental carbon. All three of these aerosol categories are dominated by man-made sources. Based on a review of that study, a reasonable judgment for the RESOLVE region is that man-made sources contribute about 85% ± 10% of combined extinction from sulfates, nitrates plus NO_2, and elemental carbon. (Note that the ± 10% uncertainty is a judgmental estimate of a single standard error, i.e., a 68% confidence interval.)

The origin of organic aerosols in the Mojave Desert was the subject of a RESOLVE special study funded by WOGA and carried out by Global Geochemistry Corp. (GGC). That study included measurements of carbon isotope ratios and analyses of organic molecular composition. Overall, the data from that study suggest that about 80% ± 15% of organic aerosols are from man-made sources.**

---

* The difficulties concern the requirements for (1) detailed emissions data regarding all five aerosol components, (2) aerometric data on transformation/deposition processes for all five components, (3) detailed wind data to characterize transport and diffusion, and (4) a model framework capable of handling the complex terrain of the study region.

** The basis for this estimate is as follows: The GGC isotope tests consistently show that about 65% (±5%) of total carbon is fossil. Assuming that 85% of elemental carbon is fossil (a noncritical assumption), and noting that 80% of total carbon is organic, we find that an estimated 60% of organic carbon is fossil. All these fossil organics are assumed to be anthropogenic. In addition, some of the contemporary organics are anthropogenic (i.e., residential wood burning, agricultural burning, food cooking) as opposed to natural (wild or controlled forest burning, plant waxes, secondary aerosols from plant terpenes). Actually, the 60% fossil fraction is representative of anthropogenic primary organic emissions (Reference 65), so one could argue that the organics are essentially all anthropogenic. However, natural sources are known to be non-negligible based both on a literature review (Reference 38) and on obvious wild-fire impacts seen in the RESOLVE data (e.g., July 1985). Somewhat arbitrarily, we will assume that the 40% contemporary fraction is half man-made and half natural, yielding an 80% total for anthropogenic. A high anthropogenic percentage is supported qualitatively by the results of the molecular composition studies that suggest that organic aerosols are dominated by urban sources.

With respect to soil dust, it is highly problematical to quantify the relative contributions of man-made sources (e.g., road dust, construction, mineral industry, agriculture, etc.) and natural sources (wind-blown dust). First, the definition of natural is ambiguous. Should wind-blown dust be considered natural if it is significantly affected by land-use practices such as disruption of soil surfaces or drying of lake beds? Second, an extensive literature review regarding dust sources in the RESOLVE region was unable to produce reliable estimates of emission rates for wind-blown dust (Reference 66). Faced with these difficulties, we will assume an arbitrary value with a large uncertainty, 50% ± 25%, as the anthropogenic contribution to soil dust. Fortunately, the assumption here is not critical because soil dust does not account for a large part of light extinction.

Combining the results of the last three paragraphs with the extinction budget of Chapter 7, and using routine error propagation methods, yields an overall estimate of man-made contributions to light extinction. Averaged over the three RESOLVE receptor sites, the estimate is that 77% ± 14% of non-Rayleigh extinction is from man-made sources. Adding in natural Rayleigh scatter, the fraction of total extinction from man-made sources is 59% ± 12%.

The above line of analysis can be taken a step further. The emissions data in Section 4.1.3 indicate that the two upwind air basins (Los Angeles and San Joaquin Valley) have man-made emissions about 10 to 20 times greater than those of the RESOLVE region (see Figure 15). If, based on emissions data, we assume that 90% of the man-made nonsoil components are from transport, we arrive at the estimate that about five-eighths of non-Rayleigh extinction is transported anthropogenic material from upwind air basins, and three-eighths local or natural.

Because sulfates, nitrates, organics, and elemental carbon are apparently dominated by man-made transport, a review of the major source categories for these species (or their precursors) in the upwind air basins was conducted. Table 26 summarizes 1983 SO_x and NO_x emissions for both the Los Angeles basin and San Joaquin Valley (Reference 39) as well as 1982 organic and elemental carbon emissions for Los Angeles (Reference 67). Several features stand out in the table. The petroleum industry is the largest single source category for SO_x, especially in the San Joaquin Valley. Emissions of NO_x are dominated by three categories: gasoline-powered vehicles, the petroleum industry, and diesel trucks. Primary organic emissions come from a large number of relatively small source categories. Elemental carbon comes mostly from engines burning diesel type fuel.

8.2 TRACER-ELEMENT MODEL FOR SOURCE AREAS

An important aspect of source characterization is the quantification of the contributions of major source areas to visibility degradation in the RESOLVE study area. The two obvious upwind source areas are the Los Angeles basin (LAB) and the San Joaquin Valley (SJV). The local Mojave Desert region, i.e., the study region itself, must also be considered. The proximity of these areas creates the necessity to separate the individual contributions using some chemical or tracer-element approach instead of relying on a purely meteorological approach. In this section, measurements at the Cajon and Soledad Passes are used to determine the elemental composition of particles leaving the Los Angeles basin, while Tehachapi Pass is used to characterize particles from the San Joaquin Valley (see Figure 1). These elemental signatures are then combined with particle composition measurements in the high desert to estimate the contributions of the source areas to aerosol loadings at the receptor sites.

TABLE 26. Emissions Inventories for SO_x, NO_x, Primary
Organics, and Elemental Carbon.

SO emissions[a]			NO emissions[a]		
	LAB	SJV		LAB	SJV
Petroleum industry	27%	47%	Gasoline vehicles	47%	22%
Diesel road vehicles	16%	16%	Petroleum industry	9%	31%
Gasoline vehicles	18%	5%	Diesel road vehicles	16%	20%
Ships	15%	0	Off-road equipment	7%	13%
Miscellaneous	25%	32%	Miscellaneous	21%	14%

Fine organic particle emissions[b]		Fine elemental carbon emissions[b]	
	LAB		LAB
Forest fires	16%	Diesel road vehicles	44%
Paved road dust	14%	Off-road equipment	12%
Charcoal broilers	12%	Gasoline vehicles	10%
Gasoline vehicles	10%	Miscellaneous	33%
Primary metallurgical	8%		
Fireplaces	8%		
Miscellaneous	28%		

NOTE: All source categories contributing greater than 8% of the total in either air basin
are listed. The gasoline vehicles category includes motorcycles. The off-road equipment
category is dominated by diesels. The petroleum industry category includes both fuel
combustion and processes in both production and refining.

[a] 1983 inventory by CARB (Reference 39), except petroleum SO_x emissions in the San
Joaquin Valley, were updated to 1986 to reflect the very large recent changes in that
category.
[b] 1982 inventory by Gray (Reference 67).

8.2.1 Analysis Overview

The basis for distinguishing the contribution of the San Joaquin Valley to the Mojave
Desert aerosol is displayed in Figure 47. Fine particles from the San Joaquin Valley exhibit
consistently higher Ni/Pb ratios than do fine particles from the Los Angeles basin. The ratio
of average Ni and Pb contents measured on days with concurrent outflow from both source
basins was 0.64 at Tehachapi and 0.062 at Soledad, an order-of-magnitude difference.

The Ni/Pb ratios measured at the receptor sites range between those characteristic of
the San Joaquin Valley and of the Los Angeles basin. Figure 48 shows an example (for
Edwards AFB) of these ratios. These intermediate ratios reflect varying mixes of Ni-rich
San Joaquin Valley aerosol with relatively Pb-rich aerosols from the Los Angeles basin
and the local desert. High Ni/Pb ratios at the receptor must represent large relative
contributions from the San Joaquin Valley, which is the only source of Ni-rich aerosol.

Nickel and lead were chosen as the basis for the analysis after screening the
composition profiles at the pass sites for elemental indicators of the source region. The Ni-
Pb pair yielded the clearest separation between Tehachapi and the Los Angeles or local
desert source signatures.
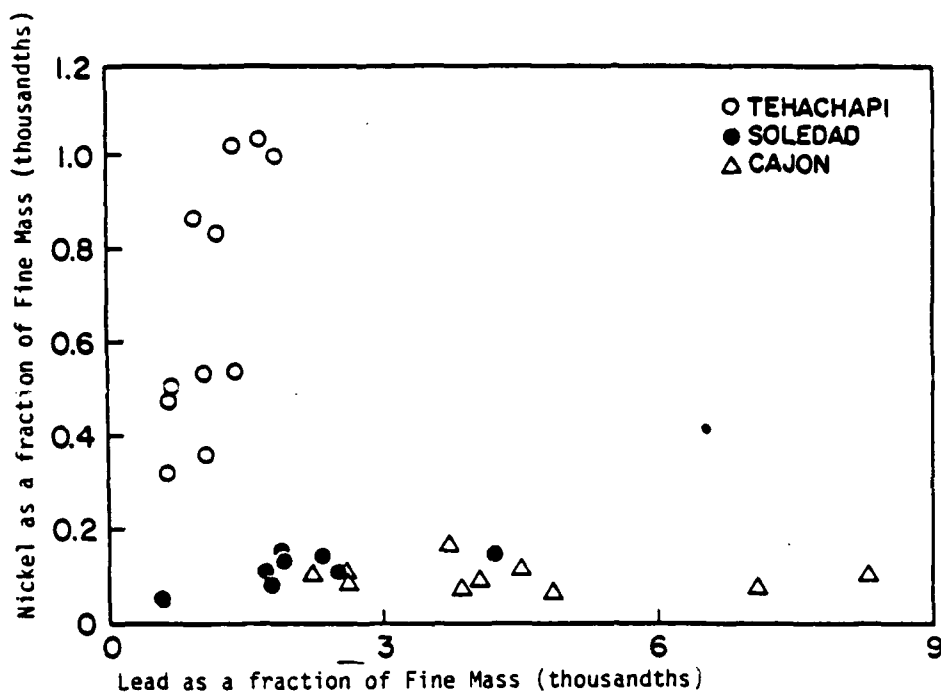
NOTE: Each point represents a 24-hour period with no backflow and at least 18 hours (Tehachapi and Soledad) or 12 hours (Cajon) of outflow.

FIGURE 47. Trace-Element Content of Fine-Particle Samples Collected in Passes on Outflow Days Leading from the San Joaquin Valley (Tehachapi) and the Los Angeles Basin (Soledad and Cajon).
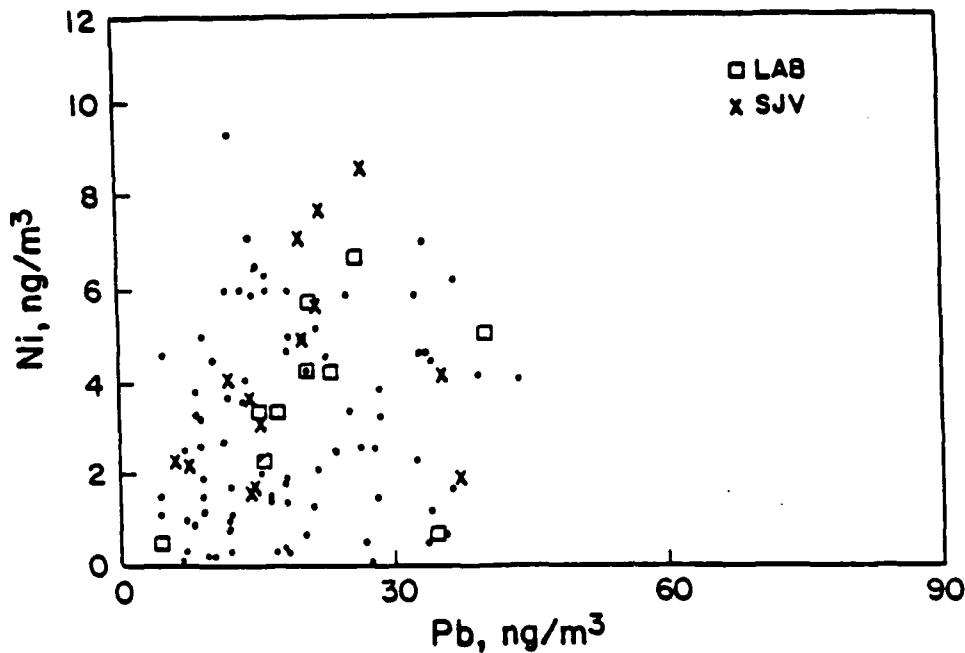
NOTES: • The Ni and Pb scales are in the same ratio as those of Figure 47.
• The symbols distinguish days on which morning 850 mb winds were from the direction of the Los Angeles basin (SE-WSW), the San Joaquin Valley (W-NW), or other.

FIGURE 48. Trace-Element Concentrations of Fine-Particle Samples at Edwards AFB.

No elements were found that reliably resolved Soledad, Cajon, or the local desert from each other. Nickel and lead were also among the most consistently detected and precisely measured of all elements. The average precision was ± 6% for Ni and ± 8% for Pb (see Table 6). A final consideration is that Ni and Pb come from known sources, the combustion, respectively, of residual oil and leaded gasoline, and the physical basis for the observed geographic differences is thus understood (see, for example, the relative contributions of gasoline vehicles and the petroleum industry in the NO_x emission inventories of Table 26).

The correlation level with extinction and fine mass was not one of the criteria for tracer selection. For example, bromine accounts for 55% of tne observed variance in fine mass at Edwards AFB, whereas nickel and lead together account for only 25%. However, the statistical relationship of fine mass to bromine offers little guidance in source-area apportionment because bromine composition does not vary greatly between the regions.

With respect to our approach, information on air mass origin does not appear to be readily available in the synoptic regimes based on Edwards AFB upper-air winds. As seen in the data plotted with various symbols in Figure 48, the synoptic regimes are poor predictors of the Ni/Pb ratio.* Thus, the following analysis does not use data stratifications based on synoptic regimes.

8.2.2 Source Area Characterization

To obtain a representative characterization of the Ni and Pb composition of particles leaving the source areas, pass measurements were chosen based on two pass wind conditions. Individual outflow days had no backflow and substantial outflow from the pass in question; data that met this requirement were used in Figure 47. Joint outflow days had no hours of backflow at any of the three passes. Elemental data that meet both criteria are given in Table 27. Note that the mean composition on joint outflow days is similar to that on individual outflow days.

8.2.3 Theory

The theory for the method employed here is described in detail in Appendix D. This section provides a brief overview and explanation.

Elemental concentrations at each receptor site are assumed to be linear combinations of source contributions from the San Joaquin Valley, the Los Angeles basin, and the high desert. The percentage of Ni and Pb in the primary aerosol from San Joaquin Valley and Los Angeles basin are supplied from measurements in the passes on outflow days. The source contributions represent only material that was already in the particle phase on leaving the source basins. This material can be considered "primary" in the sense that it is directly "emitted" by the source basins. To the degree that gas-to-particle conversion continues downwind of the passes, the primary contributions thus understate the full impact of the source basins.

---

* In retrospect, this is not surprising because air masses from both the Los Angeles basin and the San Joaquin Valley arrive at Edwards AFB from the west. It is difficult for the synoptic regimes to resolve the two source areas under westerly flows.

TABLE 27. Concurrent Ni and Pb Data from Three Pass
Sites and One Receptor Site.

Date	Tehachapi n = 11		Soledad n = 8		Cajon n = 10		Edwards AFB		
	Ni/FM ppm(m)	Pb/FM ppm(m)	Ni/FM ppm(m)	Pb/FM ppm(m)	Ni/FM ppm(m)	Pb/FM ppm(m)	Ni ng/m³	Pb ng/m³	FM µg/m³
Joint outflow days									
6/29/84	1041	1675	133	3520	77	3853	6.7	18.5	11.35
5/19/85	835	1204	156	1871	114	2601	6.5	15.2	11.26
5/25/85	1025	1378	146	2327	*	*	2.1	21.7	12.06
6/12/85	504	696	114	1710	106	2235	3.4	17.4	13.72
6/24/85	535	1055	136	1895	*	*	2.3	15.7	12.43
7/12/85	320	635	54	579	81	1720	4.1	12.2	23.33
Average	710	1107	123	1984	95	2602	4.2	16.8	14.13
CV	39%	33%	27%	44%	17%	30%	44%	18%	30%
Individual outflow days									
Average	682	1144	119	2111	102	4382			
CV	38%	34%	28%	45%	26%	42%			

* Not sampled.
CV = Coefficient of variation.
n = Sample size.

Estimates of the elemental content of primary aerosol from the high desert are available from measurements at the receptor sites under conditions minimizing transport from the San Joaquin Valley and Los Angeles basin. These measurements indicate that the Ni/Pb ratio of local source emissions is lower than that of the Los Angeles basin. This conclusion is consistent with available composition measurements for prominent local desert sources (References 66 and 68).

The method becomes understandable when you consider the fact that the San Joaquin Valley is the only source of high Ni/Pb ratios. Thus the Ni/Pb ratio at a receptor can be lowered by various combinations of aerosols from the Los Angeles basin and the high desert, but the Ni/Pb ratio can be raised only by aerosol for the San Joaquin Valley. The upper and lower bounds of the contribution of the San Joaquin Valley at a receptor are determined by assuming alternately that only one of the two other source areas exists in addition to the San Joaquin Valley—either the local high desert or the Los Angeles basin.

Figure 49 provides geometric insight into the dependence of the calculated San Joaquin Valley contribution on Ni/Pb ratios from the other source areas. In Figure 49, the point labeled EDWARDS shows the measured concentrations of Ni and Pb at Edwards AFB on 12 July 1985. The solid lines labeled TEHACHAPI, SOLEDAD, and CAJON show the Ni and Pb concentrations corresponding to varying dilutions of the aerosols measured at these passes on this date. The solid line labeled DESERT shows the Pb concentrations corresponding to varying dilutions of the average aerosol measured at Edwards AFB on

other days when outflow from all three passes was minimal. The fine-mass concentrations of the pass and desert aerosols are indicated by ticks at 1 μg/m³ intervals.

The combining of aerosols in the atmosphere corresponds to the addition of composition vectors in Figure 49. The dotted and dashed lines indicate two methods of representing the measured Edwards AFB aerosol as a sum of source aerosols. Just under 30 μg/m³ of the Tehachapi aerosol is required to reproduce the Ni and Pb concentrations observed at Edwards AFB if the Ni-poor high desert is taken as the only other source (dashed line) Somewhat less is required if some of the Ni is contributed by the Los Angeles basin via Soledad (dotted line).

To determine the San Joaquin Valley contribution at the receptors throughout the year, we must extract, from the limited source measurements, a statistical characterization of source composition and its variability. We made two assumptions: (1) that the measured source (pass site) variability is genuine, and (2) that this source variability is uncorrelated with receptor concentrations. Each of these assumptions is examined briefly here. A more complete discussion is presented in Appendix E.
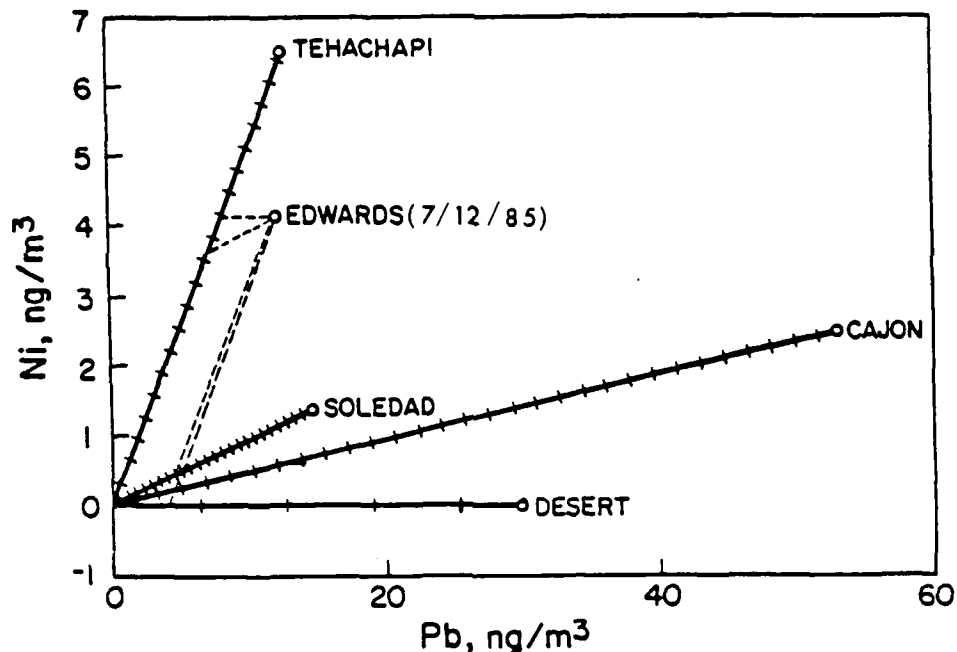
FIGURE 49. A Geometric Interpretation of Source Apportionment. See text for explanation of symbols.

1. Probably, the bulk of the observed variability of Ni and Pb contents in the passes represents real variations in source composition. Measurement precision was good, and averaging over 24 hours of outflow should have minimized the impact of inhomogeneities. Substantial correlations between passes, particularly for Pb content, support the reality of source variability. Note, for example, the uniformly low Ni and Pb contents at all three passes on 12 July 1985, which is suggestive of synoptic conditions favorable to gas-to-particle conversion.

2. The characteristics of the Ni and Pb fractions of fine mass of an upwind basin are controlled by the within-basin source mix and gas-to-particle conversion, while the

concentrations of Ni and Pb at a receptor are controlled by interbasin transport factors. In this case, the covariance of source characteristics and receptor concentration can be expected to be small.

8.2.4 Results

At Edwards AFB during the RESOLVE base year, 84 routine samples were analyzed. Average concentrations for the base year were Ni = 3.1 ng/m³, Pb = 19.3 ng/m³, and FM = 8.5 µg/m³.

A lower bound for the San Joaquin Valley contribution is obtained by attributing all of the remaining aerosol to the Los Angeles basin emissions vented from Soledad. Based on the above averages at Edwards AFB, and the observed Ni and Pb contents at Tehachapi and Soledad on joint outflow days, this lower bound for the average contribution of the San Joaquin Valley primary fine mass at Edwards AFB is 3.2 (±0.5) µg/m³, or 38% of fine mass. The indicated uncertainty in this estimate is the standard deviation attributable to the small sample (n = 6) of source characterizations on which this estimate is based.

An upper bound for the San Joaquin Valley contribution is obtained by attributing all Ni to the San Joaquin Valley. Based on the observed Ni content at Tehachapi on individual outflow days and the average Ni concentration at Edwards AFB, this upper bound for the average contribution of the San Joaquin Valley to primary fine mass at Edwards AFB is 5.3 (±0.7) µg/m³, or 63% of fine mass. Again, the indicated uncertainty is the standard deviation attributable to the small sample (n = 11) of source characterizations on which this estimate is based.

The statistical uncertainty of the above bounds is substantially smaller than their spread. Consequently, we shall be more concerned in what follows with possible biases in characterizing the source areas and implementing the model rather than with random sampling fluctuations.

Table 28 shows results for Edwards AFB under various specific conditions: base year (July 1984 to June 1985), grand average (April 1984 to August 1985), summer (April to September average), easterly upper winds (morning 850 mb wind at Edwards AFB from ENE to SE), no Tehachapi outflow (no outflow for 48 hours on the sampling day and the previous day), and 48-hour Tehachapi outflow (continuous outflow for 48 hours on the sampling day and the previous day). The estimated San Joaquin Valley contributions in Table 28 are consistent with expectations and add confidence to the receptor model results. Meteorological conditions, such as easterly upper winds or an absence of outflow at Tehachapi, should isolate the high desert from the San Joaquin Valley. The San Joaquin Valley contributions estimated for these conditions are, in fact, indistinguishable from zero at all three receptors. Conversely, sustained outflows from Tehachapi should maximize the impact of the San Joaquin Valley on the high desert. The estimated San Joquin Valley contributions for this condition are indeed above average.

Table 29 (calculated as in Table 28) summarizes results for all three RESOLVE receptor sites. Two conditions are considered for each site, the average of all routine measurement days and the average over the 25% of days with highest Bscat. As a fraction of observed fine-particle mass, the estimated contribution from the San Joaquin Valley is fairly uniform overall. However, hazy days at Edwards AFB and Fort Irwin NTC (the receptors nearest the Los Angeles basin) are accompanied by higher than average estimated relative contributions from the Los Angeles basin and high desert.

TABLE 28. Estimated Contributions of the San Joaquin Valley to Fine-Particle Mass Concentrations at Edwards AFB Under Various Conditions.

	Number of days	Measured fine mass, µg/m³	Estimated contributions of San Joaquin Valley, %	
			Lower bound	Upper bound
Edwards AFB				
RESOLVE base year	84	8.5	38	63
Grand average (4/84-8/85)	104	9 3	40	62
April-September average	57	11 7	39	59
Easterly upper winds	5	4 6	0	24
No Tehachapi outflow	5	6 0	0	13
48-hour Tehachapi outflow	24	10 1	66	77

NOTES:
- Lower bounds are based on the data from Tehachapi and Soledad for the 6 joint outflow days and the average concentrations at Edwards AFB for the indicated subsample. Upper bounds are based on the data from Tehachapi for the 11 individual outflow days and the average concentrations at Edwards AFB for the indicated subsample.
- The source characterization days are not necessarily included among the receptor subsamples; for example, the category "No Tehachapi outflow" obviously includes no source-characterization days.

TABLE 29. Estimated Contributions of the San Joaquin Valley to Fine-Particle Mass Concentrations at Three Receptor Sites.

	Measured fine mass, µg/m³	Estimated contributions of San Joaquin Valley, %	
		Lower bound	Upper bound
Edwards AFB			
RESOLVE base year	8.5	38	63
Worst quartile Bsp	13.6	30	51
NWC			
RESOLVE base year	8.9	36	57
Worst quartile Bsp	12.6	42	56
Fort Irwin NTC			
RESOLVE base year	6 5	37	53
Worst quartile Bsp	11 8	32	46

8.2.5 Assumptions and Limitations

The apportionments presented in Tables 27 and 28 rest on the following two critical assumptions:

1. The San Joaquin Valley is the only source of Ni/Pb ratios higher than those measured at Soledad.

2. The Ni/fine-mass (Ni/FM) ratios measured at Tehachapi are representative of the San Joaquin Valley contributions at the receptors.

It is appropriate at this point to reconsider these assumptions and the consequences of any violations.

The assumption that the San Joaquin Valley is the only Ni-rich source is strongly supported by the available data. We have seen that windflows minimizing transport from the San Joaquin Valley were consistently associated with low Ni/Pb ratios at the receptors. The conditions considered here include minimal outflow from all passes (2 days), no outflow from Tehachapi for 48 hours (5 days), and easterly morning 850 mb winds (5 days, 3 with no Tehachapi outflow). The only serious qualification to this result is that all 9 of these minimal-transport days were from 3 winter months: December, January, and February.

The assumption that the Tehachapi Ni/FM ratios are representative of the San Joaquin Valley contributions is more difficult to test. At least four sources of bias can be imagined.

1. San Joaquin Valley aerosol on outflow days might be unrepresentative of San Joaquin Valley aerosol on other days. The identification of outflow days was based solely on wind data, without requiring high mass concentrations or scattering coefficients, precisely to avoid the introduction of a downward bias in Ni/FM and Pb/FM ratios. Seasonal variations do not appear to be a major problem; although 9 of the 11 Tehachapi outflow days were from 4 summer months (May to August), estimated relative contributions for April to September averages differ little from estimated relative contributions for the RESOLVE base year (Table 27). The possibility remains that ventilation itself could, by decreasing residence times in the San Joaquin Valley, produce unrepresentatively high Ni/FM ratios.

2. San Joaquin Valley aerosol might be modified downwind of Tehachapi by gas-to-particle conversion. Little indication exists in the data of significant gas-to-particle conversion downwind of the source basins; "primary" aerosols from the San Joaquin Valley and Los Angeles basin together can account for most or all of the fine mass observed in the high desert. If some residual conversion exists, its effect is to reduce Ni/FM ratios below those observed at Tehachapi.

3. Aerosol leaving the San Joaquin Valley via Tehachapi might be unrepresentative of aerosol leaving the San Jaquin Valley via other routes. Oil recovery operations, the presumed source of high Ni concentrations from the San Joaquin Valley, are clustered in certain southern areas of the valley, e.g., near Lake Isabella Pass. Aerosols leaving the valley at Lake Isabella Pass might be even more rich in Ni, while aerosols from further north might be less rich in Ni.

4. Also, the possibility exists of particle-to-gas conversion (e.g., nitrates and organics). However, the RESOLVE thermidograph nephelometer experiments suggest that the effect on total fine mass should be rather small.

The first two of these sources of bias imply that the model would underestimate San Joaquin Valley contributions. The third source of bias could produce either an overestimate (if hypothesized Lake Isabella Pass effects were critical) or an underestimate (if overall north/south effects were dominant). The last minor point would imply an overestimate. Our qualitative judgment is that the overall bias is probably in the direction of underestimating San Joaquin Valley contributions.

8.2.6 An Alternative Tracer Element Model

To provide a quality assurance check on the Ni/Pb tracer model and to quantify some of the uncertainties in the results, an alternative tracer element model was applied with different solution methods and different data configurations. Appendix D gives a detailed description of this alternative analysis. Only a synopsis will be presented here.

The EPA chemical mass balance (CMB) software (Reference 69) was used to apportion fine mass at each receptor site among the source regions. The EPA CMB software calculates source contributions and associated uncertainties by applying the effective variance solution method (Reference 70) to the CMB equations. The software includes several performance measures that can be used to evaluate the validity of the model application. The most important performance measures with respect to the RESOLVE applications are the "source uncertainty clusters" that identify source profiles that are very similar to each other and thereby produce large uncertainties. The CMB application and validation protocol of Pace and Watson (Reference 71) was followed to assess the validity of the input data and compliance with model assumptions.

The EPA CMB model requires source profiles and ambient concentration profiles, both with specified uncertainties. These were determined from the ambient data at the pass and receptor sites. The source profiles needed selection criteria to identify days thought to be representative of source area composition. These selection criteria were chosen independently from (and differed considerably from) those used in the Ni/Pb tracer model. Furthermore, the data sets for the EPA CMB model were varied to investigate how different averaging methods and different numbers of species affected the solution.

The first part of the analysis involved feasibility testing using the methodology from an early RESOLVE design evaluation study (Reference 3). The conclusions were as follows: (1) the RESOLVE pass site profiles from the Los Angeles basin and the San Joaquin Valley can be used to distinguish these source areas; (2) the key distinguishing species appear to be lead and nickel (or vanadium); (3) profiles at the Soledad and Cajon sites are too similar to be separated from each other; and (4) the addition of a third (local) source profile would interfere with the source apportionment.

The second, more extensive, part of the analysis was to apply the EPA CMB model for various receptor sites, averaging periods, source area profiles, and sets of elemental species. The major findings from this application were as follows:

- Only two source areas can be resolved from each other regardless of the receptor site, averaging period, or set of elemental species. This is consistent with the feasibility testing and with the results of the Ni/Pb tracer model.

- The source contributions for the San Joaquin Valley calculated by the EPA CMB model using only Ni and Pb are generally consistent with those of the Ni/Pb tracer model. The EPA CMB model usually yields values toward the lower end of the

range produced by the Ni/Pb tracer model, but the uncertainties calculated by the EPA CMB model cover most of those ranges.

- The San Joaquin Valley contributions from the EPA CMB model for either 17 or 20 elemental species and two averaging times are generally similar to those of the Ni/Pb tracer model when a nonwinter, local-source profile is included. When such a source profile is excluded, the San Joaquin Valley contributions are much higher, exceeding the upper bound of the Ni/Pb tracer model. The uncertainties are large (about 50% of the source contribution), however, because of the great similarity among the source profiles used with the EPA CMB model.

The overall conclusion of this complementary analysis is that the San Joaquin Valley can be resolved from other source areas but only with uncertainties of 50% or more. The San Joaquin Valley contribution is probably in the range of 25 to 75% of fine-particle mass at the receptor sites. Some of the conclusions may change if the estimates of the local source profile are refined and improved. In addition to the uncertainties discussed in this section, the above results are subject to all the limitations described in Section 8.2.5.

8.3 CONLCUSIONS REGARDING SOURCE AREAS

The purpose of this section is to synthesize all available information about source area contributions to arrive at the most reasonable conclusions possible based on the current data and understanding. Unlike many other areas of this report (e.g., spatial visibility patterns, temporal visibility patterns, or light extinction budget) where firm quantitative conclusions are attained, the findings regarding source area contributions are only semiquantitative. Although the individual analyses concerning source areas are quantitative and objective, they all involve significant uncertainties, and none provides a complete answer covering all source areas. Engineering judgments are required to synthesize the results. The format here will be to state the conclusion and then to list the evidence and considerations behind the conclusion.

On the average at NWC, about one-half (maybe somewhat more) of non-Rayleigh extinction appears to be anthropogenic transport from the San Joaquin Valley, with the remainder of non-Rayleigh extinction arising from local and natural sources. Contributions from the Los Angeles basin seem to be very minor. The evidence is as follows:

- The Ni/Pb tracer model of Section 8.2 predicts average fine-mass contributions from the San Joaquin Valley of 36 to 57%. The tracer model, however, includes natural as well as anthropogenic contributions from the San Joaquin Valley.

- The line of reasoning in Section 8.1 suggests that about five-eighths of non-Rayleigh extinction at NWC is anthropogenic transport from upwind air basins, with the remaining three-eighths being local and/or natural. Wind-flow patterns (Section 4.1.2), spatial visibility patterns (Section 5.1), and SF_6 tracer studies (Reference 14) all indicate that anthropogenic transport at NWC is on the average dominated by the San Joaquin Valley with relatively infrequent contributions from the Los Angeles basin.

- Particle scattering at remote elevated sites near NWC is 64 to 89% of that at NWC itself (Section 3.5). Among other things, this 64 to 89% may be a reflection of regional sources (basically transport) as opposed to local sources.

On the average at Edwards AFB, about one-half of non-Rayleigh extinction seems to represent anthropogenic transport from the San Joaquin Valley, with the Los Angeles basin and natural/local sources also contributing significantly. The source area allocation at Fort Irwin NTC seems similar to that at Edwards AFB, with a slight shift from the anthropogenic transport category to the natural and local categories.

- The Ni/Pb tracer model for Edwards AFB indicated average fine-mass contributions from the San Joaquin Valley of 38 to 63%. (Note that the tracer model results include natural as well as anthropogenic transport from the San Joaquin Valley.)

- Wind-flow patterns (Section 4.1.2), spatial visibility patterns (Section 5.1), and SF_6 tracer studies (Reference 14) all indicate that Edwards AFB is affected significantly by anthropogenic transport from both the San Joaquin Valley and the Los Angeles basin. Local emissions data (Reference 68), the calculation methods of Section 8.1, and various Bscat/meteorology relationships in Chapter 4 suggest that Edwards AFB should have slightly greater total anthropogenic transport (relative to local and/or natural sources) than NWC. However, local and/or natural categories (e.g., portions of organics and soil dust) are certainly not negligible at Edwards AFB.

- Wind-flow patterns and geographical visibility patterns indicate that Fort Irwin NTC, like Edwards AFB, is affected significantly by anthropogenic transport from both the San Joaquin Valley and the Los Angeles basin. The lower pollutant concentrations and geographic location of Fort Irwin NTC, however, suggest that anthropogenic transport should be somewhat less important (relatively) there than at Edwards AFB. This is consistent with the slightly lower San Joaquin Valley contributions predicted by the Ni/Pb model at Fort Irwin NTC (37 to 53%, as opposed to 38 to 63% at Edwards AFB).

For worst-case days at Edwards AFB and Fort Irwin NTC, transport from the Los Angeles basin appears to be more important than it is for average contributions.

- The Ni/Pb tracer model for Edwards AFB and Fort Irwin NTC indicates fine-mass contributions from the San Joaquin Valley of about 40 to 60% on the average, but only 30 to 50% for the worst-case quartile (see Table 29).

- The illustrative case studies of Chapter 9, although very limited in scope, feature the importance of transport from Los Angeles under worst-case conditions at Edwards AFB and Fort Irwin NTC.

- For worst-case days, light extinction at Edwards AFB is slightly greater than at Tehachapi, suggesting the importance of sources other than the San Joaquin Valley (see Table 13).

8.4 EXTINCTION CONTRIBUTIONS FROM MAJOR ANTHROPOGENIC SOURCES

It is interesting to identify the important source categories that contribute to light extinction in the RESOLVE study region. Appendix B presents estimates of the contributions from individual source categories to man-made light extinction. The results pertain to the study region as a whole (i.e., to an average of the three RESOLVE receptor sites) and to annual mean conditions (rather than worst-case days).

The estimation procedure involves three steps:

1. Allocating anthropogenic extinction in the RESOLVE region among three source areas (San Joaquin, Los Angeles, and local desert)

2. For each source area, apportioning man-made extinction among the five aerosol components (organics, sulfates, elemental carbon, soil dust, and nitrates plus NO_2)

3. For each source-area/aerosol-component, allocating the relevant emissions among source categories

In the last step, emission inventories representative of the early/mid-1980s are used, with SO_x emissions in the San Joaquin Valley updated to 1986 to include the large recent decreases in petroleum industry SO_x (References 72 and 73).*

The results indicate that only three individual source categories exist that contribute significantly to man-made extinction in the RESOLVE region as a whole. These source categories are diesel vehicles/equipment (basically highway trucks and off-road mobile equipment but excluding planes/ships/trains), the petroleum industry (mostly from the San Joaquin Valley), and gasoline vehicles (including both exhaust and suspended dust). Together, these sources account for about 60% of anthropogenic extinction, with the diesel category alone contributing about one-quarter of man-made extinction. No other source categories individually account for more than about 5% of man-made extinction in the region as a whole. These findings are consistent with our discussion of emission inventories in Section 8.1. (There we noted that diesels, gasoline vehicles, and the petroleum industry dominated the emission inventories for NO_x, SO_x, and elemental carbon, and that emissions of primary organics came from a large number of relatively small source categories.)

Table 30 summarizes the results, along with overall uncertainties and a breakdown according to aerosol components. The overall uncertainties are based on propagation of judgmental error estimates for the various parameters in the analysis.

We emphasize that these results represent percentage contributions to average anthropogenic extinction. To obtain percentage contributions to non-Rayleigh extinction (including natural aerosols) or total extinction (including natural aerosols and Rayleigh scatter), the above results should be multiplied by 0.77 or 0.59, respectively. For example, the overall allocation for average total extinction is estimated as 24% from natural Rayleigh scatter, 17% from natural particles, 15% from diesel vehicles/equipment, 11% from the petroleum industry, 9% from gasoline vehicles, and 24% from other man-made sources.

We stress that the above results refer to the impact of aggregated source categories on the region as a whole. Historically, DOD personnel have been interested in the effect of specific local sources at individual receptor sites, particularly the impacts of Owens Valley dust storms and Searles Valley air pollution at NWC. Particulate air quality standards have been severely violated in the Owens Valley (Reference 74) and Searles Valley (Reference 75) and concern exists regarding spillover effects at NWC. Qualitatively, this report has provided some insights into air quality effects from the Owens and Searles Valleys. Examples are the visibility isopleths around the Searles Valley in Figure 37, the

---

* From 1983 to 1986, petroleum industry emissions for SO_x in the San Joaquin Valley were approximately as follows (rounded to the nearest 5 tons per day): 1983 = 110 T/D, 1984 = 85 T/D, 1985 = 55 T/D, and 1986 = 45 T/D.

mention of Searles Valley trajectories in Section 9.2.3, and the various discussions throughout this report of suspended dust (which might involve Owens Valley). However, to estimate quantitatively the impact of local source categories at individual receptor sites would require different methodologies than those used herein.

TABLE 30. Man-Made Extinction Allocated Among Major Source Categories.

Source category	Total contribution to man-made extinction	Contribution via each aerosol component				
		Organics	Sulfates	Elemental carbon	Soil dust	Nitrates + NO_2
Diesel vehicles/ equipment	26% ± 7%	3%	6%	12%	1%	4%
Petroleum industry	18% ± 5%	4%	11%	0	0	3%
Gasoline vehicles	16% ± 5%	3%	2%	1%	6%	4%

9.0 ILLUSTRATIVE CASE STUDIES

We have shown that visibility in the RESOLVE region is affected by at least three major source areas—the San Joaquin Valley, the Los Angeles basin, and local desert sources. On many days, the impacts of these source areas at a given receptor site may be combined. However, on some days, only one or two of these sources affect a particular receptor site. A detailed analysis of these latter days can lead to a better understanding of the atmospheric processes that link emissions in the source area to air quality at the receptor site. This is the objective of illustrative case study analysis.

The analyses here will focus on flow patterns, trajectories, transport times, and aerosol compositions for a few days. This approach is different from that of Chapter 8, where general statistical associations and long-term averages were considered. The shorter time scale allows the possibility of direct evidence of the path and time of transport from source region to receptor. However, since the detailed evaluations are time-consuming and expensive, only 4 specific days are analyzed. These days are fairly clear examples of particular types of impacts at the receptors. Keep in mind that the days represent only those specific types of impacts, not the average mixture of source area impacts at the receptor sites.

Appendix F presents a detailed description of the wind trajectories and diurnal air-quality patterns for each day.

9.1 SELECTION OF CASE STUDY DAYS

The days for the illustrative case studies were selected by scrutinizing time series plots of aerosol and extinction data (e.g., Figures 43 through 45) as well as data on hourly/daily wind flows throughout the region. This process not only revealed days when one or two of the three source areas seemed to predominate, but also, in a few cases, even implicated specific source categories, such as dust from dry lake beds (e.g., 20 February and 25 April 1985) and smoke from forest fires (e.g., the second week of July 1985).

General criteria for choosing the case study days were established so that the goals could be achieved within project resources. These criteria included (1) availability of data for the sites of interest, (2) meteorology that allows isolation of only one or two specific source areas at each receptor, (3) a large impact of a particular source area, and (4) time duration of the impact long enough to dominate the 24-hour particle samples. We also wanted to ensure that the examples had variety, including impacts from all the major source areas.

Table 31 lists the days chosen for the analysis and some of the basic characteristics of those days. The days represent transport from the San Joaquin Valley, the Los Angeles basin, and local sources. The days also include examples of wind-blown dust and forest fires. Significant impacts occur at all of the RESOLVE receptor sites on the days shown.

TABLE 31. The RESOLVE Case Study Days.

Date	Characteristics
4 October 1984	Transport from both upwind basins into the desert. All desert sites affected.
14 July 1985	Transport from both upwind basins into the high desert, with all receptor sites affected. Impacts from Ojai forest fires.
25 December 1984	Transport effects at Edwards AFB early in the day. Local and regional impacts at Edwards AFB the rest of the day and at other receptor sites all day.
20 February 1985	Wind-blown dust impact at all receptor sites and the two Los Angeles pass sites. Some transport impacts at receptor sites early in the day.

9.2 DISCUSSION OF THE CASE STUDY DAYS

The following subsections discuss the results for the 4 case study days. Most of the discussion centers on wind trajectories and diurnal patterns of particle scattering. Trajectories are intended to represent the general path of air parcels on their way to the sampling sites. The details of this analysis are presented in Appendix F.

9.2.1   4 October 1984

4 October 1984 was a day of transport to the RESOLVE receptor sites from both the San Joaquin Valley and the Los Angeles basin. On this day, all four RESOLVE desert sites showed a dramatic increase in particle scattering in the early-to-late afternoon. Particle scattering at both Tehachapi and Cajon Passes slowly increased most of the day, while the particle scattering at Soledad Pass increased dramatically in the afternoon. Outflow (flow into the high desert) occurred all day from all three passes.

Trajectories for Edwards AFB indicate that morning air parcels took about 6 hours to travel from the pass regions. However, by late afternoon, the trajectories were significantly shorter and traveled along a more direct route from the Los Angeles basin. An increase in particle scattering at Edwards AFB (between 1400 and 1600 PST) occurred in an air parcel that had passed into the desert about the same time as a large increase in particle scattering was measured at Soledad. According to the 1600 PST trajectory, this air parcel was in the San Fernando Valley area most of the morning before crossing the mountains near Castaic Lake (northwest of Soledad Canyon) and arriving at Edwards AFB.

The Ni/Pb ratio at Edwards AFB on 4 October was slightly higher than the Soledad Pass Ni/Pb, but still significantly lower than the Tehachapi Pass Ni/Pb. (See Section 3.2 and Appendix F for discussion of the significance of the Ni/Pb ratio.) This situation shows that, even in a case when the trajectories indicate transport from the Los Angeles basin all day, the 24-hour average sample still can show a small influence from the San Joaquin Valley.

The wind at NWC was light and variable until about 1600 PST, then the wind increased in velocity and came from the south-southwest. The trajectories indicate that the air parcels had been within about 15 miles of NWC for the last day or more until late afternoon. By 2000 PST, trajectories indicate that transport from the Tehachapi Pass region was established. This occurrence matches a significant increase in particle scattering that lasted the rest of the day. This action is a typical pattern at NWC.

The particle scattering diurnal pattern at Fort Irwin NTC was very similar to that at NWC. However, the wind was higher than at NWC and was consistently from the west to southwest all day. Trajectories were from Tehachapi until late in the day, when transport shifted to the Soledad region, the transport time decreased, and a sharp increase in particle scattering occurred. Later trajectories indicate transport from Cajon Pass.

The data for Fort Irwin NTC on 4 October contain an interesting phenomenon. During the worst particle scattering hours of the day, the Los Angeles basin was the major contributor to the aerosols measured at Fort Irwin NTC (as indicated by the trajectories). However, the major source area contributing to the 24-hour average concentrations (as indicated by the Ni/Pb ratio) was the San Joaquin Valley. Thus, the source area contributions during the worst hours of this particular day seem to be very different than the source area contributions averaged over the complete day. This may not be the typical situation at Fort Irwin NTC, since we have only looked at a very small subset of the RESOLVE data in this manner.

9.2.2   14 July 1985

14 July 1985 is another day of transport from both the San Joaquin Valley and the Los Angeles basin to the RESOLVE receptor sites. However, this day provides an interesting contrast, since many of the characteristics are significantly different than those of 4 October 1984.

At NWC, winds were light and variable until almost noon. Then the winds picked up and came from the south to the southwest for the rest of the day. The particle scattering was modest and steady until the wind speed increased and a pulse arrived from the Tehachapi region. This particle scattering pulse coincided with a shorter transport time and an air parcel that had been in the southern San Joaquin Valley during the early morning. NWC particle scattering dropped back to its prenoon value in the midafternoon, even though transport was still quick (about 4 hours) and from the Tehachapi region. These later air parcels were in the southern San Joaquin Valley about noon, rather than early morning, and may have experienced less emissions and less reacting time before arriving at NWC.

Trajectories show that a similar air parcel, along with a scattering pulse, arrived at both Edwards AFB and Randsburg Wash. However, right after this pulse, an air parcel from the Los Angeles basin began arriving at both Edwards AFB and Randsburg Wash.

The trajectories indicate that all air parcels arriving at Fort Irwin NTC on this day had originated in the Los Angeles basin. The particle scattering pulse in the late afternoon corresponds to a shorter transport time. The interpretation of the Fort Irwin Ni/Pb data is again confusing (see discussion for 4 October 1984). The hourly trajectories indicate transport from Los Angeles all day, while the 24-hour Ni/Pb ratio suggests significant San Joaquin Valley influence.

The case study days were chosen to represent specific types of effects at the RESOLVE receptor sites, not to represent average impacts. However, a comparison of the chemistry measurements for the case study days and the RESOLVE base year is valuable. Table 32 presents the chemical component data for this comparison.

TABLE 32. Percentage of Various Components at the RESOLVE Sites.

Day	Component	EDW	CHL	FOR	RAW	TEH	SOL	CAP
RESOLVE base year	Organics	32	37	29	30	34	30	36
	Sulfate	30	24	28	32	26	32	27
	EC	6	6	7	5	4	8	7
	Soil	16	20	27	17	15	10	8
	Remainder	16	13	9	16	21	20	22
10/4/84	Organics	43	44	40	36	34	39	40
	Sulfate	43	32	39	28	27	39	40
	EC	3	3	3	2	1	2	2
	Soil	9	9	9	12	9	6	5
	Remainder	2	12	9	22	29	14	13
7/14/85	Organics	59	65	56	61	43	58	59
	Sulfate	19	17	19	15	21	15	23
	EC	2	2	2	2	0	2	2
	Soil	8	11	10	18	13	6	6
	Remainder	12	5	13	4	23	19	10
12/25/84	Organics	28	37	–*	--	--*	--	57
	Sulfate	11	2	--	--	--	--	9
	EC	0	0	--	--	--	--	6
	Soil	2	2	--	--	--	--	11
	Remainder	59	59	--	--	--	--	17
2/20/85	Organics	33	--	12	11	52	21	26
	Sulfate	20	--	19	--	32	19	22
	EC	2	--	1	1	3	2	2
	Soil	38	--	77	--	16	44	51
	Remainder	7	--	–5	--	–3	14	–1

* Fine mass less than 1.5 µg/m³

The two transport days (4 October 1984 and 14 July 1985) had markedly different chemical patterns. Organics were much higher than average at all receptor sites on 14 July, while sulfates were somewhat higher than average at three of the four sites on 4 October. Organic aerosol from the Ojai fires was a major contributor on 14 July (the Ojai fires had gone into a smoldering stage about 10 July and were emitting copius smoke without strong vertical venting from fire heat). It appears that atmospheric conditions were especially conducive to producing sulfate aerosol on 4 October 1984.

9.2.3   25 December 1984

In general, 25 December 1984 was a day with mostly local, high-desert effects on the RESOLVE receptor sites. The wind speeds were light most of the day (and the previous day) and wind direction was more variable than on other days.

Air parcels arriving at NWC apparently spent the last 10 to 20 hours within about 25 miles of that site. The trajectories indicate that the air parcels arriving between 1500 and 2000 PST probably passed through Searles Valley.

Even on this day, with slow winds and mostly local effects, the situation at Edwards AFB is complicated because Edwards AFB is so close to the passes. The morning trajectories indicate slow transport from either the San Joaquin Valley or Los Angeles basin. However, the air parcels that arrived in the late afternoon and evening probably spent at least the last 16 hours in the desert.

Air parcels arriving at Randsburg Wash between about 1300 and 1800 PST had come from the northwest and spent the last 9 to 24 hours within about 45 miles of the monitoring site. Two of the trajectories indicate that air parcels passed through the Searles Valley.

Fort Irwin NTC was much cleaner on this day than the other sites. The morning trajectories indicate that the air parcels had spent at least the last 6 hours north of the sampling site. The air parcels that arrived around noon had spent 10 to 16 hours traveling from the south and southwest, possibly passing through the Barstow area. Late in the day, the air parcels came directly from the east.

The chemical components on this day show an extremely large unmeasured component at Edwards AFB and NWC. Other parts of this report indicate that this unmeasured component may be an indicator of nitrate aerosols.

9.2.4   20 February 1985

20 February 1985 was a day when very high wind speeds and blowing dust were reported at many locations in the high desert and much of Southern California. The synoptic conditions showed strong winds from the north early in the day. However, surface winds were from the west in the western part of the desert until early afternoon, even though extremely strong winds from the north covered the remainder of the desert. On a day such as this, surface winds and trajectories can be misleading about the origin of air parcels. Upper-level winds can carry aerosols long distances, after which the aerosols can be mixed down into a surface layer that had traveled in the opposite direction.

The trajectories indicate transport from the upwind basins at Edwards AFB, Randsburg Wash, and Fort Irwin NTC early in the morning. However, trajectories for NWC (all day) and the other three sites after 1000 PST show strong winds and transport from the north. The high particle scattering levels that occurred throughout the day at all of the sites reflect the influence of wind-blown dust.

The measurement of the soil component at Edwards AFB and Fort Irwin NTC (measurements are not available at NWC and Randsburg Wash) were much higher than normal, confirming a large wind-blown dust component. On this day, even Soledad and Cajon Passes show the strong influence of wind-blown dust (they both had flow from the desert late in the day). The only exception is Tehachapi Pass, where the chemical composition measurements and wind data suggest impacts from the San Joaquin Valley.

9.3 CONCLUSIONS

The case study analysis evaluated a number of days where fairly obvious source impacts existed at the RESOLVE receptor sites. This information helped to provide a better understanding of how visibility impacts occur at the RESOLVE receptor sites. The analysis of flow patterns, transport routes and times, and aerosol concentration patterns in the RESOLVE region provided direct evidence of transport from both the San Joaquin Valley and the Los Angeles basin to the receptor sites.

Large increases in particle scattering at the RESOLVE receptor sites can occur when arriving air parcels contain early-morning concentrations from either the San Joaquin Valley or Los Angeles. Air parcel trajectories indicate that this increase often happens when the wind speed increases and aerosols are quickly transported from the upwind basins to the receptor sites. Under these conditions, transport time from the pass regions to Edwards AFB is often 2 or 3 hours, whereas the corresponding transport time to the more distant RESOLVE receptor sites is often 6 to 8 hours. Particle scattering is generally lower at the receptor sites when the transport time is longer.

On the four case study days, NWC was never impacted by transport of aerosols from the Los Angeles basin. Edwards AFB was often impacted by aerosols transported from the San Joaquin Valley early in the day and by aerosols transported from Los Angeles later in the day. On the case study days, Edwards AFB was never impacted by Los Angeles via Cajon Pass. Randsburg Wash was impacted by both upwind basins. Since Fort Irwin NTC is so far from the San Joaquin Valley, it was hard to document transport from the San Joaquin Valley. However, the large increases in particle scattering at Fort Irwin NTC did occur during transport of aerosols from Los Angeles via Soledad Pass or Cajon Pass.

On one case study day, only local impacts were documented at NWC, Randsburg Wash, and Fort Irwin NTC. Some of the air parcel trajectories passed through the Searles Valley before they arrived at NWC and Randsburg Wash.

Some of the case study analyses are consistent with the concept that, to some extent, the study region is a large, fairly uniform mixing vessel with a relatively long characteristic residence time (on the average, greater than 1 day). The significant residence time implies that daily carryover and background concentrations are substantial. Shorter-term pulses are added to this background from the upwind basins (or local sources) to produce a daily maximum. These pulses and some of the background that day, in turn, become part of the next day's background.

Other aspects of this report that support this view are as follows: (1) the consistent, but weak, average diurnal variations of aerosol concentrations (Section 6.2); (2) the lack of a correlation between Ni/Pb ratios and current-day wind direction (Section 8.2.1); (3) the low spatial variability in extinction budgets and Ni/Pb ratio (Sections 7.3.1 and 8.2.4); and (4) the fact that worst-case conditions at the receptors are more dominated by the nearest air basins than are average conditions (Section 8.2.4).

Appendix A

PRECISION ESTIMATES FOR RESOLVE DATA SETS

The purpose of this appendix is to estimate the precision of various RESOLVE data sets. The discussion is organized according to four types of data: mass/absorption samples, carbon measurements, PIXE/XRF data, and nephelometer measurements.

In general, precision refers to the reproducibility of measurements (the case of random error as opposed to the case of systematic error). Here, precision is defined as one standard error of random deviation away from the stable value (the value with no imprecision). We can estimate from a series of independent, simultaneous, duplicate measurements as the standard deviation of the difference between the two duplicates divided by the square root of two, that is

$$\text{Precision} = \frac{1}{\sqrt{2}} \sqrt{\frac{\sum_{i=1}^{N} (X_{1i} - X_{2i})^2}{N}} \qquad (A.1)$$

The square root of 2 factor is needed because the standard error of the difference between the duplicates should be a $\sqrt{2}$ greater than the standard error of either measurement relative to the stable value.

A-1 MASS AND ABSORPTION DATA

The duplicate fine samples taken throughout RESOLVE should represent all three fundamental sources of error: mass (or absorption) determination, flow rate measurement, and blank uncertainty. Accordingly, the overall precision should be completely characterized by the errors observed in comparing the alternative fine samples. In this section we use the duplicate 2x4 samples to estimate the precision of the 2x4 sampler data for mass and absorption, including the fine, coarse, and total mass fractions.

Figures A.1 and A.2 illustrate the 2783 duplicate samples for fine mass and the 2333 duplicate samples for fine absorption, respectively. The relevant statistics are presented in Table A.1. From Table A.1, it is apparent that the average precision of an individual RESOLVE fine mass sample is .73 µg/m^3 (7.4%), while the average precision of an individual fine absorption sample is .45 Mm^{-1} (7.5%).

Table A.2 shows how precision varies with overall loading. Approximate formulas for the absolute precision of an individual sample as a function of mass or absorption can be derived from Table A.2:

FP:	Precision = .15 + .082*FP$^{.84}$ (µg/m^3)	(A.2a)
ABFL:	Precision = .24 + .034*ABF (Mm^{-1})	(A.2b)

Note that the absorption formula is linear, while the fine mass formula is slightly nonlinear.

Table A.2 and the formulas given above should also characterize the precision of the measurements for total mass and total absorption. At the average TP level of 19.5 µg/m^3, the formula indicates that the precision of total mass is 1.0 µg/m^3 (5.1%). Similarly, at the average ABT level of 7.3 Mm^{-1}, the precision for total absorption is .49 Mm^{-1} (6.7%).
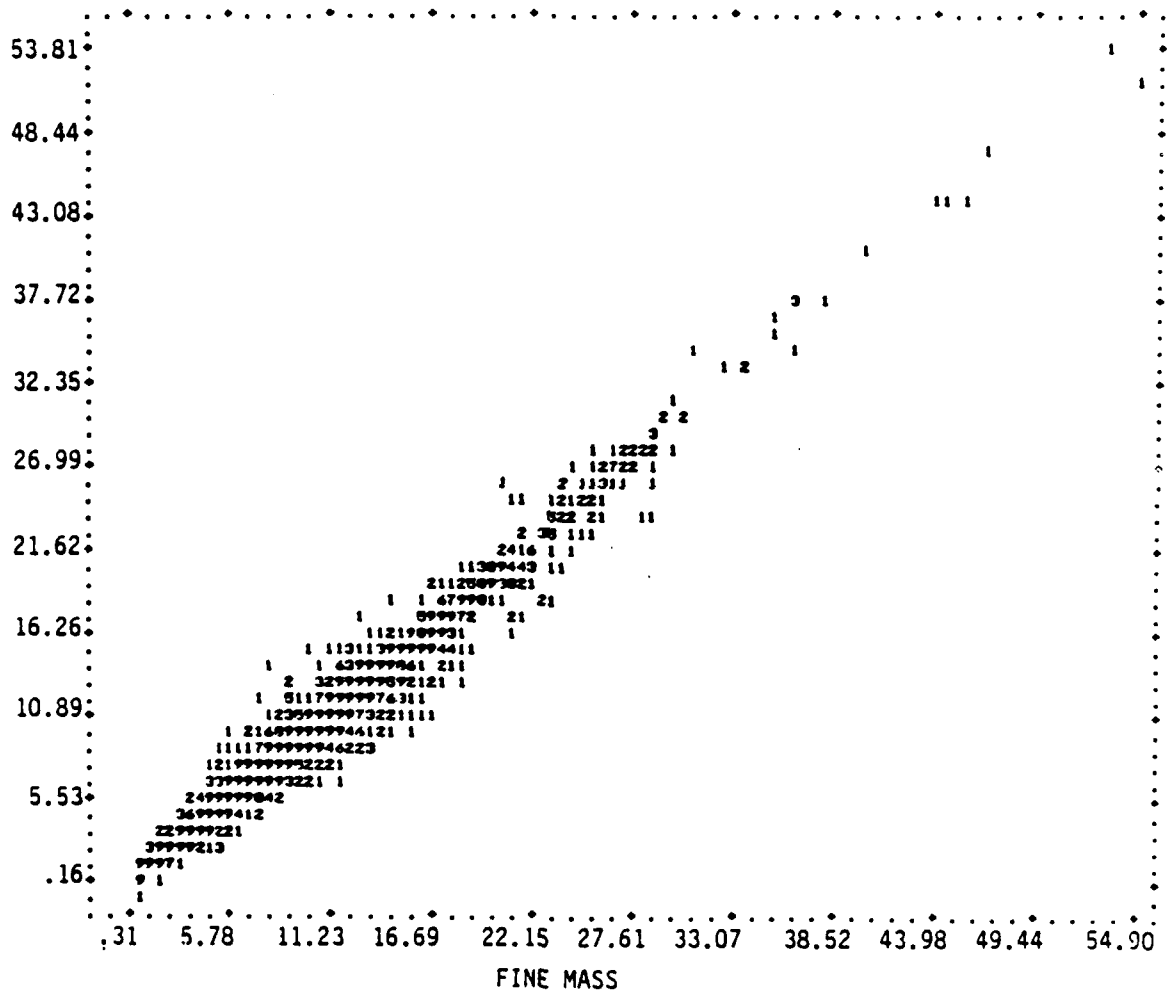
FIGURE A.1 Scatterplot of Simultaneous Fine Mass Measurements
From the Two Alternate Channels of the RESOLVE 2x4 Sampler.
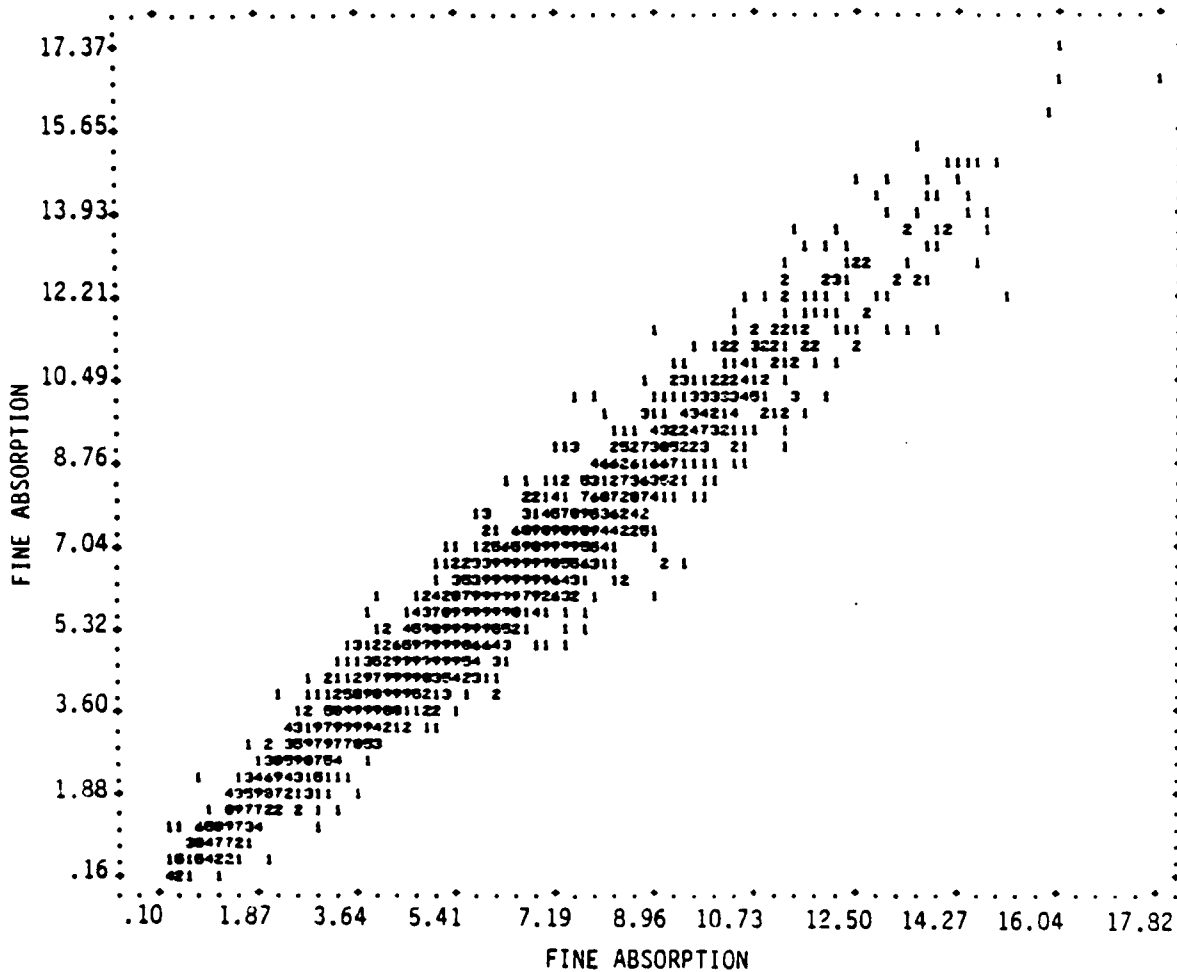
FIGURE A.2 Scatterplot of Simultaneous Fine Absorption
Measurements From the Two Alternate Channels of the RESOLVE 2x4
Sampler.

TABLE A.1. Statistics from Duplicate 2x4 Samples for Mass and Absorption.

	Fine mass	Fine absorption
Sample size	2783	2333
Mean concentration (± standard deviation)	9.93 ± 6.2 µg/m³	6.00 ± 2.8 Mm⁻¹
R (R²) for duplicate samples	.986 (.973)	(.981) (.962)
Precision standard error*	.73 µg/m³ (7.4%)	.45 Mm⁻¹ (7.5%)

* The precision standard error is defined as $\sigma/\sqrt{2}$, where σ is the standard deviation of the difference between the two duplicates.

TABLE A.2. Variation of Precision with Overall Loadings.

Fine mass		Fine absorption	
Concentration, µg/m³	Precision, µg/m³ (%)	Level, Mm⁻¹	Precision, Mm⁻¹ (%)
3.3	36 (10.9)	2.7	33 (12.2)
7.4	59 (8.0)	5.0	41 (8.2)
10.9	86 (7.8)	6.6	46 (6.9)
18.1	96 (5.3)	9.6	57 (5.9)

Note: The results in Table A.2 and Equation 2 pertain to individual fine-particle samples. The fine mass and fine absorption data actually used in the RESOLVE data analysis represent averages of two samples, so that uncertainty is decreased by a factor of $\sqrt{2}$ from the values listed above.

Actually, the RESOLVE data analysis uses averages of the two fine samples for mass and absorption. Thus, for fine mass and fine absorption, the error of the data in the analysis is decreased by a factor of $\sqrt{2}$. The precision of the data in the RESOLVE analysis is thus .73 µg/m³ ÷ $\sqrt{2}$ = .52 µg/m³ (5.2%) for fine mass and .45 Mm⁻¹ ÷ $\sqrt{2}$ = .32 Mm⁻¹ (5.3%) for fine absorption.

Coarse mass and coarse absorption are obtained by subtraction, so the precision is just the root mean square of the fine and total errors. At the average coarse mass of 9.6 µg/m³, the coarse mass precision is $\sqrt{.52^2 + 1.0^2}$ = 1.13 µg/m³ (12%). At the average coarse absorption of 1.3 Mm⁻¹, the coarse absorption precision is $\sqrt{.32^2 + .49^2}$ = .59 Mm⁻¹ (45%).

To summarize briefly, the average precision of the data for the RESOLVE analysis is as follows: FP (5.2%), TP (5.1%), CP (12%), ABF (5.3%), ABT (6.7%), and ABC (45%). The formulas given can be used to estimate the precision of individual samples at various overall loadings.

A.2 ORGANIC AND ELEMENTAL CARBON

This section summarizes the results of the GGC duplicate carbon analyses and derives overall precision estimates based on those results. Figures A.3 and A.4 illustrate the 68 duplicate analyses for organic carbon and elemental carbon, respectively. The relevant statistics are presented in Table A.3. From Table A.3 we see that the precision of the GGC organic carbon analysis is .13 $\mu g/m^3$ (4%), while the precision of the GGC elemental carbon is .14 $\mu g/m^3$ (19%).

The above error figures for analysis do not represent total errors for organic and elemental carbon concentrations. To derive the precision for the concentrations, we must add the errors for the blank values and the flow rates. From a RESOLVE memorandum on carbon blanks (see Section A.5), the blank uncertainty is about .15 $\mu g/m^3$ for organic carbon and .1 $\mu g/m^3$ for elemental carbon. The uncertainty in blank adjusted carbon, obtained by subtraction, equals the root mean square of the analysis and blank uncertainties, $\sqrt{.13^2 + .15^2} = .20$ $\mu g/m^3$ for organic carbon, and $\sqrt{.14^2 + .1^2} = .17$ $\mu g/m^3$ for elemental carbon. The flow rate error is about 5% (Reference 76). Because the flow rate enters as a division, the total relative uncertainties, $\sqrt{.20^2/3.16^2 + .05^2} = \pm 8\%$ for organic carbon and $\sqrt{.17^2/.72^2 + .05^2} = \pm 24\%$ for elemental carbon.

How the precision varies with overall loading was investigated by sorting the data according to quartiles. Table A.4 presents the results. The absolute error decreases with reduced loading, but not in direct proportion, so the percentage error increases at lower loadings. In fact, the generally low concentration of elemental carbon in the RESOLVE samples is a basic cause of the relatively high percentage error for elemental carbon analysis.

A.3 XRF AND PIXE ELEMENTAL CARBON

As was the case with the carbon measurements, the total uncertainty in the elemental data represents the compounded errors in blank values, flow rates, and laboratory analysis. The uncertainty in the blank value is negligible compared to the other two sources of error (Reference 77). The flow rate precision is ± 5% (Reference 78). For the XRF data, the precision of the laboratory analysis was estimated by using the results of 18 duplicate analyses of RESOLVE filters. For the PIXE data, Flocchini (Reference 75) provided estimates of the analytical precision for various elements.

Table A.5 summarizes the total uncertainty for elements of greatest interest in the RESOLVE program. The middle column of the table denotes the analytical technique (XRF versus PIXE) that provides the greatest percent of data above detection threshold. This is the analytical technique that was chosen for the final RESOLVE data set whenever both XRF and PIXE data are available for an element.

Table A.5 shows that, with the exception of vanadium, most of the random uncertainties in the elemental data range from about 5 to 15%. Several of the elements (S, Ca, Fe, K, and Ni) have such low analytical uncertainties that the total imprecision is nearly equal to the volume (flow rate) uncertainty.
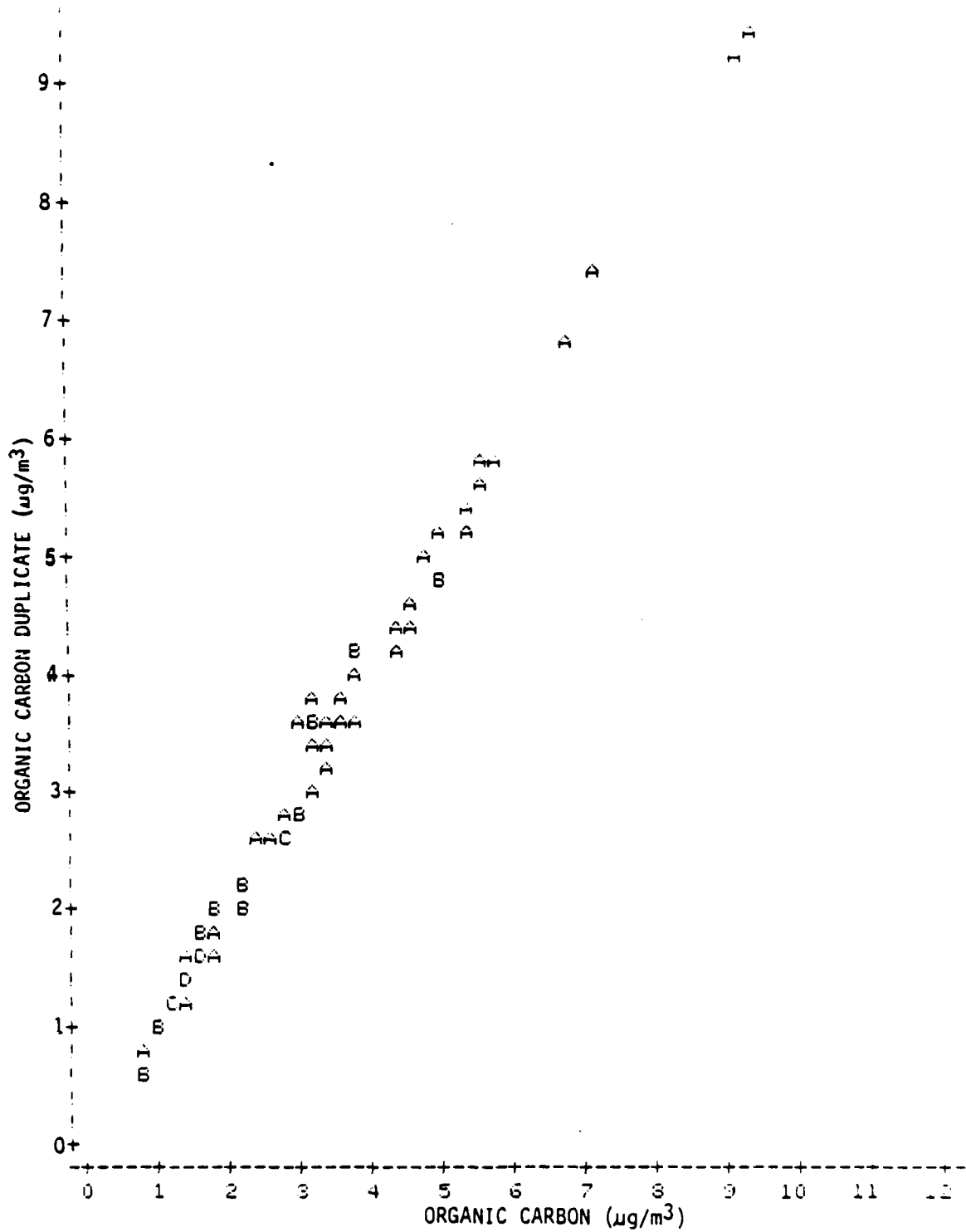
FIGURE A.3. Duplicate Organic Carbon Analyses.
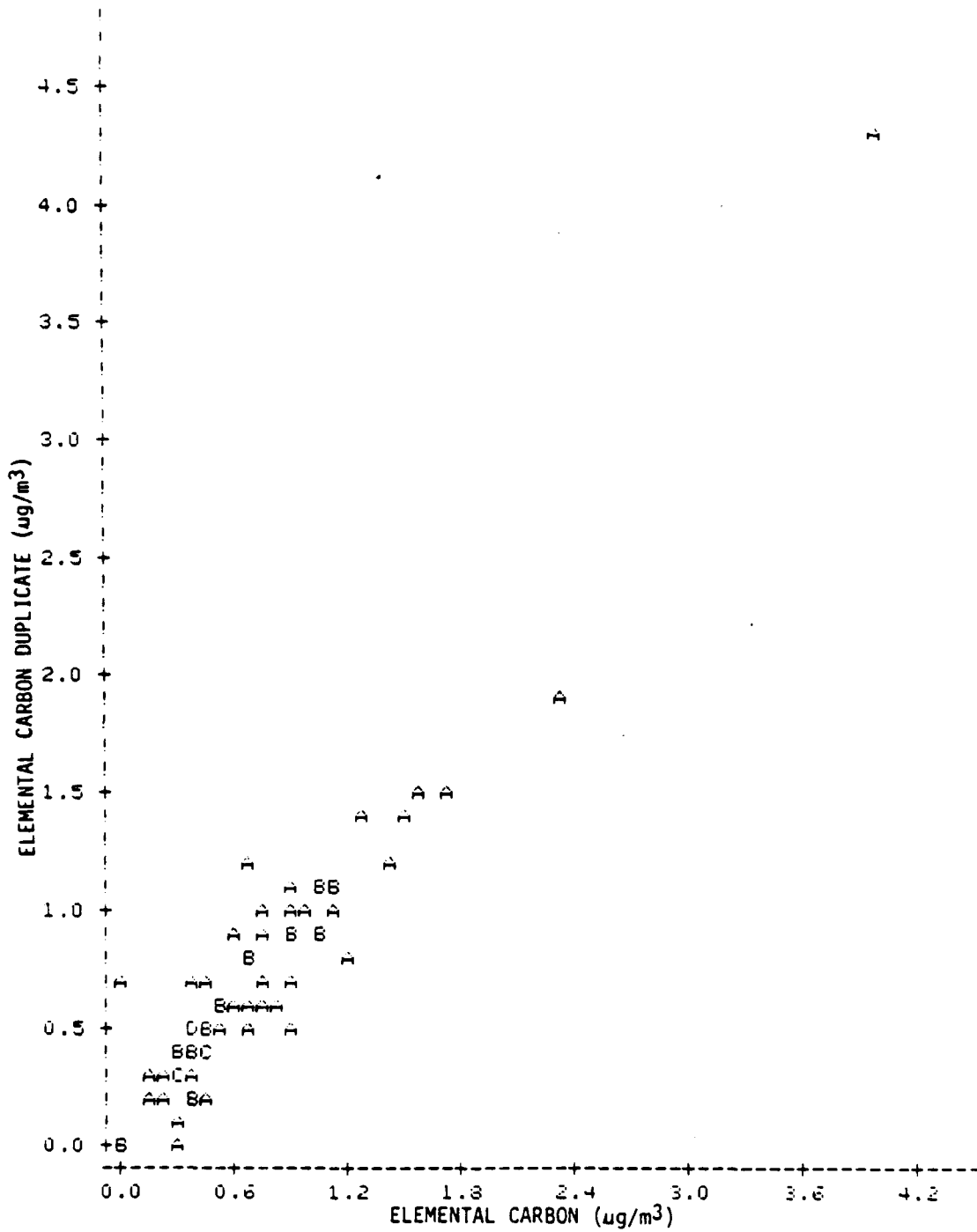
FIGURE A.4. Duplicate Elemental Carbon Analyses.

TABLE A.3. Statistics from GGC Duplicate Carbon Analyses.

	Organic carbon	Elemental carbon
Sample size	68	68
Mean concentration (± standard deviation)	3.16 ± 1.90 µg/m³	72 ± 59 µg/m³
R (R²) for duplicate analysis	.995 (.991)	.947 (.898)
Standard error of analysis*(%)	.127 µg/m³ (4.0%)	136 µg/m³(18.9%)

* The standard error of the analysis is defined as σ/√2, where σ is the root mean square error of the difference between the two duplicates.

TABLE A.4. Precision of Carbon Concentrations as a Function of Loading.

Organic carbon		Elemental carbon	
Average concentration, µg/m³	Precision absolute, µg/m³ (%)	Average concentration µg/m³	Precision absolute, µg/m³ (%)
1st quartile 1.24	17 (14)	1st quartile .24	13 (54)
2nd quartile 2.18	22 (10)	2nd quartile .46	17 (38)
3rd quartile 3.47	28 (8)	3rd quartile .77	.18 (24)
4th quartile 5.78	35 (6)	4th quartile 1.40	.18 (13)

TABLE A.5. Precision of RESOLVE Elemental Data.

	Element	Analysis method	Precision, ± %
Sulfates	S	XRF	5
Soil elements	Si	PIXE	10
	Al	PIXE	12
	Ca	XRF	6
	Fe	XRF	5
	Mn	XRF	11
	Mg	PIXE	12
	K	XRF	5
Others	Pb	XRF	8
	Ni	XRF	6
	V	XRF	25
	Cl	PIXE	8
	Na	PIXE	15
	Zn	XRF	16
	Br	XRF	7

A.4 NEPHELOMETER DATA

In the nephelometer measurements of particle scattering (Bscat), two sources of imprecision exist—zero uncertainty and span uncertainty. The zero uncertainty is additive, while the span uncertainty is multiplicative. Results from RESOLVE special studies (Reference 79) indicate that, for hourly Bscat, the zero uncertainty is ± 1.5 Mm^{-1}, and the span uncertainty is ± 4.1%. Because 24-hour averages involve 8 independent zero and span calibrations, the uncertainties for 24-hour averages are less by a factor of $\sqrt{8}$.

Based on the above information, the precision of hourly and 24-hour nephelometer data can be expressed in units of Mm^{-1} as follows:

$$\text{Hourly:} \quad P_1 = \sqrt{1.5 + .0411 \text{Bscat}^2} \qquad \text{(A.3a)}$$
$$\text{24-hour:} \quad P_{24} = P_1/\sqrt{8} \qquad \text{(A.3b)}$$

At the average RESOLVE Bscat level of 33 Mm^{-1}, the hourly precision is 2.0 Mm^{-1} (6.1%), while the 24-hour precision is 0.7 Mm^{-1} (2.2%).

A.5 RESOLVE MEMO ON CARBON BLANKS (Reference 80)

As part of the RESOLVE monitoring program, quartz filters were exposed on a weekly basis to represent field blanks for the carbon analyses. Of these weekly field blanks, 151 filters—scattered among the monitoring sites and seasons—were analyzed for organic and elemental carbon. The purpose of this memorandum is to investigate the blank values statistically and to derive blank adjustment factors for the RESOLVE carbon data.

Blank values should be independent of the actual sampler flow rates. The blank values physically represent mass per filter or mass per filter area. To allow more insightful interpretation, however, we will present the blank data in units of µg/m^3 by normalizing all values to a standard daily flow of 32 m^3.

Averaged over all sites and seasons, the mean blank values for organic carbon and elemental carbon are 1.13 µg/m^3 and .27 µg/m^3, respectively. The question that immediately arises is do the blank values depend on the site and season?. Figure A.5 shows a plot of the seasonal variations (averaged for all sites) as well as a plot of the site variations (averaged for all seasons).* Obviously, a pronounced, statistically significant seasonal pattern exists for organic carbon blanks. The seasonal variations for elemental carbon as well as the site variations for both organic and elemental carbon are of marginal statistical significance (many t-scores on the order of 1.0 to 1.5).

It seems reasonable that both seasonal and site variations should be included in the specification of carbon blanks.

One possible method to include both seasonal and site variations in the specification of carbon blanks is to use the average blank values by site and by seasonal quarter, as shown in Table A.6. However, the individual quarterly averages contain large statistical

---

* Note that, in the production of Figure A.5, biases introduced by different sample sizes for various seasons and sites were eliminated. For example, the seasonal patterns were computed by first averaging within each site and then averaging the 7 site values each season. Also, the site patterns were determined by first averaging within each season and then averaging the 4 seasons for each site.
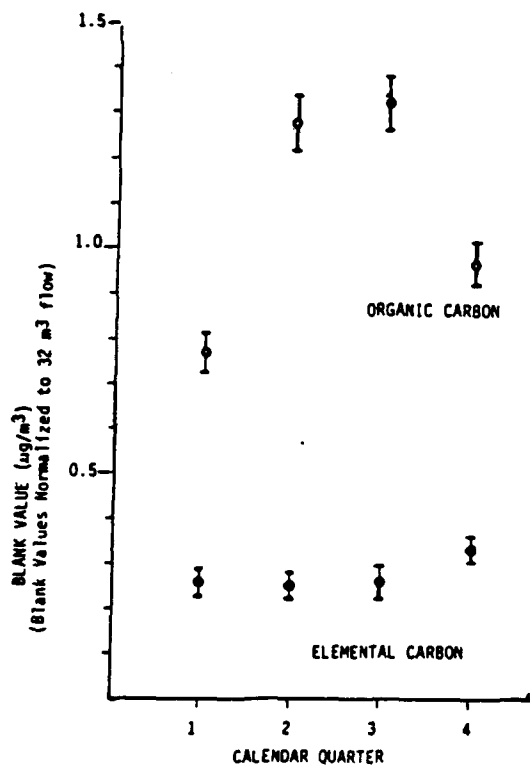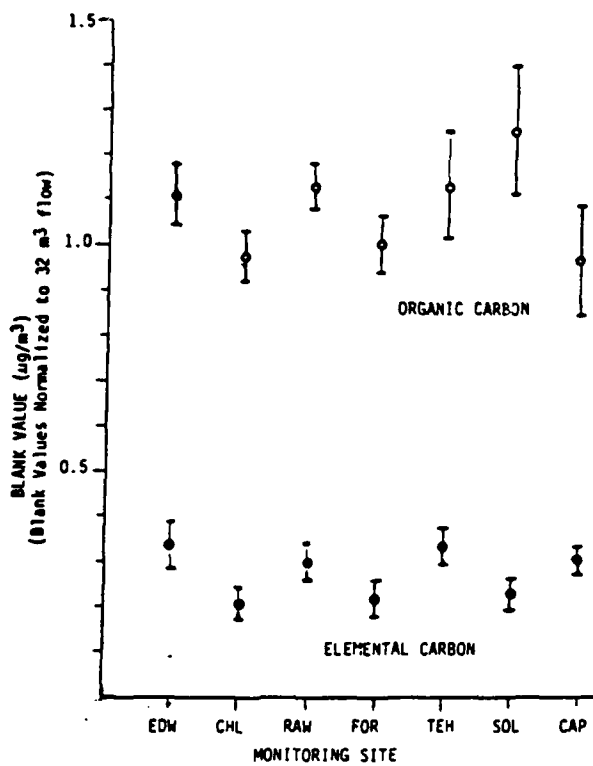
NOTE: Uncertainty bars represent standard errors of the mean values.

FIGURE A.5. Seasonal and Site Variations in RESOLVE Carbon Blanks.

TABLE A.6. Average Carbon Blank Values by Site and Quarter.
(All values correspond to a standard flow of 32 cubic meters per day.)

	Organic carbon (µg/m³), mean ± standard error of mean (sample size)					Elemental carbon (µg/m³), mean ± standard error of mean (sample size)			
	Q1	Q2	Q3	Q4		Q1	Q2	Q3	Q4
EDW	.72 ± .10 (3)	1.15 ± .08 (11)	1.36 ± .14 (8)	1.22 ± .10 (4)	EDW	.13 ± .07 (3)	.35 ± .09 (11)	.47 ± .10 (8)	.37 ± .02 (4)
CHL	.80 ± .12 (4)	1.12 ± .14 (7)	1.15 ± .05 (9)	.82 ± .11 (4)	CHL	.17 ± .09 (4)	.21 ± .07 (7)	.18 ± .06 (9)	.26 ± .07 (4)
RAW	1.12 ± .11 (4)	.95 ± .12 (5)	1.20 ± .02 (5)	1.23 ± .06 (4)	RAW	.28 ± .07 (4)	.26 ± .06 (5)	.19 ± .05 (5)	.47 ± .12 (4)
FOR	.70 ± .04 (5)	1.39 ± .10 (5)	1.02 ± .05 (7)	.90 ± .04 (4)	FOR	.23 ± .07 (5)	.23 ± .08 (5)	.05 ± .07 (7)	.28 ± .06 (4)
TEH	.78 ± .07 (4)	1.39 ± .13 (6)	1.53 ± .28 (6)	.84 ± .10 (4)	TEH	.35 ± .06 (4)	.30 ± .08 (6)	.32 ± .10 (6)	.35 ± .03 (4)
SOL	.67 ± .06 (4)	1.69 ± .22 (7)	1.71 ± .28 (6)	.95 ± .08 (4)	SOL	.26 ± .08 (4)	.16 ± .03 (7)	.23 ± .07 (6)	.26 ± .07 (4)
CAP	.59 ± .11 (4)	1.24 ± .21 (7)	1.26 ± .28 (6)	.79 ± .06 (4)	CAP	.36 ± .03 (4)	.18 ± .03 (7)	.35 ± .05 (6)	.31 ± .04 (4)

aberrations because of the small sample sizes (e.g., third quarter for elemental carbon at Fort Irwin NTC) and substantial discontinuities from quarter to quarter (e.g., organic carbon at Soledad going from .67 µg/m³ to 1.69 µg/m³ from 31 March to 1 April).

A second possibility involves seeking more general patterns in the data. For example, perhaps all sites have similar seasonal patterns so that the yearly mean at each site should be adjusted by the same general set of seasonal factors. This possibility, however, does not appear defensible because the seasonal patterns are, in actuality, not that constant from site to site (see Figure A.6).

A third possibility (the author's recommended possibility) is the scheme presented in Table A.7. Here, to increase the sample size yet include the basic summer/winter dichotomy for organics shown in Figure A.5, the blanks have been averaged over the entire winter 6 months and the entire summer 6 months. To avoid large discontinuities, transition months are taken as the average of the summer and winter values.

A separate question involves the issue as to whether the carbon blank values changed significantly at some time during the monitoring program. This question can be addressed by comparing the average blank values for the summers of 1984 and 1985 (Quarters 2 and 3), the first 2 and last 2 quarters of sampling. These values (including standard errors of the means) are as follows:

	Summer 1984	Summer 1985
Organic carbon blanks	1.33 ± .06	1.18 ± .07
Elemental carbon blanks	.25 ± .03	.27 ± .04
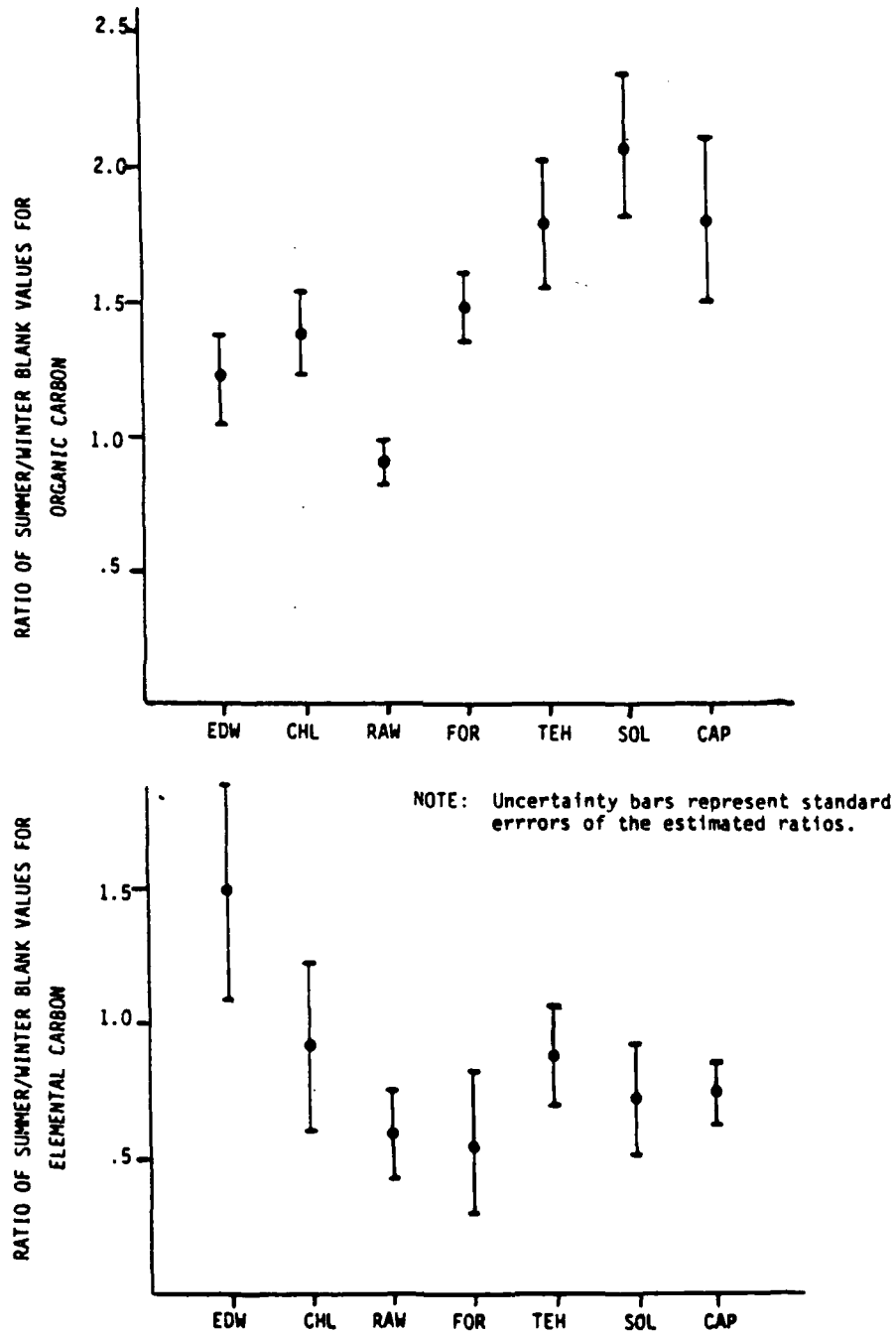
FIGURE A.6. Summer/Winter Ratios of Carbon Blank
Values for the RESOLVE Sites.

TABLE A.7. Average Carbon Blank Values by Site and Seasons.

(All values correspond to a standard flow of 32 cubic meters per day.)

	Organic carbon (µg/m³),				Elemental carbon (µg/m³),		
	Winter Nov-Feb	Summer May-Aug	Transition Mar/Apr/Sep/Oct		Winter Nov-Feb	Summer May-Aug	Transition Mar/Apr/Sep/Oct
EDW	.97	1.25	1.11	EDW	.25	.41	.33
CHL	.81	1.14	.98	CHL	.22	.19	.20
RAW	1.18	1.08	1.13	RAW	.38	.22	.30
FOR	.80	1.20	1.00	FOR	.25	.16	.21
TEH	.81	1.46	1.14	TEH	.35	.31	.33
SOL	.81	1.70	1.26	SOL	.26	.19	.23
CAP	.69	1.25	.97	CAP	.34	.26	.30

No differences are apparent in these numbers.

A final question is what is the uncertainty in the blank values that should be used in assessing the overall uncertainty of carbon concentrations. Apparently, no definitive answer is given by the data. The blank uncertainties are surely not as high as the standard deviations of individual blanks (about 4 µg/m³ for organic carbon and .2 µg/m³ for elemental carbon) because these individual data points contain the carbon analysis uncertainties that are treated separately (about .25 µg/m³, see Reference 80). On the other hand, the blank uncertainties may be greater than the standard errors of the site/quarter means given in Table A.6 because there will be some real week-to-week variations in actual blank exposures. The uncertainty in carbon blanks, in the end, is a judgment call. The author's judgment is that the uncertainty approximately corresponds to a .2 µg/m³ standard error for organic carbon and a .1 µg/m³ standard error for elemental carbon.

Appendix B

ESTIMATION OF EXTINCTION CONTRIBUTIONS FROM MAJOR SOURCE CATEGORIES

This appendix presents calculations to estimate the most important source categories contributing to man-made visibility impairment in the RESOLVE study region. The calculations pertain to an average of the three RESOLVE receptor sites (i.e., to the study region as a composite) and to annual mean conditions (rather than worst-case days).

The procedure for estimating source category contributions to man-made light extinction involves three parts. First, we allocate man-made extinction in the RESOLVE study region among three source areas—San Joaquin Valley, Los Angeles basin, and local desert region. Second, for each of these source areas, man-made extinction contributions are apportioned among the five aerosol components: organics, sulfates, elemental carbon, soil dust, and nitrates plus NO_2. Third, for each source area/aerosol type, the corresponding emissions are allocated among the source categories.

B.1 SOURCE AREA CONTRIBUTIONS TO ANTHROPOGENIC EXTINCTION

In Section 8.3 we concluded that, on the average, approximately one-half of non-Rayleigh extinction represents anthropogenic transport from the San Joaquin Valley. Section 8.1 includes the estimate that, on the average, three-fourths of non-Rayleigh extinction is anthropogenic. Combining these results, we conclude that about two-thirds of anthropogenic extinction in the RESOLVE region comes from the San Joaquin Valley.

The remaining one-third of anthropogenic extinction is assumed to come from local desert sources and the Los Angeles basin. Although our analyses indicate that both of these sources are significant, we do not have an objective method of apportionment for them. We assume that the remaining one-third of anthropogenic extinction arises equally from the local sources and the Los Angeles basin. Accordingly, the overall, regional source area allocation for anthropogenic extinction is as follows: San Joaquin Valley = 2/3, local desert sources = 1/6, and Los Angeles basin = 1/6.

B. 2 ANTHROPOGENIC EXTINCTION COMPONENTS

The average non-Rayleigh extinction budget for the RESOLVE region is as follows (see Table 21): organics 26%, sulfates 24%, elemental carbon 19%, soil dust 18%, and nitrates plus NO_2 13%, with a total non-Rayleigh extinction of 35 Mm^{-1}. It is argued in Section 8.1 that 85% of sulfates/elemental-carbon/nitrates-plus-NO_2, 80% of organics, and 50% of soil dust are anthropogenic. When we combine these two results, the budget for anthropogenic extinction is organics 27%, sulfates 26%, elemental carbon 21%, soil dust 12%, and nitrates plus NO_2 14%, with a total anthropogenic extinction of 27 Mm^{-1}.

For the purpose of this appendix, we need extinction budgets for anthropogenic contributions from each of the three source areas individually. A reasonable estimate of these extinction budgets can be made by noting three constraints:

1. The weighted sum of the three source areas must equal the total anthropogenic extinction budget listed at the end of the first paragraph in Section B.2.

2. The coarse soil dust component should be assigned predominantly to local sources because of the relatively short atmospheric life of coarse particles.

3. With minor exceptions, the budget for transported San Joaquin extinction should resemble that of transported Los Angeles extinction because of similar "five-component" composition for the two source regions (see Table 7). Table B.1 presents source-area

anthropogenic extinction budgets that meet these constraints. All values in the table are stated to the nearest 5 or 10% to more appropriately reflect uncertainties.

TABLE B.1. Extinction Budgets for Anthropogenic
Contributions in the RESOLVE Region.

	San Joaquin Valley[a]	Los Angeles basin[a]	Local desert sources[b]	RESOLVE region
Organics	30%	25%	20%[c]	27%
Sulfates	30%	30%	10%	26%
Elemental carbon	20%[d]	30%[c]	10%	21%
Soil dust	5%[e]	0%[d]	50%	12%
Nitrates plus NO$_2$	15%	15%	10%	14%

[a] With the minor exceptions discussed below, budgets for these two source areas should be similar because of similar "five-component" composition at the pass sites. Because together they dominate the total, they each should be similar to the RESOLVE region anthropogenic budget (except for soil dust).

[b] Coarse soil dust is basically all assigned to the local source category

[c] Emission and ambient data for the desert suggest the possibility of relatively high organics compared to sulfates and elemental carbon.

[d] Tehachapi pass shows relatively less elemental carbon than the Los Angeles passes.

[e] Tehachapi pass shows relatively more soil dust than the Los Angeles passes. Also, transport distances are shorter from Tehachapi, a factor that may be more critical for soil components.

B.3 ANTHROPOGENIC EMISSION INVENTORIES

The third part of the engineering calculation is to assign the anthropogenic components (by source area) to emission source categories. For each source area, man-made sulfates, elemental carbon, and soil dust will be allocated according to anthropogenic inventories for SO$_x$, elemental carbon, and soil dust, respectively. Based on the assumption that two-thirds of man-made organics are primary (Reference 65), two-thirds of organics will be allocated by primary organic aerosol emissions, with one-third apportioned by reactive organic gas (ROG) emissions.

It is reasonable to allocate NO$_2$ according to NO$_x$ emissions (Reference 81), but the situation for nitrates is problematical. Fine aerosol nitrates predominately consist of ammonium nitrate that forms in the atmosphere from gaseous nitric acid and ammonia. Ammonia availability, rather than NO$_x$ availability, may be the controlling factor for aerosol nitrates (References 51 and 82). Nevertheless, because of the lack of ammonia emission inventories, we will apportion nitrates according to NO$_x$ emissions.

An initial set of rough calculations demonstrates that only three source categories contribute significantly to anthropogenic extinction, with any other source category individually accounting for at most about 5% of man-made extinction in the region as a whole. The three important source categories are diesel vehicles/equipment (highway trucks and off-road mobile equipment, but not planes, ships, or trains), the petroleum industry (mostly from the San Joaquin Valley), and gasoline-powered vehicles (including exhaust and suspended dust). The calculations here are restricted to these three source categories.

Table B.2 presents the required emission data. As indicated by the footnotes to the table, three critical references exist: a 1983 emission inventory for California (Reference 39), a

1982 carbon-particle emission inventory for Los Angeles (Reference 67), and an early/mid-1980s particle inventory for the RESOLVE region (Reference 68). The SO_x emissions inventory for the San Joaquin Valley was updated to 1986 to include the large recent decreases in petroleum industry SO_x (References 72 and 73). (See footnote in Section 8.4.)

TABLE B.2. Percent of Emissions from Major Source Categories.

Source category	ROG			Organic particles			SO_x			Elemental carbon			NO_x			Soil dust
	SJV[a]	LAB[a]	Local[a]	SJV[b]	LAB[c]	Local[d]	SJV[a]	LAB[c]	Local[a]	SJV[b]	LAB[c]	Local[d]	SJV[a]	LAB[a]	Local[a]	(SJV + Local)[d]
Diesel vehicles equipment	4	3	7	14	5	9	22	20	22	66	57	43	33	23	27	5
Petroleum industry	48	8	4	4	1	0	47	27	0	1	0	0	31	9	0	0
Gasoline vehicles	19	46	29	5	10	3	5	18	3	2	10	1	22	47	13	50

[a] Based on the 1983 inventory by CARB (Reference 39), the SO_x inventory for the San Joaquin Valley has been updated to 1986 using data from Cleary (Reference 72) and Ouimette (Reference 73). To separate out diesel light/medium-duty vehicles, it is assumed that diesel vehicles account for 10% of total light/medium-duty SO_x, 5% of total light/medium duty NO_x, and a negligible amount of total light/medium-duty ROG (Reference 83).

[b] Based on applying the fine-organic carbon and fine-elemental carbon fractions of Gray (Reference 67) to all source categories in the PM-10 inventory by CARB (Reference 39).

[c] Based on the 1982 inventory by Gray (Reference 67).

[d] Based on the early/mid-1980s inventory by Nero (Reference 68). Vehicular emissions are split between gasoline and diesel using data in CARB (Reference 39) and Gray (Reference 67).

B.4 RESULTS AND UNCERTAINTIES

The anthropogenic contribution of each source category via each aerosol component from each source area is obtained by multiplying the factors of Sections B.1, B.2, and B.3. For example, diesel vehicles/equipment via elemental carbon from the San Joaquin Valley contribute 9% of man-made extinction—67% (contribution of San Joaquin Valley to man-made extinction) times 20% (portion of San Joaquin Valley man-made extinction due to elemental carbon) times 66% (portion of San Joaquin elemental carbon from diesels). Table B.3 presents the composite results for each source category, with a breakdown according to aerosol components.

Table B.3 indicates that the three source categories together account for about 60% of anthropogenic extinction. The diesel vehicle/equipment category alone accounts for about one-quarter of man-made extinction.

One method of estimating uncertainties for the total contribution from each source category is to apply simple error propagation to potential errors in all three sets of factors discussed in Sections B.1, B.2, and B.3. However, this method would not be strictly correct because some of the errors are mutually dependent. Moreover, it would not take advantage of an important simplification that is usually possible in error propagation. This simplification is that, because errors are added according to root mean sums of squares, one or two sources of error usually dominate the total uncertainty. This phenomen is illustrated

in Appendix C, where only one source of error was found to dominate for four of the five extinction budget categories, and only two sources of error were significant in the fifth category.

TABLE B.3. Man-Made Extinction Allocated Among Source Categories.

Source category	Total contribution to man-made extinction	Contribution via each aerosol component				
		Organics	Sulfates	EC	Soil dust	Nitrates + NO$_2$
Diesel vehicles/equipment	25.7%	2.7%	5.8%	12.3%	6%	4 3%
Petroleum industry	18.0%	3 8%	10.8%	.1%	0	3 3%
Gasoline vehicles	15.7%	3 5%	2.0%	8%	5 8%	3 6%

A review of potential errors for the diesel vehicles/equipment category indicates that the predominant source of error is in the largest component, elemental carbon. For this component, errors in the source area contributions (Section B.1) are not important because elemental carbon from diesels has similar significance in all three source areas (so that the result is not very sensitive to source area allocation). The relative error for elemental carbon in the anthropogenic extinction budget allocation (Section B.2) should be nearly the same as the relative error for elemental carbon in the extinction budget ($\pm 32\%$, see Appendix C). For all three source areas, diesels account for about one-half of elemental carbon emissions (Section B.3); the relative error in this third factor is judged to be $\pm 35\%$ based on experience with emission inventories for elemental carbon (References 67 and 83). Accordingly, the total relative error for the elemental carbon category is $\sqrt{32\%^2 + 35\%^2} = \pm 47\%$, and the absolute error on the diesel elemental carbon component is $\pm 47\% \times 12.3\% = \pm 5.8\%$. Arbitrarily assuming a $\pm 50\%$ relative error for the other diesel components, and assuming the errors can be combined by root mean square, gives an overall absolute error of $\pm 7\%$ for the diesel category.

For the petroleum industry, the largest error is in the sulfate contribution from the San Joaquin Valley (the estimated contribution for this category is 9.4%). The relative error in the first factor, source area contribution (Section B.1), is judged to be $\pm 25\%$ based on a review of Chapter 8. The relative error in the sulfate component of the extinction budget (Section B.2) is $\pm 21\%$ (see Appendix C). From experience with emission inventories, the relative error in the percentage contribution by the petroleum industry is judged to be $\pm 30\%$. Propagating these errors yields a relative error of $\pm 44\%$ for the San Joaquin Valley petroleum SO$_x$ category, or an absolute error of 4.2%. Arbitrarily assuming a $\pm 50\%$ relative error for the organics and NO$_x$ categories brings the total root mean square absolute error up to only $\pm 5\%$.

The contribution from gasoline vehicles is generally insensitive to errors in the source area allocation and extinction budgets because gasoline vehicles are significant in all three source areas and in nearly all components of the extinction budget. Also, emissions data are fairly well documented for motor vehicles. The one major exception is in the soil dust category. Uncertainty exists regarding the portion of soil dust that is anthropogenic and the fraction of anthropogenic dust that is caused by motor vehicles. Allowing for a $\pm 50\%$ relative error in both these fractions yields an overall relative error of $\pm 71\%$ and an absolute error of $\pm 71\% \times 5.8\% = \pm 4.1\%$. Assuming a relative error of $\pm 40\%$ for the other four gasoline vehicle components, and assuming root mean square propagation, we arrive at a total absolute error of $\pm 5\%$.

In summary, the contributions of the three source categories to average, regional anthropogenic extinction are as follows:

Diesel vehicles/equipment	26% ± 7%
Petroleum industry	18% ± 5%
Gasoline vehicles	16% ± 5%

To obtain the contributions to average non-Rayleigh extinction (including natural aerosols), these results should be multiplied by 0.77. To obtain the contributions to average total extinction (including natural aerosols and Rayleigh scatter), the above results should be multiplied by 0.59.

Appendix C

UNCERTAINTY ANALYSIS FOR THE EXTINCTION BUDGET

The purpose of this appendix is to estimate the uncertainty in the RESOLVE extinction budget. Specifically, error propagation methods are used to determine the standard errors in the average percentage contributions to non-Rayleigh extinction for five components: organics (ORG = 1.5·OC), sulfates (SUL = 4.12·S), elemental carbon (ELC), soil (SOIL), and nitrates (NO_3) plus NO_2. The error propagation methods are applied to judgmental estimates of uncertainty that encompass instrument imprecisions, climatological variations, potential measurement inaccuracies, and potential modeling errors (e.g., in extinction efficiencies).

Estimates of uncertainty are themselves extremely uncertain. A minimal estimate of uncertainty is supplied by the analytical uncertainty (imprecision) that is determined by replicate measurements of the same observable. The temporal representativeness of the samples contributes an additional uncertainty to average values derived from individual measurements. Further uncertainty is added when measurement and modeling assumptions are not entirely met. The uncertainties here reflect an aggregate of these individual causes of uncertainty. Quantitative values for imprecision were drawn from analytical error propagation specific to RESOLVE measurements and from measurement methods tests performed in RESOLVE and other studies. A year-to-year climatological variability in average values of ±10% was applied to all data based on previous analysis of long-term air quality data.

These estimates have been justified, and modified, in a peer review process that examined the rationale for their selection. A conservative approach was taken, so, if anything, these uncertainties probably overestimate the true uncertainty. Note that all units are $\mu g/m^3$, Mm^{-1}, and m^2/g and that all uncertainties pertain to long-term averages.

For total non-Rayleigh extinction, we have $B_{NR} = B_{NO_2} + Bsp + Bap$. The three terms and the associated uncertainties are as follows:

1. NO_2 absorption, $B_{NO_2} = (4\% \pm 1.5\%)\cdot Bscat$. The uncertainty of B_{NO_2} as a percentage of nephelometer scattering (Bscat) represents judgment of the net effects of instrument accuracy, instrument precision (minor), and climatological representativeness for various data sets. For this formula, $Bscat = 25.6 \pm 2.5$ Mm^{-1}, where the uncertainty here represents judgment of climatological representativeness (inflated well above simple $\sigma/\sqrt{N}$ because of nonindependent sampling).

2. Particle scattering, $Bsp = 28.2 \pm 4.5$ Mm^{-1}. The significant uncertainties here are climatological representativeness (3 Mm^{-1}) and potential error in our estimate as to how the nephelometer must be corrected for missing coarse-particle scattering and water (± 3 Mm^{-1}).

3. Particle absorption, $Bap = 6.2 \pm 2$ Mm^{-1}. The significant uncertainties here are the accuracy correction factor for Teflon absorption ($\pm 30\%$) and climatology ($\pm 10\%$).

Scattering and absorption by particles are allocated among aerosol constituents as described in Section 7.2. The uncertainties are quantified in the following paragraphs.

For organics, the contribution to extinction is $B_{ORG} = (3.75 \pm 1.25)[ORG]/1.13 + (4\% \pm 3\%)$ Bspc. The first term represents fine-particle scattering. The uncertainty in the fine-scattering efficiency (3.75 ± 1.25 m^2/g) is meant to represent all errors in the scattering efficiency appropriate to [ORG], including errors produced by sampling artifacts. The value of 1.13 is a correction factor that makes fine-particle scattering be exactly apportioned (see Section 7.2.3). The error in the concentration of fine organics, [ORG] = $2.7 \pm .1$ $\mu g/m^3$, should represent the error in the relative contribution of organics to fine mass. This error is

extremely small because of the large sample size and because accuracy considerations have been obviated by considering the scattering efficiency as appropriate to whatever [ORG] represents. The second term is coarse-particle scattering, with $4\% \pm 3\%$ assumed to be from organics. Total coarse scattering, Bspc = 5.1 ± 3 Mm^{-1}, has a substantial uncertainty because of the large potential error in our estimate of this parameter.

For sulfates, we again have fine and coarse scattering, $B_{SUL} = (4.25 \pm 1)$[SUL]/1.13 + $(3\% \pm 1.5\%)$Bspc. The uncertainty in the fine-scattering efficiency (4.25 ± 1 m^2/g) is meant to represent all errors in the scattering efficiency appropriate to [SO$_4$]. The error in the concentration of fine sulfates, [SUL] = $2.2 \pm .1$ µg/m^3, again represents the error in the relative contribution of sulfates to fine mass. The second term is scattering by coarse sulfates, $3\% \pm 1.5\%$ of total coarse scattering.

For elemental carbon, $B_{ELC} = (1.5 \pm 2)$[ELC]/1.13 + $(3\% \pm 3\%)$ Bspc + Bapf + $(80\% \pm 10\%)$Bapc. The first term represents fine scattering, with [ELC] = $.5 \pm .04$ µg/m^3. The second term is coarse-particle scattering. The third term is fine-particle absorption, with Bapf = 5.0 ± 1.5 Mm^{-1} (see previous discussion for total absorption). The fourth term is coarse-particle absorption, Bapc = $1.2 \pm .5$ Mm^{-1}, with $80\% \pm 10\%$ of this assumed to be from elemental carbon.

For soil dust, $B_{SOIL} = (1.25 \pm .5)$[SOIL]/1.13 + $(85\% \pm 10\%)$ Bspc + $(20\% \pm 10\%)$ Bapc. The three terms represent fine scattering ([SOIL] = $1.7 \pm .2$ µg/m^3), coarse scattering, and coarse absorption.

For nitrates, $B_{NO_3} = (4.25 \pm 1.5)$[NO$_3$]/1.13 + $(5\% \pm 4\%)$ Bspc. The first term, fine scattering, includes a relatively high uncertainty in the scattering efficiency (± 1.5 m^2/g) because of the lack of a specific modeling analysis for nitrates. The error in the concentration term, [NO$_3$] = $0.9 \pm .3$, is also large because of uncertainties as to the climatological representativeness of the sparse winter sampling. The second term represents coarse scattering.

Carrying out the uncertainty analysis using routine error propagation techniques leads to the following conclusions. Average non-Rayleigh extinction is $B_{NR} = 35.4 \pm 5$ Mm^{-1}, with the dominant source of error being the uncertainty in the degree to which nephelometer scattering needs to be increased to account for missing coarse-particle scattering, and a secondary source of error being the uncertainty in the accuracy correction for particle absorption. The light extinction budget, including one-standard-error uncertainties, is

Organics	$25\% \pm 9\%$
Sulfates	$24\% \pm 5\%$
Elemental carbon	$19\% \pm 6\%$
Soil dust	$18\% \pm 8\%$
Nitrates plus NO$_2$	$13\% \pm 5\%$

It is apparent that the errors for the species contributions range from 5 to 9% of total non-Rayleigh extinction, with the greatest absolute errors being in the organics and soil-dust categories.

The analysis further demonstrates that the error in the extinction budget is dominated by only four types of uncertainty as follows:

1. Uncertainties in the fine-scattering efficiencies for organics, sulfates, and nitrates account for basically all of the error in the organic and sulfate categories, and about half of the error in the nitrate category. (Note that potential errors introduced by sampling artifacts have been included within the uncertainty of the scattering efficiencies.)

2. Uncertainty in the accuracy correction factor for Teflon absorption accounts for the major part of the error in the elemental carbon category.

3. Uncertainty in our estimate of coarse-particle scattering dominates the error in the soil-dust category.

4. Uncertainty in the concentration of nitrate particles contributes about half of the error in the nitrate category.

With respect to the extinction budget, the uncertainties related to measurement imprecision and climatological representativeness are quite negligible (except for the sparse nitrate sampling) because of the large number of observations in the RESOLVE data set. Furthermore, uncertainties related to the allocation of coarse scattering among the five species as well as to the allocation of fine scattering and coarse absorption between elemental carbon and soil dust are of minor importance because of the small magnitude of most of these terms.

Appendix D

THEORY FOR THE Ni/Pb TRACER MODEL

This appendix presents a detailed discussion of the theory behind the Ni/Pb tracer model. Essentially, the discussion here is an expanded, more mathematical version of Section 8.2.3.

The elemental concentrations at a receptor can be expressed as linear combinations from various sources as follows:

$$c_{Ni} = a_{Ni,SJ}\,s_{SJ} + a_{Ni,LAs}\,s_{LAs} + a_{Ni,LAc}\,s_{LAc} + a_{Ni,HD}\,s_{HD} \quad \text{and}$$

$$c_{Pb} = a_{Pb,SJ}\,s_{SJ} + a_{Pb,LAs}\,s_{LAs} + a_{Pb,LAc}\,s_{LAc} + a_{Pb,HD}\,s_{HD} \quad \text{where}$$

(D.1)

c_{Ni} and c_{Pb} = elemental concentrations (mass of element per volume of air) at the receptor.

s_{SJ}, s_{LAs}, s_{LAc} and s_{HD} = source contributions (mass of primary aerosol per volume of air) at the receptor from the San Joaquin Valley, the Los Angeles basin via Soledad Pass, the Los Angeles basin via Cajon Pass, and the high desert.

$a_{i,j}$ = content (mass of element per mass of primary aerosol) of element i in the aerosol from source j.

The coefficients $a_{i,SJ}$, $a_{i,LAs}'$, and $a_{i,LAc}$ in Equation D.1 are supplied by the measurements in the passes on outflow days. The coefficients $a_{i,HD}$ are available from measurements at the receptor sites under conditions minimizing transport from the San Joaquin Valley and Los Angeles basin. The concentrations c_i are measured at the receptor. This leaves four unknowns in the two equations, the source contributions s_j.

D.1 BOUNDING CONTRIBUTIONS

Although Equation D.1 is underdetermined, admitting an infinite number of solutions, it yields useful bounds in the San Joaquin Valley contribution s_{SJ} because the San Joaquin Valley is the only source of Ni/Pb ratios higher than those typical of the receptors. The Ni/Pb ratio of a trial mixture can be lowered by various combinations of aerosols from Soledad Pass, Cajon Pass, and the high desert, but it can be raised only by aerosol from the San Joaquin Valley. It is hard to show that the nonnegative solution to Equation D.1 yielding the minimum value of s_{SJ} is that for which the non-SJV source with the highest Ni/Pb ratio is the only other contributor. Similarly, the nonnegative solution to Equation D.1 yielding the maximum value of s_{SJ} is that for which the non-SJV source with the lowest Ni/Pb ratio is the only other contributor. Figure 49 provides geometric insight into this dependence of the calculated SJV contribution on other sources' Ni/Pb ratios.

For an example of the calculations involved we will bound the contribution of the San Joaquin Valley to Edwards on 12 July 1985. This was an outflow day at all three passes, with Ni/Pb ratios ranked Tehachapi, Edwards, Soledad, Cajon (see Table D.1). The Ni/Pb ratio attributable to local high desert sources can be assumed to be similar to the Ni/Pb ratios measured at Edwards AFB on other days when transport from the San Joaquin Valley and Los Angeles basin was minimal. On two days (23 December 1984 and 16 January 1985), when no more than 4 hours of outflow had been through any of the three passes during a 48-hour period, the average contents Ni/FM and Pb/FM were 86 and 6361 ppm(m), yielding an Ni/Pb ratio that is lower than either of the ratios for the Los Angeles basin.

TABLE D.1 Estimated Contributions of the San Joaquin Valley and Los Angeles Basin to Fine-Particle Mass Concentrations at Edwards AFB on 6 Joint Outflow Days.

Input data	Calculation	Estimated contributions to Edwards AFB fine mass			
		San Joaquin Valley		Los Angeles basin	
		Lower bound	Upper bound	Lower bound	Upper bound
Source distributions and receptor distributions	$S - A^{-1}C$	39	47	0	45
Source distributions and receptor averages	$S - (A^{-1})C$	40	50	0	53
Source averages and receptor averages	$S - (A)^{-1}C$	35	42	0	41

It follows that the lower bound for the contribution s_{SJ} is provided by the (unique) solution to Equation D.1 with $s_{LAc} = s_{HD} = 0$. Setting the contributions from Cajon and the high desert to zero leaves two equations in two unknowns, easily solved for

$$s_{SJ}(lower) = \frac{a_{Ni,LAs} c_{Pb} - a_{Pb,LAs} c_{Ni}}{a_{Ni,LAs} a_{PB,SJ} - a_{Pb,LAs} a_{Ni,SJ}} \tag{D.2}$$

The upper bound for s_{SJ} is provided by the solution to Equation D.1 with $s_{LAs} = s_{LAc} = 0$. Significant uncertainties exist in the Ni and Pb contents of the high desert contribution that were not measured directly as those of the San Joaquin Valley and Los Angeles basin were. The most conservative bound for s_{SJ} is obtained by assuming the Ni content $a_{Ni,HD}$ to be zero, so that the San Joaquin Valley is the sole source of all Ni. The San Joaquin Valley contribution is then simply

$$s_{SJ}(upper) = \frac{c_{Ni}}{a_{Ni,SJ}} \tag{D.3}$$

The contribution of the San Joaquin Valley at Edwards AFB on 12 July 1985 is thus estimated to have been between 49 and 55% of the observed fine-particle mass.

The contributions of the Los Angeles basin and high desert are only loosely constrained by Equation D.1 because they are largely interchangeable. For example, attributing all of the non-SJV aerosol at Edwards AFB on 12 July 1985 to transport through Soledad yields the following estimates: $s_{SJ} = 11.4$ µg/m³, $s_{LAs} + s_{LAc} = 8.6$ µg/m³, and $s_{HD} = 0$ µg/m³. Alternatively, attributing all of the non-SJV aerosol to transport through Cajon yields $s_{SJ} = 12.2$ µg/m³, $s_{LAs} + s_{LAc} = 2.6$ µg/m³, and $s_{HD} = 0$ µg/m³. Alternatively, attributing all of the non-SJV aerosol to high desert aerosol of the type measured at Edwards AFB on the two minimal outflow days yields $s_{SJ} = 12.6$ µg/m³, $s_{LAs} + s_{LAc} = 0$ µg/m³, and $s_{HD} = 0.7$ µg/m³. The estimates for the San Joaquin Valley contribution to fine-particle mass fall within the relatively narrow bounds of 49 and 55% determined earlier, while those for the Los Angeles basin range from 37% down to 0%. Even the sum of all primary contributions is comparatively poorly determined, ranging between 86% down to 57% of the observed total.

This last observation is consistent with the results of regression analysis that shows that Ni and Pb together account for only 25% of the observed variance in fine mass at Edwards AFB.

D.2 AVERAGING CONTRIBUTIONS

We want to determine the San Joaquin Valley contribution at the receptors throughout the year, not just for the few joint outflow days shown in Table D.1. Most receptor measurements were made without concurrent characterization of the source basins. However, sampling frequencies at the passes were about one-third those at the receptors, and many of the pass measurements were compromised by backflow. The full set of receptor measurements can be utilized only by extracting from the limited source measurements a statistical characterization of source composition and its variability.

The equations giving rise to the bounds 2 and 3 can be expressed in matrix terms as C = AS, where

$$C = c_{Ni}, \quad A = a_{Ni,SJ}, a_{Ni,X} \quad \text{and} \quad S = s_{SJ} \tag{D.4}$$
$$c_{Pb} \qquad a_{Pb,SJ}, a_{Pb,X} \qquad s_X$$

where the subscript X denotes a non-SJV source. The solution to Equation D.4 then has the simple form

$$S = A^{-1}C \tag{D.5}$$

We write daily values in terms of their deviation from the mean, the mean denoted by an overbar

$$S = \overline{S} + (S - \overline{S}), A^{-1} = \overline{A^{-1}} + (A^{-1} - \overline{A^{-1}}), C = C + (C - \overline{C})$$

The mean source contribution S can be written in terms of the means and covariance of A^{-1} and C as follows:

$$S = \overline{A^{-1}C} = \overline{(\overline{A^{-1}} + (A^{-1} - \overline{A^{-1}}))(C + C - \overline{C}))} = \overline{(\overline{A^{-1}})C} + \overline{(A^{-1} - \overline{A^{-1}})(C - \overline{C})} \tag{D.6}$$

Equation D.6 shows that the mean contribution S of a source to a receptor can be accurately estimated from mean source characteristics A^{-1} and mean source receptor concentrations C only if the covariance $(A^{-1} - \overline{A^{-1}}) (C - \overline{C})$ between source characteristics Ni/FM and Pb/FM of an upwind basin are controlled by the within-basin source mix and gas-to-particle conversion, while the concentrations Ni and Pb at a receptor are controlled by interbasin transport and dispersion. Only indirect linkages exist between these two sets of factors so that there is reason to expect the covariance of source characteristics and receptor concentrations to be small.

The only data available for calculating source-receptor covariance are those from the 6 joint outflow days of Table D.1, when both source basins were characterized concurrently with measurements at Edwards AFB. The effects of the observed covariance on these days are summarized in the top two rows of Table D.1, which compare the mean source contributions calculated according to the exact Equation D.6 with those calculated neglecting the covariance term. The simplest example is provided by the upper bound for the San Joaquin Valley contribution, for which the matrix equation, Equation D.5, reduces to the scalar equation, Equation D.3: $s_{SJ}(\text{upper}) = a_{Ni,SJ}^{-1} c_{Ni}$. The true mean is $s_{SJ}(\text{upper})$

$= 6^{-1}(0.001041^{-1}0.0067 + ... + 0.000320^{-1}0.0041) = 6.7\ \mu g/m^3$ while the estimate derived from mean values is $6^{-1}(0.001041^{-1} + ... + 0.000320^{-1})0.0042 = 7.0\ \mu g/m^3$. The difference arises from a slight negative correlation ($r = -0.26$) between $a_{Ni,SJ}^{-1}$ and c_{Ni}. Ni concentrations at Edwards AFB tended to be a little higher than average when the Ni content of the San Joaquin Valley aerosol was higher than average. This correlation is statistically insignificant, as are the others underlying the differences between rows one and two. Six samples are too few to provide a reliable test of independence, however, and the decision to neglect source-receptor covariance ultimately must rest on the a priori reasoning outlined in the preceding paragraph.

Another point in Equation D.6 concerns the proper averaging of source characteristics. One interpretation of the observed variability of Ni/FM and Pb/FM in the passes is that it stems from measurement errors and local inhomogeneities, and represents random deviations from true source compositions that are more or less constant. This interpretation underlies the "effective variance" method of Watson, et al., (Reference 70) and leads to the use of $(\overline{A})^{-1}$, the inverse of the mean source composition matrix, in calculating source contributions. An alternative interpretation is that the observed variability reflects real variations in source composition, arising from variations in emissions and gas-to-particle conversion. This interpretation leads to the use of $(\overline{A^{-1}})$, the mean of the inverse source composition matrixes as in Equation D.6. The bottom two rows of Table D.1 compare the source contributions calculated according to the two interpretations. The upper bound for the San Joaquin Valley contribution again provides a simple illustration of the distinction. The inverse mean San Joaquin Valley Ni content on the 6 joint outflow days is $(a_{Ni,SJ})^{-1} = 0.000710^{-1} = 1408$, while the mean inverse is $(\overline{a_{Ni,SJ}^{-1}}) = 6^{-1}(0.001041^{-1} + ... + 0.000320^{-1}) = 1685$.

It seems possible that the bulk of the observed variability of Ni and Pb contents in the passes represents real variations in source composition. Measurement precision was good, and averaging over 24 hours of outflow should have minimized the impact of inhomogeneities. Substantial correlations between passes, particularly for Pb content, support the reality of source variability. (Note, for example, the uniformly low Ni and Pb contents at all three passes on 12 July 1985, suggesting synoptic conditions favorable to gas-to-particle conversion.) The estimates of average source contributions to follow will accordingly be calculated by the formula

$$\overline{S} = \overline{(A^{-1})}\ \overline{C} \tag{D.7}$$

To summarize the discussion in this subsection, use of Equation D.7 implies an assumption that measured source variability is genuine, and uncorrelated with receptor concentrations.

Appendix E

CHEMICAL MASS BALANCE APPROACH TO SOURCE APPORTIONMENT

Section 8.2 described a tracer solution to the CMB equations for determining the upper and lower limits of contributions from the San Joaquin Valley to fine-particle concentrations at RESOLVE receptor sites. This appendix reports the results of the same conceptual model applied with different solution methods and different data configurations. The purpose of this independent application is to provide quality assurance for the results reported in Section 8.2.4 and to provide quantitative estimates of the uncertainties of those results.

E.1 CHEMICAL MASS BALANCE MODELING

The CMB software developed for EPA (Reference 69) was used to apportion annual average fine-particle mass concentrations at Edwards AFB, Fort Irwin NTC, and NWC to regional sources. This software applies the effective variance solution (Reference 70) to a set of chemical mass balance equations to calculate source contributions and their uncertainties. The software provides several performance measures that indicate the validity of each application. The most useful of these performance measures are the "source uncertainty clusters" that identify source profiles that are very similar to each other and cannot be resolved without large degrees of uncertainty. A separate CMB applications and validation protocol (Reference 71) was followed to estimate the validity of the input data and the compliance with model assumptions.

The fundamental assumptions of the CMB are

1. Compositions of source emissions, as perceived at the receptor, are constant over the period of ambient and source sampling.

2. Chemical species concentrations add linearly.

3. All sources with a potential for significantly contributing to the receptor have been identified and had their emissions characterized.

4. Source compositions are linearly independent of each other.

5. The number of sources is less than or equal to the number of pollutant properties.

6. Measurement uncertainties are random, uncorrelated, and normally distributed.

These assumptions are never completely complied with in actual practice. Model testing studies show that substantial deviations from them can be tolerated. The degree of this tolerance is situation-specific, however, and some testing is required for each application of the model. Assumption 4 is the most critical assumption for source apportionment in the RESOLVE study, and model testing and uncertainty analysis is focused on this assumption.

E.2 MODEL INPUT DATA

The CMB receptor model requires source profiles and their uncertainties, and ambient concentrations and their uncertainties. Source profiles were derived from ambient measurements at the source and receptor sampling sites and are presented in Table E.1. Profiles for air exiting the South Coast Air Basin via the Soledad and Cajon Passes and for air exiting the San Joaquin Valley Air Basin via the Tehachapi Pass were calculated from

days in which wind directions pointed from each basin to the desert for more than two-thirds of the 24-hour sampling period. The average fraction of fine mass and the standard deviation were calculated for each of these subsets of samples, with the results appearing in the first three columns of Table E.1.

"Local" source profiles were derived from receptor data at Edwards AFB, NWC, and Fort Irwin NTC by selecting cases for which flow from the deserts into the air basins was greater than one-third of the 24-hour sampling period at all three pass sites simultaneously. These subsets were further divided into winter (November through February, indicated with a W suffix) and nonwinter (March through September, indicated with an NW suffix) subsets prior to calculation of the average and standard deviation of fractional fine-mass composition. Undoubtedly, some contamination of these local profiles exists with contributions from the Los Angeles and San Joaquin Valley air basins, since there was some outflow from these basins during the sampling periods. However, these are the best nonregional profiles obtainable with current data.

Annual averages for the base year for Al, Si, S, K, Ca, Ti, V, Cr, Mn, Fe, Ni, Cu, Zn, Br, and Pb were calculated for each receptor site. The standard error of these averages (standard deviation divided by the square root of the number of samples) was used as an estimate of their uncertainty. Cases were eliminated when any single species did not have valid data reported. Another set of annual averages was calculated for the above species plus Cl, Oc, and EC for the entire data set from April 1984 through August 1985. All valid data were included in each average. The CMB applied to these two different data sets allows the effects of different averaging methods and different numbers of species in the solution to be determined.

E.3 FEASIBILITY TESTING

The source apportionment of nonlocal fine particles at Edwards AFB, NWC, and Fort Irwin NTC depended on the uniqueness of fine-particle chemical composition exiting the South Coast Air Basin and the San Joaquin Valley. These are the only potentially significant regional source contributors to desert sampling sites. The analytical approach applied by Trijonis, et al. (Reference 3), to hypothetical RESOLVE data was applied a posteriori to the actual data taken at Cajon, Soledad, and Tehachapi Passes.

Coefficients of variation for most species in the Soledad, Cajon, and Tehachapi source profiles are generally in a range of 30 to 80%, a range that Trijonis, et al. (Reference 3), found marginal for the resolution of five different sources used in their tests. However, the fractional compositions for the Tehachapi Pass source profile (representing the San Joaquin Valley) is significantly different from the Soledad and Cajon source profiles. The Tehachapi profile was enriched in vanadium and nickel with respect to the other profiles. The Cajon profile (representing the eastern South Coast Air Basin) was enriched in chromium, chlorine, bromine, and lead with respect to the other profiles. The Soledad profile (representative of the northern South Coast Air Basin) exhibited levels for the measured species that were similar to one or the other of the remaining two profiiles.

Random uncertainty proportional to the coefficients of variation was applied to ambient concentrations generated from these three source profiles and equal contributions from each source. The procedure of Trijonis, et al. (Reference 3), was followed to maintain equivalence to the *a priori* tests made for RESOLVE. The results were that contributions from Tehachapi and Cajon could be resolved from each other at an uncertainty level of about 40%. Contributions from Soledad are apparently colinear with Cajon and these contributions

TABLE E.1. Source Compositions and Uncertainties.

Species	SOL	CAP	TEH	EDW,NW	EDW,W	FOR,NW	FOR,W	CHL,NW	CHL,W
AL	.0094	.0130	.0171	.0145	.0037	.0392	.0143	.0386	.0109
	.0057	.0162	.0099	.0068	.0036	.0286	.0102	.0293	.0111
SI	.0180	.0206	.0377	.0473	.0145	.1072	.0398	.0918	.0380
	.0091	.0103	.0207	.0163	.0183	.0779	.0332	.0665	.0316
S	.0915	.0735	.0653	.0812	.0345	.0591	.0806	.0368	.0399
	.0269	.0175	.0195	.0325	.0333	.0257	.0241	.0245	.0084
CL	.0001	.0020	.0005	.0009	.0022	.0005	.0059	.0002	.0019
	.0002	.0014	.0014	.0008	.0020	.0010	.0059	.0005	.0010
K	.0073	.0049	.0107	.0094	.0026	.0139	.0070	.0130	.0085
	.0081	.0032	.0050	.0049	.0034	.0060	.0036	.0080	.0041
CA	.0040	.0042	.0061	.0099	.0017	.0232	.0082	.0155	.0044
	.0024	.0023	.0041	.0040	.0027	.0171	.0059	.0125	.0032
TI	.0005	.0003	.0010	.0010	.0001	.0024	.0010	.0019	.0006
	.0004	.0003	.0006	.0002	.0003	.0015	.0007	.0014	.0006
V	.0001	.0001	.0004	.0003	.0000	.0003	.0004	.0003	.0003
	.0001	.0001	.0002	.0001	.0001	.0001	.0003	.0002	.0002
CR	.0000	.0002	.0001	.0000	.0000	.0001	.0003	.0001	.0001
	.0000	.0001	.0001	.0000	.0001	.0001	.0003	.0001	.0000
MN	.0002	.0004	.0003	.0002	.0001	.0005	.0008	.0005	.0003
	.0001	.0002	.0002	.0001	.0002	.0004	.0008	.0004	.0001
FE	.0053	.0059	.0098	.0112	.0021	.0206	.0068	.0182	.0060
	.0034	.0026	.0059	.0027	.0028	.0126	.0049	.0130	.0054
NI	.0001	.0001	.0007	.0005	.0001	.0004	.0002	.0003	.0003
	.0001	.0001	.0004	.0003	.0001	.0004	.0002	.0003	.0001
CU	.0001	.0005	.0004	.0004	.0002	.0002	.0010	.0004	.0004
	.0001	.0005	.0007	.0003	.0003	.0003	.0013	.0005	.0002
ZN	.0007	.0020	.0008	.0035	.0008	.0019	.0045	.0018	.0016
	.0003	.0014	.0006	.0044	.0008	.0007	.0042	.0028	.0015
BR	.0007	.0013	.0005	.0005	.0004	.0004	.0009	.0004	.0009
	.0003	.0009	.0001	.0001	.0004	.0002	.0006	.0002	.0002
PB	.0026	.0086	.0013	.0028	.0020	.0013	.0033	.0017	.0045
	.0010	.0053	.0005	.0009	.0019	.0010	.0026	.0010	.0012
OC	.3304	.3981	.3515	.3696	.1669	.4413	.6127	.2335	.4229
	.0624	.1409	.1307	.1682	.2755	.1231	.3504	.2020	.1214
EC	.0716	.1505	.0807	.1085	.0606	.1502	.2185	.0470	.1295
	.0272	.0672	.0504	.0274	.0733	.0875	.1202	.0809	.0371

could not be resolved, in the presence of a Cajon contribution, with an uncertainty better than about 90%.

The conclusions from this analysis are

1. RESOLVE source profiles from the South Coast Air Basin and the San Joaquin Valley can be used to separate these sources.

2. The key resolving species appear to be lead, vanadium, and nickel.

3. South Coast Air Basin source profiles measured at Cajon and Soledad are too similar, at least for the species measured in this study, to allow these sources to be separated.

Local source profiles may still interfere with the source apportionment. The nonwinter source compositions reported in Table E.1 for local sources contain higher concentrations for soil-related species such as Al, Si, and Ca when compared to the regional source profiles derived from the mountain passes. Winter profiles contain a larger proportion of organic carbon. The nonwinter profiles also contain from 50 to 75% of the fractional Ni and V found in the Tehachapi profile, which indicates that these profiles are influenced by aerosol from the San Joaquin Valley.

These feasibility testing results significantly relax the original conclusions of Trijonis, et al. (Reference 3), which did not benefit from actual data.

E.4 CHEMICAL MASS BALANCE RESULTS

Table E.2 presents the results of CMB model applications to average receptor concentrations at Edwards AFB, NWC, and Fort Irwin NTC. The source mnemonics refer to the source compositions and their uncertainties presented in Table E.1. Source contributions were calculated by the CMB in several different configurations to estimate the uncertainty of the source apportionments. These configurations consisted of

- Different averaging periods. Chemical concentration averages were calculated for the base year and for all samples taken between April 1984 and August 1985 to determine the effect of different averaging periods on the source attribution process.

- Different receptor sites. Edwards AFB, NWC, and Fort Irwin NTC were treated separately to observe differences. Edwards AFB, being closer to the San Joaquin Valley and Los Angeles air basins, is expected to show a larger contribution from these regions than are NWC and Fort Irwin NTC.

- Different source profiles included in the CMB. It is possible that different source profiles will provide equivalent performance measures. These performance measures are too numerous and complex to report here, but they were examined and compared for each case to determine which of alternative mixtures of source profiles could reproduce the annual average chemical compositions observed at the receptors.

- Different sets of chemical species included in the CMB. The Ni and Pb used in the tracer solution reported in Section 8.2 were used with the base year averages to verify the conclusions of Section 8.2. Seventeen species were

included in CMB calculations for base year data and 20 species were included in the CMB calculations for the averages over all data.

TABLE E.2. Source Contributions and Their Uncertainties
for Different CMB Cases in μg/m³.

(Uncertainty is shown directly under source contribution.)

Case	SOL	CAP	TEH	EDW,NW	EDW,W
EDW Base year Ni, Pb			3.0		8.5
			2.4		9.1
	6.5		2.9		
	3.0		1.7		
		1.8	3.7		
		1.2	1.8		
			4.3	6.0	
			2.6	2.4	
EDW Base year Al, Si, S, K, Ca, Ti, V, Cr, Mn, Fe, Ni, Cu, Zn, Br, Pb	1.0		4.4	4.0	1.9
	3.9		2.4	3.0	5.8
	4.3		6.7		
	2.0		1.9		
				9.5	1.5
				1.8	3.8
			4.3	6.0	
			2.6	2.4	
	2.9	0.5	7.0		
	3.1	1.1	2.0		
EDW All samples Al, Si, S, Cl, K, Ca, Ti, V, Cr, Mn, Fe, Ni, Cu, Zn, Br, Pb, EC, OC	-2.7		14.3	-4.6	13.8
	9.0		6.5	7.2	12.0
				9.9	1.4
				1.4	3.0
	-6.2	5.0	11.9		
	5.7	2.9	3.6		
			12.5	1.0	
			3.1	2.3	
	11.2	1.7			7.0
	4.0	3.1			7.3
			10.3		6.2
			2.3		4.4

TABLE E.2. (Contd.)

Case	SOL	CAP	TEH	CHL.NW	CHL.W
CHL			3.1		2.9
Base year			1 7		1 0
Ni, Pb					
	4.8		3.3		
	2.3		1 8		
		1.4	3.9		
		0.9	1 9		
			- 3	10.2	
			7 4	10.3	
CHL	3.2		1 8	4.5	- 3
Base year	2.4		2.3	2.1	2.0
Al, Si, S, K, Ca, Ti,					
V, Cr, Mn, Fe, Ni,	0.1		7.9		1.3
Cu, Zn, Br, Pb	2.6		1.9		1.6
			8.0		1.3
			1 7		1.1
			4.5	4.4	
			2.2	2.0	
		0.2	8.1		1 0
		2.5	2.4		5.1
CHL	-2.9		4.6	6.0	3 5
All samples	3.1		3.4	2.9	2.4
Al, Si, S, Cl, K, Ca,					
Ti, V, Cr, Mn, Fe,				8.3	3.3
Ni, Cu, Zn, Br, Pb,				2.5	1.9
EC, OC					
	-1.1		12.9		
	2.6		3.0		
			4.3	7 5	
			3.0	3.1	
		1 6	3.4	6.5	
		1.1	2.7	2.8	
			10.0		1.3
			2.0		1.3

TABLE E.2. (Contd.)

Case	SOL	CAP	TEH	FOR.NW	FOR.W
FOR			1.9		2.2
Base year			2.2		2.1
Ni, Pb					
	2.8		1.9		
	1.4		1.1		
		0.8	2.3		
		0.6	1.2		
			-3.8	11.4	
			17.6	24.2	
FOR	1.9		1.3	2.3	0.2
Base year	1.1		1.3	1.0	0.5
Al, Si, S, K, Ca, Ti,					
V, Cr, Mn, Fe, Ni,	1.0		5.6		
Cu, Zn, Br, Pb	1.2		1.4		1.6
				3.5	1.3
				1.3	0.9
			2.2	2.2	0.9
			1.4	1.1	0.7
	1.0	0.0	5.6		
	2.2	0.7	1.5		
FOR	-0.1		2.1	2.5	1.6
All samples	1.8		2.2	1.6	1.2
Al, Si, S, Cl, K, Ca,					
Ti, V, Cr, Mn, Fe,				4.7	1.3
Ni, Cu, Zn, Br, Pb,				1.2	0.8
EC, OC					
	-1.2		9.8		
	2.0		2.3		
			4.3	7.5	
			3.0	3.1	
	0.1		2.8	2.9	1.0
	1.3		1.8	1.3	0.7

While a wealth of information can be gleaned from Table E.2 and the individual outputs from the CMB model applications used to produce Table E.2, the important conclusions to be drawn from these data are the following:

- Only two source types can be resolved from each other for the annual average receptor data, regardless of the averaging period or the chemical species included in the CMB. This statement is consistent with the feasibility testing, which found that when three source types were tested (with the species measured in RESOLVE in excess of detection limits), one or more of the source contributions was associated with uncertainties that far exceeded

the source contribution. In general, the CMB, which included the Tehachapi source profile with a nonwinter local source profile, returned the best performance measures and the lowest uncertainties. In every case, however, the uncertainty-similarity clusters showed that these source profiles are very similar and that the uncertainty associated with their resolution is large (Reference 71). This uncertainty is, however, adequately reflected in Table E.2.

● For the base year averages, the source contributions from the San Joaquin Valley calculated by the CMB are generally consistent with those determined by the Ni and Pb tracer solutions of Section 8.2. The CMB Ni and Pb solutions yield values toward the low end of the ranges cited in Section 8.2, but the uncertainties calculated by the CMB cover most of the ranges specified in the previous section. These uncertainties are large, however, amounting to more than 50% of the source contribution in most cases. These large uncertainties are caused by the great similarity among the source profiles as well as the substantial variability in those profiles as indicated in Table E.1.

● The San Joaquin Valley contributions for the base year with 17 species in the CMB are similar to those of the Ni/Pb solution when a nonwinter local source is included. When such a source type is excluded, however, these San Joaquin Valley contributions are much higher and they exceed the upper bound for the San Joaquin Valley contribution of Section 8.2. This higher contribution is generally because of the much lower concentration of geologically-related material in the Tehachapi source profile when compared to the local nonwinter profiles. These geological species concentrations are reproduced more accurately with the inclusion of the local source profile. Unfortunately, local geological profiles are not available. The geological profiles would substantially improve the results. The conclusion to be drawn here is that the composition of local soil sources must be included in the CMB when a large number of species concentrations are used. The nonwinter local source profile provides the best, though by no means perfect, representation of this.

● Source contribution estimates for the April 1984 to August 1985 averages and 20 CMB species are also consistent with the other analyses when a nonwinter local source profile is included.

The overall conclusion of this complementary CMB analysis is that San Joaquin Valley sources can be resolved from other sources, but only with uncertainties of 50% or more. This means that the San Joaquin Valley contribution is probably in the range of 25 to 75% of the fine-particle mass at NWC and Fort Irwin NTC.

Appendix F

DETAILED ANALYSIS OF CASE STUDY DAYS

This appendix presents a detailed description of the 4 case study days. Most of the discussion centers on wind trajectories and diurnal patterns of particle scattering.

To provide a better understanding of this appendix, we will discuss two issues. One issue is related to the RESOLVE source sites, and the other to the receptor sites.

Photographs and observations of the regions near Tehachapi and Soledad Passes as well as the wind fields developed for the trajectory analysis indicate that significant outflow occurs across whole sections of these mountain ranges, not just through the pass itself. This outflow occurs because the cross section of the particular pass is not always sufficient for all of the flow required by the synoptic conditions, even though the pass is at a lower elevaton than the surrounding mountain range. Thus, both the aerosol and wind measurements at these two passes can only be used as indicators of the material being transported, not as complete representations of the flow. In contrast, wind fields and observations indicate that most of the transport in the Cajon Pass region occurs at the pass. This might be expected, since the mountains around Cajon Pass are much higher than those surrounding Tehachapi and Soledad, and the pass is lower.

The RESOLVE desert sites naturally divide into two groups, Edwards AFB and the other three, because the distance to (and thus transport time from) the pass areas is much shorter for Edwards AFB than the other sites. Edwards AFB is about 30 miles from Tehachapi and Soledad Passes. This distance implies an average transport time of about 6 hours when the wind speed is 5 miles per hour, and about 3 hours when the wind speed is 10 miles per hour. However, the three other desert sites are 65 to 110 miles from any of the pass areas and thus are 13 to 22 hours away at 5 miles per hour, or 6.5 to 11 hours away at 10 miles per hour. The longer transport times make it much more difficult to track air masses from the passes to the more distant desert sites. Pollutant dilution and mixing also reduce the potential impact of a particular pass at the more distant sites. Thus, the analysis of transport to the Edwards AFB site is more straightforward than the analyses for the other three desert sites.

F.1   4 OCTOBER 1984

Figure F.1 shows the hourly wind speed, wind direction, temperature, relative humidity, and particle scattering for Edwards AFB on 4 October 1984. Generally, western flow was established quite early at Edwards AFB. By noon, the flow was southwesterly, becoming quite strong by 1500 PST. The temperature and relative humidity plots show a typical diurnal profile, with the temperature increasing and the relative humidity decreasing during the daylight hours. However, the relative humidity increased quite early (after about 1400 PST) when air from the coastal region began to arrive. The particle scattering increased significantly about the same time.

Figure F.2 shows similar plots for particle scattering at the four RESOLVE desert sites. All four sites showed a dramatic increase in particle scattering in the early to late afternoon. Figure F.2 also shows similar plots for the three pass sites. Particle scattering at both Tehachapi and Cajon slowly increased most of the day, while particle scattering at Soledad increased dramatically in the afternoon. There was outflow (flow into the desert) all day from all three passes.

Figure F.3 shows some example trajectories for air parcels that arrived at Edwards AFB, NWC, and Fort Irwin NTC on 4 October. Such trajectories are intended to represent the general paths of air parcels on their way to the sampling sites. These trajectories were calculated using surface-wind streamline maps drawn from hourly wind speed and wind
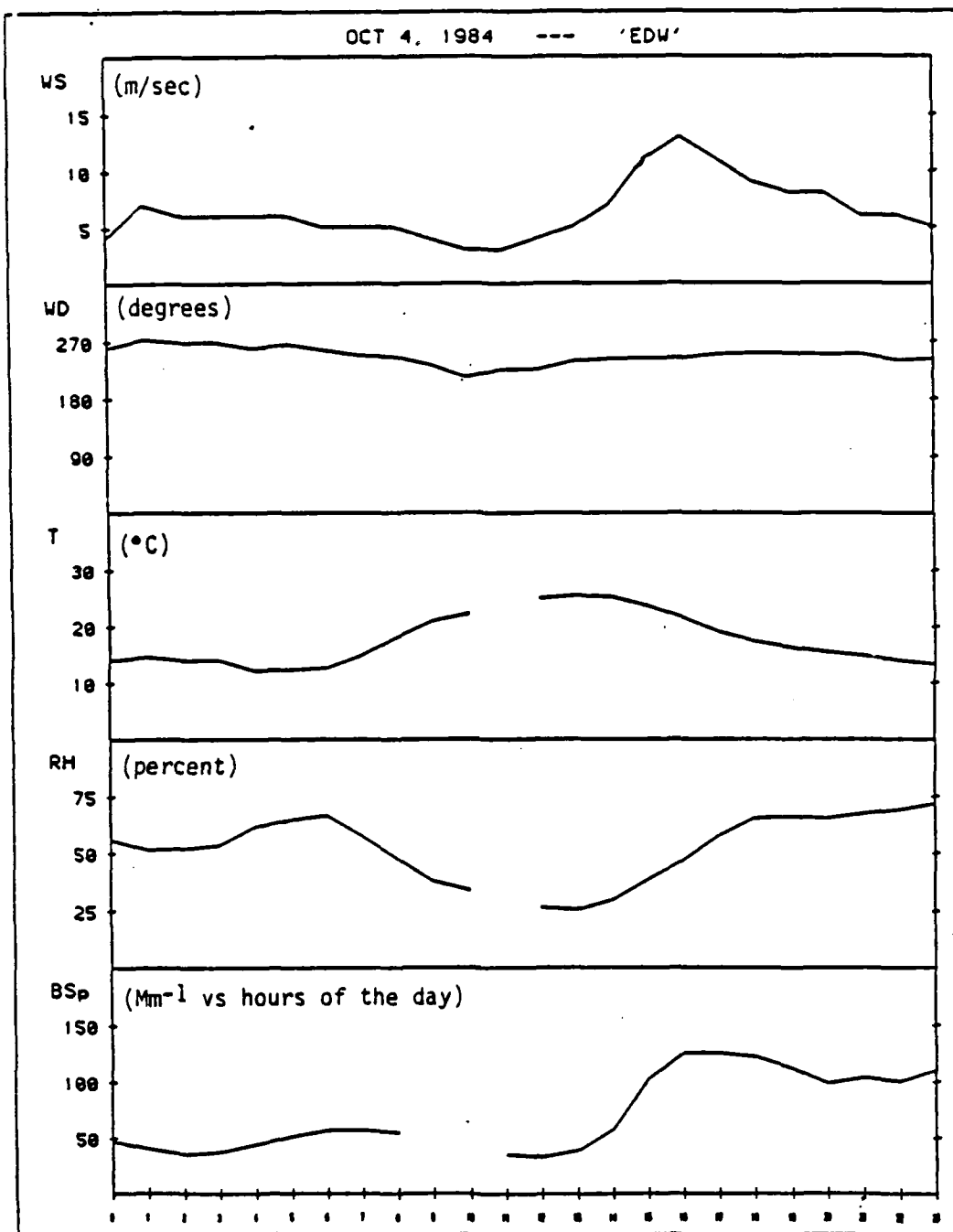
FIGURE F.1. Hourly-Averaged Measurements at Edwards AFB on 4 October 1984.
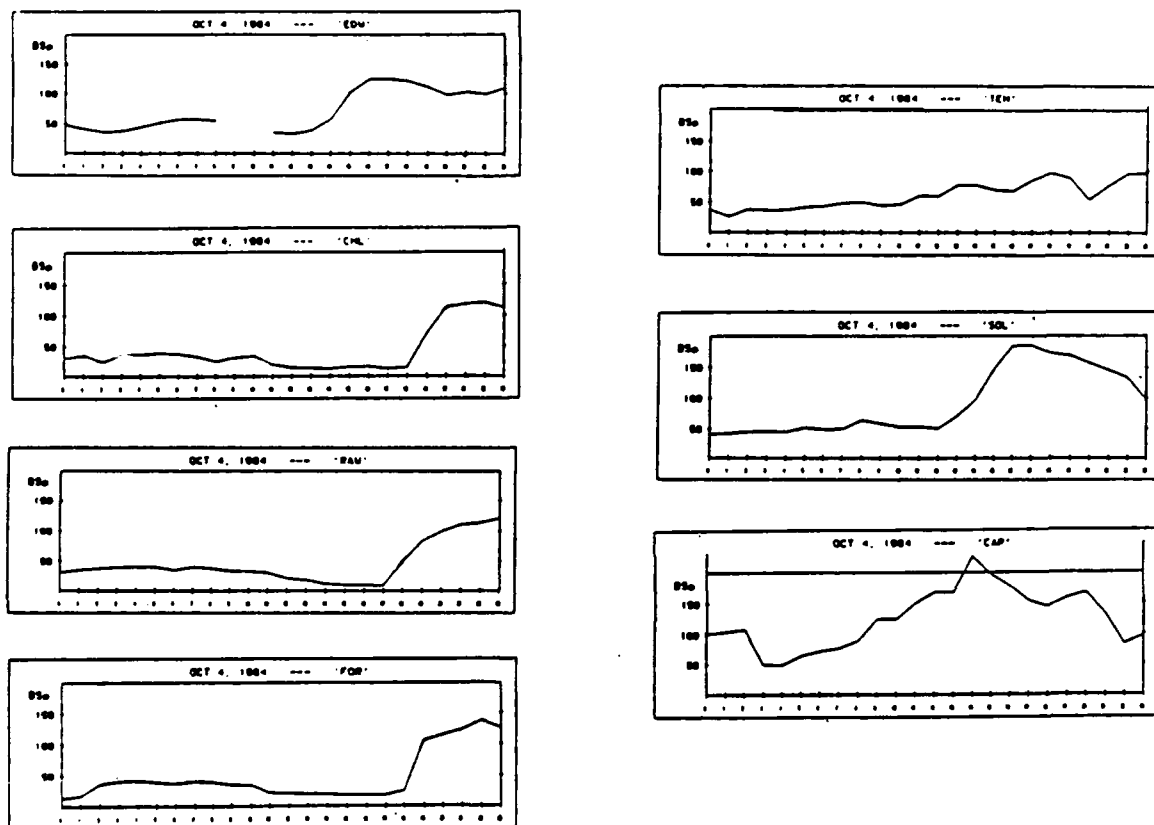
FIGURE F.2. Hourly-Averaged Particle Scattering Measurements at the Seven RESOLVE Sites on 4 October 1984. Particle scattering (Bscat) in Mm^{-1} versus hours of the day.
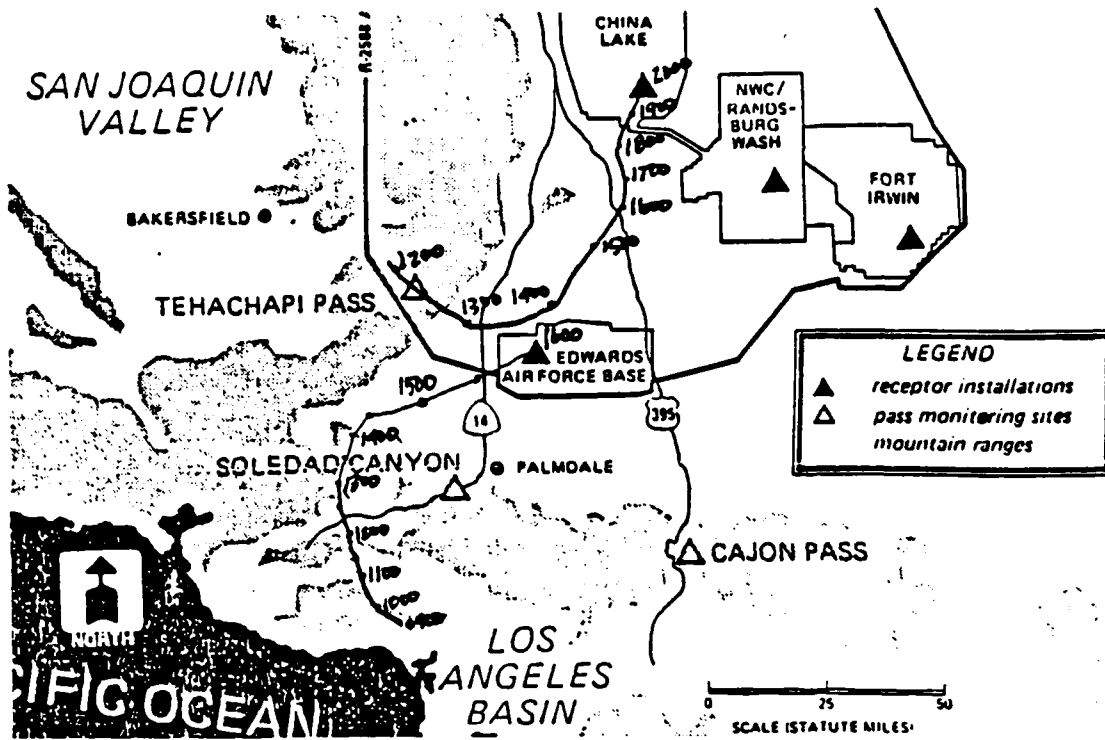
FIGURE F.3a. Example Trajectories of Air Parcels Arriving at Edwards AFB and NWC on 4 October 1984.
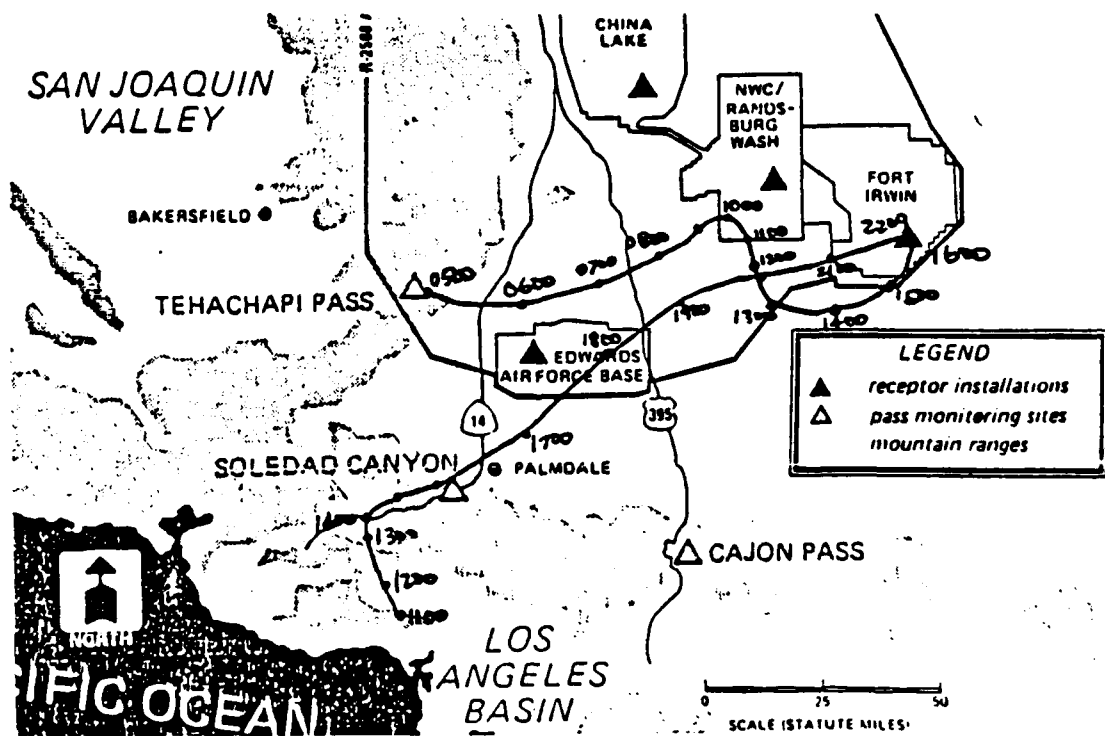

FIGURE F.3b. Example Trajectories of Air Parcels Arriving at Fort Irwin NTC on 4 October 1984.

direction data taken at the RESOLVE sites, air pollution district sites, and NWS stations in the region. The characteristics of the streamline maps discussed in this section are similar to the average ones shown in Chapter 4 of References 7 and 35. The trajectory calculation procedure is similar to that used in the Los Angeles basin by Angell, et al. (Reference 84). Shorter trajectories are generally more reliable than longer ones because of the variability of wind speed and direction. Trajectories were not calculated for every hour during the day, only for the most interesting periods (especially when particle scattering was high or changing dramatically).

Figure F.4 shows particle scattering and information on trajectories for Edwards AFB during the day. The 1600 PST trajectory is shown in Figure F.3a. Earlier trajectories had similar paths, but longer transport times. By 1600 PST, the trajectories were significantly shorter and traveled along a more direct route from the Los Angeles basin. According to the 1600 PST trajectory, this air parcel was in the San Fernando Valley area most of the morning before crossing the mountains just northwest of Soledad Canyon and arriving at Edwards AFB. The air parcel associated with the increase in particle scattering at Edwards AFB (between 1400 and 1600 PST) had passed into the desert about the same time as a large increase in particle scattering was measured at the Soledad Canyon site (see Figure F.2).

The Ni/Pb ratio at Edwards AFB on 4 October is 0.12 (see Table F.1). This ratio is slightly lower than the average for the RESOLVE base year at Edwards AFB. Also, it is slightly higher than the Soledad Pass Ni/Pb, and significantly lower than the Tehachapi Pass Ni/Pb on 4 October. These data show that even on a day when the trajectories indicate transport from the Los Angeles basin all day, the 24-hour average sample still shows a small influence from the San Joaquin Valley.

Figure F.4 also shows particle scattering and trajectory information for NWC during the day. The winds were light and variable until about 1600 PST, when they increased in velocity and came from about the south-southwest. Both the 0600 PST and the 1500 PST trajectories indicate that the air parcels had been within about 15 miles of NWC for the last day or more. The 2000 PST trajectory (shown in Figure F.3a) indicates that transport from the Tehachapi Pass region was established. This transport matches a significant increase in particle scattering that lasted the rest of the day. Note in Figure F.4 that the 2000 PST trajectory was significantly shorter than the 1900 PST trajectory and thus had traveled more quickly along a direct route from the San Joaquin Valley.

The Ni/Pb ratio at NWC on 4 October is 0.31 (see Table F.1). This ratio is slightly higher than the average for the RESOLVE base year at NWC. Also, the ratio is significantly higher than the Soledad Pass Ni/Pb and slightly lower than the Tehachapi Pass Ni/Pb on 4 October.

Figure F.4 also presents information for Fort Irwin NTC. The particle-scattering diurnal pattern is very similar to that at NWC. However, the winds were higher (7 to 16 miles per hour) than at NWC and consistently from the west to southwest all day. Figure F.3b shows how the trajectories shifted during the day. The 1600 PST trajectory (from Tehachapi Pass) probably represents most of the day before 1800 PST. However, note the sharp increase in particle scattering at 1900 PST that occurred just as the transport shifted to the Soledad Pass region and the transport time decreased. Later trajectories indicate transport was from Cajon Pass.

The Ni/Pb ratio at Fort Irwin NTC on 4 October is 0.35. This ratio is slightly higher than the average for the RESOLVE base year at Fort Irwin NTC. Also, the ratio is significantly higher than the Soledad Ni/Pb and slightly lower than the Tehachapi Ni/Pb on 4 October.
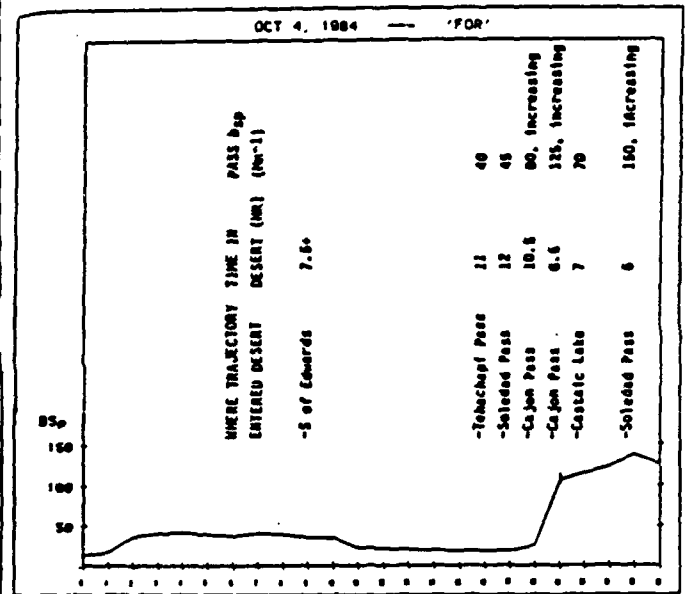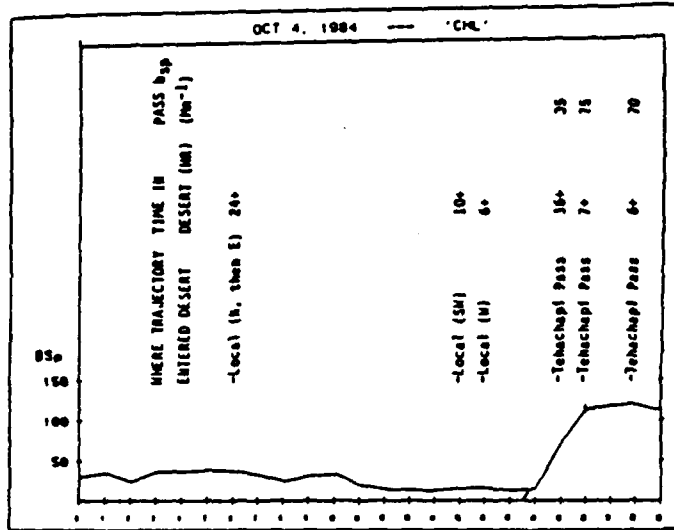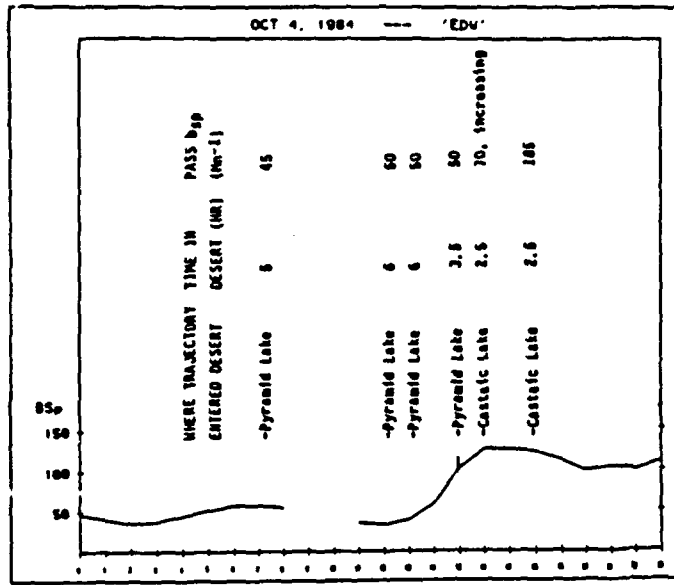
FIGURE F.4. Particle Scattering and Trajectory Information for Edwards AFB, NWC, and Fort Irwin NTC on 4 October 1984. Particle scattering (Bscat) in Mm-1 versus hours of the day. Note that Pyramid and Castaic Lakes are 10 to 25 miles west of Soledad Canyon.

TABLE F.1. Ni/Pb Ratios on Case Study Days.

Site	Average nickel to average lead		12/25/84	10/4//84	7/14/85	2/20/85
	For individual outflow days	For RESOLVE base year				
Cajon Pass	0.023	---	---	0.022	0.056	0.061
Soledad pass	0.056	---	---	0.055	0.074	0.087
Tehachapi pass	0.60	---	---	0.43	1.14	0.49
Edwards AFB	---	0.16	0.003	0.12	0.21	0.58
NWC	---	0.18	0.075	0.31	0.53	---
Randsburg Wash	---	---	---	0.47	0.52	0.45
Fort Irwin NTC	---	0.20	0.0	0.35	0.52	0.43

This result for Fort Irwin NTC on 4 October illustrates an interesting phenomenon. During the worst particle-scattering hours of the day, the trajectories indicate that the Los Angeles basin was the major contributor to aerosols at Fort Irwin NTC. However, the Ni/Pb ratio suggests that the major source contributor to the 24-hour aerosol concentrations was the San Joaquin Valley. Thus, the source contributions during the worst hours of this particular day seem to be different than the source contribution averaged over the complete day. This may not be the situation for other days at Fort Irwin NTC, since we have only looked at this one day. Also the Ni/Pb ratio is not a reliable tracer for individual days (see Chapter 8).

F.2 14 JULY 1985

14 July 1985 is another day of transport from both the San Joaquin Valley and the Los Angeles basin to the RESOLVE receptor sites. However, this day provides an interesting contrast to the other transport day, since many of its characteristics are significantly different than those for 4 October.

Particle scattering and trajectory information are shown for NWC in Figure F.5. Temperature increased and relative humidity decreased during the daylight hours in a typical diurnal pattern. Winds were light and variable until almost noon. The winds then increased and came from the south to the southwest for the rest of the day. The particle scattering was modest and constant until the wind increased and a large pulse arrived from the Tehachapi Pass region. Actually, trajectories throughout the day at NWC entered the desert near Tehachapi Pass.

The NWC trajectories (see Figure F.6) show that the particle-scattering pulse coincided with a shorter transport time and an air parcel with early morning (0600 to 0900 PST) concentrations in the southern San Joaquin Valley. In fact, this same pulse also arrived at Edwards AFB (about 0700 to 1000 PST), and at Randsburg Wash (about 1100 to 1300 PST). NWC particle scattering dropped back to its prenoon value after 1700 PST, even though transport was still quick (about 4 hours) and from the Tehachapi Pass region. These air parcels were in the southern San Joaquin Valley about noon, rather than early morning, and may not have resided in the San Joaquin Valley as long under conditions of poor dispersion.
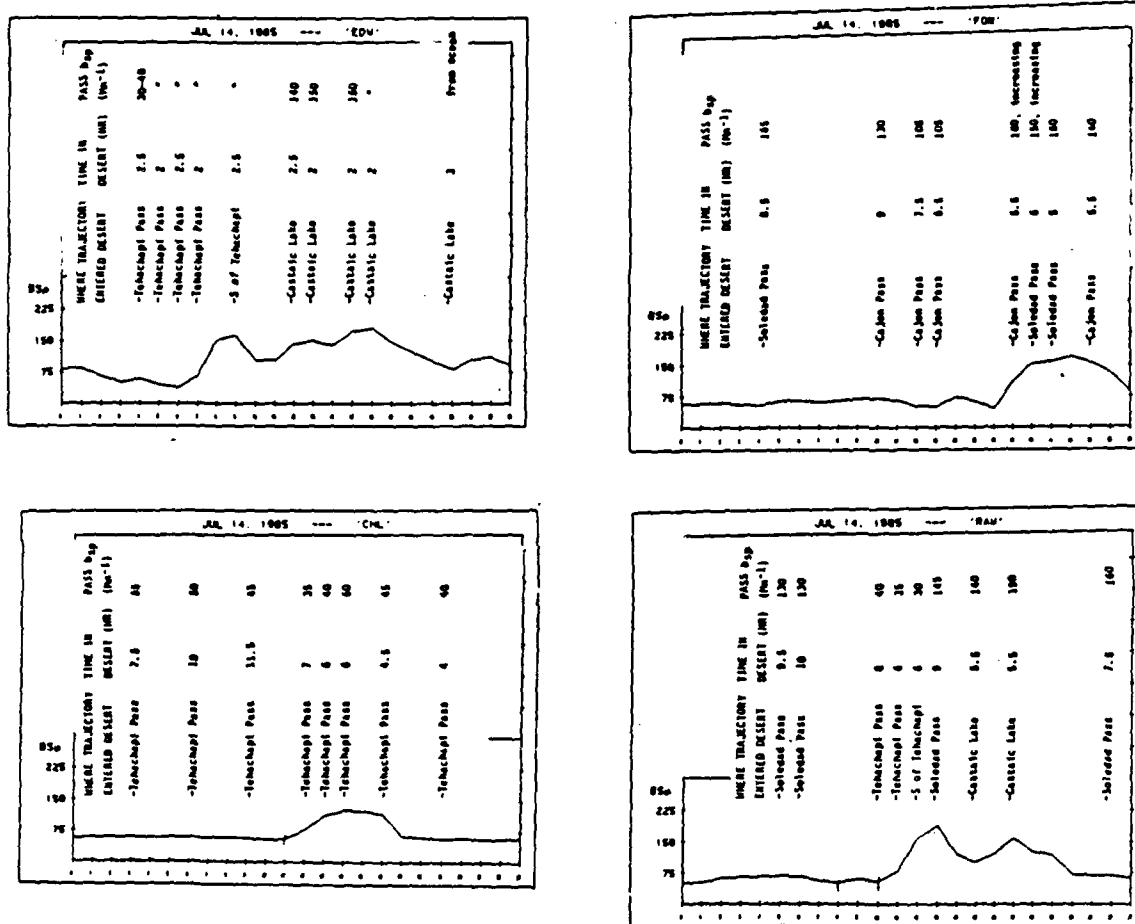
FIGURE F.5. Particle Scattering and Trajectory Information for Edwards AFB, NWC, Randsburg Wash, and Fort Irwin NTC on 14 July 1985. Particle scattering (Bscat) in Mm^{-1} versus hours of the day.
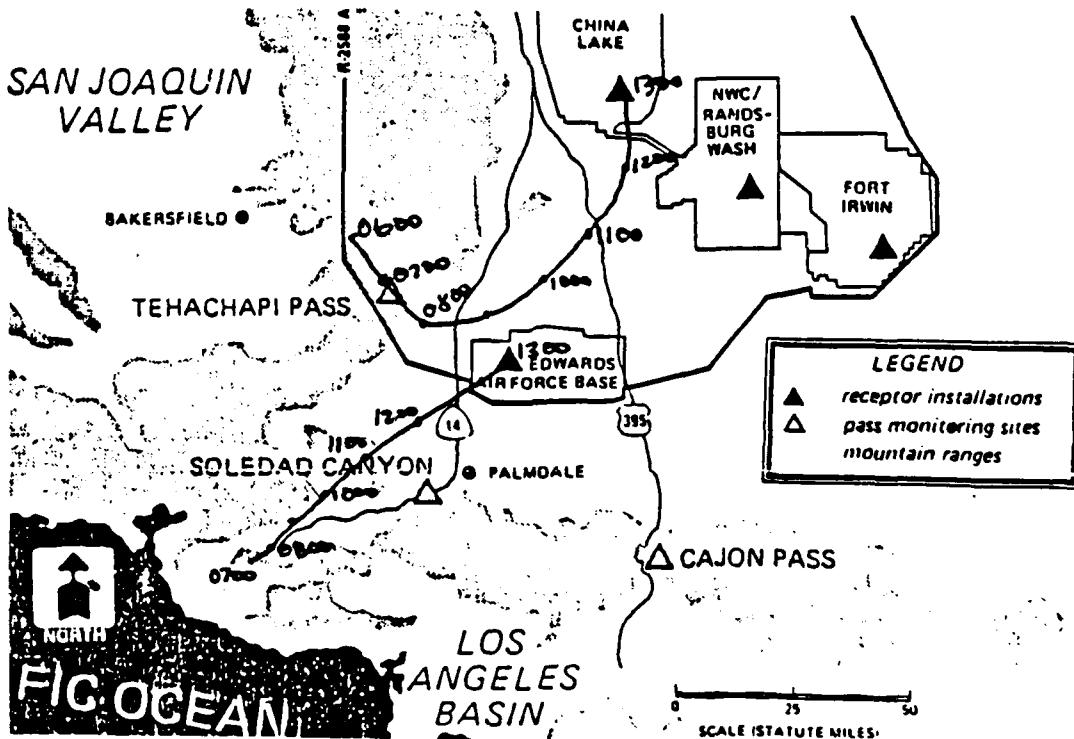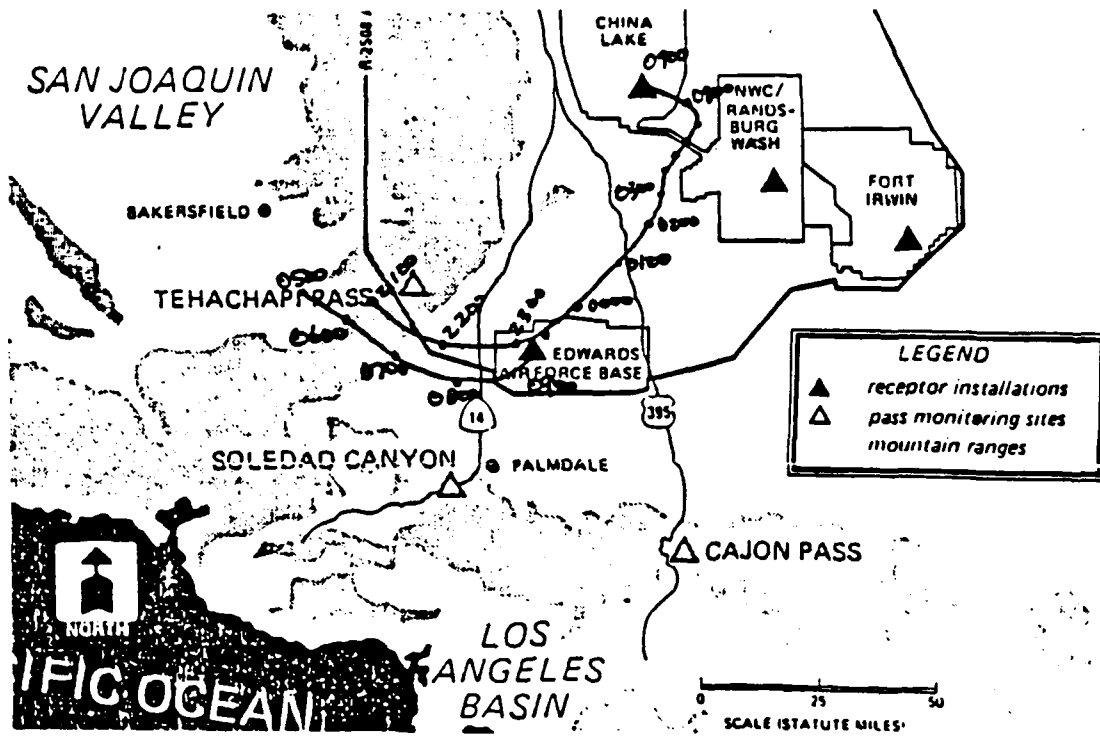
FIGURE F.6. Example Trajectories of Air Parcels Arriving at Edwards AFB and NWC on 14 July 1985.

Figure F.5 also shows the particle scattering and trajectory information for Edwards AFB and Randsburg Wash on 14 July. For Edwards AFB, the particle-scattering pulse between 0700 and 1000 PST was the one with early-morning San Joaquin Valley concentrations. Trajectories show that a similar air parcel arrived at Randsburg Wash at the front end of a particle-scattering pulse (about 1100 to 1300 PST). However, right after this pulse, air parcels from the Los Angeles basin began arriving at both Edwards AFB and Randsburg Wash. Figure F.6 shows two sample Edwards AFB trajectories, one from the San Joaquin Valley and one from the Los Angeles basin. Both trajectories show that the air parcels would have included early-morning concentrations.

Particle scattering and trajectory information for Fort Irwin NTC on 14 July is also shown in Figure F.5. The trajectories show that all air parcels that arrived at Fort Irwin NTC had originated in the Los Angeles basin. The particle-scattering pulse in the late afternoon corresponds to a shorter transport time and morning Los Angeles basin concentrations.

Ni/Pb ratios for all sites on 14 July are shown in Table F.1. All of the receptor sites show a significant influence from the San Joaquin Valley. The interpretation of the Fort Irwin NTC data is again confusing (see discussion of 4 October data); the hourly trajectories indicate transport from the Los Angeles basin all day, while the 24-hour Ni/Pb ratio suggests significant San Joaquin Valley influence.

Part of the influence on this day was because of extremely large forest fires during two weeks of mid-July in Southern California. On 14 July, as on surrounding days, the organic component of the aerosol was high throughout the RESOLVE network.

F.3 25 DECEMBER 1984

In general, 25 December 1984 was a day with mostly local desert effects on the RESOLVE receptor sites. The wind speeds were light most of the day (and the previous day) and wind direction was more variable than on other days. Consequently, the calculated trajectories are less reliable. This could be especially true east of NWC, where the wind flow can be very complicated. However, the trajectories should still be adequate, since we have wind data at three locations in the vicinity: NWC, Trona, and Randsburg Wash.

Particle scattering and trajectory information for NWC are shown in Figure F.7. Air parcels that arrived at NWC probably spent the last 10 to 20 hours within about 25 miles of NWC. The trajectories indicate that the air parcels that arrived between about 1500 and 2000 PST probably passed through the Searles Valley before arriving at NWC.

Particle scattering and trajectory information for Edwards AFB are also shown in Figure F.7. Even on this day, with slow winds and mostly local effects, the situation at Edwards AFB was complicated, since Edwards AFB is so close to the passes. The morning trajectories indicated slow transport from the San Joaquin Valley and possibly the Los Angeles basin. However, the air parcels that arrived in the late afternoon and evening probably spent at least the last 16 hours in the desert.

Particle scattering and trajectory information for both Randsburg Wash and Fort Irwin NTC are also shown in Figure F.7. Air parcels that arrived at Randsburg Wash between about 1300 and 1800 PST came from the northwest and had spent the last 9 to 24 hours within about 45 miles of the site. Two of the trajectories indicated that the air parcels passed through the Searles Valley. Fort Irwin NTC was much cleaner on this day than the
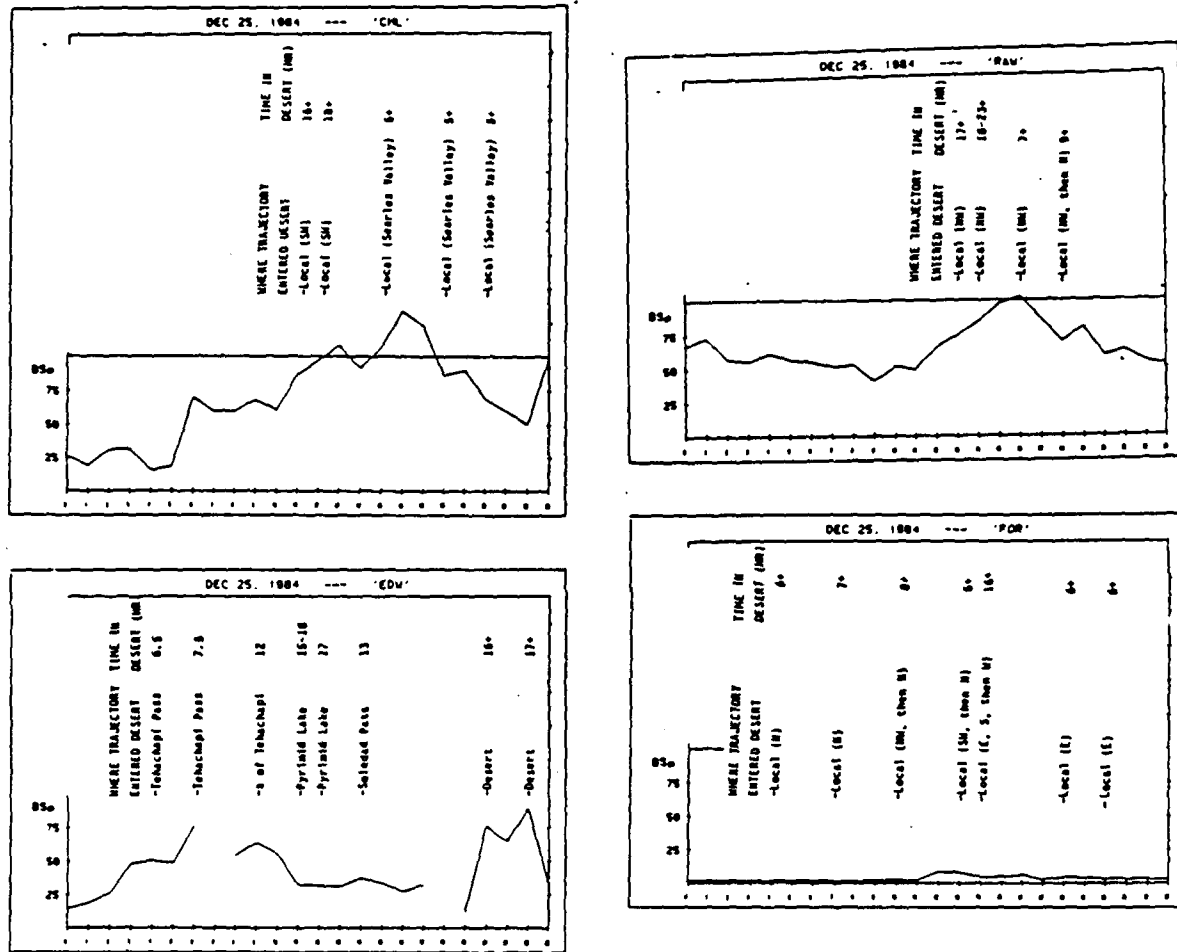
FIGURE F.7. Particle Scattering and Trajectory Information for Edwards AFB, NWC, Randsburg Wash, and Fort Irwin NTC on 25 December 1984. Particle scattering (Bscat) in Mm⁻¹ versus hours of the day.

other sites. The trajectories before about 1000 PST indicate that the air parcels had spent at least the last 6 hours north of the sampling site. The air parcels that arrived around noon had spent 10 to 16 hours traveling from the south and southwest, possibly passing through the Barstow area. Late in the day, the air parcels came directly from the east.

F.4 20 FEBRUARY 1985

Very high wind speeds and blowing dust were reported at many locations in the high desert and much of Southern California on 20 February 1985. The synoptic conditions showed strong winds from the north early in the day (0500 PST). However, surface winds were from the west in the western end of the high desert (between Edwards AFB and Palmdale) until early afternoon, even as extremely strong winds from the north covered the rest of the high desert. Lancaster reported blowing dust at 0600 PST with westerly winds. On a day such as this, surface winds and trajectories can be misleading about the origin of particular air parcels. Upper-level winds can carry pollutants long distances, after which the pollutants can be mixed down into a surface-layer air parcel that is traveling from the opposite direction. Good examples of this phenomenon are Edwards AFB and Fort Irwin NTC early in the day.

Particle scattering and trajectory information for the four desert sites is shown in Figure F.8. The trajectories indicate transport from the upwind basins at Edwards AFB, Randsburg Wash, and Fort Irwin NTC early in the morning. At all three pass sites, this corresponds to a large particle scattering peak late on 19 February that decreased to background by about 0600 PST on 20 February.

Trajectories for NWC all day, and for the other three desert sites after 1000 PST, show strong winds and transport from the north. The high particle-scattering levels occurring throughout the day at all of the sites demonstrate the influence of wind-blown dust. The measurement of the soil component at Edwards AFB and Fort Irwin NTC (measurements are not available at NWC and Randsburg Wash) are much higher than normal, also indicating a large wind-blown dust component.
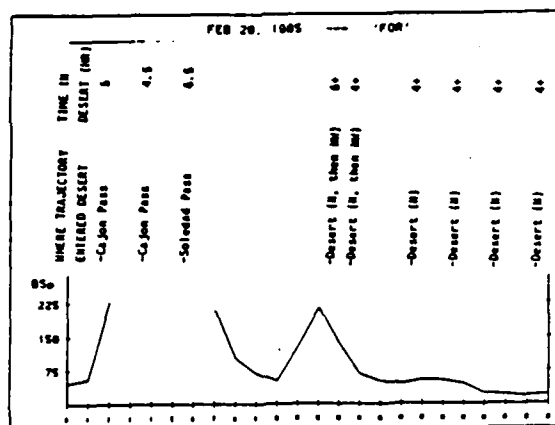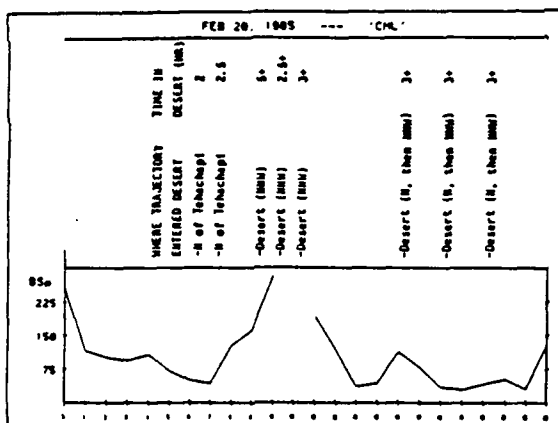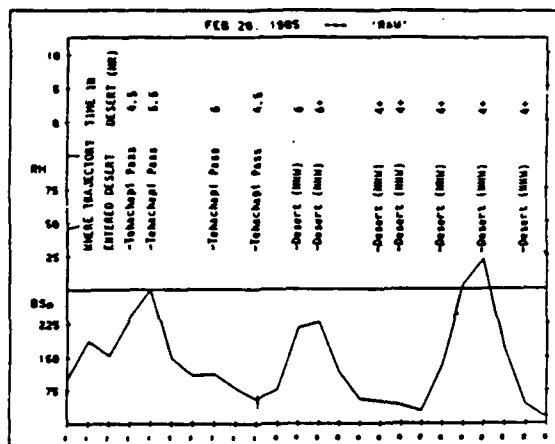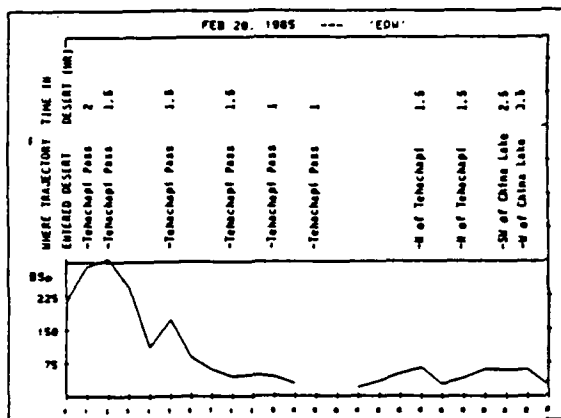
FIGURE F.8. Particle Scattering and Trajectory Information for Edwards
AFB, NWC, Randsburg Wash, and Fort Irwin NTC on 20 February 1985.
Particle scattering (Bscat) in Mm^{-1} versus hours of the day.

REFERENCES

1. Naval Weapons Center. *Visibility Monitoring in the Southern California Desert for the Department of Defense: Research on Operations-Limiting Visual Extinction,* by D Blumenthal and J. Trijonis. China Lake, Calif., NWC, September 1984. (NWC TP 6566.)

2. J. Trijonis. *RESOLVE Data Analysis Plan,* prepared for the Naval Weapons Center, China Lake, Calif., January 1985.

3. J. Trijonis, et al. *RESOLVE Monitoring Program Plan Evaluation Using Historical Data and Error Analysis,* prepared for Lockheed-EMSCO, Las Vegas, Nev., June 1984.

4. Naval Weapons Center. *Quality Assurance for RESOLVE-A Visibility Study in the California Desert,* by A. Pitchford, et al. China Lake, Calif., NWC, January 1985. (NWC TP 6591.)

5. M. McGown, et al. *RESOLVE Data Summary, Vol. I: Annual Report,* prepared for the Naval Weapons Center, China Lake, Calif., 1987.

6. _____. *RESOLVE Data Summary, Vol. II: Quarterly Reports,* prepared for the Naval Weapons Center, China Lake, Calif., 1987.

7. T. Smith, et al. *The Impact of Transport from the South Coast Air Basin on Ozone Levels in the Southeast Desert Air Basin,* prepared for California Air Resources Board, Sacramento, Calif., 1983.

8. R. Husar, et al. "Three-Dimensional Distribution of Air Pollutants in the Los Angeles Basin," *Journal of Applied Meteorology,* 16:1089-96, 1977.

9. M. Pitchford. "The Relationship of Regional Visibility to Coarse and Fine Particle Concentration in the Southwest," *Journal of Air Pollution Control Association,* 32: 814, 1982.

10. J. Ouimette, et al. "Chemical Species Contributions to Light Scattering by Aerosols at a Remote Arid Site," proceedings of ACS Symposium Series 167 on Atmospheric Aerosol, Las Vegas, Nev., 1980.

11. California Air Resources Board. *Visibility Reduction as Related to Aerosol Constituents,* by B. Appel, et al., Sacramento, Calif., CARB, 1983. (Report ARB/A1-081-32.)

12. Environmental Protection Agency. *Determination of the Feasibility of the Long-Range Transport of Ozone and Ozone Precursors,* by D. Blumenthal, et al. Research Triangle Park, N.C., EPA, 1974. (Report 450/3-74-061.)

13. P. Drivas and F. Shair. "A Tracer Study of Pollutant Transport and Dispersion in the Los Angeles Area," *Atmospheric Environment,* 8:1155-63, 1984.

14. D. Reible, et al. "Atmospheric Transport of Visibility Degrading Pollutants into the California Mojave Desert," *Atmospheric Environment,* 16: 599-613, 1982.

15. California Air Resources Board.. *Assessment of Aerosol Transport into the Mojave Desert*, by L. Myrup and R. Flocchini. Sacramento, Calif. CARB, 1986. (Report for contract A1-153-32.)

16. J. Barone, et al. "The Effect of Owens Dry Lake on Air Quality in the Owens Valley with Implications for the Mono Lake Area." ACS *Symposium Series* 167, 1981. Pp. 328-346.

17. D. Chaloud. Standard Operating Procedures and Quality Assurance Manual for RESOLVE. Lockheed Engineering and Management Services Report to Naval Weapons Center, China Lake, Calif. February 1984.

18. M. Pitchford. EPA Environmental Monitoring Systems Laboratory, Las Vegas, Nev. Personal communication, 1986.

19. C. Mathai, et al. "Intercomparison of Ambient Aerosol Samplers Used in Western Visibility and Air Quality Studies," presented at annual meeting of the Air Pollution Control Association, Detroit, Mich., 1985.

20. A. Waggoner, et al. Waggoner Electronics, Inc., Seattle, Wash. Private communication, 1988.

21. _____. "Optical characteristics of Atmospheric Aerosols," *Atmospheric Environment*, 15:1891, 1981.

22. _____. *University of Washington, Seattle, Wash. Private communication, 1986.*

23. Sandia National Laboratories. *The Albuquerque Winter Visibility Study, Vol. I: Overview and Data Analysis*, by B. Zak, et al. Albuquerque, N. Mex., SNL, 1984. (SAND84-0173-1, UC-71.)

24. G. Wolff. General Motors Research Laboratories, Warren, Mich. Private communication, 1986.

25. J. Trijonis. "Effect of Diesel Vehicles on Visibility in California," *The Science of the Total Environment*, 36: 131, 1984.

26. R. Weiss and A. Waggoner. "Aerosol Optical Absorption: Accuracy of Filter Measurement by Comparison with In-Situ Extinction," *Aerosols*, Elsevier Science Publishing Co., New York, N. Y., 1984.

27. Electric Power Research Institute. *Comparison of Visibility Measurement Techniques: Eastern United States*, by I. Tombach and D. Allard. Palo Alto, Calif., EPRI, October 1983. (Report EA-3292.)

28. I. Tombach. AeroVironment, Inc., Monrovia, Calif. Private communication, 1986.

29. W. Richards. Sonoma Technology, Inc., Santa Rosa, Calif. Private communication, 1986.

30. J. Ouimette. "Aerosol Chemical Species Contributions to the Extinction Coefficient," Ph.D. thesis, California Institute of Technology, Pasadena, Calif. (1981).

31. E. Felton. *California's Many Climates*. Pacific Books, Palo Alto, Calif. (1968).

32. Edwards Air Force Base. Monthly Weather Summaries for July 1984-June 1985, prepared by Meteorlogical Office, Det 21, 2WS (1985).

33. National Oceanic and Atmospheric Administration. "Climate of California." *Climatography of the United States*, Vol. 60, 1982.

34. Naval Weapons Center. *Winds Aloft at the Naval Weapons Center*, by the Range Meteorological Office. China Lake, Calif., NWC, January 1984. (NWC TM 5209.)

35. California Air Resources Board. *Application of Climatological Analysis to Minimize Air Pollution Impacts in California*, by T. Smith, et al. Sacramento, Calif., CARB, 1984.

36. Naval Weapons Center. *Surface Winds at NWC: 1964-1982*, by R. Kelso and R. Evert. China Lake, Calif., NWC, February 1985. (NWC TP 6572.)

37. US Air Force. *Limited Surface Observations, Climatic Summary for Edwards AFB*, prepared by Environmental Technical Application Center, Asheville, N.C., December 1984.

38. California Air Resources Board. *California Surface Wind Climatology*, by T. Hayes, et al. Sacramento, Calif., CARB, June 1984.

39. _____. *Emission Inventory 1983*. Sacramento, Calif., CARB, December 1986.

40. J. Trijonis. "Visibility in California," *Journal of Air Pollution Control Association*, 32:165-69, 1982.

41. Naval Weapons Center. Monthly Summary of Weather for July 1984-June 1985, prepared by the Range Meteorological Office. China Lake, Calif., NWC, 1985.

42. U.S. Air Force. *Uniform Summary of Rawinsonde Observation, Edwards AFB: Temperatures by Month, for July 1952-October 1960 and January 1961-February 1967*, prepared by the Environmental Technical Application Center, Asheville, N.C. (1969).

43. California Air Resoures Board, *Mean Monthly 850 mb Temperatures at Vandenberg AFB for 1956 and 1985*, and *Daily 850 mb Temperatures at Vandenberg AFB for 1984 and 1985 at 1200 Z*, obtained from A. Lorenzen. Sacramento, Calif., CARB, February 1987.

44. T. Smith, et al. *Climatological, Meteorological, and Dispersion Study of Regional and Selected Local Environments of Northern California*, U.S. Army Atmospheric Sciences Laboratory, 1985. (Report CR-85-0008-I.)

45. D. Blumenthal, et al. "Anatomy of a Los Angeles Smog Episode: Pollutant Transport in the Daytime Sea Breeze Regime," *Atmospheric Environment*, 12:893-907, 1978.

46. California Air Resources Board. *Air Quality Benefit Analysis for Los Angeles and San Francisco Based on Housing Values and Visibility*, by J. Trijonis, et al. Sacramento, Calif., CARB, 1985.

47. R. Kelso. Naval Weapons Center, China Lake, Calif. Private communication, 1987.

48. D. Wilbur. AeroVironment, Inc., Monrovia, Calif. Private communication of data, 1987.

49. J. Ouimette and R. Flagan. "The Extinction Coefficient of Multicomponent Aerosols," *Atmospheric Environment*, 16:2405, 1982.

50. A. Davidson. "Visibility in the South Coast Air Basin: Patterns, Relationship to Particulate Concentrations, and Trends," presented at the annual meeting of the Air Pollution Control Association, West Coast Chapter, Scottsdale, Ariz., October 1983.

51. A. Stelson, et al. "A Note on the Equilibrium Relationship Between Ammonia and Nitric Acid and Particulate Ammonium Nitrate," *Atmospheric Environment*, 13:369-71, 1979.

52. A. Stelson and J. Seinfeld. "Relative Humidity and Temperature Dependence of the Ammonium Nitrate Dissociation Constant," *Atmospheric Environment*, 16:983-92, 1982.

53. California Air Resources Board. *Impact of Transport from South Coast Basin on Ozone Levels in the Southeast Desert Air Basin*, by D. Lehrman, et al. Sacramento, Calif., CARB, 1982. (Vol. IV, MRI report.)

54. D. Hegg. Private communication concerning data from University of Washington Cloud Physics Aircraft funded by Southern California Edison, 1983.

55. R. Crume, et al. *Scattering Efficiencies of Sulfate and Nitrate Aerosols in an Outdoor Smog Chamber*. University of North Carolina, Environmental Sciences and Engineering Dept., Chapel Hill, N.C. 1987. (Working paper.)

56. H. Hasan and T. Dzubay. "Apportioning Light Extinction Coefficients to Chemical Species in Atmospheric Aerosol," *Atmospheric Environment*, 17:1573-81, 1983.

57. P. Groblicki, et al. "Visibility-Reducing Species in the Denver 'Brown Cloud'-I: Relationships Between Extinction and Chemical Composition," *Atmospheric Environment*, 15:2473, 1981.

58. C. Sloane. General Motors Research Laboratories, Warren, Mich. Private communication, 1986.

59. G. Jennings. National Center for Atmospheric Research, Boulder, Colo. Private communication, 1986.

60. R. Draftz. Illinois Institute of Technology Research, Chicago, Ill. Private communication, 1986.

61. W. Malm and C. Johnson. "Optical Characteristics of Fine and Coarse Particulates at Grand Canyon, Arizona," *Atmospheric Environment*, 18:1231, 1984.

62. C. Sloane. "Effect of Composition on Aerosol Light Scattering Efficiencies," *Atmospheric Environment*, 20:1025, 1986.

63. A. Madansky. "The Fitting of Straight Lines When Both Variables are Subject to Error," *American Statistical Association Journal*, March 1959.

64. W. White and E. Macias. "The Empirical Relationship of Atmospheric Extinction to Aerosol Composition in the Nonurban West," presented at APCA International Specialty Conference on Visibility, Jackson, Wyo., September 1986.

65. G. Cass. California Institute of Technology, Pasadena, Calif. Private communication, 1987.

66. AeroVironment, Inc. *Chemical Composition Profiles for Dust Sources Near R-2508 Airspace*, prepared for the Naval Weapons Center, China Lake, Calif, October 1986. (Report AV-FR-86/570.)

67. California Institute of Technology, Environmental Quality Laboratory. *Control of Atmospheric Fine Primary Carbon Particle Concentrations*, by H. Gray. Pasadena Calif., CIT, 1986. (EQL Report 23.)

68. Nero and Associates. *Review of Emissions Inventory for the Three Counties in the Southeast Desert Air Basin*, prepared for the Naval Weapons Center, China Lake, Calif., August 1986.

69. U.S. Environmental Protection Agency. *Revised CMB User Manual*, by K. Axetell, et al. Research Triangle Park, N.C., EPA, 1987.

70. J. Watson, et al. "The Effective Variance Weighting for Least Squares Calculations Applied to the Mass Balance Receptor Model," *Atmospheric Environment*, 18:1347, 1984.

71. U.S. Environmental Protection Agency. *Protocol for Applying and Validating the CMB Model*, by T. Pace and J. Watson. Research Triangle Park, N.C., EPA, 1987.

72. K. Cleary. California Air Resources Board, Sacramento, Calif. Private communication, 1987.

73. J. Ouimette. Chevron Research Corp., Richmond, Calif. Private communication, 1987.

74. W. Cox. Great Basin Unified Air Pollution Control District, Bishop, Calif. Private communication, April 1988.

75. California Energy Commission. *Final Staff Assessment for Kerr-McGee Chemical Corporation's Argus Co-Generation Expansion (ACE Project)*. Sacramento, Calif., CEC, March 1987.

76. M. Pitchford and M. McGown. EPA-EMSL, Las Vegas, Nev. Private communications, 1986.

77. R. Flocchini. University of California, Davis, Calif. Private communication, 1986.

78. M. Pitchford, EPA-EMSL, Las Vegas, Nev. Private communication, 1985.

79. R. Weiss. University of Washington, Seattle, Wash. Private communication, 1986.

80. Santa Fe Research Corp. *Blank Adjustments for RESOLVE Carbon Concentrations*, by J. Trijonis. Bloomington, Minn., 1985. (Working memorandum.)

81. J. Trijonis. "Dependence of Ambient NO_2 on Precursor Control," *Air*. American Institute of Chemical Engineers Symposium series, 1979.

82. A. G. Russell, et al. "Mathematical Modeling of the Formation and Transport of Ammonium Nitrate Aerosol," *Atmospheric Environment*, 17:949-64, 1983.

83. California Air Resources Board. *Effect of Diesel Vehicles on Visibility in California*, by J. Trijonis. Sacramento, Calif., CARB, July 1983. (Contract No. A2-072-32.)

84. J. Angell, et al. "Three-Dimensional Air Trajectories Determined from Tetroon Flights in the Plantery Boundary Layer of the Los Angeles Basin," *Journal Applied Meteorology*, 11:451, 1972.